

Brain connectivity from micro to macro scale

*Hersenconnectiviteit van micro- tot macroschaal
(met een samenvatting in het Nederlands)*

proefschrift

ter verkrijging van de graad van doctor aan de Universiteit Utrecht op gezag van de rector magnificus, prof. dr. G.J. van der Zwaan, ingevolge het besluit van het college voor promoties in het openbaar te verdedigen op dinsdag 3 april 2018 des middags te 12.45 uur

door

Lianne Heleen Scholtens

geboren op 11 mei 1989
te Wageningen

Promotor: Prof. dr. R.S. Kahn

Copromotor: Dr. M.P. van den Heuvel

Brain connectivity from micro to macro scale

Lianne Heleen Scholtens

The studies described in this thesis were performed at Brain Center Rudolf Magnus, Department of Psychiatry, University Medical Center Utrecht, Utrecht University, The Netherlands.

Scholtens, Lianne Heleen

Brain connectivity from micro to macro scale

Printed by Proefschriften.net – Ipskamp printing Enschede

Cover design Ruud Barth & Lianne Scholtens using a neural algorithm of artistic style transfer (<https://arxiv.org/abs/1508.06576>)

ISBN 978-94-028-0967-1

Copyright: © Lianne Heleen Scholtens, 2018. All rights reserved. No part of this publication may be reproduced in any form by any electronic or mechanical means without the prior written permission of the author.

voor Ruud ♡

Contents

Page

1 Introduction 1

Theme I

2 Linking macroscale graph analytical organization to microscale neuroarchitectonics in the macaque connectome 15

3 Associated microscale spine density and macroscale connectivity disruptions in schizophrenia 59

4 Bridging cytoarchitectonics and connectomics in human cerebral cortex 105

5 Converging evidence of interplay between neural connectivity at the micro- and macroscale of connectome organization in human, mouse and rat brain 123

6 Rich layer III pyramidal morphology of highly connected macroscale regions: a pilot study 143

Theme II

7 Cortical chemoarchitecture shapes macroscale effective functional connectivity patterns in macaque cerebral cortex 159

8 Multimodal Analysis of Cortical Chemoarchitecture and Macroscale fMRI Resting-State Functional Connectivity 185

Theme III

9 Linking Contemporary High Resolution Magnetic Resonance Imaging to the Von Economo Legacy: A Study on the Comparison of MRI Cortical Thickness and Histological Measurements of Cortical Structure 213

10 An MRI Von Economo Koskinas atlas 237

Theme IV

11 Affected anatomical rich club and structural-functional coupling in young offspring of schizophrenia and bipolar disorder patients 269

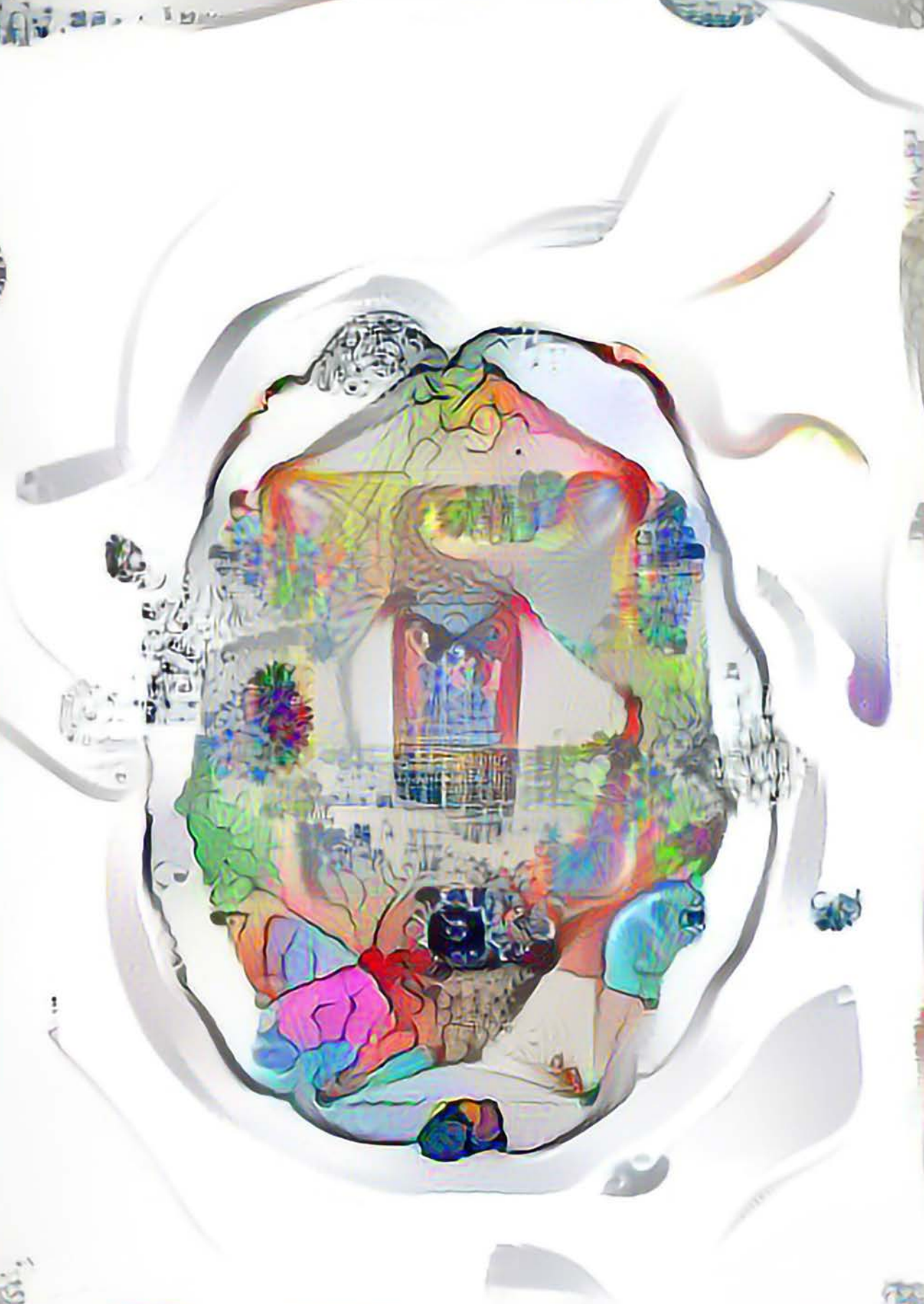
12 Summary and Discussion 301

List of publications 317

Nederlandse samenvatting 319

Acknowledgments – Dankwoord 323

Curriculum Vitae 326



Chapter 1

Introduction

[Parts of this introduction have been submitted as a review paper to Biological Psychiatry: Cognitive Neuroscience and Neuroimaging]

Brain connectivity from micro to macro scale

The mammalian brain is a highly complex organ, with a broad range of regional microscale cellular morphologies and macroscale global properties, together forming an efficient system for processing and integration of multimodal information. Scientists investigating the brain across different species and across scales of observation have reported on a large regional variability in brain organization. For example on the microscale, large variation in cortical microscale cyto-, myelo- and chemoarchitecture has been observed (see for review (Amunts and Zilles, 2015)). On the macroscale of corticocortical connectivity, regions have widely differing connectivity profiles with some regions connecting to regions broadly distributed across the cortex, while others have mostly local connections (Sporns, 2011). Variability in both scales of organization has been observed to coincide with differentiated functional roles of cortical regions within the healthy brain, as well as with disease-related biomarkers (Crossley et al., 2014; Penzes et al., 2011). How cortical organization on the micro and macroscale interact – and how this interaction influences brain function in disease – remains largely an open question.

Aim of this thesis

The work presented here explores the association between whole-brain patterns of microscale architecture and macroscale region-to-region connectivity. Much of the work

presented in this thesis would not have been possible without the availability of literature sources on microscale architecture of the brain, nor without strong collaboration with neuroimaging colleagues for the diverse sources of macroscale connectivity data. In linking data across scales – and sometimes across centuries – we aimed to learn how a region’s microscale characteristics are related to its macroscale corticocortical connectivity.

General introduction

Microscale patterns of cortical organization

Microscale cortical variation has been described in a multitude of different modalities (see for some examples Figure 1 a-d), and has been proposed to reflect functional differences in the role of a particular region in brain function.

In an effort to elucidate brain structure and (localization of) brain function, pioneering neuroanatomists have extensively demonstrated a large heterogeneity of cortical morphology on the microscale of brain organization. At the turn of the twentieth century, microscale variation was observed in neuronal cell type, size and layer distribution by neuroanatomy pioneers such as Hammarberg (Hammarberg, 1895), Campbell (Campbell, 1905), Brodmann (Brodmann, 1909) and Von Economo and Koskinas (Von Economo and Koskinas, 1925), as well as in cortical myelinated fiber distribution by amongst others Smith (Smith, 1907), Flechsig (Flechsig, 1920) and Vogt and Vogt (Vogt, 1919). These observations led to increasingly detailed subdivisions of the cortical mantle into up to 150 to 200 (Amunts and Zilles, 2015) cytoarchitecturally and/or myeloarchitecturally distinct regions, which often – but not yet always – could be associated with the observation of similarly diverse regional functional profiles. Following these findings, modern-day studies employing chemoarchitectural quantifications of neurotransmitter receptor densities have shown great variability in the presence, density and layer distribution of both inhibitory and excitatory neurotransmitter receptors, describing a microscale regional variation which has enabled even more fine-grained delineation of cortical regions (Amunts et al., 2010).

In addition to parcellating the cortex into distinct sub regions, cortex-wide patterns of microscale characteristics have been associated to general functional profiles of cortical regions. *Cortical type* (ranging from granular to agranular, broadly defined based on the definition of cortical (sub)layers, the distribution of neuronal cell types, as well as neuronal cell size) has been related to the general function of a cortical area, with for instance primary sensory areas having a very clearly defined granular layer structure, whereas more higher order association areas are mostly agranular and tend to have a much less clearly defined cortical layer IV (Barbas, 2015; Brodmann, 1909; Mesulam,

1998; Von Economo and Koskinas, 1925). Additionally, studies investigating layer III *pyramidal cell complexity* across regions in both macaque and human cortex have reported clear differences in both cell size and spine density between cortical regions, with those areas involved in higher order processing having larger and more spinous pyramidal neurons (Elston, 2003; Jacobs et al., 2001), aspects of neuronal organization suggested to be related to increased processing and integration capacity of neurons (Koch, 1997; McCulloch and Pitts, 1943).

Gene expression analysis (transcriptomics), reflecting localized modulation of gene function, is another measure showing great regional variability at the micro scale of cortical organization (Hawrylycz et al., 2012). Recent studies exploring the brain-wide transcriptome of the developing primate (Bakken et al., 2016) and human (Miller et al., 2014) brain, as well as the adult mouse (Lein et al., 2007), macaque (Bernard et al., 2012) and human brain (Hawrylycz et al., 2012), and have reported on differentiated expression profiles across cortical brain regions, where regions with more similar expression profiles are located in spatial proximity of each other (Bernard et al., 2012; Hawrylycz et al., 2012; Lein et al., 2007).

Macroscale patterns of cortical organization

At the macroscale organizational level of brain connectivity, the field of connectomics aims to study the comprehensive set of connections between all regions of the brain (Sporns, 2011) (Figure 1 e-i). Macroscale connectivity patterns vary across regions, and have been associated with functional organization and efficiency of information processing in the brain.

In the mammalian brain, anatomical connections are mostly studied using invasive tract-tracing or non-invasive neuroimaging methods such as diffusion weighted magnetic resonance imaging (DWI). On top of mapping anatomical connections, functional connectivity is defined as the statistical dependency between remote physiological events in the brain (Friston et al., 1993) and is often examined by means of resting state functional magnetic resonance imaging (rsfMRI), electroencephalography (EEG) and/or magnetoencephalography (MEG). Findings across different macroscale connectome modalities in the human brain have consistently shown a strong genetic component in brain connectivity patterns (Fornito et al., 2011; Glahn et al., 2010; van den Heuvel et al., 2013), regional connectivity patterns that have been related to differentiated functional profiles of regions (Bullmore and Sporns, 2009; Tomasi and Volkow, 2011).

Based on its topology, the brain network can be divided into modules consisting of highly interconnected regions clustered together, with relatively sparse connections

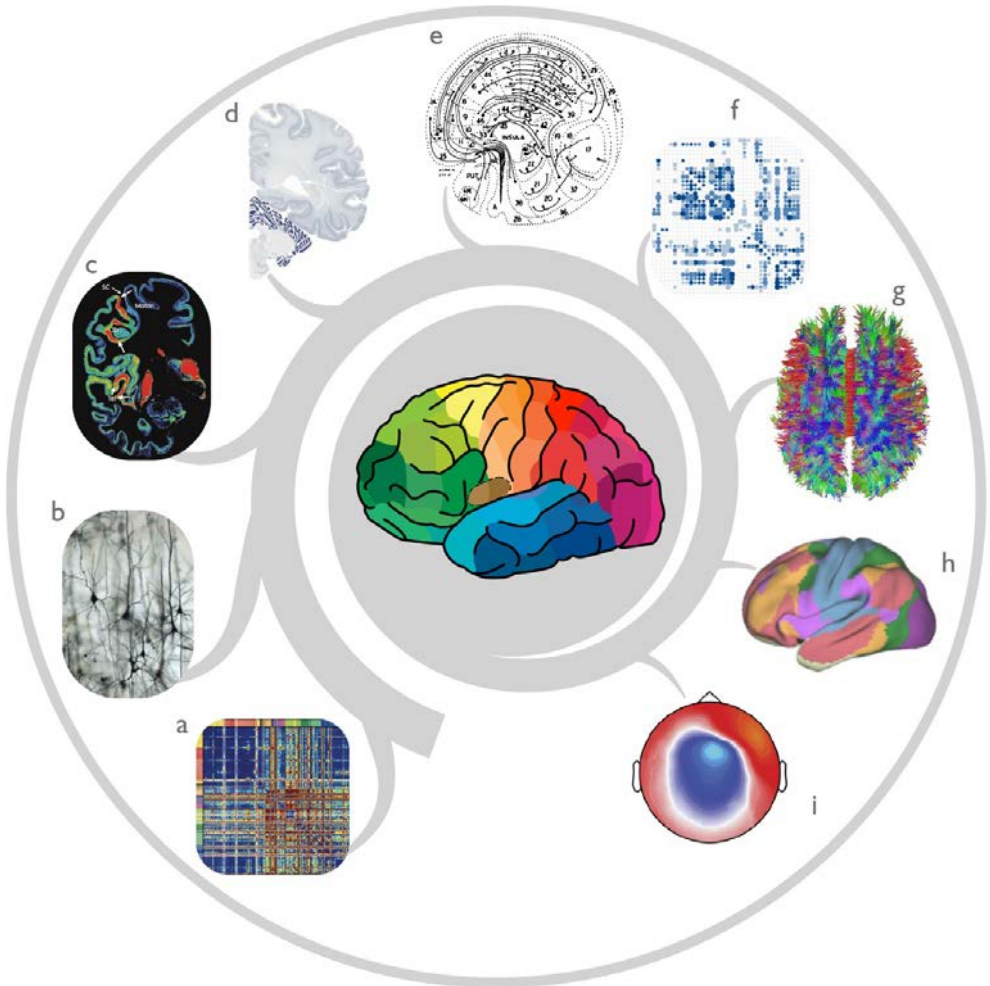


Figure 1. Brain organization has been studied on a wide range of scales, each providing a unique and complementary perspective on brain structure and function. Selected examples of micro (a-d) and macroscale (e-i) measurement modalities of brain structure and function: **a)** gene expression (Hawrylycz et al., 2012); **b)** pyramidal cell morphology; **c)** neurotransmitter receptor fingerprint (chemoarchitecture) (Zilles and Amunts, 2010); **d)** Nissl staining based cortical laminar architecture (Ding et al., 2016); **e)** macaque strychnine-based effective functional connectivity (McCulloch, 1944); **f)** macaque tract-tracing structural connectome (Scholtens et al., 2014); **g)** diffusion-weighted imaging; **h)** resting state functional MRI networks (Yeo et al., 2011); **i)** magnetoencephalography (Baillet, 2017).

between modules (Newman and Girvan, 2004). Following this characteristic, most cortical regions tend to primarily be linked to other regions within their own functional module (Meunier et al., 2010; Newman and Girvan, 2004). In contrast, a select subset of regions – also described as hubs – has widely distributed lines of communication across the cortical mantle (Harriger et al., 2012; van den Heuvel et al., 2012). These

highly – and widely – connected hub regions have been hypothesized to play an important role in information integration in the brain, and to form a link between different functional modules. Integrating different types and sources of information across the cortex, hub regions could provide a scaffold or backbone for the brain in performing important higher order processes, such as cognition, and have been shown to overlap with all resting state functional networks (van den Heuvel and Sporns, 2013; Zamora-López et al., 2010, 2011). Simulated selective lesioning studies show removal of rich club hub nodes from the brain network to have a much larger effect on the brain's integrative capacity than removal of other non-hub nodes (de Reus and van den Heuvel, 2014; Schmidt et al., 2015; Zamora-López et al., 2010). Extending on the observations and simulations in the healthy connectome, rich club hubs have been shown to be affected across a range of brain disorders (Crossley et al., 2014), and to play an important role in for example Alzheimer's disease (Buckner et al., 2009) and schizophrenia (van den Heuvel et al., 2013).

Linking micro and macro scale patterns of organization in the brain

Studies on both the micro and the macro scale of observation have shown links between variation in cortical organization and a region's functional role in the brain. Some investigations into the connectivity of individual selected regions in the the macaque monkey (e.g. (Rockland and Pandya, 1979; Seltzer and Pandya, 1978)) and cat brain (as collated and analyzed by (Scannell et al., 1995)) have shown that the majority of cortical regions are predominantly connected to regions with a similar cytoarchitectural layout, hypothesizing that a large portion of cortical connections occur between regions with similar functional profiles (Barbas, 2015). In this thesis we aim to further explore these observations and to extend them to all regions of the cortical connectome, in an effort to expand our understanding of the interplay between the micro and macro scale of brain organization.

Outline of this thesis

The aim of the research presented in this thesis is to explore the association between the cortical architecture of the mammalian brain at the micro and macro scale of organization. The content of this thesis has been divided into four themes, describing micro – macro comparisons in the structural [**chapter 2 – 6**] and functional [**chapter 7 & 8**] connectome, as well as in historical microscale data [**chapter 9 & 10**], followed by a study into connectome disconnectivity in offspring of schizophrenia and bipolar disorder patients [**chapter 11**].

Theme I – linking micro to macro scale in the structural connectome

In the first part of this thesis we aim to explore the putative relation between cortical microscale characteristics and macroscale connectivity in the structural connectome. **Chapter 2** describes a broad investigation of possible micro – macro associations in the structural connectome of the macaque monkey. In this chapter we aim to explore the possible relation between a wide range of characteristics describing aspects of the microscale cortical organization of the macaque cortex, including layer III pyramidal complexity, neuron density, metabolic rate and neurotransmitter receptor density, and macroscale corticocortical connectivity. Next, in **chapter 3 – part I** we aim to extend our micro – macro analyses to the structural connectome of the human brain, by linking information on microscale neuron morphometry to macroscale connectivity and in **part II** of the same chapter we aim to apply the same principle to schizophrenia, by looking into the putative relation between microscale spine density of layer III pyramidal cells and macroscale structural disconnectivity. In **chapter 4**, we make use of the detailed data on cortex-wide microscale layer-specific neuron size and density included in the legacy 1925 Von Economo & Koskinas cytoarchitectural atlas of the human brain to further extend our exploration of micro – macro associations in the structural connectome to *layer-specific* analyses. The aim of **chapter 5** is to further extend our micro – macro observations to the rodent brain, combining neuron reconstructions as stored in the Neuromorpho.org online repository with data on corticocortical connectivity.

In the previous chapters we used a combination of collated data from literature and historical sources to explore the association between microscale neuron morphology and macroscale connectivity. The aim of the pilot presented in **chapter 6** is to acquire our own data on microscale neuron morphology in an attempt to gain a more complete insight into the relation between micro and macro scale in the human connectome.

Theme II – linking micro to macro scale in the functional connectome

The second part of this thesis focuses on a comparison between microscale cortical architecture and macroscale functional connectivity. **Chapter 7** deals with a comparison of regional variation in the microscale ratio between excitatory and inhibitory neurotransmitter densities and regional macroscale effective functional connectivity in the macaque monkey. The aim of **chapter 8** is to confirm the observations of chapter 7 in resting state functional connectivity in the macaque monkey, and to extend these findings to the human functional connectome.

Theme III – linking micro to macro across centuries

In this third part of the thesis, **chapter 9** presents a comparison between width of the

cortical mantle as provided by Von Economo and Koskinas in their 1925 cytoarchitectural atlas of the human brain and MRI-based cortical thickness estimates as calculated using the commonly used FreeSurfer neuroimaging software suite. Next, in **chapter 10** we present a digitized version of the Von Economo & Koskinas atlas for the FreeSurfer software, aimed to assist in bringing the legacy atlas into MRI space in order to make the atlas and its accompanying morphological data more accessible to the neuroimaging community.

Theme IV – macroscale connectomics in young offspring of schizophrenia and bipolar disorder patients

The aim of **chapter 11** presented in this fourth and last part of the thesis is to assess the putative disruption of hub connectivity in young offspring of schizophrenia and bipolar disorder patients. This study, although at first glance not directly linked to the rest of this thesis, aims to add to the existing body of evidence that disconnectivity observed in schizophrenia patients has a strong hereditary component, which could point toward a underlying biological mechanism at play – something that could potentially also be picked up at the microscale of brain organization.

Finally, **chapter 12** summarizes the findings discussed in this thesis in the context of recent literature, and proposes directions for future research.

References

- Amunts K, Lenzen M, Friederici AD, Schleicher A, Morosan P, Palomero-Gallagher N, Zilles K (2010) Broca's region: novel organizational principles and multiple receptor mapping. *PLoS biology* 8:e1000489.
- Amunts K, Zilles K (2015) Architectonic mapping of the human brain beyond Brodmann. *Neuron* 88:1086–1107.
- Baillet S (2017) Magnetoencephalography for brain electrophysiology and imaging. *Nature Neuroscience* 20:327–339.
- Bakken TE, Miller JA, Ding SL, Sunkin SM, Smith KA, Ng L, Szafer A, Dalley RA, Royall JJ, Lemon T, Shapouri S, Aiona K, Arnold J, Bennett JL, Bertagnolli D, Bickley K, Boe A, Brouner K, Butler S, Byrnes E, Caldejon S, Carey A, Cate S, Chapin M, Chen J, Dee N, Desta T, Dolbeare TA, Dotson N, Ebbert A, Fulfs E, Gee G, Gilbert TL, Goldy J, Gourley L, Gregor B, Gu G, Hall J, Haradon Z, Haynor DR, Hejazinia N, Hoerder-Suabedissen A, Howard R, Jochim J, Kinnunen M, Kriedberg A, Kuan CL, Lau C, Lee CK, Lee F, Luong L, Mastan N, May R, Melchor J, Mosqueda N, Mott E, Ngo K, Nyhus J, Oldre A, Olson E, Parente J, Parker PD, Parry S, Pendergraft J, Potekhina L, Reding M, Riley ZL, Roberts T, Rogers B, Roll K, Rosen D, Sandman D, Sarreal M, Shapovalova N, Shi S, Sjoquist N, Sodt AJ, Townsend R, Velasquez L, Wagley U, Wakeman WB, White C, Bennett C, Wu J, Young R, Youngstrom BL, Wohnoutka P, Gibbs RA, Rogers J, Hohmann JG, Hawrylycz MJ, Hevner RF, Molnar Z, Phillips JW, Dang C, Jones AR, Amaral DG, Bernard A, Lein ES (2016) A comprehensive transcriptional map of primate brain development. *Nature* 535:367–75.
- Barbas H (2015) General cortical and special prefrontal connections: Principles from structure to function. *Annual Review of Neuroscience* 38:269–289.
- Bernard A, Lubbers L, Tanis K, Luo R, Podtelezchnikov A, Finney E, McWhorter ME, Serikawa K, Lemon T, Morgan R, Copeland C, Smith K, Cullen V, Davis-Turak J, Lee CK, Sunkin SM, Loboda A, Levine D, Stone D, Hawrylycz M, Roberts C, Jones A, Geschwind D, Lein ES (2012) Transcriptional architecture of the primate neocortex. *Neuron* 73:1083–1099.
- Brodmann K (1909) *Vergleichende Lokalisationslehre der Grosshirnrinde in ihren Prinzipien dargestellt auf Grund des Zellenbaues* Barth.
- Buckner RL, Sepulcre J, Talukdar T, Krienen FM, Liu H, Hedden T, Andrews-Hanna JR, Sperling RA, Johnson KA (2009) Cortical hubs revealed by intrinsic functional connectivity: mapping, assessment of stability, and relation to Alzheimer's disease. *J Neurosci* 29:1860–73.
- Bullmore E, Sporns O (2009) Complex brain networks: graph theoretical analysis of structural and functional systems. *Nat Rev Neurosci* 10.
- Campbell AW (1905) *Histological studies on the localisation of cerebral function* University Press.

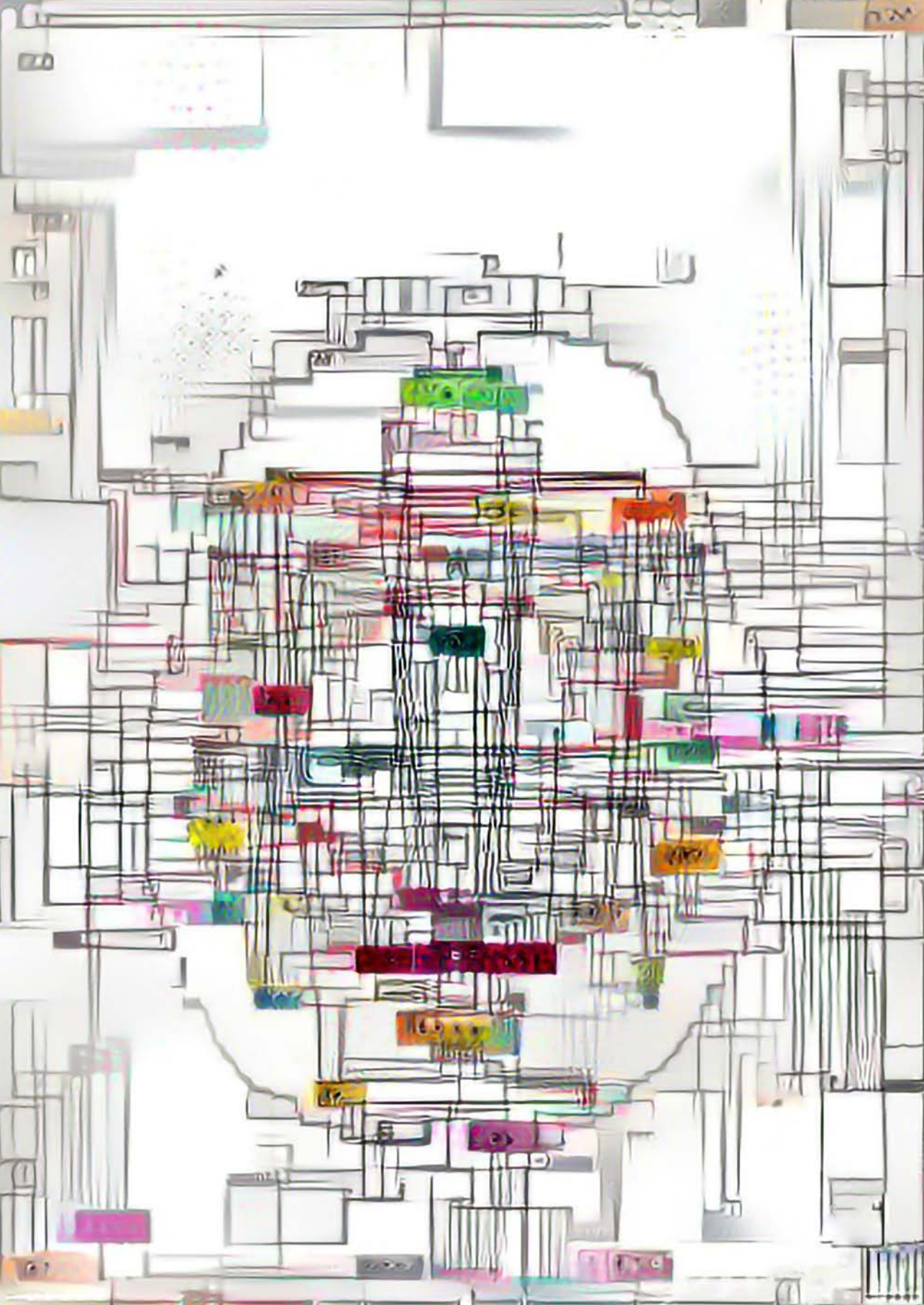
- Crossley NA, Mechelli A, Scott J, Carletti F, Fox PT, McGuire P, Bullmore ET (2014) The hubs of the human connectome are generally implicated in the anatomy of brain disorders. *Brain* 137:2382–95.
- de Reus MA, van den Heuvel MP (2014) Simulated rich club lesioning in brain networks: a scaffold for communication and integration? *Frontiers in Human Neuroscience* 8.
- Ding S, Royall JJ, Sunkin SM, Ng L, Facer BA, Lesnar P, Guillozet-Bongaarts A, McMurray B, Szafer A, Dolbeare TA (2016) Comprehensive cellular-resolution atlas of the adult human brain. *Journal of Comparative Neurology* 524:3127–3481.
- Elston GN (2003) Cortex, cognition and the cell: New insights into the pyramidal neuron and prefrontal function. *Cerebral Cortex* 13:1124–1138.
- Flechsig P (1920) *Anatomie des menschlichen Gehirns und Rückenmarks auf myelogenetischer Grundlage* G. Thieme.
- Fornito A, Zalesky A, Bassett DS, Meunier D, Ellison-Wright I, Yücel M, Wood SJ, Shaw K, O'Connor J, Nertney D, Mowry BJ, Pantelis C, Bullmore ET (2011) Genetic influences on cost-efficient organization of human cortical functional networks. *The Journal of neuroscience : the official journal of the Society for Neuroscience* 31:3261–70.
- Friston K, Frith C, Liddle P, Frackowiak R (1993) Functional connectivity: the principal-component analysis of large (pet) data sets. *Journal of Cerebral Blood Flow & Metabolism* 13:5–14.
- Glahn DC, Winkler A, Kochunov P, Almasy L, Duggirala R, Carless M, Curran J, Olvera R, Laird A, Smith S (2010) Genetic control over the resting brain. *Proceedings of the National Academy of Sciences* 107:1223–1228.
- Hammarberg C (1895) *Studien über Klinik und Pathologie der Idiotie, nebst untersuchungen über die normale Anatomie der Hirnrinde* Druck der Edv. Berling.
- Harriger L, van den Heuvel MP, Sporns O (2012) Rich club organization of macaque cerebral cortex and its role in network communication. *PloS one* 7:e46497.
- Hawrylycz MJ, Lein ES, Guillozet-Bongaarts AL, Shen EH, Ng L, Miller JA, van de Lagemaat LN, Smith KA, Ebbert A, Riley ZL, Abajian C, Beckmann CF, Bernard A, Bertagnolli D, Boe AF, Cartagena PM, Chakravarty MM, Chapin M, Chong J, Dalley RA, David Daly B, Dang C, Datta S, Dee N, Dolbeare TA, Faber V, Feng D, Fowler DR, Goldy J, Gregor BW, Haradon Z, Haynor DR, Hohmann JG, Horvath S, Howard RE, Jeromin A, Jochim JM, Kinnunen M, Lau C, Lazarz ET, Lee C, Lemon TA, Li L, Li Y, Morris JA, Overly CC, Parker PD, Parry SE, Reding M, Royall JJ, Schulkin J, Sequeira PA, Slaughterbeck CR, Smith SC, Sodt AJ, Sunkin SM, Swanson BE, Vawter MP, Williams D, Wohnoutka P, Zielke HR, Geschwind DH, Hof PR, Smith SM, Koch C, Grant SGN, Jones AR (2012) An anatomically comprehensive atlas of the adult human brain transcriptome. *Nature* 489:391–399.

- Jacobs B, Schall M, Prather M, Kapler E, Driscoll L, Baca S, Jacobs J, Ford K, Wainwright M, Trembl M (2001) Regional dendritic and spine variation in human cerebral cortex: a quantitative golgi study. *Cerebral Cortex* 11:558–571.
- Koch C (1997) Computation and the single neuron. *Nature* 385:207–210.
- Lein ES, Hawrylycz MJ, Ao N, Ayres M, Bensinger A, Bernard A, Boe AF, Boguski MS, Brockway KS, Byrnes EJ, Chen L, Chen L, Chen TM, Chi Chin M, Chong J, Crook BE, Czaplinska A, Dang CN, Datta S, Dee NR, Desaki AL, Desta T, Diep E, Dolbeare TA, Donelan MJ, Dong HW, Dougherty JG, Duncan BJ, Ebbert AJ, Eichele G, Estin LK, Faber C, Facer BA, Fields R, Fischer SR, Fliss TP, Frensley C, Gates SN, Glattfelder KJ, Halverson KR, Hart MR, Hohmann JG, Howell MP, Jeung DP, Johnson RA, Karr PT, Kawal R, Kidney JM, Knapik RH, Kuan CL, Lake JH, Laramée AR, Larsen KD, Lau C, Lemon TA, Liang AJ, Liu Y, Luong LT, Michaels J, Morgan JJ, Morgan RJ, Mortrud MT, Mosqueda NF, Ng LL, Ng R, Orta GJ, Overly CC, Pak TH, Parry SE, Pathak SD, Pearson OC, Puchalski RB, Riley ZL, Rockett HR, Rowland SA, Royall JJ, Ruiz MJ, Sarno NR, Schaffnit K, Shapovalova NV, Sivisay T, Slaughterbeck CR, Smith SC, Smith KA, Smith BI, Sodt AJ, Stewart NN, Stumpf KR, Sunkin SM, Sutram M, Tam A, Teemer CD, Thaller C, Thompson CL, Varnam LR, Visel A, Whitlock RM, Wohnoutka PE, Wolkey CK, Wong VY et al. (2007) Genome-wide atlas of gene expression in the adult mouse brain. *Nature* 445:168–176.
- McCulloch WS, Pitts W (1943) A logical calculus of the ideas immanent in nervous activity. *The bulletin of mathematical biophysics* 5:115–133.
- McCulloch W (1944) The functional organization of the cerebral cortex. *Physiological Reviews* 24:390–407.
- Mesulam MM (1998) From sensation to cognition. *Brain* 121:1013–1052.
- Meunier D, Lambiotte R, Bullmore E (2010) Modular and hierarchically modular organization of brain networks. *Frontiers in neuroscience* 4:200.
- Miller JA, Ding SL, Sunkin SM, Smith KA, Ng L, Szafer A, Ebbert A, Riley ZL, Royall JJ, Aiona K, Arnold JM, Bennet C, Bertagnolli D, Brouner K, Butler S, Caldejon S, Carey A, Cuhaciyan C, Dalley RA, Dee N, Dolbeare TA, Facer BAC, Feng D, Fliss TP, Gee G, Goldy J, Gourley L, Gregor BW, Gu G, Howard RE, Jochim JM, Kuan CL, Lau C, Lee CK, Lee F, Lemon TA, Lesnar P, McMurray B, Mastan N, Mosqueda N, Nalwai-Cecchini T, Ngo NK, Nyhus J, Oldre A, Olson E, Parente J, Parker PD, Parry SE, Stevens A, Pletikos M, Reding M, Roll K, Sandman D, Sarreal M, Shapouri S, Shapovalova NV, Shen EH, Sjoquist N, Slaughterbeck CR, Smith M, Sodt AJ, Williams D, Zollei L, Fischl B, Gerstein MB, Geschwind DH, Glass IA, Hawrylycz MJ, Hevner RF, Huang H, Jones AR, Knowles JA, Levitt P, Phillips JW, Sestan N, Wohnoutka P, Dang C, Bernard A, Hohmann JG, Lein ES (2014) Transcriptional landscape of the prenatal human brain. *Nature* 508:199–206.
- Newman ME, Girvan M (2004) Finding and evaluating community structure in networks. *Physical*

- review E* 69:026113.
- Penzes P, Cahill ME, Jones KA, VanLeeuwen JE, Woolfrey KM (2011) Dendritic spine pathology in neuropsychiatric disorders. *Nat Neurosci* 14:285–293.
- Rockland K, Pandya D (1979) Laminar origins and terminations of cortical connections of the occipital lobe in the rhesus monkey. *Brain research* 179:3–20.
- Scannell JW, Blakemore C, Young MP (1995) Analysis of connectivity in the cat cerebral cortex. *The Journal of neuroscience : the official journal of the Society for Neuroscience* 15:1463–83.
- Schmidt R, LaFleur KJ, de Reus MA, van den Berg LH, van den Heuvel MP (2015) Kuramoto model simulation of neural hubs and dynamic synchrony in the human cerebral connectome. *BMC neuroscience* 16:54.
- Scholtens LH, Schmidt R, de Reus MA, van den Heuvel MP (2014) Linking macroscale graph analytical organization to microscale neuroarchitectonics in the macaque connectome. *The Journal of Neuroscience* 34:12192–12205.
- Seltzer B, Pandya DN (1978) Afferent cortical connections and architectonics of the superior temporal sulcus and surrounding cortex in the rhesus monkey. *Brain Research* 149:1–24.
- Smith GE (1907) A new topographical survey of the human cerebral cortex, being an account of the distribution of the anatomically distinct cortical areas and their relationship to the cerebral sulci. *Journal of anatomy and physiology* 41:237.
- Sporns O (2011) *Networks of the Brain* MIT press.
- Tomasi D, Volkow ND (2011) Association between functional connectivity hubs and brain networks. *Cerebral cortex* 21:2003–2013.
- van den Heuvel MP, van Soelen IL, Stam CJ, Kahn RS, Boomsma DI, Hulshoff Pol HE (2013) Genetic control of functional brain network efficiency in children. *Eur Neuropsychopharmacol* 23:19–23.
- van den Heuvel MP, Kahn RS, Goñi J, Sporns O (2012) High-cost, high-capacity backbone for global brain communication. *Proceedings of the National Academy of Sciences of the United States of America* 109:11372–11377.
- van den Heuvel MP, Sporns O (2013) An anatomical substrate for integration among functional networks in human cortex. *The Journal of neuroscience : the official journal of the Society for Neuroscience* 33:14489–500.
- van den Heuvel MP, Sporns O, Collin G, Scheewe T, Mandl RCW, Cahn W, Goñi J, Hulshoff Pol HE, Kahn RS (2013) Abnormal rich club organization and functional brain dynamics in schizophrenia. *JAMA psychiatry (Chicago, Ill.)* 70:783–92.

- Vogt C (1919) Allgemeinere ergebnisse unserer hirnforschung. *J. Psychol. Neurol.* 25:279–462.
- Von Economo CF, Koskinas GN (1925) *Die cytoarchitektur der hirnrinde des erwachsenen menschen* J. Springer.
- Yeo BT, Krienen FM, Sepulcre J, Sabuncu MR, Lashkari D, Hollinshead M, Roffman JL, Smoller JW, Zöllei L, Polimeni JR (2011) The organization of the human cerebral cortex estimated by intrinsic functional connectivity. *Journal of neurophysiology* 106:1125–1165.
- Zamora-López G, Zhou C, Kurths J (2010) Cortical hubs form a module for multisensory integration on top of the hierarchy of cortical networks. *Frontiers in Neuroinformatics* 4.
- Zamora-López G, Zhou C, Kurths J (2011) Exploring brain function from anatomical connectivity. *Frontiers in neuroscience* 5:83.
- Zilles K, Amunts K (2010) Centenary of brodmann’s map—conception and fate. *Nature reviews. Neuroscience* 11:139–45.

Theme I – linking micro to macro scale in the structural connectome



Chapter 2

Linking macroscale graph analytical organization to microscale neuroarchitectonics in the macaque connectome

Lianne H. Scholtens, Ruben Schmidt, Marcel A. de Reus, Martijn P. van den Heuvel

The Journal of Neuroscience 2014; 34 (36): 12192–12205

Macroscale connectivity of the mammalian brain has been shown to display several characteristics of an efficient communication network architecture. In parallel, at the microscopic scale, histological studies have extensively revealed large interregional variation in cortical neural architectonics. However, how these two “scales” of cerebrum organization are linked remains an open question. Collating and combining data across multiple studies on the cortical cytoarchitecture of the macaque cortex with information on macroscale anatomical wiring derived from tract tracing studies, this study focuses on examining the interplay between macroscale organization of the macaque connectome and microscale cortical neuronal architecture. Our findings show that both macroscale degree as well as the topological role in the overall network are related to the level of neuronal complexity of cortical regions at the microscale, showing (among several effects) a positive overall association between macroscale degree and metrics of microscale pyramidal complexity. Macroscale hub regions, together forming a densely interconnected “rich club” are noted to display a high level of neuronal complexity, findings supportive of a high level of integrative neuronal processes to occur in these regions. Together, we report on cross-scale observations that jointly suggest that a

region's microscale neuronal architecture is tuned to its role in the global brain network.

Introduction

A fundamental characteristic of the architecture of neural systems is their combined ability to process specialized information and to efficiently integrate information across segregated domains. Embracing network science as a theoretical framework to examine the topological organization of neural systems, studies have consistently shown features of an efficient communication architecture of macroscale brain networks, showing high local clustering of connections, pronounced community structure, short communication pathways (Bullmore and Sporns, 2009), and the formation of densely connected and centrally embedded hub regions (Sporns et al., 2007; van den Heuvel and Sporns, 2011, 2013b).

For the mammalian brain, network organizational features have mostly been studied at the macroscopic scale, describing and examining neural systems in terms of large-scale brain regions interconnected by bundles of long-distance white matter axonal projections (Goldman-Rakic, 1988; Hagmann et al., 2008; Iturria-Medina et al., 2008; van den Heuvel et al., 2012). In parallel, decades of pioneering histological studies have provided a wealth of evidence about the neuroarchitectonic organization of cortical regions at the microscopic scale, illustrating that cortical regions can differ widely in variety of receptor binding sites, cell types, neuronal count, synaptic connectivity, etc. (Amunts and Zilles, 2012; Brodmann, 1909; Schüz and Miller, 2002). However, how the macroscale network topological architecture of the brain network is linked to the neuroarchitectonic organization of cortical regions at the microscale remains an open question.

To start addressing this question, the present report focuses on the relationship between network organizational features of the large-scale anatomical wiring of the primate brain and cellular and neuronal properties of the interconnected cortical regions. At the macroscale, a connectome map describing the organization of corticocortical wiring of the macaque cortex was reconstructed on the basis of metadata from anatomical tracer studies (Stephan et al., 2001), which was combined with information on the functional role of these edges as collated from metadata of strychnine connectivity studies (Stephan et al., 2000). At the microscale, information on the cytoarchitectonics of cortical regions was collated from a series of studies examining the neuronal architecture of cortical regions of the macaque cerebral cortex, including information on cortical cell and neuronal count (Collins and Airey, 2010), dendritic branching of cortical layer III pyramidal neurons (Elston, 2000), and glucose metabolism and

neurotransmitter binding levels (Kötter et al., 2001), aspects that have all been suggested to relate to the processing and integration capacity of neurons. Examining the neuroarchitectonic embedding of macroscopic topological network attributes can provide new insights into the workings of the mammalian connectome.

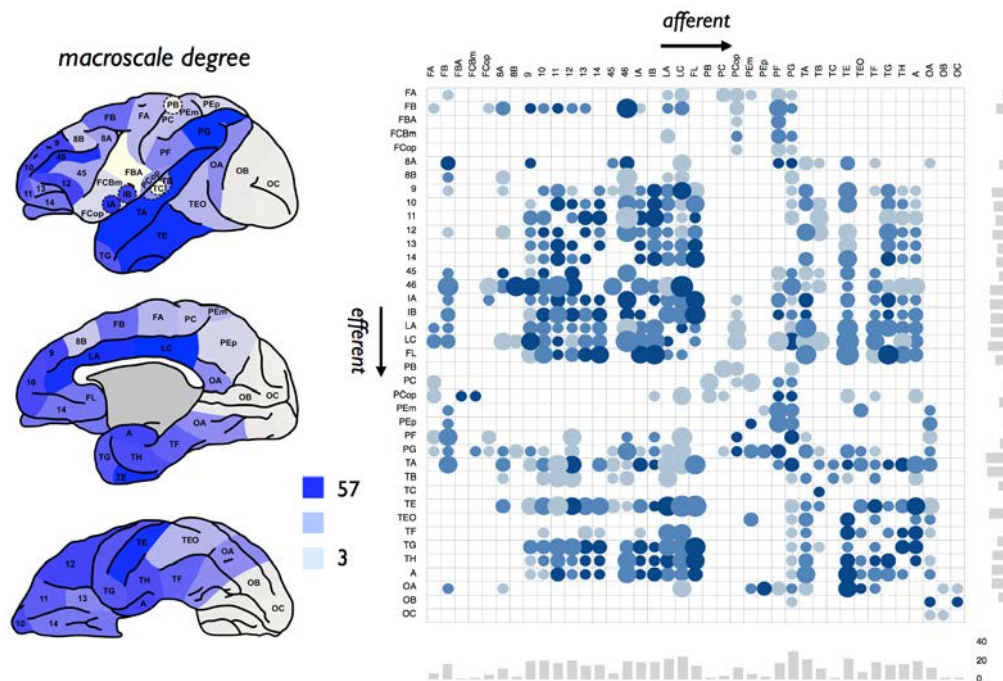


Figure 1. Anatomical connectivity matrix. Left, Degree (i.e., total number of efferent and afferent connections) of cortical regions. The figure represents a lateral, medial, and ventral view, as originally presented by Stephan et al. (2000). Right, Matching directed weighted connectivity matrix derived from the CoCoMac database (Stephan et al., 2001). Rows represent the efferent anatomical connections of regions; columns represent afferent connections of regions. Dots represent anatomical projections; size reflects estimated projection distance (small to large), color (light blue to dark blue), the averaged reported connectivity strength. Bottom and side bar plots represent, respectively, the in-degree and out-degree of the 39 cortical regions.

Materials and Methods

In what follows, we first describe the parcellation atlas and connectivity matrices used in our analyses, followed by the methods used for the macroscale graph analysis and collation of the microscale neuroarchitectonic information.

Parcellation atlas

Connectivity and cytoarchitectonic data were analyzed using the combined Walker-von Bonin and Bailey (WBB47) parcellation atlas, dividing the macaque cortical surface into 39 nonoverlapping cortical regions, as introduced by Stephan et al. (2000). The WBB47

atlas forms a conjunction of the cortical parcellation of the 1947 von Bonin and Bailey atlas (von Bonin and Bailey, 1947) for parietal, occipital, and temporal regions and the 1940 Walker atlas for prefrontal brain areas (areas 8A, 8B, 9, 10, 11, 12, 13, 14, 45, and 46) (Walker, 1940) (see Figure 1 and Table 1 for regions).

Macroscale structural connectivity (SC) data

Information on the presence (and absence) of macroscale corticocortical white matter axonal projections between WBB47 regions was obtained from the open source CoCoMac neuroinformatics database of published macaque anatomical tracer studies (Stephan et al., 2001) (CoCoMac, RRID: nif-0000-00022). This database includes information on cortical parcellation schemes of the macaque cortical surface, including the combined von Bonin and Bailey (1947) and Walker (1940) atlas. The CoCoMac database contains information on studies making report of the specific presence (i.e., an examined and observed anatomical tract between brain regions) as well as the specific absence (i.e., an examined, but not found tract) of anatomical projections between brain regions. The database was queried for the existence of tracer studies reporting on the presence (or absence) of anatomical projections between each pair of regions in the WBB47 atlas. An anatomical tract between region i and region j was included in the SC matrix if at least 5 reports were made on this potential tract in the CoCoMac database, and if the number of positive reports (i.e., reports of the presence of an anatomical connection of any strength) or “prevalence” across these 5 studies was at least two-thirds (66%) (de Reus and van den Heuvel, 2013). Testing other settings (e.g., number of reports being 4 or 6 and the prevalence set to 60% or 70%) revealed consistent findings. Based on these query results, a 39×39 SC matrix was constructed between the 39 cortical WBB47 regions. As the CoCoMac database provides information on the source and target site of each tracer injection, the connectivity matrix included a directed SC matrix. No clear information on the sex or age of the macaque monkeys was available from the CoCoMac database; the included dataset therefore most likely consists of combined information on connectivity in both male and female macaque cortex. Spatial coordinates of the included WBB47 regions were taken from information provided by the CARET software package (Van Essen et al., 2001), and from which the Euclidean distance between region pairs was computed as a proxy of the projection distance of anatomical pathways.

Macroscale functional connectivity data

Information on corticocortical functional connectivity (stryFC) was obtained from a meta-study by Stephan et al. (2000). Using the WBB47 parcellation scheme, the macaque functional connectivity (stryFC) dataset, as presented by Stephan et al. (2000), contains information on directed unihemispheric corticocortical functional connections between the 39 WBB47 regions of the macaque cortex collated from strychnine neuronography studies (Stephan et al., 2000). The technique of

strychninization as developed by Dusser de Barenne (1924) and Dusser de Barenne and Mcculloch (1938) involves the application of the γ -aminobutyric acid receptor A and glycine receptor antagonist strychnine on the cortical surface, leading to local disinhibition, thereby facilitating glutamatergic transmission of action potentials, causing multisynaptic spread of the signal across long-distance axonal projections (Dusser de Barenne, 1924; Dusser de Barenne and Mcculloch, 1938). Early studies have shown that strychnine induced patterns of cortical activation are highly reproducible within a single animal, stable for any given area across individuals, and highly similar to those found after electrical stimulation (Dusser de Barenne and Mcculloch, 1938). This method has thus been suggested as an approach to map functional connections between brain regions (Dusser de Barenne and Mcculloch, 1938). Interestingly, literature does not just describe anatomically connected areas to become activated after strychninization, but regular reports have been made on anatomical projections to have no net excitatory effect on target regions or even to consistently induce deactivation in target areas (Dusser de Barenne et al., 1941). The application of strychninization techniques thus provides the unique opportunity to map net excitatory as well as net inhibitory influence of brain regions on each other, information that is not directly accessible by means of modern functional neuroimaging techniques, such as EEG or fMRI.

Macroscale graph analytical analysis

Network science was used to elucidate aspects of topological organization of the SC network, including the assessment of nodal and edgecentric metrics (Rubinov and Sporns, 2010) (Brain Connectivity Toolbox, RRID nlx_143925). The following commonly used nodal metrics were computed from the SC matrix:

1. Nodal total degree and in-degree and out-degree, being the number of afferent and efferent connections of a node;
2. Clustering coefficient, describing the level of local connectedness of a node, computed as the proportion of connected triangles around a node;
3. Shortest path length, describing the number of binary steps needed to travel from source node i to target node j in the network, averaged over all j ;
4. Eigenvalue centrality, describing the largest eigenvector of the eigenvalue decomposition of the connectivity matrix, providing an estimate of the centrality of each node in the overall network (de Lange et al., 2014; Rubinov and Sporns, 2010; Zuo et al., 2012).

Community structure

Functional domains of the macaque brain were extracted from the stryFC matrix by means of Newman's modularity algorithm as present in the Brain Connectivity Toolbox (Rubinov and Sporns, 2010) (1000 runs, taking the highest modularity value Q) (Kofuji and Newman, 2004). Similar to the community analysis performed by Stephan et al. (2000) on the stryFC matrix, community detection resulted in three communities (see Results). In addition, performing a two-step approach in which each of these main communities was again examined individually for the existence of sub-clusters using Newman's modularity algorithm revealed a total of 8 smaller subnetworks (see Results). These communities were taken as a functional modular partitioning of the macaque cortex. A similar two-step approach was used to detect possible community structure in the anatomical SC matrix.

Testing robustness of community structure

Robustness of community structure was examined by means of a random rewiring procedure (Karrer et al., 2008). This procedure involves the random rewiring of $p\%$ edges (randomly selected) of the matrix across a set of iterations, followed by a subsequent comparison of the community structure of each of the randomized matrices with the community structure of the original matrix. Here, 1000 random matrices were computed with $p = 10\%$, and the overlap in community structure between the original and randomized situations was computed using the Rand-index (Rand, 1971), which involves the pairwise count of the number of node pairs that are classified in the same or different modules across the module assignments of the two compared matrices (Karrer et al., 2008) (a Rand-index of 0 indicates no overlap, 1 indicates complete overlap). To assess a null distribution of Rand-indices that might occur at chance level (Bassett et al., 2008; van den Heuvel et al., 2010), module assignment of the original matrix was randomized (10,000 runs) and the Rand-index with the original module assignment was computed. A p -value was then assigned to the original observed Rand-indices (i.e., between original module assignment and module assignments of the 10% randomized matrices) by testing for statistical difference between the two distributions.

Comparison of the community structure of anatomical and functional data

The Rand-index was also used to directly compare the modularity structure of the SC and stryFC matrix. The Rand-index between the two-step community structure of the SC and stryFC was computed, and statistical significance was assessed by permutation testing using a similar approach as described above: The modular assignments of the nodes of both the SC and stryFC were randomized (thus keeping the number and size of the modules intact) across 10,000 permutations, and the Rand-index in the random situations was computed. This resulted in a null distribution of effects occurring at chance level. Using this null distribution, the original Rand-index of overlapping

community structure of the SC and stryFC matrix was assigned a p -value as the percentage of observations in the random condition exceeding the original value.

Intramodular and intermodular connectivity profile of nodes

Within-module degree z-score. With the functional modules describing a modular decomposition of the network, the level of intramodular involvement of each node i was examined by means of the within-module degree z -score z_i , describing the extent to which node i is structurally connected to the other nodes in its module (Rubinov and Sporns, 2010), with a high z_i -score reflecting a relatively high involvement of a node within its own community.

Participation coefficient. The intermodular character of a node in the network was assessed by computing the participation coefficient P_i of each node i , formally given by the following:

$$P_i = 1 - \sum_{S=1}^m \left(\frac{k_{iS}}{k_i} \right)^2 \quad (2.1)$$

with k_{iS} being the number of structural links from node i to nodes in functional module S , m the number of modules, and k_i the total degree of node i . A high P_i indicates a strong intermodular character of node i , showing that its connections are relatively equally distributed over the modules in the network.

Rich club organization

A rich club organization of a network reflects the existence of a series of sets of nodes with increasing degree k that display a level of interconnectivity exceeding the level of connectivity that can be expected on basis of chance alone. Formally, the unweighted rich club coefficient (k) is computed as the fraction of the number of connections present within the subnetwork S of nodes with a degree $> k$ (van den Heuvel and Sporns, 2011) and the total number of possible connections in S (Colizza et al., 2006):

$$\Phi(k) = \frac{E_{>k}}{N_{>k}(N_{>k} - 1)} \quad (2.2)$$

$\Phi(k)$ is typically normalized by $\Phi_{random}(k)$, being the average rich club coefficient for each k of a set of randomized graphs (acquired by randomizing the adjacency matrix, while preserving the degree sequence of the network), resulting in a normalized rich club coefficient $\Phi_{norm}(k)$. $\Phi_{random}(k)$ was computed for a set of a 1000 random networks (van den Heuvel and Sporns, 2011). A network is said to display rich club organization if $\Phi(k) > \Phi_{random}(k)$ (or, equivalently, $\Phi_{norm}(k) > 1$) for a range of increasing k . Taking $\Phi_{random}(k)$ as a null distribution of the level of connectivity between nodes of degree k , the level $\Phi(k)$ (and thus the ratio $\Phi_{norm}(k)$) was assigned a p -value as the percentage of observations in $\Phi_{random}(k)$ exceeding $\Phi(k)$. Previous studies have described consistent

structural rich club organization of the mammalian brain: human (van den Heuvel et al., 2012; van den Heuvel and Sporns, 2011, 2013a), cat (de Reus and van den Heuvel, 2013; Zamora-López et al., 2009, 2011), and macaque (Harriger et al., 2012) brain, for different resolutions and for different parcellation schemes.

Rich club selection

In this study, the cortical rich club was taken as the set of nodes showing a total degree $k > 38$ (Harriger et al., 2012; van den Heuvel and Sporns, 2011). Nodes participating in the rich club were classified as “rich club hub nodes”; other nodes were categorized as “peripheral nodes” (Towlson et al., 2013; van den Heuvel et al., 2012).

Classification of edges

This classification of network nodes into rich club hub nodes and peripheral non-hub nodes allowed for the categorization of edges into the following: (1) rich club connections, edges between two rich club nodes; (2) feeder connections, edges linking peripheral nodes to hub nodes (feeder-in connections) and vice versa (feeder-out connections); and (3) local connections, edges interlinking peripheral nodes (van den Heuvel et al., 2012). In addition, edges were classified according to their role with respect to module formation in the network. Edges were labeled as intramodular when they connected nodes within the same functional module, and intermodular when they linked two nodes in two different modules (de Reus and van den Heuvel, 2013; van den Heuvel and Sporns, 2013a).

Microscale regional measures of layer III pyramidal neurons: soma size, spine count, spine density, and dendritic tree size

At the cellular level, basal dendrites are the largest target site for synaptic input onto cortical pyramidal neurons (Larkman, 1991; Lübke and Feldmeyer, 2007). To examine regional variation in neuronal morphology, Elston and colleagues performed a series of studies (e.g., Elston et al. (2010)) investigating layer III pyramidal neurons across multiple sites of the macaque cortex. Combining information from their studies (for a list of all included papers, see Table 1), we collated morphological data from cortical layer III pyramidal neurons of 25 distinct regions. These regions were manually mapped by two anatomy experts to the cortical regions defined in the WBB47 atlas, obtaining pyramidal information of 22 of the 39 cortical regions of the WBB47 parcellation atlas. Table 1 provides detailed information on the performed regional mapping, including information on the original source of each metric value. Collated data on the morphology of layer III pyramidal cells included information on the following: (1) size of the pyramidal dendritic tree, (2) estimated total count of spines per cortical area of an average pyramidal neuron, (3) dendritic spine density, and (4) soma size of the layer III pyramidal neurons.

Microscale regional measures of cell count, cell density, and neural cell density of cortical regions

Information on the total cell count of regions of the macaque cortex was taken from the recent study of Collins and colleagues (2010), quantifying cell count and cell density of the entire cortex of a single macaque. In their study, Collins and colleagues (2010) divided the cortical mantle of the right hemisphere into 41 distinct blocks and acquired detailed information on the following: (1) total cell count (including glial cells and neurons), (2) neural cell count, (3) ratio of neurons to non-neuron cells, (4) total cell density (including non-neuron cells) (millions/g), and (5) neuronal cell density (millions/g) and neuronal cell percentage of each tissue block. The spatial locations of the 41 cortical blocks, as reported by Collins et al. (2010), were manually allocated to the regions in the WBB47 parcellation atlas (Table 1 provides a description of the mapping). The average neuronal characteristics of the brain pieces contained in each of the WBB47 cortical regions were computed (Table 1), obtaining cellular information of all regions of the WBB47 parcellation atlas.

Hierarchical organization of the visual system

In addition to information on the neuronal organization of cortical regions, information on the hierarchical ordering of regions of the visual system, as published by Hilgetag (2000), was included in our network analysis. Hilgetag (2000) defined the hierarchical ordering of visual regions based on interlaminar differences in cortical source and target layers, using the classification as proposed by Felleman and Van Essen (1991), classifying the interareal connections as ascending, descending, or lateral. Based on these classifications, Hilgetag (2000) defined a hierarchical arrangement of 30 cortical areas of the visual system of a single hemisphere of the macaque cortex, assigning to each area a peak frequency of its location in the hierarchical arrangement, ranging from 1 (low hierarchy with predominantly feedforward (ascending) efferent connections and feedbackward (descending) afferent connections) to 16 (high in hierarchy with predominantly feed-backward efferent connections and feedforward afferent connections). The spatial location of all regions and their hierarchical scores were mapped to the WBB47 atlas (for the mapping, see Table 1), providing information on visual hierarchy of 13 of the 39 cortical areas of the WBB47 atlas.

Regional measures of metabolic activity

Cortical regional variation in cerebral glucose metabolism was obtained from a glucose metabolic PET imaging study by Cross et al. (2000), examining 6 young macaques (mean \pm SD: 6.2 \pm 2 years of age). After intravenous injection of the glucose uptake tracer fludeoxyglucose, tomographic (PET) images were acquired and overlaid with an anatomical T1 image, yielding quantitative reports of the rate of glucose metabolism of cortical regions. In addition to whole-brain levels, Cross et al. (2000) reported levels of

glucose metabolism for 11 cortical structures (and 4 subcortical structures). These cortical structures were mapped to 11 regions in the WBB47 atlas. Table 1 summarizes the assignments across the used parcellation schemes.

Receptor fingerprint

Interregional variation in neurotransmitter receptor densities in the macaque cortex was taken from the study by Kötter et al. (2001), providing a “receptor fingerprint” (Zilles et al., 2002) of the chemoarchitecture of the unihemispheric cortical visual and motor system. For the motor and visual regions, ligand binding densities for five receptor types were reported, including the glutamatergic AMPA receptor, γ -aminobutyric acid receptor A (GABA_A), serotonergic receptor 5-HT₂, and the muscarinic acetylcholine receptors M₁ and M₂. All 29 reported areas were mapped to 11 areas in the WBB47 parcellation atlas, of which Table 1 provides a detailed description.

Statistical analyses

Overlap between macroscale structural and functional connectivity data. Potential overlap between the anatomical SC connectivity matrix and strychnine derived stryFC connectivity matrix was assessed by means of the Mantel test for comparison of matrices (Mantel, 1967; van den Heuvel et al., 2014). A distance matrix was computed between the binary SC and stryFC, expressing which cell entries displayed a 1 or 0 in both matrices, with the level of overlap O computed as the density of distance matrix. Permutation testing was used to obtain a null distribution of overlap scores that are present under the null-hypothesis of no overlap between the two matrices, randomizing the entries of the SC and stryFC matrix for 10,000 iterations (using the Maslov and Sneppen algorithm; (Maslov and Sneppen, 2002; Rubinov and Sporns, 2010)) with the overlap computed for each iteration. Based on this null distribution, the original observed overlap O between the SC and stryFC matrix was given a p -value as the fraction of the null distribution that exceeded O (e.g., Bassett et al. (2008); van den Heuvel and Sporns (2011, 2013a)).

Associations between macroscale network and microscale architectonic metrics

Assessment of potential associations between graph topological metrics at the macroscale (in total 13 metrics, e.g., degree metrics, clustering, path length, participation coefficient) and architectonic metrics at the microscale (in total 18 metrics, e.g., metrics of pyramidal complexity, neuronal count, metabolism, receptor densities) was performed by computing Pearson’s correlations. Between the two scales, the evaluation of a total of 234 tests would be possible, yielding the need for a proper correction to the α level. In situations of multiple testing, a correction method that balances Type I and Type II errors is needed, that is, a correction method that controls for the occurrence of false discoveries, without jeopardizing sensitivity (i.e., including

too many false negatives). Classical Bonferroni correction is known to provide good control for family-wise error, but in case of existence of strong dependencies between the examined metrics, most often at the cost of Type II errors. In our study, and as commonly reported, the examined macroscale graph metrics showed an average correlation of .375 (SD: .28) (Lynall et al., 2010; van den Heuvel and Sporns, 2011), and the microscale metrics showed an average correlation of .37 (SD: .32). Several correction methods in such situations of correlated variables have been proposed. The false discovery rate (FDR) is designed to control for the expected proportion of incorrectly rejected null hypotheses (i.e., Type I errors) and can also incorporate information on the correlation between the examined variables Benjamini and Yekutieli (2001). Across the set of microscale–macroscale correlations, the FDR corrected α level $q = .05$ yielded .0121.

FDR methods provide a less stringent control compared to methods that control for family-wise error rate (e.g., Bonferroni), which are designed to reduce the probability of even one false discovery. To control for Type I error in a more conservative way while still keeping enough sensitivity, methods to estimate the effective number of tests from which a “partial Bonferroni”-corrected α can be computed have been designed (Gao et al., 2008; Li and Ji, 2005; Shriner et al., 2008). To this end, we applied a method based on principal component analysis (PCA) (Gao et al., 2008). A PCA analysis involves the transformation of a dataset of related variables to a set of linearly uncorrelated variables, named “principal components”, with the extracted components ordered according to the amount of explained variance. The procedure involved the following steps (Gao et al., 2008): First, at the macrolevel, a PCA was performed on the data matrix of the macroscale metrics, and the number of largest components together explaining $> 95\%$ of the total variance in the data was selected. Following the same approach, a second PCA was performed on the data matrix of the microscale metrics, and the number of components together explaining $> 95\%$ of the total variance of the microscale data was selected. For the macroscale graph theoretical data, the first three largest components were found to explain $> 95\%$ of the variance; for the microscale data, the first two largest components were found to explain $> 95\%$ of the variance. Finally, based on these PCA results, a partial Bonferroni correction factor was computed as the number of tests performed between the 3 and 2 PCA components, resulting in an adjusted α of $.05/(3 \times 2) = .0083$.

Based on these two statistical thresholds (with FDR controlling for FDR and partial Bonferroni for family-wise error), evaluated macroscale–microscale correlations reaching FDR correction were taken as trend-level effects, and effects reaching the more conservative partial Bonferroni correction were taken as significant. All other correlations were labeled as statistically nonsignificant effects.

Statistical analysis of differences in microscale metrics between hub and non-hub regions

Nonparametric permutation testing was used to examine potential differences of microscale metrics between hub and non-hub regions. For the microscale metric of interest, the group difference between the mean values of rich club regions and peripheral regions was computed. A null distribution was computed by randomizing group assignment (i.e., hub vs peripheral), and the difference between the group means of the random groups was computed for 10,000 permutations. A p -value was then assigned to the original difference (i.e., rich club vs peripheral nodes) as the fraction of observations of the null distribution exceeding the observed group difference. Based on the PCA results of the microscale metrics (see above), effects reaching a partial Bonferroni corrected of $.05/2$ were interpreted as statistically significant.

Statistical analysis of differences on edge metrics

Potential differences between rich club, feeder, and local edges on edge properties were tested using permutation testing by random group assignment, using a similar approach as described above. In total, across 3 edge metrics (edge directionality, edge projection length, stryFC) and across 4 classes (i.e., rich club, feeder-in, feeder-out and local), a total of $3 \times 4 = 12$ tests were performed. Tests reaching a strict Bonferroni corrected level of $.05/12 = .004$ were interpreted as statistically significant.

FE91 atlas

The WBB47 atlas was taken as the primary parcellation approach in our study. Across the literature, several parcellation atlases of the macaque cortex have been presented. To verify that observed microscale–macroscale correlations in our study were independent of the selected WBB47 atlas, we validated our findings in the context of a second parcellation atlas. Another commonly used parcellation atlas of the macaque cortex is the Felleman and Van Essen 91 (FE91) atlas (Felleman and Van Essen, 1991). The FE91 atlas also describes a single hemisphere and includes a parcellation of the cerebral cortex into 78 nonoverlapping regions. Similar to the approach used for the WBB47 atlas, data on the anatomical connectivity between the FE91 regions were extracted from the CoCoMac database. To obtain good coverage of all region-to-region combinations of the more fine-grained FE91 atlas, information on all node-pairs was included without requiring a minimum number of reports, with a “1” included in the SC matrix when at least 66% (two-thirds) of the reports on a node-pair were positive; otherwise, a “0” was included in the matrix. This resulted in an SC connectivity matrix of 18.4% density. Next, using a similar approach as described for the main WBB47 analysis, the collated microscale data (i.e., metrics of pyramidal complexity, neuronal count, receptor levels, etc.) was manually mapped to the FE91 regions. Macroscale–microscale associations observed in the WBB47 dataset were validated with the FE91 dataset. Mapping resulted in pyramidal complexity data of 25 cortical regions

(32% of all FE91 regions), neuronal and total cell count data of 78 regions (100%), visual hierarchy of 32 regions (41%), receptor levels of 20 regions (26%), and metabolism data of 11 regions (14%). Remapping of the stryFC data to the FE91 parcellation was not feasible because of the nature of the stryFC dataset, so we limited the FE91 analysis to anatomical SC effects.

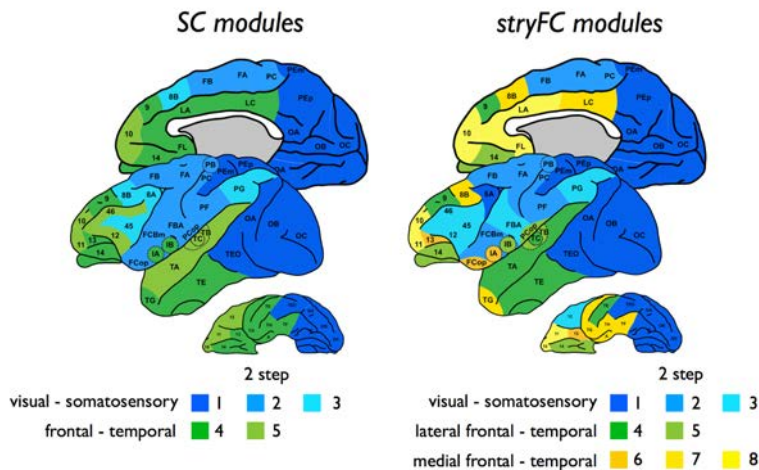


Figure 2. Anatomical and functional community structure. Figure represents a side-to-side presentation of the community structure of the anatomical and strychnine functional macaque brain network. Left, Community structure of the anatomical SC network. Community detection revealed two main communities, including a community overlapping somatosensory and visual regions (blue) and a community overlapping frontal and temporal cortical regions (green). Using a two-step community detection approach (in which the main first-level communities were subject to community detection themselves; see Materials and Methods) revealed the existence of, respectively, three sub-clusters (light, medium, and dark blue) and two sub-clusters (light and dark green). Right, Community structure of the stryFC network. First-level community detection revealed three main communities, including a visual–somatosensory community (blue), a lateral frontal–temporal cluster (green), and a medial frontal–temporal cluster (yellow). Two-step community detection revealed three functional sub-clusters of the visual–somatosensory network, overlapping a visual (dark blue), motor and sensory network (medium and light). In addition, two-step community detection of the lateral frontal–temporal network revealed two sub-clusters (light and dark green) and three sub-clusters in the medial frontal–temporal network (light, medium, and dark yellow). Formal statistical testing of the anatomical and functional community structure revealed significant overlap between the two-step community structures ($p < .001$; see Results).

Results

We will first describe the results of the graph analytical analysis of the macaque cortical network, followed by the cross-resolution analysis of the graph analytical findings in relation to collated microscale information of the cortical regions, associating macroscale network attributes with information on regional variation in dendritic complexity of layer III pyramidal cells, total cell and neuronal count, receptor binding levels, hierarchical ordering, and glucose metabolic activity.

WBB47 Atlas	Pyramidal complexity	Cell & neuronal count	PET Glucose metabolism	Receptor densities	Visual hierarchy
FA	4 (ER02)	30, 36 (CA10)	Pre- / Postcentral gyrus	F1 (KO01)	–
FB	6 (ER02)	33, 34, 36, 38 (CA10)	–	F2v, F2d, F3, F6, F7 (KO01)	–
FBA	–	29, 30, 35, 38 (CA10)	–	F4v, F4d (KO01)	–
FCBm	–	26, 35 (CA10)	–	F5 (KO01)	–
FCop	–	26 (CA10)	–	–	–
8A	–	40 (CA10)	Lateral frontal	–	FEF (HI00)
8B	–	37, 38 (CA10)	–	–	–
9	9d (EB11)	37, 40 (CA10)	–	–	–
10	10 (E00, EB11)	41 (CA10)	Principal sulcus	–	–
11	11 (E00)	40 (CA10)	–	–	–
12	12 (E00, EB11)	26, 35, 40 (CA10)	–	–	–
13	13 (EB11)	26 (CA10)	–	–	–
14	–	26, 40 (CA10)	–	–	–
45	–	40, 41 (CA10)	–	–	–
46	46 (EB11)	41 (CA10)	–	–	reg46 (HI00)
IA	–	26 (CA10)	–	–	–
IB	–	24, 26, 35 (CA10)	–	–	–
LA	Ant cing (EBD05)	39, 41 (CA10)	Anterior cingulate	–	–
LC	Post cing (EBD05)	39 (CA10)	Posterior cingulate	–	–
FL	–	41 (CA10)	–	–	–
PB	3b (ER02)	29 (CA10)	–	–	–
PC	–	29 (CA10)	Pre- / Postcentral gyrus	–	–
PCop	–	32, 35 (CA10)	–	–	–
PEm	5 (ER02)	31, 32 (CA10)	–	VIP (KO01)	PIP, VIP (HI00)
PEp	7m (EO1)	15, 31 (CA10)	–	PO, MIP, PEP (KO01)	–
PF	7b (ER02)	32 (CA10)	Lateral parietal, Supra-marginal gyrus	–	7a (HI00)
PG	MT, LIPv, 7a (ER97)	19, 20, 28, 32 (CA10)	Lateral parietal, Supra-marginal gyrus	LIP, PG, MT, MTp, MST (KO01)	7a, LIP (HI00)
TA	STP (ETR99, E01)	23, 27, 28 (CA10)	–	FST (KO01)	MSTl, FST, STPa, STPp, MSTd (HI00)
TB	–	25 (CA10)	–	–	–
TC	A1 (EO10)	24 (CA10)	–	–	–
TE	TE (E99, EO11), IT (EBD05)	18, 22, 23 (CA10)	–	–	PITd, PITv, CITv, AITv, AITd, CITd (HI00)
TEO	TEO (ER98)	17, 18, 20, 21, 22 (CA10)	Lateral temporal	–	VP, V3, V3A, V4, PO, DP, VOT, V4t (HI00)
TF	–	22 (CA10)	–	–	TF (HI00)
TG	–	23 (CA10)	–	–	–
TH	–	22 (CA10)	–	–	TH (HI00)
A	–	22 (CA10)	–	–	–
OA	MT (ER97), V4 (ER98)	14, 15, 16, 17, 19, 20, 21, 22 (CA10)	Lateral occipital	V3v, V3d, V3A, V4v, V4d, V6A, V4t, MT (KO01)	V2, VP, V3, V3A, V4, PO, DP, VOT, MT (HI00)
OB	V2 (ER97, ER98)	1, 2, 3, 4, 5, 8, 19, 20, 21 (CA10)	–	V2v, V2d (KO01)	V2 (HI00)
OC	V1 (ER97, ER98, ETR99)	6, 7, 9, 10, 11, 12, 13 (CA10)	Cuneus / Lingual gyrus	V1 (KO01)	V1 (HI00)

Table 1. Mapping to the WBB47 parcellation of all neuronal measures included in the meta-analysis.

Pyramidal complexity mapped from studies by Elston and colleagues: E00 (Elston, 2000), E01 (Elston et al., 2001), EB11 (Elston et al., 2011), EBD05 (Elston et al., 2005), EO10 (Elston et al., 2010), EO11 (Elston et al., 2011), ER02 (Elston and Rockland, 2002), ER97 (Elston and Rosa, 1997), ER98 (Elston and Rosa, 1998), and ETR99 (Elston et al., 1999); cell and neuronal count from a study by Collins and colleagues: CA10 (Collins and Airey, 2010); PET glucose metabolism from Cross and colleagues: CR00 (Cross et al., 2000); receptor fingerprint from Kötter and colleagues: KO01 (Kötter et al., 2001); and visual hierarchy from Hilgetag and colleagues: HI00 (Hilgetag, 2000).

Macroscale graph analytical findings

Anatomical connectivity

The macaque cortical brain network, represented by a 39×39 unweighted directed anatomical connectivity matrix (SC) (Figure 1), was found to be 35.0% dense, to show a high level of clustering (.73, normalized clustering: 1.14, $p < .0001$, 10,000 permutations) and to have a short path length close to that of random networks (1.75, normalized shortest path length: 1.04), together indicating a small-world organization (small-world index: 1.09). Consistent with previous observations (Harriger et al., 2012; Goulas et al., 2014), the macaque anatomical network displayed an overall rich club organization, showing a $\Phi_{\text{norm}} > 1$ for $11 < k < 41$ ($p < .0001$, surviving Bonferroni correction for 42 performed tests of different k levels). Community detection (Figure 2, left) showed the existence of two main structural modules (Rand index at 10% random rewiring: .72, $p < .0001$, 10,000 permutations), overlapping visual–somatosensory and frontal–temporal regions. Two-step community detection revealed 2 and 3 submodules, respectively, resulting in a total of 5 anatomical (sub)clusters (Rand index at 10% random rewiring: .86, $p < .0001$, 10,000 permutations).

stryFC

Cross-reference of the stryFC with the anatomical SC matrix revealed a significant overlap (1.55 times more overlap than in the random condition, $p < .0001$, Mantel test, 10,000 permutations). Overlapping the analysis of Stephan et al. (2000), community detection revealed the existence of 3 main functional communities, including a visual–somatosensory cluster (consisting of 18 regions), a lateral frontal–temporal cluster (8 regions), and a medial frontal–temporal cluster (13 regions) (Rand index at 10% random rewiring: .82, $p < .0001$, 10,000 permutations) (Figure 2, right). Two-step community detection revealed further sub-clustering (Rand index at 10% random rewiring: .84, $p < .0001$, 1000 permutations). The visual–somatosensory community revealed 3 sub-clusters, consisting of 6, 7, and 5 regions, respectively, including visual (dark blue) and motor and sensory regions (medium and light blue shades). The medial temporal–frontal cluster included 3 sub-clusters, describing a frontal sub-cluster of 4 regions, including 10/11/FL and cingulate region LA (light yellow), a sub-cluster of 6 regions, including cingulate cortex LC, frontal region 8B and temporal regions (e.g., TH, TF, A) (medium yellow) and a sub-cluster of 3 regions including insular region IA and frontal regions 13 and FCoP (dark yellow). Community structure of the lateral frontal–temporal community involved 2 sub-clusters, including a sub-cluster overlapping auditory regions and frontal region 14 (4 regions, light green) and a sub-cluster overlapping superior/inferior temporal cortex (3 regions, dark green) and frontal area 9. Figure 2 shows a side-by-side comparison of the two-step structural and functional community structure, demonstrating a relatively high level of overlap

between the anatomical and functional community structure. Formal statistical testing of this overlap (see Materials and Methods) revealed a significant level of consistency between functional and structural module structure (Rand index: .81, $p < .0001$, 10,000 permutations). Furthermore, the stryFC (sub)clusters, despite the relatively coarse parcellation of the cortex, tend to show overlap with functional networks as reported from resting-state fMRI recordings in the macaque (Hutchison and Everling, 2012; Hutchison et al., 2011). Examining this potential overlap in detail is out of the scope of our paper, but future studies examining the consistency (and differences) between stryFC and resting-state fMRI derived functional networks would be of interest.

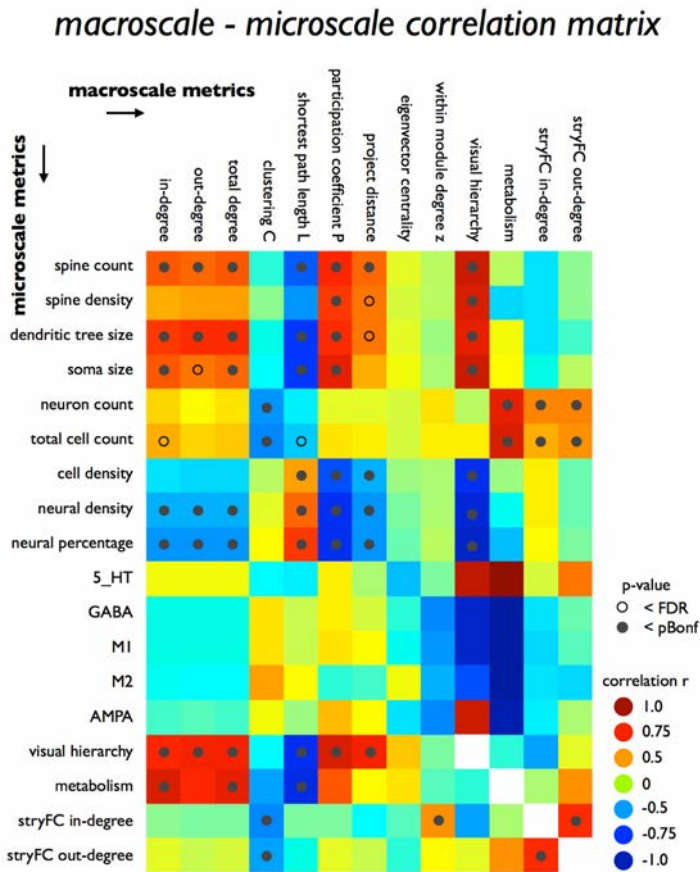


Figure 3. Macroscale–microscale metrics correlations. Figure plots all correlations between macroscale metrics (columns) and microscale metrics (rows). Green to blue represent negative associations; yellow to red represent positive correlations. Open circle represents effects reaching FDR correction for multiple testing; filled circle represents effects reaching the stricter partial Bonferroni correction. Metrics of stryFC, visual hierarchy, and metabolism were compared both to microscale metrics as well as to the class of macroscale metrics and are thus included in both categories.

Macroscale network-microscale metric associations

Figure 3 reports the correlations between all possible microscale–macroscale metrics and indicates which effects survived statistical evaluation. In what follows, we describe the most prominent findings, focusing on effects reaching FDR (labeled as trend-level effects) and partial Bonferroni corrected levels (for the computation of these corrected levels, see Materials and Methods).

Relationship between macroscale connectome organization and cytoarchitectural and dendritic architectural properties of layer III pyramidal neurons.

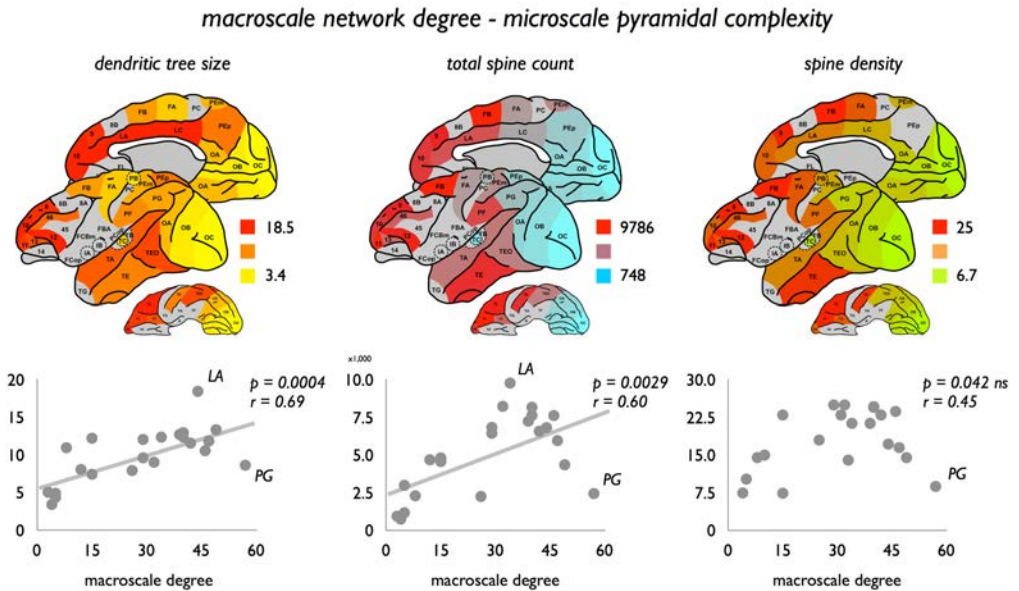


Figure 4. Association between macroscale degree and microscale layer III pyramidal complexity. Top, Dendritic tree size, total spine count, and spine density as derived for 22 cortical regions on basis of the studies of Elston and colleagues (Table 1). Bottom, Associations between macroscale degree and pyramidal complexity, showing a positive significant relationship between macroscale total degree (i.e., sum of in-degree and out-degree) and dendritic tree size (left, effect reaching partial Bonferroni correction) and total spine count (middle, effect reaching partial Bonferroni correction). Spine density did not show a significant correlation with macroscale degree (right, effect not reaching correction for multiple testing). Exploratory exclusion of region PG as a potential data outlier from the correlation analysis did reveal a potential relationship with total degree ($p = .0026$, $r = .64$).

Association with macroscale degree

Basal dendrites are the largest target site for synaptic input of cortical pyramidal neurons (Larkman, 1991; Lübke and Feldmeyer, 2007). Microscale data on regional variation in pyramidal cell complexity, as obtained from a series of studies by Elston et al. (2010),

included information on the length of dendritic tree, estimated total count of spines per cortical area of an average pyramidal neuron, dendritic spine density, and soma size of layer III pyramidal neurons. Cross-correlating these microscale cellular metrics with macroscale network properties revealed several associations:

Pyramidal dendritic tree size positively correlated to macroscale anatomical degree (in-degree, $p = .0005$, $r = .68$; and out-degree, $p = .0004$, $r = .69$), indicating that pyramidal cells with the largest dendritic tree are found in those regions with the highest total number of efferent and afferent macroscale connections (Figure 4). In addition, total spine count, reflecting the total amount of (possible) synaptic terminals on the dendritic tree of a neuron, positively correlated with regional variation in the number of macroscale efferent ($p = .0027$, $r = .60$) and afferent connections ($p = .0039$, $r = .59$) (effects reaching partial Bonferroni corrected α). However, no significant effects were found between degree and spine density (i.e., the number of spines per section of the dendritic tree; Elston (2000)) (in-degree, $p = .0502$, not significant, $r = .43$; out-degree, $p = .0374$, not significant, $r = .47$). A positive relationship between soma size of layer III pyramidal neurons and macroscale in-degree was observed (in-degree, $p = .0049$, $r = .60$; out-degree: $p = .0101$ FDR; $r = .56$). An exception to the positive association between macroscale degree and layer III pyramidal neuron characteristics was region PG (Figure 4). Cortical region PG, well recognized as a key region in the so-called visual “where pathway” (Felleman and Van Essen, 1991; Ungerleider and Haxby, 1994) of the macaque visual system, was found to display a relatively high macroscale degree, but a (relative to the fitted linear relationship) small dendritic tree size (Figure 4, region PG), low spine count, and low spine density. Excluding region PG from the correlation analysis revealed stronger correlations for all pyramidal metrics, now showing a potential positive association between macroscale degree and spine density (in-degree, $p = .0022$, $r = .60$; out-degree, $p = .0037$, $r = .62$). Interestingly, in contrast to region PG, region LA (anterior cingulate cortex) and LC (posterior cingulate cortex) formed a positive exception scoring above the fitted linear relationship (Figure 4), with layer III pyramidal neurons in region LA showing the most elaborate dendritic trees of all reported regions, with region LC in second place. These findings led to the hypothesis of high-degree region PG being mostly involved in local neuronal processes, potentially the processing of mostly unimodal information, whereas regions LA and LC have a more globally orientated profile involved in the processing and integration of multimodal information across the whole network.

Association with macroscale projection distance

A possible local versus global connectivity profile of cortical regions was further examined by looking at a region’s projection distance of afferent macroscale connections in relationship to microscale neuronal architecture. The white matter

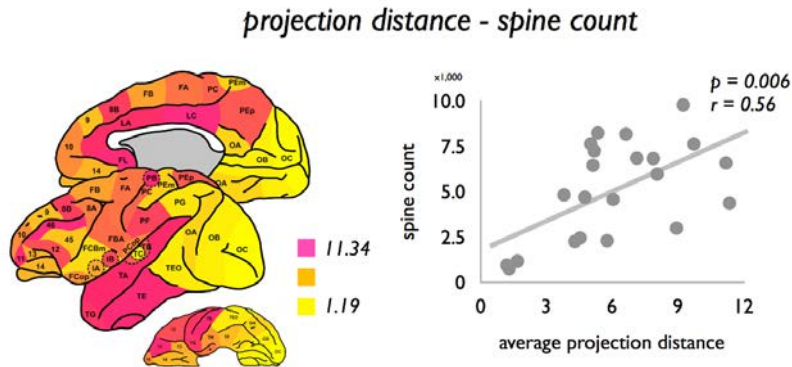


Figure 5. Association between average projection distance of cortical regions and microscale layer III spine count. Left, Mean projection distance of all connections (efferent and afferent combined) of each cortical region. Right, Association between mean projection length of connections of cortical regions (afferent and efferent connections) and spine count.

projections of outlier region PG were found to have a relatively short average projection distance (mean \pm SD: 4.53 ± 3.06 , averaged over 31 afferent connections; 26 efferent connections: $4.52/3.11$), consistent with a potential local connectivity profile of this region. The connections of high-degree region LA (afferent/efferent 7.97, 23 connections) and LC (11.37, 25 connections) were found to display on average the longest white matter projections of the macaque macroscale connectome, thus on average receiving projections from more distant regions in the cortex (efferent connections, respectively, 4.98, 21 connections; and 5.61, 24 connections). These findings are consistent with the observation of LA and LC to have a high dendritic complexity. Next, we examined this association across the entire cortex. Projection distance of afferent connections was significantly correlated to spine count ($p = .0060$, $r = .56$; Figure 5). Trend-level (FDR) effects were observed between projection distance and dendritic tree size ($p = .0091$, $r = .54$) and spine density ($p = .0084$, $r = .57$) (Figure 3). Figure 3 summarizes the results of all examined correlations with projection distance.

Association with macroscale visual hierarchy

Information on the hierarchical ordering of cortical regions of the macaque visual system, as obtained by the study of Hilgetag (2000) (see Materials and Methods), revealed further insight into a potential association between the topological organization of macroscale connectivity and the microstructural organization of cortical regions. Hierarchical ordering of visual regions, based on interlaminar differences in cortical source and target layers of afferent and efferent projections (Felleman and Van Essen, 1991) (see Materials and Methods), showed a positive correlation with

visual hierarchy - spine density

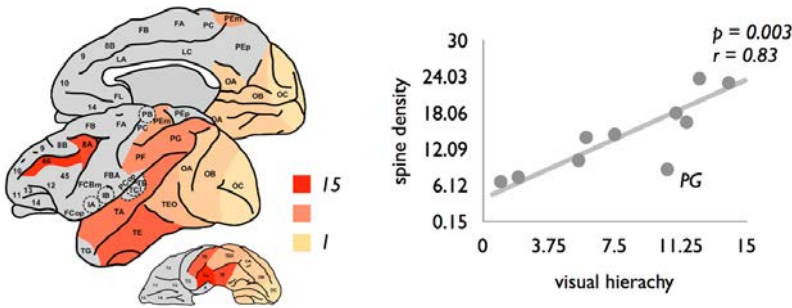


Figure 6. Association between macroscale visual hierarchy and microscale layer III spine density. Left, Scored hierarchical ordering of regions of the visual system (based on the laminar projection patterns of a region’s efferent and afferent projections), as translated from Hilgetag (2000) plotted on the cortical surface. Right, Positive relationship between visual hierarchy and spine density.

dendritic tree size ($p = .0058$, $r = .80$), spine count ($p = .0021$, $r = .85$), and spine density ($p = .0030$, $r = .83$) (Figure 6), with regions ranking higher in hierarchy showing the most complex pyramidal neuronal organization.

macroscale graph metrics - pyramidal complexity

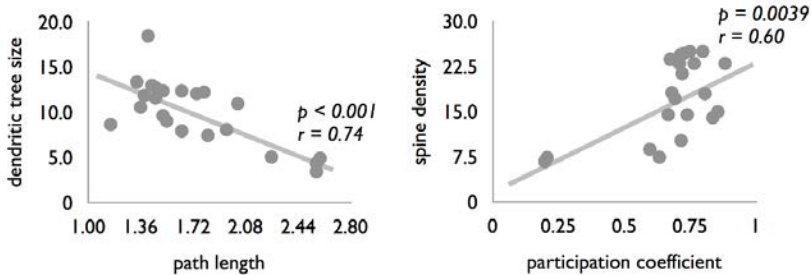


Figure 7. Relationship between macroscale graph organizational features and microscale complexity. Both nodal intermodular participation coefficient P_i and normalized path length L_i were found to be significantly correlated with pyramidal complexity. Relationship between L_i and dendritic tree size (left) and P_i (degree corrected) and spine density (right) are shown.

Association with topological graph metrics

No significant relationships between network clustering C_i and pyramidal complexity metrics were observed (all $p > .05$; see also Figure 3). In contrast, global shortest path length L_i significantly negatively correlated to dendritic tree size ($p = <.001$, $r = .74$; Figure 7), spine count ($p = .0011$, $r = .64$), and soma size ($p = .0064$, $r = .59$). These findings tend to suggest that regions with a shorter path length show a

more complex architecture, a relationship influenced by the positive association between dendritic complexity and degree (see above). Indeed, correcting for this interaction (by regressing out the effect of degree) revealed only a remaining effect for soma size ($p = .0028$). A potential link between topological architecture and microarchitecture is further supported by an observed positive association between the intermodular participation coefficient P_i and dendritic complexity, with regions with a more extensive intermodular connectivity profile showing a larger dendritic tree size ($p = .0003$, $r = .70$), higher spine count ($p = .0002$, $r = .71$), higher spine density ($p = .0009$, $r = .67$), and larger layer III pyramidal soma size ($p = .0001$, $r = .77$). Correcting P_i for nodal degree revealed a remaining effect for spine density ($p = .0039$, $r = .60$; Figure 7).

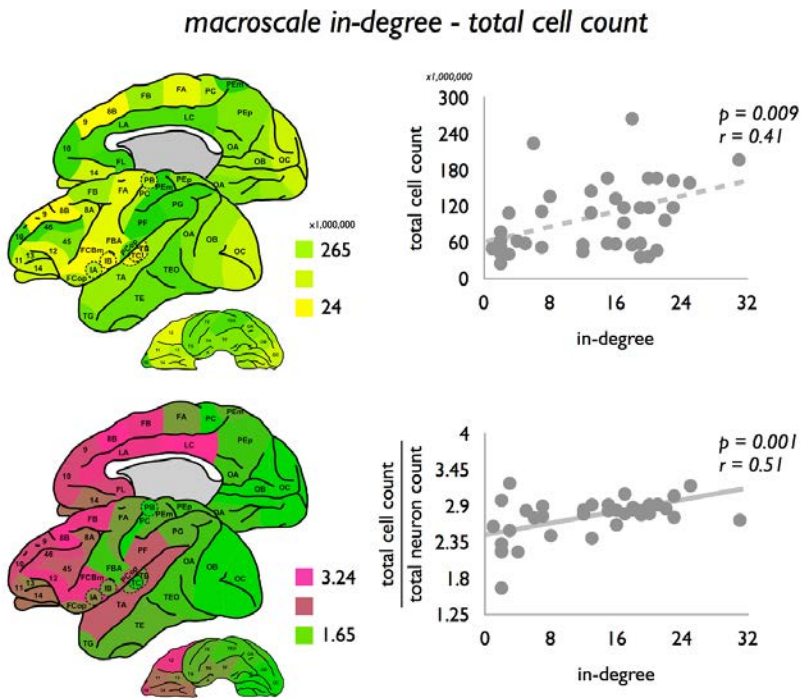


Figure 8. Association between macroscale in-degree and neuronal count. Left, Total cell count and ratio total cell count/neuronal count. Cell count and neuronal count were translated from the study by Collins and Airey (2010). Interestingly, a correlation was present not only between macroscale degree and total cell count (top right, effect reaching FDR correction), but also between macroscale degree and the ratio total cell count/neuronal count (bottom right), suggesting that macroscale degree is also related to regional variation in non-neuronal tissue at the microscale.

Regional covariation in microarchitectural organization

Next, we examined the level of similarity in dendritic organization across the included cortical regions, computed as $1/\text{distance}$ (Euclidean) between the pyramidal metric values of each pair of cortical regions. Covariation in microstructural organization was

found to be significantly higher for regions interconnected by a macroscale projection, compared with region pairs not directly connected ($p < .001$, 10,000 permutations), suggesting that anatomically connected regions tend to show overlap in their neuronal architecture.

Macroscale connectome organization and regional variation in total cell count, cell density, and neural cell density

Information on regional variation in total cell and neuronal count across all cortical laminae was obtained from a recent study by Collins and Airey (2010), in which the cortical mantle of a single macaque was divided into distinct blocks and examined for total cell count, total cell density, neuronal cell count, percentage of neurons, and neuronal cell density. Macroscale in-degree revealed a trend-level positive relationship with total cell count ($p = .0091$ FDR, $r = .41$; Figure 8).

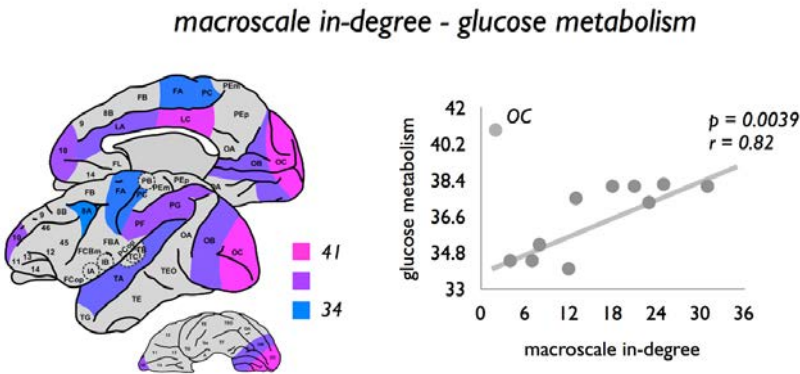


Figure 9. Association between macroscale in-degree and glucose metabolism. Left, Regional variation of glucose metabolism across the macaque cortex, with metabolic rates obtained from the study by Cross et al. (2000). Regional in-degree was found to be positively correlated with regional variation in glucose metabolism, suggesting that regions with a higher macroscale degree show a higher level of glucose metabolism. Region OC was interpreted as an outlier, and not taken into account in the statistical analysis.

Relationship between macroscale connectivity and regional variation of glucose metabolism

Examining graph organizational properties in relation to the level of glucose metabolism of cortical regions as reported by the study of Cross et al. (2000) (see also Materials and Methods) revealed a positive correlation between glucose metabolism and macroscale in-degree ($p = .0039$, $r = .82$, primary visual OC taken as outlier; Figure 9). A positive relationship was also found between glucose metabolism and total cell ($p = .0030$, $r = .83$, region OC taken as outlier) and total neuronal count ($p = .0071$, $r = .78$, region OC taken as outlier).

Receptor fingerprints

Information on the chemoarchitecture of cortical regions of the macaque cortex was collated from the study of Kötter et al. (2001), summarizing levels of quantitative receptor binding in the motor and visual system of the macaque brain (see Materials and Methods), which were mapped to the WBB47 atlas. No direct correlations were found between macroscale anatomical degree and binding levels (all $p > .05$), indicating that our findings provide no evidence for the notion of receptor metrics to be associated with the network topological profile of regions (for the correlations, see Figure 3). No clear difference between similarity in receptor binding levels (computed as $1/\text{distance}$ (Euclidean) between the metric values of each pair of cortical regions) of anatomically connected and non-connected regions was observed ($p = .0212$, not significant, 10,000 permutations).

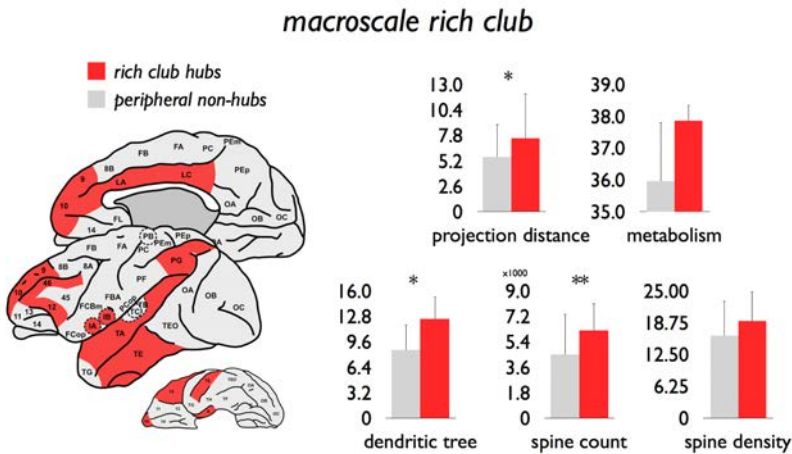


Figure 10. Macroscale properties of graph analytically derived hub regions. Left, Red represents the 12 hub regions ($k > 38$). Gray represents all other peripheral non-hub nodes. Right, Differences between hub and peripheral non-hub nodes on several macroscale and microscale metrics. * $p < .025$ (reaching partial Bonferroni correction). ** $p < .0208$ excluding outlier region PG (reaching partial Bonferroni correction).

Microscale architectonics of macroscale rich club

The rich club was selected as the set of nodes showing a combined in-degree and out-degree $k > 38$, including a set of in total 12 cortical regions (region 9, 10, 12, 46, IA, IB, LA, LC, PG, TA, TE, and A) (Figure 10). Similar to previous observations (de Reus and van den Heuvel, 2013; Harriger et al., 2012), different rich club levels (e.g., $k > 36$ or $k > 40$) revealed consistent findings. Consistent with an overall rich club organization, these hub regions showed a dense level of mutual connectivity (98%), significantly higher than in a set of randomly connected networks ($1.12 \times$ higher, $p < .001$, 1000 random networks preserving degree sequence) (van den Heuvel and Sporns, 2011).

stryFC

Efferent anatomical rich club edges (i.e., connections spanning between rich club nodes) were found to have significantly less often a net excitatory strychnine effect (15% of edges) on their target regions compared with the class of local connections (i.e., connections spanning between local nodes, 86%, $p < .001$, 10,000 permutations, surviving Bonferroni correction; feeder: 47%). In addition, examining the neuronal architecture of rich club regions, rich club hubs were found to be present in 3 of the 3 functional communities (100%) and 6 of the 8 (75%) functional subnetworks (as revealed by two-step community detection). Rich club and feeder edges were found to be well represented among intermodular connections (88% and 87% of connections, respectively), more than local connections (69% of connections), as computed on the basis of the two-step community approach. For the first-level stryFC communities, a similar pattern was observed, with rich club edges involving 72% intermodular connections, feeder connections 57%, and local connections 39%. Figure 10 summarizes mean values of macroscale and microscale metrics of rich club and non-rich club regions. Rich club edges were found to be predominantly bidirectional (98%), more frequently than feeder (86%) and local connections (76%). Rich club edges were found to span significantly longer physical distances compared with local connections (i.e., edges connecting peripheral nodes, $p < .001$, 10,000 permutations, surviving Bonferroni correction). Rich club hub regions showed a significantly larger dendritic tree compared with non-rich club regions ($p = .0024$, 10,000 permutations; Figure 10). No significant effects were found for spine count ($p = .0788$), spine density ($p = .0958$), soma size ($p = .11$), or metabolism ($p = .0584$). Excluding region PG (see text above; Figure 4) revealed a difference in spine count between hub and non-hub peripheral nodes ($p = .0208$, 10,000 permutations; Figure 10).

FE91 validation

Associations found to be significant in the main analysis were validated using the FE91 parcellation dataset, now involving CoCoMac extraction of macroscale anatomical connectivity on basis of the FE91 atlas, and mapping of the collated microscale pyramidal complexity data to the FE91 regions. The FE91 analysis results revealed high consistency with the associations reported for the WBB47 datasets. A summary of these findings include the following, with the computed FDR correction for the FE91 atlas set yielding a corrected of .0175 and a partial Bonferroni corrected of $.05/(2 \times 2)$.0125 (based on PCA analysis as described in Materials and Methods).

The FE91 network revealed a significant community structure (mean Rand index: .93, 10% rewiring, $p < .001$, 1000 iterations, two-step communities), including 5 main communities and in total 12 subcommunities (Figure 11A), together with a significant rich club formation ($12 < k < 62$, $p = .001$, reaching Bonferroni correction).

FE91

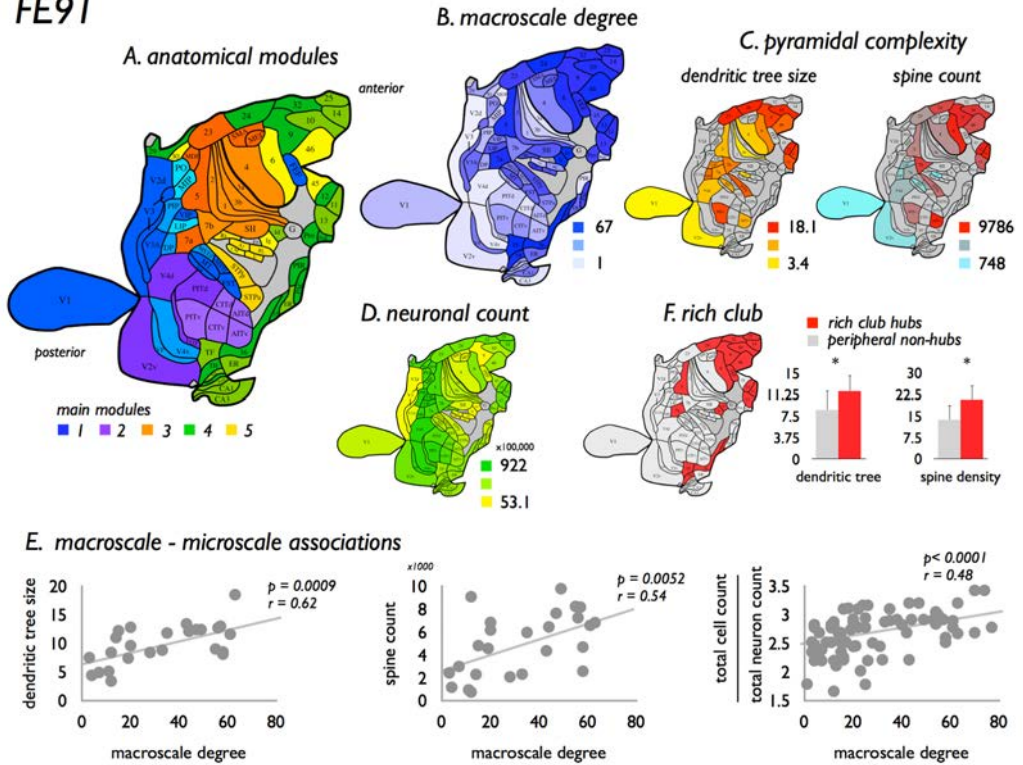


Figure 11. FE91 validation analysis. Figure summarizes findings of the validation analysis using the Felleman and Van Essen (1991) FE91 atlas. **A**, The 78 regions of the FE91 atlas (Felleman and Van Essen, 1991), color coded according to their anatomical modular structure (five main modules, color coded in blue, purple, orange, yellow, and green; and sub-clusters of the two-step module depicted in color shades). **B**, Map of the degree distribution across the FE91 regions. **C**, Two distribution maps of pyramidal complexity values as collated from the Elston papers, showing a map of dendritic tree size (left) and spine count (right). **D**, Distribution map of neuronal count as mapped by Collins and Airey (2010). Consistent with the main analysis based on the WBB47 atlas (e.g., Figure 4), analysis of the FE91 dataset revealed several associations between macroscale network organization and microscale neuroarchitectonics. **E**, Summary of three of these associations, showing a significant positive relationship between macroscale degree and dendritic tree size, spine count, and the ratio between total cell count and total neuronal count (surviving partial Bonferroni correction). **F**, Distribution of high-degree rich club nodes across the cortex as observed in the FE91 dataset (left). Consistent with the main analysis (Figure 10), rich club nodes were observed to show a significantly larger dendritic tree size and higher spine count compared with the class of peripheral nodes. * $p < .05$ (surviving partial Bonferroni correction).

Confirming the WBB47 analysis, macroscale nodal degree (taken as the total sum of in-degree and out-degree) was found to show significant associations to pyramidal complexity (dendritic tree size, $p = .0009$, $r = .62$; spine count, $p = .0052$, $r = .54$; soma size, $p = .0046$, $r = .57$), the ratio of neuronal count and cell count ($p < .0001$, $r = .48$), neural percentage ($p = .0033$, $r = .45$), and an effect with neural cell density ($p = .0051$, $r = .44$) (Figure 11). Pyramidal complexity also showed a positive correlation

with visual hierarchy (e.g., dendritic tree size, $p = .0013$, $r = .84$; spine count, $p = .0030$, $r = .80$). No significant correlation was observed between degree and spine density ($p = .0296$, not significant, $r = .44$). Pyramidal complexity correlated negatively with network path length (e.g., dendritic tree, $p = .0009$, $r = .62$; spine count, $p = .0052$, $r = .54$). No significant relationship was observed between macroscale degree and regional metabolism ($p = .30$, not significant, $r = .36$) or between macroscale projection distance and pyramidal complexity (e.g., dendritic tree size, $p = .29$, not significant, $r = .29$; spine count, $p = .51$, not significant, $r = .183$). The latter may have been influenced by the notion that, of only 45 FE91 regions (58% of total), information on spatial coordinates was available. Consistent with the results of the WBB47 analysis and recent reports (Harriger et al., 2012; Goulas et al., 2014), the FE91 dataset revealed the existence of hub regions and a densely connected rich club (selected as regions with a combined degree 43, including 20 regions [25.6% of total], density 87%, 1.22 times more than random, $p < .001$, permutation testing) (selecting other rich club levels, e.g., $k > 41$ or $k > 45$, revealed consistent findings). Rich club and feeder edges were found to be strongly present among intermodular edges (rich club: 72%, feeder-in: 68%, feeder-out 75%, local: 53%, based on the revealed two-step communities), to mostly involve bidirectional connections (92% and significantly more than local edges, $p < .001$, with feeder-in: 59%, feeder-out 63%, local: 62%) and to project over longer distances than local edges ($p < .001$, 10,000 permutations); effects all reaching Bonferroni correction. Validating rich club observations of the WBB47 results, rich club nodes showed higher levels of pyramidal complexity (dendritic tree size, $p = .0164$ reaching FDR; spine count, $p = .0042$ partial Bonferroni; spine density, $p = .0108$ partial Bonferroni; soma size, $p = .0142$ FDR; Figure 11). Figure 11 shows a summarized overview of the results of the FE91 dataset.

Discussion

Combining information on the topological organization of the macroscale macaque connectome with collated data on the neuroarchitectonic organization of cortical regions, our findings show several potential links between between macroscale network organization and microscale neuronal architecture. The number of macroscale white matter anatomical connections (i.e., network degree) was found to be associated with cortical variation in metrics of complexity of layer III pyramidal neurons, with higher connected regions showing more elaborate dendritic branching, larger soma size, and higher total spine count compared with macroscale low degree regions. In addition, macroscale degree also significantly correlated to the ratio between regional variation in total cell and neuronal count and thus negatively with neural density, suggesting that macroscale wiring may also be potentially related to the relative density of other

non-neural cortical tissue, for example, glial cells and capillaries (Collins and Airey, 2010). Furthermore, hierarchical position in the visual system was associated with dendritic organization (Figure 6), with regions higher in the visual hierarchy showing both a higher pyramidal complexity as well as a more central role in the overall network. These observations point to the direction of regions low in hierarchy, processing predominantly unimodal information and having a low number of connections, to show a relatively low-degree and low pyramidal complexity, whereas more richly connected regions positioned higher in the hierarchy and assumed to process more transmodal and multimodal information, display a more complex pyramidal architecture.

Our findings are in line with previous observations of macroscale and microscale organization of the mammalian brain. Across their experiments, Elston et al. (2009, 2010) noted a systematic trend for an increasing complexity of dendritic trees of functionally ordered regions, with pyramidal neurons becoming progressively larger, more branched, and more spinous when traveling in anterior direction through the visual system. Elston et al. (2010) already hypothesized that such a specialization of pyramidal cells could have an impact on the functioning of cortical regions at both the cellular and whole-brain levels. Our cross-resolution findings now indeed tend to suggest that a putative gradient of increasing microscale pyramidal organization goes hand in hand with a more and more central role of cortical regions at the macroscale network level. Furthermore, human and animal studies have noted that macroscale high-degree regions tend to predominantly overlap with functional multimodal areas of the cortex (de Reus and van den Heuvel, 2013; Goldman-Rakic, 1988; Power et al., 2013; Tomasi and Volkow, 2011), and neuroimaging studies have indeed already suggested that these high-degree regions belong to the most metabolically active regions of the cortex (Collins and Airey, 2010; Liang et al., 2013; Vaishnavi et al., 2010), with high levels of energy usage hypothesized to be potentially related to high synaptic turnover and synaptic plasticity (Lim and Isaac, 2005) and maintenance of elaborate dendritic trees of cortical neurons (Vaishnavi et al., 2010).

In addition to the total number of pathways, our study also provides indications of a possible link between the macroscale topological role of cortical regions and microscale architectonics. The average projection distance of a region's connections was observed to be positively related to pyramidal spine count (Figs. 3 and 5), with regions with a broad connectivity profile showing the most elaborate dendritic trees. Furthermore, network metrics, such as topological connection distance (shortest path length) and participation coefficient (reflecting the intermodular connectivity profile of a network node), were found to be associated with microscale dendritic tree length and spine count, suggesting a potential relationship between topological position of cortical regions in the macroscale

brain network and microscale neuronal architecture.

Consistent with other recent studies, the anatomical macaque connectome showed the formation of macroscale neural hubs (Harriger et al., 2012; Markov et al., 2013). Because of their central embedding in the macroscale network, rich club hubs have been proposed to form a topologically central structure for global communication and information integration (Crossley et al., 2013; Park and Friston, 2013; van den Heuvel et al., 2012; van den Heuvel and Sporns, 2013b). Extending these findings, our study now suggests that on both the macroscale as well as on the microscale, high-degree hub regions display an architecture potentially suited for facilitating functional neural integration processes (Elston, 2000; Elston et al., 2001; Jacobs et al., 2001; Schüz and Miller, 2002; van den Heuvel and Sporns, 2013b).

Although tract tracing data are often seen as a “gold standard” of white matter pathway reconstruction, it is important to realize that animal connectome reconstructions (as also implemented here) are often based on a collation of data across a wide range of experiments, experiments that have not always reported consistent results. For a robust reconstruction, pathways were included on which CoCoMac contained information from ≥ 5 studies and of which the majority of these studies (66%) involved a positive report, but there is no clear consensus on these settings. Sparse sampling of other settings (e.g., ≥ 4 ; 60% or ≥ 5 and 50%) resulted in consistent results, but it is important to note that recent studies have suggested much denser wiring diagrams of the macaque cortex (Markov et al., 2013) than resulting from our CoCoMac extraction. In addition, in the main analysis of this study, the WBB47 atlas was used to parcellate the cortex, providing complete coverage of the macaque cortex and allowing for the analysis of functional strychnine data, but many other parcellation atlases (as, e.g., the FE91 replication atlas) are available, with most of these atlases containing a more fine-grained parcellation. Last, the examined microscale data involved a collation of data across studies from the literature, thus also including information across multiple experiments, and moreover including only a relatively coarse sampling of the cortex with missing data on microscale metrics for several cortical regions (Table 1). These effects limit the sensitivity of our study.

Our study should only be seen as a first attempt to examine a potential microscale–macroscale relationship. Many open questions of course remain. For example, microscale–macroscale associations were assessed by means of a series of simple correlations. As shown by the correlation and PCA analysis, both microscale and macroscale metrics show strong intraclass correlations, suggesting that most presented macroscale–microscale associations are driven by global underlying organizational effects. Interestingly, although the strong dependency of network metrics on degree is

well reported (Lynall et al., 2010; van den Heuvel and Sporns, 2011), PCA results also revealed strong correlations between several microscale metrics, effects that are potentially nontrivial. Future studies examining these microscale relationships, together with how they relate to global underlying macroscale network descriptors, would be of particular interest. Furthermore, the important question of “what is driving what” remains unanswered. Is the neuroarchitectonic organization of cortical regions tuned to accommodate large-scale macroscale projections, or does a high complexity of cortical regions allow for the existence of a large number of macroscale efferent and afferent white matter projections? Earlier studies have hypothesized differences in global connectivity patterns to have consequences for the structural and histological organization of cortical regions, with macroscale connectivity patterns potentially including an important factor for architectonic differentiation of cortical regions, bringing to attention the need for studies examining the link between macroscale connectional patterns and microscale architectonics (Kaas et al., 2002; Schüz and Miller, 2002). More experimental studies are needed to provide insight into a potential causal relationship between neuroarchitectural organization of cortical regions and macroscale connectivity patterns, as well as their interaction to the formation of large-scale hierarchies, community structure, and neural hubs (Buckner and Krienen, 2013; Elston et al., 2009). In addition, in this study we have primarily been focusing on the examination of anatomical architectonic features, but examination of the potential influence and interplay of microscale architectonics and macroscale connectome formation on the emergence of functional dynamics and functional hierarchical systems (Breakspear and Stam, 2005; Kiebel et al., 2008; Meunier et al., 2010; Zhou et al., 2006) would be of particular interest. Pioneering cross-species studies have noted that resting-state networks in the macaque as derived from resting-state fMRI data resemble those observed in the human (Hutchison et al., 2011, 2013), and similar cross-species observations have been made regarding anatomical connectivity (Goulas et al., 2014; Miranda-Dominguez et al., 2014). Because of the inherent nature of the method, the stryFC data as analyzed in this study are different from FC estimates based on resting-state fMRI; nevertheless, the stryFC sub-clusters have been noted to show overlap with known functional domains of the macaque cortex, identifying visual, somatosensory, and frontal networks (Stephan et al., 2000). A formal comparison between resting-state fMRI-derived functional communities and stryFC-defined community structure would be of interest and might provide new information on the underlying biological foundation of resting-state network formation in the mammalian cortex.

This study provides evidence for a potential relationship between the properties of macroscale and microscale connectivity of the mammalian cortex. Our findings

Chapter 2

converge on the notion of an interplay between the neuroarchitectonic organization of cortical regions and their connectional pattern on the macroscale connectome level.

References

- Amunts K, Zilles K (2012) Architecture and organizational principles of broca's region. *Trends in cognitive sciences* 16:418–426.
- Bassett DS, Bullmore E, Verchinski BA, Mattay VS, Weinberger DR, Meyer-Lindenberg A (2008) Hierarchical organization of human cortical networks in health and schizophrenia. *J Neurosci* 28:9239–48.
- Benjamini Y, Yekutieli D (2001) The control of the false discovery rate in multiple testing under dependency. *Annals of statistics* pp. 1165–1188.
- Breakspear M, Stam CJ (2005) Dynamics of a neural system with a multiscale architecture. *Philosophical Transactions of the Royal Society of London B: Biological Sciences* 360:1051–1074.
- Brodmann K (1909) *Vergleichende Lokalisationslehre der Grosshirnrinde in ihren Prinzipien dargestellt auf Grund des Zellenbaues* Barth.
- Buckner RL, Krienen FM (2013) The evolution of distributed association networks in the human brain. *Trends Cogn Sci* 17:648–65.
- Bullmore E, Sporns O (2009) Complex brain networks: graph theoretical analysis of structural and functional systems. *Nat Rev Neurosci* 10.
- Colizza V, Flammini A, Serrano M, Vespigiani A (2006) Detecting rich-club ordering in complex networks. *Nat Phys* 2:110–115.
- Collins C, Airey D (2010) Neuron densities vary across and within cortical areas in primates. *Proceedings of the National Academy of Sciences* 107:15927–32.
- Cross DJ, Minoshima S, Nishimura S, Noda a, Tsukada H, Kuhl DE (2000) Three-dimensional stereotactic surface projection analysis of macaque brain pet: development and initial applications. *Journal of nuclear medicine : official publication, Society of Nuclear Medicine* 41:1879–87.
- Crossley NA, Mechelli A, Vértes PE, Winton-Brown TT, Patel AX, Ginestet CE, McGuire P, Bullmore ET (2013) Cognitive relevance of the community structure of the human brain functional coactivation network. *Proceedings of the National Academy of Sciences* 110:11583–11588.
- de Lange S, de Reus M, Van Den Heuvel M (2014) The laplacian spectrum of neural networks. *Frontiers in Computational Neuroscience* 7.
- de Reus MA, van den Heuvel MP (2013) Rich club organization and intermodule communication in the cat connectome. *Journal of Neuroscience* 33:12929–12939.

- Dusser de Barenne JG (1924) Experimental researches on sensory localization in the cerebral cortex of the monkey (macacus). *Proceedings of the Royal Society of London B: Biological Sciences* 96:272–291.
- Dusser de Barenne JG, McCulloch WS (1938) Functional organization in the sensory cortex of the monkey (macaca mulatta). *Journal of Neurophysiology* pp. 69–85.
- Dusser de Barenne J, Garol H, McCulloch W (1941) Functional organization of sensory and adjacent cortex of the monkey. *Journal of Neurophysiology* 4:324–330.
- Elston GN (2000) Pyramidal cells of the frontal lobe: all the more spinous to think with. *The Journal of neuroscience : the official journal of the Society for Neuroscience* 20:RC95.
- Elston GN, Benavides-Piccione R, DeFelipe J (2001) The pyramidal cell in cognition: a comparative study in human and monkey. *The Journal of neuroscience : the official journal of the Society for Neuroscience* 21:RC163.
- Elston GN, Rosa MG (1997) The occipitoparietal pathway of the macaque monkey: comparison of pyramidal cell morphology in layer iii of functionally related cortical visual areas. *Cerebral cortex (New York, N.Y. : 1991)* 7:432–52.
- Elston GN, Rosa MG (1998) Morphological variation of layer iii pyramidal neurones in the occipitotemporal pathway of the macaque monkey visual cortex. *Cerebral cortex (New York, N.Y. : 1991)* 8:278–94.
- Elston GN, Tweedale R, Rosa MG (1999) Cellular heterogeneity in cerebral cortex: a study of the morphology of pyramidal neurones in visual areas of the marmoset monkey. *The Journal of comparative neurology* 415:33–51.
- Elston GN, Benavides-Piccione R, Defelipe J (2005) A study of pyramidal cell structure in the cingulate cortex of the macaque monkey with comparative notes on inferotemporal and primary visual cortex. *Cerebral cortex (New York, N.Y. : 1991)* 15:64–73.
- Elston GN, Benavides-Piccione R, Elston A, Manger PR, Defelipe J (2011) Pyramidal cells in prefrontal cortex of primates: marked differences in neuronal structure among species. *Frontiers in neuroanatomy* 5:2.
- Elston GN, Oga T, Fujita I (2009) Spinogenesis and pruning scales across functional hierarchies. *The Journal of neuroscience : the official journal of the Society for Neuroscience* 29:3271–5.
- Elston GN, Oga T, Okamoto T, Fujita I (2011) Spinogenesis and pruning in the anterior ventral inferotemporal cortex of the macaque monkey: An intracellular injection study of layer iii pyramidal cells. *Frontiers in neuroanatomy* 5:42.
- Elston GN, Okamoto T, Oga T, Dornan D, Fujita I (2010) Spinogenesis and pruning in the primary

- auditory cortex of the macaque monkey (*macaca fascicularis*): an intracellular injection study of layer iii pyramidal cells. *Brain research* 1316:35–42.
- Elston GN, Rockland KS (2002) The pyramidal cell of the sensorimotor cortex of the macaque monkey: phenotypic variation. *Cerebral cortex (New York, N.Y. : 1991)* 12:1071–8.
- Felleman DJ, Van Essen DC (1991) Distributed hierarchical processing in the primate cerebral cortex. *Cerebral cortex (New York, N.Y. : 1991)* 1:1–47.
- Gao X, Starmer J, Martin ER (2008) A multiple testing correction method for genetic association studies using correlated single nucleotide polymorphisms. *Genetic epidemiology* 32:361–369.
- Goldman-Rakic PS (1988) Topography of cognition: parallel distributed networks in primate association cortex. *Annual review of neuroscience* 11:137–156.
- Goulas A, Bastiani M, Bezgin G, Uylings HB, Roebroek A, Stiers P (2014) Comparative analysis of the macroscale structural connectivity in the macaque and human brain. *PLoS Comput Biol* 10:e1003529.
- Hagmann P, Cammoun L, Gigandet X (2008) Mapping the structural core of human cerebral cortex. *PLoS biology* 6:e159.
- Harriger L, van den Heuvel MP, Sporns O (2012) Rich club organization of macaque cerebral cortex and its role in network communication. *PloS one* 7:e46497.
- Hilgetag C (2000) Hierarchical organization of macaque and cat cortical sensory systems explored with a novel network processor. *Philos Trans R Soc Lond B Biol Sci* .
- Hutchison RM, Everling S (2012) Monkey in the middle: why non-human primates are needed to bridge the gap in resting-state investigations. *Frontiers in neuroanatomy* 6.
- Hutchison RM, Leung LS, Mirsattari SM, Gati JS, Menon RS, Everling S (2011) Resting-state networks in the macaque at 7 t. *NeuroImage* 56:1546–55.
- Hutchison RM, Womelsdorf T, Allen EA, Bandettini PA, Calhoun VD, Corbetta M, Della Penna S, Duyn JH, Glover GH, Gonzalez-Castillo J (2013) Dynamic functional connectivity: promise, issues, and interpretations. *Neuroimage* 80:360–378.
- Iturria-Medina Y, Sotero RC, Canales-Rodríguez EJ, Alemán-Gómez Y, Melie-García L (2008) Studying the human brain anatomical network via diffusion-weighted mri and graph theory. *Neuroimage* 40:1064–1076.
- Jacobs B, Schall M, Prather M, Kapler E, Driscoll L, Baca S, Jacobs J, Ford K, Wainwright M, Trembl M (2001) Regional dendritic and spine variation in human cerebral cortex: a quantitative golgi study. *Cerebral Cortex* 11:558–571.

- Kaas JH, Schüz A, Miller R (2002) Cortical areas and patterns of cortico-cortical connections. *Cortical areas: unity and diversity* pp. 179–191.
- Karrer B, Levina E, Newman ME (2008) Robustness of community structure in networks. *Physical Review E* 77:046119.
- Kiebel SJ, Daunizeau J, Friston KJ (2008) A hierarchy of time-scales and the brain. *PLoS Comput Biol* 4:e1000209.
- Kofuji P, Newman E (2004) Potassium buffering in the central nervous system. *Neuroscience* 129:1045–1056.
- Kötter R, Stephan KE, Palomero-Gallagher N, Geyer S, Schleicher a, Zilles K (2001) Multimodal characterisation of cortical areas by multivariate analyses of receptor binding and connectivity data. *Anatomy and embryology* 204:333–50.
- Larkman AU (1991) Dendritic morphology of pyramidal neurones of the visual cortex of the rat: I. branching patterns. *The Journal of comparative neurology* 306:307–19.
- Li J, Ji L (2005) Adjusting multiple testing in multilocus analyses using the eigenvalues of a correlation matrix. *Heredity* 95:221–227.
- Liang X, Zou Q, He Y, Yang Y (2013) Coupling of functional connectivity and regional cerebral blood flow reveals a physiological basis for network hubs of the human brain. *Proceedings of the National Academy of Sciences* 110:1929–1934.
- Lim W, Isaac JT (2005) Atp hydrolysis is required for the rapid regulation of ampa receptors during basal synaptic transmission and long-term synaptic plasticity. *Neuropharmacology* 48:949–955.
- Lübke J, Feldmeyer D (2007) Excitatory signal flow and connectivity in a cortical column: focus on barrel cortex. *Brain structure & function* 212:3–17.
- Lynall ME, Bassett DS, Kerwin R, McKenna PJ, Kitzbichler M, Muller U, Bullmore E (2010) Functional connectivity and brain networks in schizophrenia. *The Journal of Neuroscience* 30:9477–9487.
- Mantel N (1967) The detection of disease clustering and a generalized regression approach. *Cancer research* 27:209–220.
- Markov NT, Ercsey-Ravasz M, Van Essen DC, Knoblauch K, Toroczka Z, Kennedy H (2013) Cortical high-density counterstream architectures. *Science* 342:1238406–1238406.
- Maslov S, Sneppen K (2002) Specificity and stability in topology of protein networks. *Science* 296:910–913.
- Meunier D, Lambiotte R, Bullmore E (2010) Modular and hierarchically modular organization of

- brain networks. *Frontiers in neuroscience* 4:200.
- Miranda-Dominguez O, Mills BD, Grayson D, Woodall A, Grant KA, Kroenke CD, Fair DA (2014) Bridging the gap between the human and macaque connectome: a quantitative comparison of global interspecies structure-function relationships and network topology. *J Neurosci* 34:5552–63.
- Park HJ, Friston K (2013) Structural and functional brain networks: from connections to cognition. *Science* 342:1238411.
- Power JD, Schlaggar BL, Lessov-Schlaggar CN, Petersen SE (2013) Evidence for hubs in human functional brain networks. *Neuron* 79:798–813.
- Rand WM (1971) Objective criteria for the evaluation of clustering methods. *Journal of the American Statistical association* 66:846–850.
- Rubinov M, Sporns O (2010) Complex network measures of brain connectivity: uses and interpretations. *NeuroImage* 52:1059–69.
- Schüz A, Miller R (2002) *Cortical areas: unity and diversity* Conceptual advances in brain research. Taylor & Francis, London; New York.
- Shriner D, Baye TM, Padilla MA, Zhang S, Vaughan LK, Loraine AE (2008) Commonality of functional annotation: a method for prioritization of candidate genes from genome-wide linkage studies. *Nucleic acids research* 36:e26–e26.
- Sporns O, Honey C, Kötter R (2007) Identification and classification of hubs in brain networks. *PloS one* 2:e1049.
- Stephan KE, Hilgetag CC, Burns Ga, O'Neill Ma, Young MP, Kötter R (2000) Computational analysis of functional connectivity between areas of primate cerebral cortex. *Philosophical transactions of the Royal Society of London. Series B, Biological sciences* 355:111–26.
- Stephan KE, Kamper L, Bozkurt a, Burns Ga, Young MP, Kötter R (2001) Advanced database methodology for the collation of connectivity data on the macaque brain (cocomac). *Philosophical transactions of the Royal Society of London. Series B, Biological sciences* 356:1159–86.
- Tomasi D, Volkow ND (2011) Association between functional connectivity hubs and brain networks. *Cerebral cortex* 21:2003–2013.
- Towlson EK, Vertes PE, Ahnert SE, Schafer WR, Bullmore ET (2013) The rich club of the c. elegans neuronal connectome. *J Neurosci* 33:6380–7.
- Ungerleider L, Haxby J (1994) 'what' and 'where' in the human brain. *Current opinion in neurobiology* 4:157–165.

- Vaishnavi SN, Vlassenko AG, Rundle MM, Snyder AZ, Mintun MA, Raichle ME (2010) Regional aerobic glycolysis in the human brain. *Proceedings of the National Academy of Sciences* 107:17757–17762.
- van den Heuvel MP, Kersbergen KJ, de Reus MA, Keunen K, Kahn RS, Groenendaal F, de Vries LS, Benders MJ (2014) The neonatal connectome during preterm brain development. *Cereb Cortex* .
- van den Heuvel MP, Kahn RS, Goñi J, Sporns O (2012) High-cost, high-capacity backbone for global brain communication. *Proceedings of the National Academy of Sciences of the United States of America* 109:11372–11377.
- van den Heuvel MP, Mandl RCW, Stam CJ, Kahn RS, Hulshoff Pol HE (2010) Aberrant frontal and temporal complex network structure in schizophrenia: a graph theoretical analysis. *The Journal of neuroscience : the official journal of the Society for Neuroscience* 30:15915–26.
- van den Heuvel MP, Sporns O (2011) Rich-club organization of the human connectome. *The Journal of neuroscience : the official journal of the Society for Neuroscience* 31:15775–86.
- van den Heuvel MP, Sporns O (2013a) An anatomical substrate for integration among functional networks in human cortex. *The Journal of neuroscience : the official journal of the Society for Neuroscience* 33:14489–500.
- van den Heuvel MP, Sporns O (2013b) Network hubs in the human brain. *Trends in cognitive sciences* 17:683–696.
- Van Essen DC, Drury HA, Dickson J, Harwell J, Hanlon D, Anderson CH (2001) An integrated software suite for surface-based analyses of cerebral cortex. *Journal of the American Medical Informatics Association* 8:443–459.
- von Bonin G, Bailey P (1947) *The neocortex of Macaca mulatta* Univ. of Illinois Press, Urbana.
- Walker E (1940) A cytoarchitectural study of the prefrontal area of the macaque monkey. *The Journal of Comparative Neurology* 73:59–86.
- Zamora-López G, Zhou C, Kurths J (2009) Graph analysis of cortical networks reveals complex anatomical communication substrate. *Chaos* 19:015117.
- Zamora-López G, Zhou C, Kurths J (2011) Exploring brain function from anatomical connectivity. *Frontiers in neuroscience* 5:83.
- Zhou C, Zemanova L, Zamora G, Hilgetag CC, Kurths J (2006) Hierarchical organization unveiled by functional connectivity in complex brain networks. *Phys Rev Lett* 97:238103.
- Zilles K, Palomero-Gallagher N, Grefkes C, Scheperjans F, Boy C, Amunts K, Schleicher a (2002) Architectonics of the human cerebral cortex and transmitter receptor fingerprints: reconciling functional neuroanatomy and neurochemistry. *European neuropsychopharmacology : the journal*

of the European College of Neuropsychopharmacology 12:587–99.

Zuo XN, Ehmke R, Mennes M, Imperati D, Castellanos FX, Sporns O, Milham MP (2012) Network centrality in the human functional connectome. *Cerebral Cortex* 22:1862–1875.

Supplemental Materials: BB47 atlas

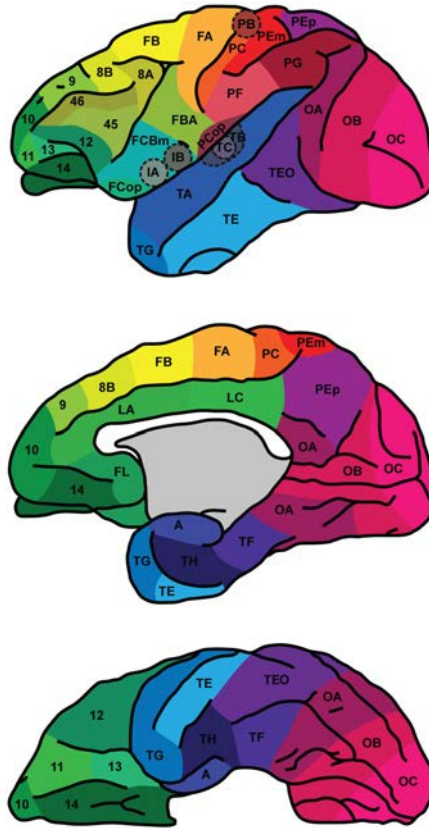


Figure S1. WBB47 map of the macaque cortical surface. All prefrontal areas are as described by Walker in 1940, all other areas are as described by von Bonin and Bailey in 1947. This figure is an artist's adaptation of the figure published by Stephan et al. (2000).

Table S1. Overview of the mapping of all neuronal measures included in the meta-analysis to the WBB47 parcellation and the values as collated from the original articles. The first column lists all cortical areas included in the WBB47 parcellation, as listed in the CoCoMac database of macaque tract tracing studies (Stephan et al., 2001), to which the areas listed in the subsequent columns were mapped. Pyramidal complexity information was mapped from a series of studies by Elston and colleagues (E00 (Elston, 2000), E01 (Elston et al., 2001), EB11 (Elston et al., 2011b), EBD05 (Elston et al., 2005), EO10 (Elston et al., 2010b), EO11 (Elston et al., 2011a), ER02 (Elston and Rockland, 2002), ER97 (Elston and Rosa, 1997), ER98 (Elston and Rosa, 1998), ETR99 (Elston et al., 1999)). Cell and neuron count was mapped from a study by Collins and colleagues (Collins et al., 2010), PET glucose metabolism from work by Cross and colleagues (Cross et al., 2000), receptor fingerprint from Kötter and colleagues (Kötter et al., 2001) and visual hierarchy from Hilgetag and colleagues (Hilgetag et al., 2000).

→

Supplemental Materials: FE91 atlas

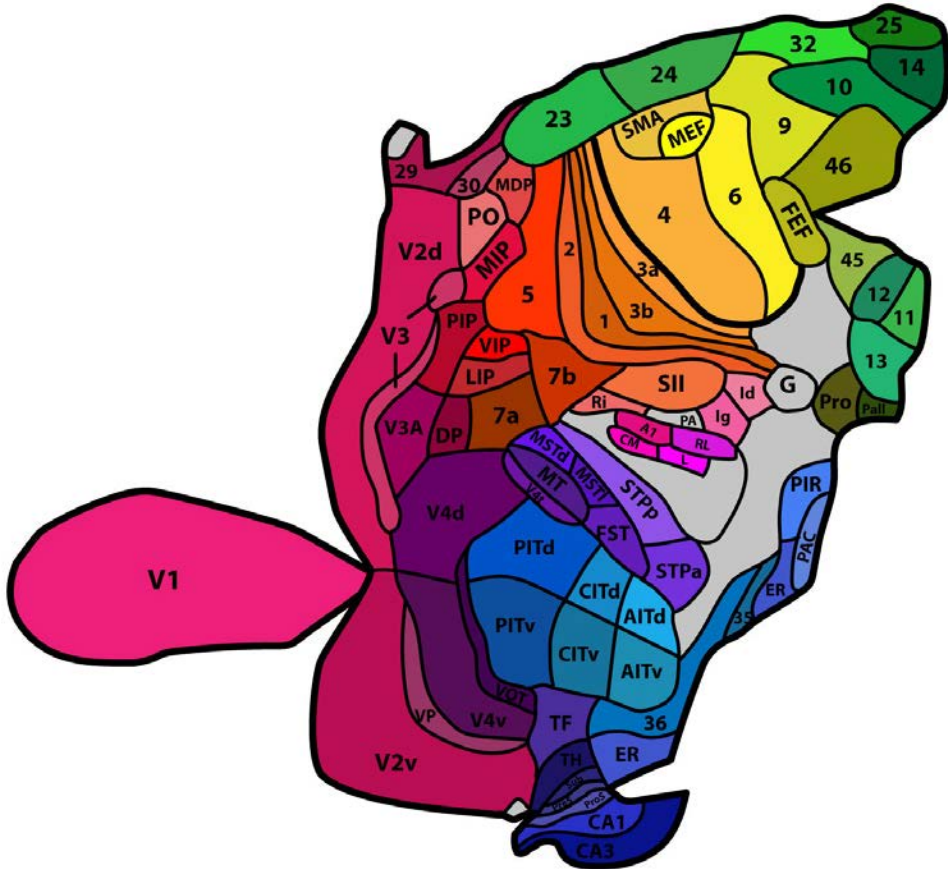


Figure S2. Flat map of a single macaque cortical hemisphere. This figure is an artist’s adaptation of the figure published in the article by Felleman & van Essen (1991) and depicts the cortical areas included in our analysis.

Table S2. Overview of the mapping of all neuronal measures included in the meta-analysis to the FV91 parcellation and the values as collated from the original articles. The first column lists the CoCoMac names of all cortical areas included in the FV91 parcellation (Stephan et al., 2001), to which the areas listed in the subsequent columns were mapped. Pyramidal complexity information was mapped from a series of studies by Elston and colleagues (E00 (Elston, 2000), E01 (Elston et al., 2001), EB11 (Elston et al., 2011b), EBD05 (Elston et al., 2005), EO10 (Elston et al., 2010b), EO11 (Elston et al., 2011a), ER02 (Elston and Rockland, 2002), ER97 (Elston and Rosa, 1997), ER98 (Elston and Rosa, 1998), ETR99 (Elston et al., 1999)). Cell and neuron count was mapped from a study by Collins and colleagues (Collins et al., 2010), PET glucose metabolism from work by Cross and colleagues (Cross et al., 2000), receptor fingerprint from Kötter and colleagues (Kötter et al., 2001) and visual hierarchy from Hilgetag and colleagues (Hilgetag et al., 2000).



FV91-1					29	62343750	0.46	28338068	155470698	70668499	
FV91-2					29	62343750	0.46	28338068	155470698	70668499	
FV91-35					23	95473633	0.37	35703747	120052687	44195992	
FV91-36					22 23	125063477	0.37	46515691	141098434	52140762	
FV91-3a					29	62343750	0.46	28338068	155470698	70668499	
FV91-3b	3b (ER02)	2987.0	4.9	187.7	15.0	62343750	0.46	28338068	155470698	70668499	
FV91-4	4 (ER02)	4568.0	7.4	286.5	23.0	51729493	0.37	18859456	148928239	57519125	
FV91-46	46 (EB11)	6584.5	11.6	289.4	23.0	111306641	0.35	38405638	139106642	48354205	
FV91-5	5 (ER02)	4689.0	8.1	247.3	14.5	183496094	0.40	72811250	159561821	63297618	
FV91-6	6 (ER02)	8238.0	9.0	268.2	25.0	131126953	0.32	43776204	127274846	40889442	
FV91-7a	7a (ER97)	2572.0	8.5	233.0	9.8	164482910	0.39	63164995	160852826	64536333	
FV91-7b	7b (ER02)	6841.0	9.6	292.1	18.0	170089844	0.34	58161071	122913300	41280032	
FV91-AIT											
FV91-AITd					18	103468750	0.35	36648734	179321924	63472201	
FV91-AITv	TEa (E99, EO11)	9085.0	8.4	250.0	27.5	117500000	0.36	42243202	161845730	58194245	
FV91-CIT											
FV91-CITd					18 21	123062500	0.40	49883214	178047734	70827846	
FV91-CITv					21	142656250	0.44	63117693	176773544	78183691	
FV91-OP	7m (EO1)	2294.0	11.0	237.1	7.3	206279297	0.37	77000130	245570592	91710494	
FV91-FF					40	56109375	0.35	19753862	139575560	49200155	
FV91-FST					18 27	92940430	0.34	31547206	143595589	49043381	
FV91-IT	IT (EBD05)	6170.0	12.8	229.5	19.9	136275391	0.41	55669494	183105180	75087041	
FV91-Id					35	24902434	0.29	7265087	118582590	34579188	
FV91-Ig					35	24902344	0.29	7265087	118582590	34579188	
FV91-LIP	LIPv	2316.0	8.8	283.0	7.7	265312500	0.35	92200798	132391467	46001496	
FV91-MDP					31	183496094	0.40	72811250	159561821	63297618	
FV91-MIP					31	183496094	0.40	72811250	159561821	63297618	
FV91-MST											
FV91-MSTd					28	74867188	0.32	24121343	113435133	36558568	
FV91-MSTI					28	74867188	0.32	24121343	113435133	36558568	
FV91-MT	MT (ER97)	2077.0	8.4	218.0	8.0	75503907	0.40	30096982	146084498	60657832	
FV91-PIP					32	265312500	0.35	92200798	132391467	46001496	
FV91-PIT											
FV91-PITd					17 18 20 21	140969238	0.42	59026067	188420043	79310240	
FV91-PITv	TEO (ER98)	4812.0	12.2	229.5	14.0	192133789	0.43	81691457	197812193	84505932	
FV91-PO					31	183496094	0.40	72811250	159561821	63297618	
FV91-Ri					32 35	145107422	0.32	49732943	125487029	40290342	
FV91-SEF					34	52554688	0.32	16591339	137938814	43558253	
FV91-SII					35 29	43623047	0.37	17801578	137026644	52623844	
FV91-SMA					34	52554688	0.32	16591339	137938814	43558253	
FV91-STP											
FV91-STPa					27	82412109	0.32	26445677	107869253	34614760	
FV91-STPp	STPp (ETR99, EO1)	5961.0	11.8	238.7	16.5	74867188	0.32	24121343	113435133	36558568	
FV91-TF					22	117500000	0.36	42243202	161845730	58194245	
FV91-TH					22	117500000	0.36	42243202	161845730	58194245	
FV91-V1	V1 (ER97, ER98, ETR99)	748.0	3.4	135.4	6.7	42006055	0.60	25248752	226030031	134711090	
FV91-V2					5	19421875	0.56	10853410	159195697	89035356	
FV91-V2v	V2 (ER97, ER98)	1170.0	4.4	128.5	7.5	121280925	0.46	49038411	209784479	97645082	
FV91-V3					2 8 19 20 21 22	29306641	0.50	14496042	181134238	89439513	
FV91-V3A					14 15 16	26912110	0.56	15081375	165814080	92688854	
FV91-V4					14 16	26912110	0.56	15081375	165814080	92688854	
FV91-V4d	V4 (ER98)	2429.0	7.5	238.7	12.5	223945313	0.39	88632675	23210717	91269334	
FV91-V4t					17	76140625	0.47	36072620	178733862	84757096	
FV91-V4v					20 21	192133789	0.43	81691457	197812193	84505932	
FV91-VIP					32	265312500	0.35	92200798	132391467	46001496	
FV91-VOT					21	142656250	0.44	63117693	176773544	78183691	
FV91-VP					19 20 21	196848958	0.41	80127681	213731659	86907453	
AIC87-ER					22	117500000	0.36	42243202	161845730	58194245	
BP89-10	10 (E00, EB11)	7247.7	12.7	296.5	21.3	91767578	0.33	31184427	144678376	47235297	
BP89-11	11 (E00)	9786.0	12.4	25.0	25.0	166503906	0.34	57057413	138637724	47508254	
BP89-12	12 (E00, EB11)	8175.0	13.0	274.1	24.7	166503906	0.34	57057413	138637724	47508254	
BP89-13	13 (EB11)	6448.5	12.1	331.5	23.0	166503906	0.34	57057413	138637724	47508254	
BP89-14					41	166503906	0.34	57057413	138637724	47508254	
BP89-25					41	166503906	0.34	57057413	138637724	47508254	
BP89-32					41 39	162587891	0.33	53267870	143742819	46963775	
BP89-9	9d (EB11)	7637.5	12.4	301.1	24.5	17031250	0.31	5311441	150719027	46962340	
BP89-Pro					26	58320313	0.35	20619313	119754236	42304705	
BP89-PalI					22 23	125063477	0.37	46515691	141098434	52140762	
IAC87a-23	Post cing (EBD05)	4357.0	13.4	286.6	14.5	158671875	0.31	49478327	148847913	46419295	
IAC87a-24	Ant cing (EBD05)	6825.0	18.5	262.8	17.2	158671875	0.31	49478327	148847913	46419295	
IAC87a-29					31	183496094	0.40	72811250	159561821	63297618	
IAC87a-30					31	183496094	0.40	72811250	159561821	63297618	
IAC87a-45					40 41	111306641	0.35	38405638	139106642	48354205	
IAC87a-PAC					26	58320313	0.35	20619313	119754236	42304705	
IAC87a-Pir					26	58320313	0.35	20619313	119754236	42304705	
MB73-A1	A1 (EO10)	943.0	5.1		7.4	44433594	0.36	16017656	135468274	48908873	
MB73-CM					24	24687500	0.45	11147650	188454198	84902134	
MB73-L					24	24687500	0.45	11147650	188454198	84902134	
MB73-RL					24	24687500	0.45	11147650	188454198	84902134	
SR88-CA1					22	117500000	0.36	42243202	161845730	58194245	
SR88-CA3					22	117500000	0.36	42243202	161845730	58194245	
SR88-PreS					22 23	125063477	0.37	46515691	141098434	52140762	
SR88-ProS					22 23	125063477	0.37	46515691	141098434	52140762	
SR88-Sub					22 23	125063477	0.37	46515691	141098434	52140762	
FV91	Elston area	spine number	dendritic tree size (10 ³ μm ²)	soma size (μm ²)	spine density (spines/10μm)	Collins et al., (2010): block ID	cell count	neuronal fraction	neuron count	cell density (cells/g)	neural density (neurons/g)

Table S2 – See caption on previous page.

FV91-1											
FV91-2											
FV91-35											
FV91-36											
FV91-3a			Pre-/postcentral gyrus	34.4							
FV91-3b											
FV91-4			Pre-/postcentral gyrus	34.4	F1		1469.0	4875.0	2424.0	791.0	380.0
FV91-46	reg46	14									
FV91-5											
FV91-6						F2v F2d F3 F4v F4d F5 F6 F7	2099.1	6484.5	3054.9	852.4	533.1
FV91-7a	7a	11									
FV91-7b			Supramarginal gyrus	39							
FV91-AIT											
FV91-AITd	AITd	16									
FV91-AITv	AITv	13									
FV91-CIT											
FV91-CITd	CITd	12									
FV91-CITv	CITv	12									
FV91-DP	DP	8									
FV91-FEF	FEF	13	Lateral frontal	34							
FV91-FST	FST	14			FST		694.0	2435.0	555.0	367.0	674.0
FV91-IT											
FV91-Id											
FV91-Ig											
FV91-LIP	LIP	10	Lateral parietal	37.2	LIP		1095.0	2391.0	712.0	334.0	697.0
FV91-MDP											
FV91-MIP					MIP		923.0	2200.0	771.0	276.0	595.0
FV91-MST											
FV91-MSTd	MSTd	10			MST		1022.0	1882.0	432.0	438.0	661.0
FV91-MSTl	MSTl	10			MST		1022.0	1882.0	432.0	438.0	661.0
FV91-MT	MT	8			MT MTp		833.0	1973.0	520.5	394.0	673.0
FV91-PIP	PIP	5									
FV91-PIT											
FV91-PITd	PITd	10									
FV91-PITv	PITv	11									
FV91-PO	PO	6			PO		758.0	2170.0	669.0	283.0	604.0
FV91-Ri											
FV91-SEF					F1		1469.0	4875.0	2424.0	791.0	380.0
FV91-Sil											
FV91-SMA					F1 F2v F2d		1669.3	5441.0	2563.3	799.0	412.7
FV91-STP											
FV91-STPa	STPa	12									
FV91-STPp	STPp	12	Lateral temporal	35.2							
FV91-TF	TF	13									
FV91-TH	TH	15									
FV91-V1	V1	1	Lateral occipital Cuneus/lingual gyrus	39.2	V1		641.0	3119.0	851.0	890.0	480.0
FV91-V2											
FV91-V2d	V2	2			V2d		888.0	2755.0	796.0	416.0	357.0
FV91-V2v	V2	2	Cuneus/lingual gyrus	40.9	V2v		793.0	2494.0	802.0	390.0	590.0
FV91-V3	V3	3			V3v V3d		855.5	2622.5	810.0	395.5	588.5
FV91-V3A	V3A	5			V3A		708.0	2547.0	407.0	305.0	610.0
FV91-V4											
FV91-V4d	V4	6			V4d		750.0	2091.0	460.0	321.0	630.0
FV91-V4t	V4t	8			V4t		1070.0	2510.0	674.0	399.0	731.0
FV91-V4v	V4	6			V4v		1037.0	2474.0	713.0	389.0	602.0
FV91-VIP	VIP	10			VIP		916.0	2125.0	515.0	322.0	706.0
FV91-VOT	VOT	8									
FV91-VP	VP	3									
AIC87-ER											
BP89-10			Principal sulcus	38.1							
BP89-11											
BP89-12											
BP89-13											
BP89-14											
BP89-25											
BP89-32											
BP89-9											
BP89-PAll											
BP89-Pro											
IAC87a-23			Posterior cingulate	38.2							
IAC87a-24			Anterior cingulate	37.3							
IAC87a-29											
IAC87a-30											
IAC87a-45											
IAC87a-PAC											
IAC87a-Pir											
MB73-A1											
MB73-CM											
MB73-L											
MB73-RL											
SR88-CA1											
SR88-CA3											
SR88-PreS											
SR88-ProS											
SR88-Sub											
FV91 area	Hilgetag et al., (2000) area	visual hierarchy	Cross et al., (2000): PET areas	meanPET-CMRglc (μmol/100g/min)	Kotter et al., (2001): Receptor areas	AMPA	GABA_A	M₁	M₂	5-HT₂	

Table S2 – continued.

Chapter 3

Associated microscale spine density and macroscale connectivity disruptions in schizophrenia

Martijn P. van den Heuvel, Lianne H. Scholtens, Marcel A. de Reus, René S. Kahn

Biological Psychiatry 2015; 80 (4): 293–301

BACKGROUND: Schizophrenia is often described as a disorder of dysconnectivity, with disruptions in neural connectivity reported on the cellular microscale as well as the global macroscale level of brain organization. How these effects on these two scales are related is poorly understood.

METHODS: First (part I of this study), we collated data on layer 3 pyramidal spine density of the healthy brain from the literature and cross-analyzed these data with new data on macroscale connectivity as derived from diffusion imaging. Second (part II of this study), we examined how alterations in regional spine density in schizophrenia are related to changes in white matter connectivity. Data on group differences in spine density were collated from histology reports in the literature and examined in a meta-regression analysis in context of alterations in macroscale white matter connectivity as derived from diffusion imaging data of a (separately acquired) group of 61 patients and 55 matched control subjects.

RESULTS: Densely connected areas of the healthy human cortex were shown to overlap with areas that display high pyramidal complexity, with pyramidal neurons that are more spinous ($p = .0027$) compared with pyramidal neurons in areas of low macroscale connectivity. Cross-scale meta-regression analysis showed a significant association between regional variation in level of disease-related spine density reduction in

schizophrenia and regional level of decrease in macroscale connectivity (two data sets examined, $p = .0028$ and $p = .0011$).

CONCLUSIONS: Our study presents evidence that regional disruptions in microscale neuronal connectivity in schizophrenia go hand in hand with changes in macroscale brain connectivity.

Introduction

Schizophrenia has a long history of being hypothesized as a disorder of dysconnectivity. Pioneering neuroanatomists and psychiatrists Meynert, Kraepelin, and Wernicke suggested that dysconnectivity of association pathways may constitute a core aspect of the etiology of schizophrenia; contemporary theories have hypothesized that affected brain connectivity and network organization play an important role in the disruption of integrative brain processes in patients with schizophrenia (Stephan et al., 2006; van den Heuvel and Fornito, 2014).

Dysconnectivity theories have been supported by empirical findings at the microscale and the macroscale levels of brain organization. Histologic examinations reported reduced spine density (Garey et al., 1998; Lewis et al., 2003; Sweet et al., 2009) and affected morphology (Glantz and Lewis, 2000; Kalus et al., 2000) of neurons in several frontal and temporal brain areas. These microscale alterations have been suggested to be localized to pyramidal neurons of layer 3 of the cerebral cortex (see Discussion) (Kolluri et al., 2005; Rajkowska et al., 1998), a cortical layer known to play an important role in long-range cortico-cortical connectivity and region-to-region communication (Schüz and Miller, 2002). At the macroscale level of brain organization, neuroimaging studies reported that schizophrenia includes disruptions of cortical structure and white matter connectivity (Ellison-Wright and Bullmore, 2009; Fornito et al., 2012; Hulshoff Pol et al., 2004; Kanaan et al., 2005; Kubicki et al., 2007; Stephan et al., 2006). Advances in diffusion-weighted imaging (DWI) techniques have led to emerging evidence that disrupted macroscale brain network organization plays an important role in the disorder (Fornito et al., 2015, 2012; Lynall et al., 2010; Repovs et al., 2011; Rubinov, 2013; van den Heuvel et al., 2010; van den Heuvel and Sporns, 2011). However, how these disease effects at these two scales of brain organization are related is poorly understood.

In this study, we present potential evidence that disease-related alterations in spine density of pyramidal neurons in schizophrenia are associated with changes in inter-areal connectivity at the macroscale level of brain organization. In part I of the study, we report an examination of a microscale-macroscale (micro-macro) relationship

in the healthy human brain, collating quantitative data on layer 3 spine density of cortical regions from histologic examinations reported in the literature and cross-referencing the data with data on regional macroscale connectivity as derived from magnetic resonance imaging (MRI). Next, in part II of our study, we continued our examination by studying a possible link between disease-related changes in spine density of cortical regions and changes in macroscale connectivity as derived from MRI analysis. We collated data from the literature on group differences in reductions in spine density in schizophrenia as measured by histologic examinations, and we cross-referenced this microscale data in a meta-regression analysis with data on macroscale dysconnectivity effects as derived from analysis of high-resolution diffusion MRI data of a (separate) group of 61 patients with chronic schizophrenia and 55 matched healthy control subjects. Using meta-regression analysis, we present evidence of neural dysconnectivity at the microscale and macroscale levels of brain organization in schizophrenia to be potentially related.

Materials and Methods

Part I: Micro-Macro Relationship in the Healthy Brain

Microscale Data.

Data on cortical variation of pyramidal layer 3 spine density in the healthy brain were collated across studies found in the literature (Table S1 in Supplement 1) (Anderson et al., 2009; Garey et al., 1998; Hutsler and Zhang, 2010; Jacobs et al., 1997, 2001; Zeba et al., 2008). With studies using different methodologies (Golgi, Golgi-Cox, rapid Golgi) (Table S2 in Supplement 1), data were standardized across studies (taking the data of the Jacobs group as a reference) to allow across-study comparison (Supplement 1).

In addition to spine density, the studies of the Jacobs group (Table S1 in Supplement 1) (Anderson et al., 2009; Jacobs et al., 1997, 2001) reported quantitative data on total length of the dendritic tree, total number of dendritic segments, total mean segment length of a dendritic branch, and total estimated spine count (Figure 1A). These additional data were collated (Table S1 in Supplement 1) and examined in the context of regional variation of macroscale connectivity (see later).

In total, across these 6 studies, data on pyramidal complexity were collected at 14 different sites of the cortex (Figure 1C). The spatial locations of the cortical patches were mapped to corresponding cortical regions of the cortical Desikan-Killiany atlas used for DWI connectome reconstruction (Figure 1C and Table S1 in Supplement 1).

Macroscale Connectome Reconstruction and Analysis. A macroscale human connectome

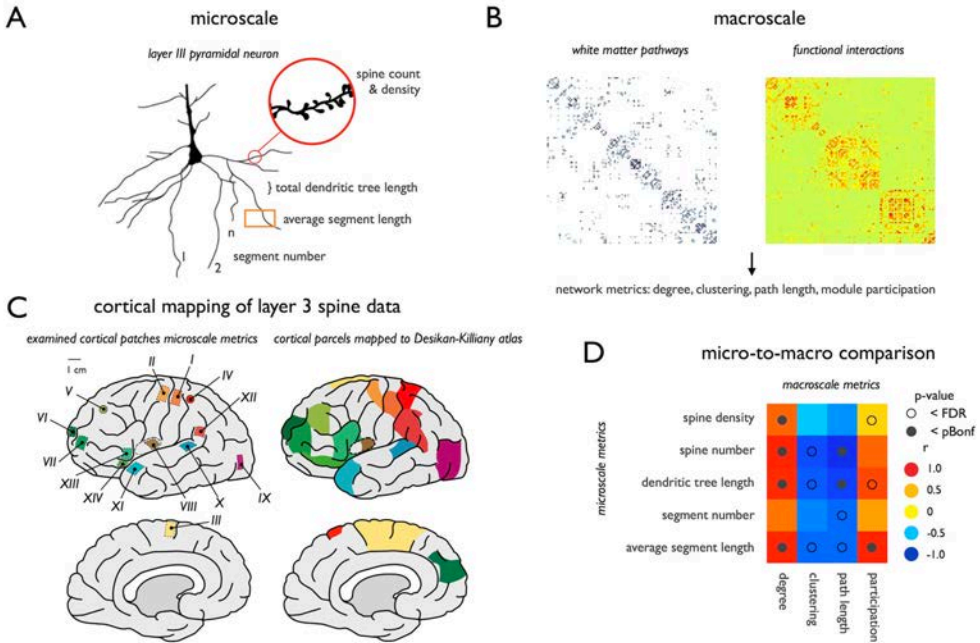


Figure 1. (A) Collated data on microscale layer 3 pyramidal neurons involved five metrics of dendritic pyramidal structure. (B) Macroscale data involved reconstruction of cortico-cortical anatomic pathways by means of diffusion magnetic resonance imaging (left matrix) and the reconstruction of functional connectivity (right matrix) derived from resting-state functional magnetic resonance imaging recordings of Human Connectome Project data. (C) The 14 cortical patches (regions I–XIV) (Table S1 in Supplement 1) from which data on layer 3 pyramidal complexity were collated from the literature. For 12 regions, the approximate size of the examined cortical patch was reported in the original article (shown as patches); for 2 regions (shown as dots), this information was absent. Roman numerals correspond to the region descriptions in Table S1 in Supplement 1. Right panel shows the corresponding selected cortical parcels of the Desikan-Killiany atlas. (D) 5×4 correlation matrix of the five microscale and four macroscale network metrics. open circles, trend-level correlations surviving false discovery rate (FDR); closed circles, correlations surviving more strict partial Bonferroni correction (pBonf). Visual representations of pyramidal dendritic tree are based on Anderson et al. (2009).

map of 114 cortical regions was derived from streamline tractography of high-resolution DWI data from the Human Connectome Project (Q3, $N = 215$ subjects) (see Supplement 1 for details) (Van Essen et al., 2013). A group-averaged structural connectivity matrix was formed by taking the nonzero mean over the individual matrices (Figure 1B, left panel).

Functional connectivity between each of the 114 cortical regions was assessed by means of analysis of resting-state functional MRI data (Human Connectome Project, Q3 release) (Supplement 1), with a group-averaged weighted functional connectivity matrix formed by averaging across the individual matrices (Figure 1B, right panel).

Nodal degree k was computed as the total number of (undirected, unweighted) anatomic connections of a region, providing a metric of how well a node is connected to the rest of the network. Nodal clustering C_i was computed as a metric of local network connectedness; the metric of nodal shortest path length L_i was computed and interpreted as a (inverse) metric of the global communication efficiency of a cortical region (Rubinov and Sporns, 2010). Functional communities were determined on the basis of modular decomposition of the functional connectivity matrix, and the anatomic intermodular connectivity profile of a node was assessed via computation of the nodal participation coefficient P_i (Rubinov and Sporns, 2010; van den Heuvel and Sporns, 2013a). Anatomic hub nodes were selected as the set of top 30% nodes with the highest degree (overlapping a selection of nodes with a degree $k > 12$) (Supplement 1) (van den Heuvel et al., 2012).

Statistical Analysis.

Relationships between regional variation in pyramidal complexity and macroscale connectivity were examined using Pearson correlation analysis. Effects reaching a strict partial Bonferroni corrected α level of 0.0083 were considered statistically significant; correlations reaching $p = 0.033$ (false discovery rate [FDR] of $q = 0.05$) were considered trend-level effects (see Supplement 1 for computation of both statistical thresholds).

Part II: Relationship Between Disease-Related Changes in Spine Density and Changes in Macroscale Connectivity in Schizophrenia

Layer 3 Pyramidal Spine Density Reductions in Schizophrenia.

A PubMed search revealed six studies examining pyramidal layer 3 spine density reductions in schizophrenia (Tables S3 and S4 in Supplement 1) (Garey et al., 1998; Glantz and Lewis, 2000; Kolluri et al., 2005; Konopaske et al., 2014; Somenarain and Jones, 2012; Sweet et al., 2009). A meta-analysis was performed, collating between-group differences in layer 3 spine density as percentage of change (i.e., effect sizes rather than quantitative levels), ruling out potential differences in measurement variables resulting from varying types of spine mapping techniques used across the different studies (Methods and Results in Supplement 1). Data on layer 3 spine effects of seven Brodmann areas (BAs) could be collated, including BA 9, BA 10, and BA 46 in the frontal lobe; BA 17 in the occipital lobe; and BA 38, BA 41, and BA 42 in the temporal lobe (Table S3 in Supplement 1). Figure S1 in Supplement 1 illustrates the locations of the seven cortical patches from which histologic data on layer 3 spine density could be collated, together with their matching cortical regions in the Desikan-Killiany atlas used for DWI connectivity reconstruction.

Layer Nonspecific Microscale Alterations.

Changes in microscale connectivity in schizophrenia were also reported by studies using synaptophysin immunostaining techniques. Most synaptophysin immunostaining studies reported synapse reductions across entire examined volumes (i.e., estimates of total synapse reduction across all layers of the cortex combined). In a PubMed search, we found 11 additional studies reporting on synapse levels in cortical regions by means of synaptophysin immunostaining of postmortem brain material (Davidsson et al., 1999; Eastwood and Harrison, 1995; Eastwood et al., 2000, 1995; Glantz and Lewis, 1997; Honer et al., 1999, 1997; Karson et al., 1999; Landén et al., 2002; Perrone-Bizzozero et al., 1996; Rao et al., 2013). We collated the results of these studies (Table S5 in Supplement 1), again grouping information on between-group differences in synapse levels in patients compared with control subjects, measured by the reported percentage of change in the patient population compared with the control population in each of the studies. The 12 cortical locations as reported in the original articles were mapped to cortical parcels of the Desikan-Killiany atlas using the same procedure as described (Figure 6A shows the mapping of the regions; see also Supplement 1), providing data on (*ex vivo* examined) spine density reductions of 12 areas of human cortex in schizophrenia.

MRI Data.

In vivo MRI data from a different group of patients with schizophrenia were analyzed. Analysis involved examination of data of 61 patients with schizophrenia and 55 age-matched and gender-matched healthy control subjects, including an MRI data set described and examined previously in the context of affected hub connectivity in schizophrenia (van den Heuvel et al., 2013). Table S6 in Supplement 1 summarizes the demographics of the included patients and healthy control subjects. The MRI data included the acquisition of a 3-tesla T1 scan (three-dimensional fast field echo using parallel imaging, repetition time = 10 ms, echo time = 4.6 ms, 200 slices, .75-mm voxel size) and a DWI scan (two sets each consisting of 5 non-diffusion-weighted volumes [b-factor = 0 sec/mm²] and 30 diffusion-weighted volumes [b-factor = 1000 sec/mm²]) (see Supplement 1 for processing details). Individual white matter connectivity connectome maps were derived from the DWI data (using a similar procedure as for the Human Connectome Project data) (Supplement 1). The strength of reconstructed pathways between regions was taken as the number of reconstructed streamlines (NOS). In addition to NOS, the strength of tracts was assessed by streamline density (the number of streamlines divided by the average volume of the target and source region). Streamline density was examined to correct for potential effects of differences in regional volumes between patient and control populations on the tract reconstruction (see Methods in Supplement 1) (Hagmann et al., 2008; van den

Heuvel and Sporns, 2013a). Next, from the derived individual structural connectivity matrices, the average level of connectivity strength per cortical region was computed for each subject as the nonzero mean of NOS (and streamline density) of the reconstructed cortico-cortical pathways of a region. Finally, patient/control subject between-group analysis involved the computation of group average effect sizes in regional connectivity strength in percentage of change compared with the group of control subjects.

Microscale-to-Macroscale Cross-Scale Analysis.

Region wise between-group effect sizes in spine density as measured using layer 3 measurements and synaptophysin immunostaining were correlated with region wise between-group effect sizes in macroscale connectivity using Pearson correlation.

Results

Part I: Micro-Macro Relationship in the Healthy Brain

Associations Between Macroscale Connectome Metrics and Microscale Pyramidal Complexity. Cross- correlation between regional data on pyramidal complexity and graph theoretical properties of macroscale connectome organization (see Supplement 1 for connectome analysis) revealed several significant associations between properties of microscale and macroscale neuronal connectivity in the healthy human brain. We describe the most prominent findings (Figure 1D shows the total set of all possible $5 \times 4 = 20$ micro-macro correlations).

The number of macroscale connections (i.e., network nodal degree) of cortical regions revealed a positive correlation with layer 3 pyramidal total spine density ($p = .0027$, $r = .74$). Including information on the strength of macroscale pathways in this comparison revealed similar findings (NOS, $p = .0184$, $r = .62$; streamline density, $p = .0023$, $r = .74$) (Supplement 1). Furthermore, post hoc analysis regressing out potential influencing effects of cortical volume (including regional volume as a covariate in the regression) revealed similar findings (degree, $p = .0032$; NOS, $p = .0112$; streamline density, $p = .0023$). Examining the other metrics of complexity of pyramidal organization similarly revealed associations with regional macroscale connectivity, with regional variation in macroscale network degree correlated with regional variation in dendritic tree length ($p = .0060$, $r = .79$), average dendritic segment length ($p = .0028$, $r = .83$), and total number of counted spines ($p = .0003$, $r = .91$) (Figure 2).

Consistent with the observations for degree and connectivity strength, higher communication efficiency of cortical regions – reflected by a shorter path length L_i – was associated with longer dendritic tree length ($p = .004$, $r = .71$), higher spine

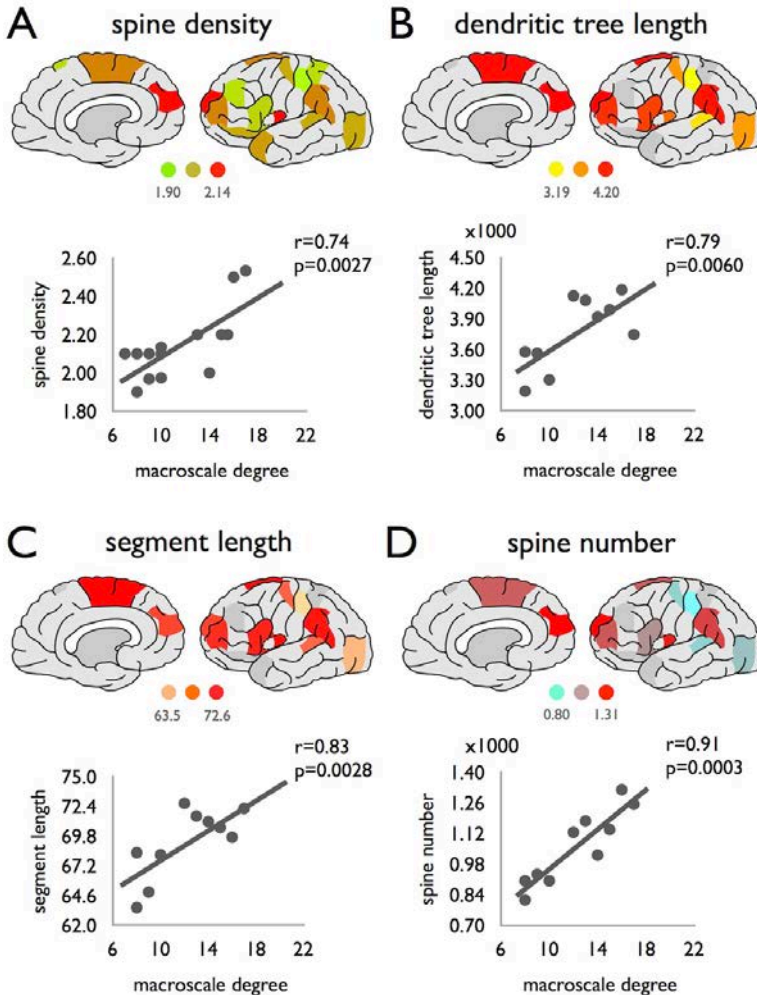


Figure 2. (A–D) Upper panels show distribution of values of layer 3 pyramidal complexity across cortical areas; lower panels show correlations between microscale pyramidal complexity metrics and macroscale network degree.

number ($p = .004$, $r = .90$), trend-level higher segment number ($p = .020$, reaching FDR, $r = .72$), and trend-level longer dendritic segments ($p = .022$, reaching FDR, $r = .71$) (Figure 3). Nodal clustering C_i also showed a significant (inverse) relationship with spine number ($p = .009$, $r = .77$) and a trend-level (inverse) relationship with dendritic tree length ($p = .016$, FDR, $r = .73$) and dendritic segment length ($p = .028$, FDR, $r = .69$). Intermodular connectivity P_i of cortical regions, expressing a node's level of intermodular connectedness, revealed trend-level correlations to cortical variation in dendritic tree length ($p = .014$, FDR, $r = .74$) and the length of dendritic

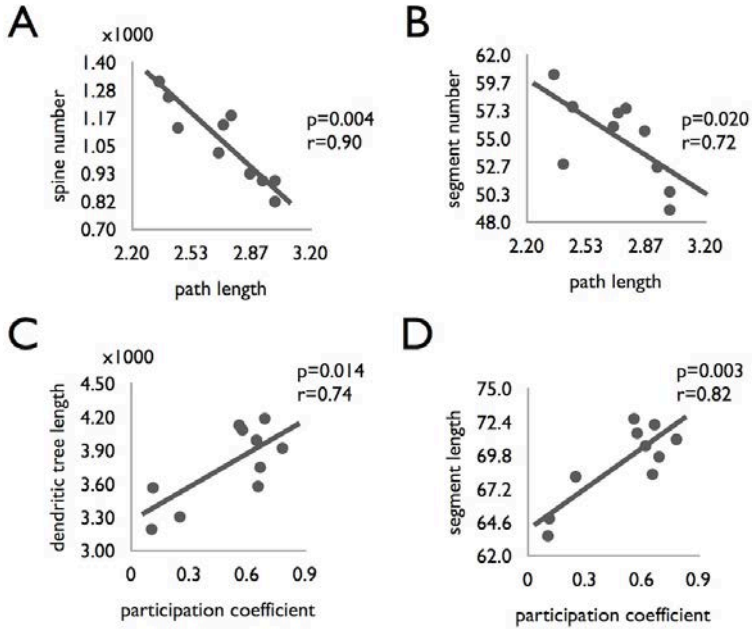


Figure 3. Correlations between macroscale topological network metrics shortest path length L_i (A,B) and participation coefficient P_i (C,D) and metrics of layer 3 pyramidal complexity.

segments ($p = .0031$, $r = .82$) (Figure 3). A post hoc partial least squares regression analysis further confirmed a significant association between microscale and macroscale metrics (three factors, explained variance 81%, $p = 1.367 \times 10^{-11}$).

Macroscale cortical hubs – cortical regions with a high level of connectivity that have been noted to form a densely, mutually connected “rich club” (Power et al., 2013; van den Heuvel and Sporns, 2011, 2013b) – were tested for a differentiating level of neuronal complexity compared with low-degree peripheral regions (Collin et al., 2013). Confirming earlier observations in the macaque cortex (Scholtens et al., 2014), layer 3 pyramidal neurons in cortical areas overlapping macroscale hub regions (Figure 4) displayed an overall more intricate neuronal organization with more spinous (spine count, $p = .0052$; spine density, $p = .0142$; 10,000 permutations), longer ($p = .007$, permutation testing, 10,000 permutations), more branched ($p = .034$, FDR), and more segmented ($p = .004$) dendritic trees (Figure 4) compared with pyramidal neurons in areas overlapping low-degree peripheral regions.

Part II: Relationship Between Disease-Related Changes in Spine Density and Changes in

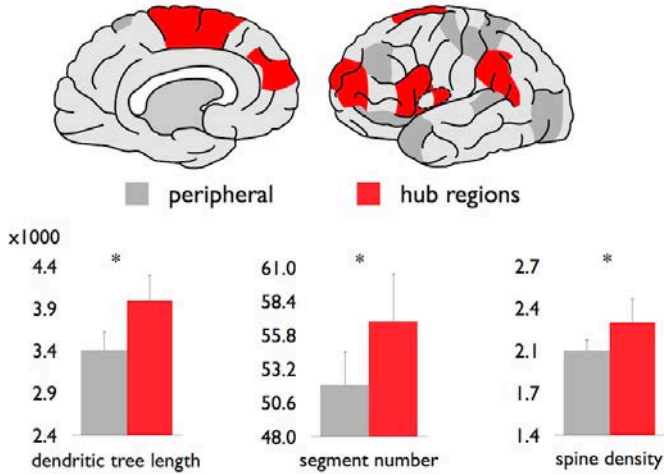


Figure 4. Upper panels highlight the Brodmann areas (for which micro-data were available) that overlapped with a high-degree hub region, shown in red; regions overlapping peripheral regions are shown in gray. Lower panels depict a higher level of pyramidal metrics of hub regions (red) compared with peripheral nodes (gray). * $p < .05$ (reaching Bonferroni correction).

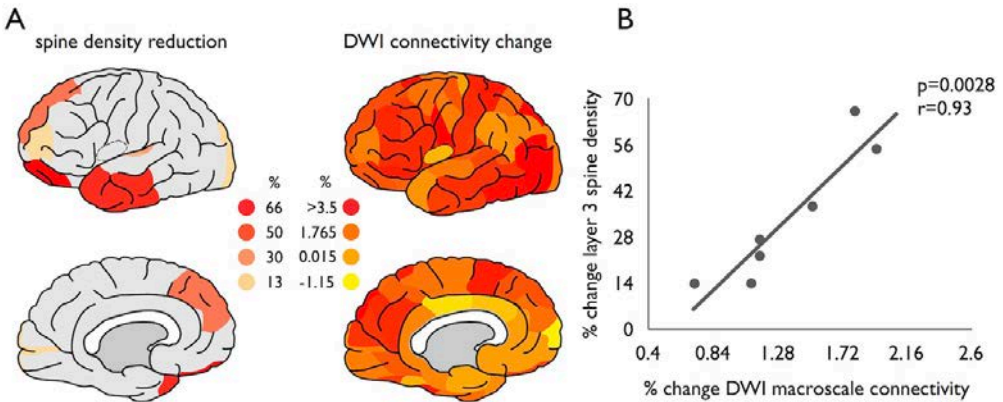


Figure 5. Cortical levels of between-group differences in layer 3 spine density ((A) left panel; (B) y-axis, in % of change compared with control subjects) positively correlated with cortical variation in between-group differences in macroscale number-of- streamlines connectivity ((A) right panel; (B) x-axis, in % of change compared with control subjects). DWI, diffusion-weighted imaging.

Macroscale Connectivity in Schizophrenia

Layer 3 Specific Effects.

In the second part of our investigation, we collated reports on regional reductions in

layer 3 pyramidal spine density in schizophrenia across postmortem histology reports in the literature (including data on seven cortical regions) (Figure S3 and Table S3 in Supplement 1) and cross-correlated these effects with alterations in macroscale white matter connectivity as examined in in vivo DWI data in a (separate) group of 61 patients with schizophrenia and 55 matched healthy control subjects (Table S6 in Supplement 1). Regional reductions in microscale layer 3 spine density significantly correlated with between-group differences in macroscale DWI connectivity (NOS, $p = .0028$, $r = .93$) (Figure 5). Examining differences in streamline density (to correct for regional volume effects on the assessment of connectivity strength of reconstructed pathways) revealed similar results ($p = .0066$, $r = .89$). Additional analysis in which potential effects of patient/control subject differences in cortical volume (Kuperberg et al., 2003; van Haren et al., 2011) were regressed out (by including regional volumes and group differences in cortical volume [percentage of change] as covariates in the regression analysis) revealed similar findings (NOS, $p = .0141$; streamline density, $p = .0262$). Further post hoc analysis showed that a micro-macro disease relationship was specific to NOS and streamline density connectivity, with no associations observed between regionally averaged fractional anisotropy (computed as the average over the collection of voxels passed by the reconstructed fiber streamlines, $p = .27$) or mean diffusivity ($p = .52$). Restricting analysis to data from studies using Golgi staining techniques [i.e., omitting data of the studies by Somenarain and Jones (Somenarain and Jones, 2012) or Sweet et al. (Sweet et al., 2009), or both] (Table S5 in Supplement 1) revealed similar findings (see Results in Supplement 1). Effects remained significant after correction for potential medication effects (regressing out haloperidol equivalent dose; NOS, $p = .0032$; streamline density, $p = .0033$) (Table S6 in Supplement 1; see Results in Supplement 1).

Layer Nonspecific Effects.

In a second analysis, data on between-group effect sizes in microscale synapse alterations as reported by synaptophysin immunostaining studies (reporting on spine effects across the entire width of the cortex, not focused on one specific layer) (Figure 6A) were collated and cross-correlated with macroscale connectivity changes as computed from DWI data of a (different) group of 61 patients with schizophrenia and 55 healthy control subjects. Meta-regression analysis between the two independent data sets revealed the regional percentage of reduction of microscale spine density to be correlated with regional between-group differences in macroscale anatomic connectivity (NOS, $p = .0011$, $r = .82$; streamline density, $p = .0027$, $r = .78$) (Figure 6B). Effects remained significant after correction for potential volume effects (NOS, $p = .0006$; streamline density, $p = .0081$) and after correction of the patient data for medication dose (haloperidol equivalent dose; NOS, $p = .0002$; streamline density, $p = .0018$).

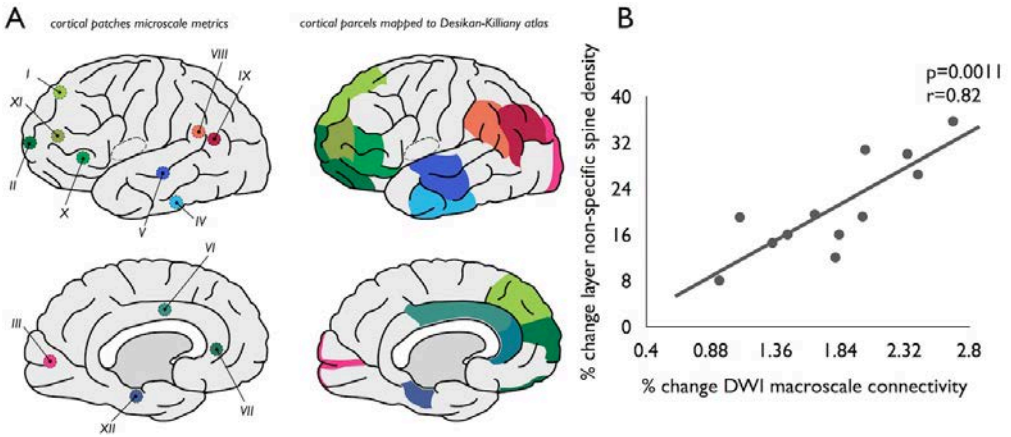


Figure 6. (A) Left panel shows the reported Brodmann area locations, and right panel shows the mapping on the Desikan-Killiany atlas. Roman numerals correspond to the region descriptions in Table S5 in Supplement 1. (B) Regional variation in between-group differences in layer nonspecific spine density as measured via layer nonspecific synaptophysin immunostaining (y-axis, % of reduction compared with control subjects) positively correlated with between-group differences in macroscale connectivity in schizophrenia (x-axis, % of change compared with control subjects) as derived from diffusion-weighted imaging (DWI) analysis.

Discussion

The first main finding of this study (part I) is the observation of a positive association between the level of macroscale connectivity of cortical regions and their level of neuronal complexity at the microscale cellular level in the healthy brain. Regional variation in layer 3 pyramidal complexity in the healthy brain positively correlated with region wise levels of macroscale connectivity, suggesting that a denser macroscale connectivity profile goes hand in hand with a more complex architecture of pyramidal neurons at the microscale cellular level. The second main finding of our study (part II) is that the level of cortical variation in reduction of spine density in schizophrenia is associated with the level of reduction of white matter connectivity at the macroscale. Data on cortical variation in between-group differences in layer 3 spine density were collated from studies in literature and cross-referenced in a meta-regression analysis with data on alterations in macroscale connectivity as derived from diffusion-weighted MRI in a separate group of patients and control subjects. Cross-correlation analysis showed a positive association between regional variation in spine density reductions and the extent of macroscale connectivity changes in patients; a micro-macro association was also observed in a further analysis correlating cortical variation in macroscale dysconnectivity with layer nonspecific cortical spine density reductions as collated across studies using synaptophysin immunostaining. Taken together, our findings suggest the possibility of an interplay between often reported disease-related

alterations in cortical spine density (Glausier and Lewis, 2013; Moyer et al., 2015) and – also common, but independently reported – alterations in connectome architecture at the macroscale level of brain organization in schizophrenia (Fornito et al., 2012; Stephan et al., 2006).

The observed association between organizational properties at different scales of brain connectivity is in line with recent observations examining micro-macro relationships. Beul et al. (Beul et al., 2015) reported cytoarchitectonic types of the cat cortex to be related to the macroscale wiring pattern of cortical regions, and we reported on a positive interaction between macroscale wiring and microscale layer 3 neuron size and complexity in the macaque (Scholtens et al., 2014) and human cortex (van den Heuvel et al., 2015). Furthermore, studies on the neuroarchitectonics of the human and animal cortex noted a gradient of increasing complexity in pyramidal architecture from unimodal to multimodal regions (Elston, 2003; Jacobs et al., 2001) with multimodal areas being distinctive in cytoarchitectonic layout from unimodal areas and theorized to be particularly involved in upstream integrative neural processing (Mesulam, 1998). At the same time, network studies of the human macroscale connectome reported a high spatial overlap between high-degree regions and functional multimodal association regions (Bullmore and Sporns, 2009; Cole et al., 2013; Tomasi and Volkow, 2011), hypothesizing that high-degree brain hubs form central “convergence zones” for information integration in the human brain (Cole et al., 2013; van den Heuvel and Sporns, 2013b). Our current findings converge on – and perhaps to some extent merge – these theories, showing evidence for macroscale high-degree regions to be strongly represented among cortical areas with a highly complex neuronal organization (Figure 4). Lewis et al. argued a relative specificity of changes to cortical layer 3 pyramidal neurons (Kolluri et al., 2005; Pierri et al., 2001) in schizophrenia, and with layer 3 argued to be an important layer for interareal communication, they already theorized that microscale abnormalities may lead to changes in macroscale white matter circuitry and conversely to disrupted global brain functioning in patients (Glantz and Lewis, 2000). Our findings provide evidence for such a micro-macro interaction, showing disease-related reductions in microscale neuronal connectivity to coincide with changes in cortico-cortical white matter connectivity in schizophrenia.

Many unanswered questions about a latent micro-macro interaction remain. In particular, the question of which underlying processes are driving the observed micro-macro associations is unresolved. The meta-regression analysis does not provide insight into whether a diverse macroscale connectivity profile leads to a more complex microstructural architecture or whether a more complex microstructural architecture allows for a larger number of macroscale pathways to emerge. One – perhaps reductionistic – explanation of the observed micro-macro association in schizophrenia

might include a genetic cascade driving dendritic dysmorphology, with a decay of long-range macroscale projections as a consequence of long-range axons not being able to attach properly to the impoverished dendritic trees. Alternatively, one could hypothesize disease effects on long-range axonal projections to lead subsequently to pruning of unused synapses. The observed micro-macro relationship might also be the result of an interaction between the two scales during development. There is a rich body of literature on developmental effects on the microscale (Elston et al., 2010) as well as the macroscale of brain organization (Collin and van den Heuvel, 2013; Fair et al., 2009; Grayson et al., 2014), and the two organizational scales of connectivity most likely involve a continuous interplay, shaped by interacting developmental processes that work on both scales (Elston et al., 2010; Fair et al., 2009; Huttenlocher and Dabholkar, 1997; Innocenti and Price, 2005). As a result, abnormal developmental processes in the transition toward and during the course of the disease might lead to interacting effects on the microscale and macroscale of brain connectivity, with associated disruptions in microscale neuronal and macroscale connectome organization (Bullmore et al., 1997; Catani and ffytche, 2005; Fornito et al., 2015; McGlashan and Hoffman, 2000).

Our findings are inherently limited by the nature of the collated microscale data and the analyzed MRI data. To our knowledge, only a few studies have examined regional spine density reductions in schizophrenia, which limits our examination to a relatively coarse sampling of cortical areas. In addition, our study involves a meta-regression type of analysis in which data of two different data sets are combined. Data on spine density and spine density differences were collated from histologic reports in the literature, whereas data on cortical macroscale connectivity were derived from diffusion MRI in a newly acquired population. A “single-cohort” examination in which information on both scales would be derived and analyzed in the same group of subjects would constitute a more powerful study design; brain banks focused on psychiatry patients [e.g., Netherlands Brain Bank for Psychiatry, available at <http://www.nbb-psy.nl>, or Australian Schizophrenia Research Bank (Loughland et al., 2010)] might make such investigations possible in the future. Also, the collated data on pyramidal complexity were derived from postmortem tissue samples taken from subjects who were generally older (age range, 30–64 years [Table S2 in Supplement 1]; patient study, 48–71 years [Table S4 in Supplement 1]) than the subjects from whom MRI data were acquired (age range, 22–35 years in Human Connectome Data, Q3 release; patient study, 20–48 years). Development and aging have well-known effects on morphologic properties of neurons (Jacobs et al., 1997) as well as on global white matter integrity and macroscale connectome organization (Betz et al., 2014; Collin and van den Heuvel, 2013). Furthermore, not all of the included postmortem studies reported details on

neuropathologic examinations (e.g., plaques, tangles, staging of neurodegenerative diseases), which is a further limitation of the included histology data. In addition, as a result of the performed meta-regression type of analysis in which data were collated from multiple studies, the microscale data could not be corrected for potential confounding effects such as disease stage, medication, or treatment differences. Finally, data on macroscale connectivity were assessed via DWI, which is known to be associated with several caveats, such as a recognized underestimation of long-range and short-range connectivity, difficulty in reconstructing complex fiber orientations, and incapability to resolve projection direction of axonal pathways (Jbabdi and Johansen-Berg, 2011; Jones, 2008). Extending examinations to include recent advances in MRI that go beyond fiber tractography, such as MRI sequences that provide in vivo estimates of axonal diameter (Alexander et al., 2010) and neurite dispersion and density (Zhang et al., 2012) would be of interest. Our study was focused on the examination of spine density effects in schizophrenia, but alterations in other aspects of cytoarchitecture and neuronal complexity may be of equal interest to examine in the context of abnormalities in macro-scale connectivity. Extending analysis to reported alterations in pyramidal neuron somal size (Pierri et al., 2001; Rajkowska et al., 1998), dendritic architecture, and dendritic branching in schizophrenia (Elston, 2003; Jacobs et al., 2001) (see Results in Supplement 1) as well as disease-related changes in neurotransmitter and receptor density levels of neurons (Hu et al., 2014) would be of interest.

In conclusion, to date, there is a dearth of evidence linking different scales of connectivity in the brain. Examination of a micro-macro interplay of brain connectivity may provide a potentially fruitful framework for examining how disease-related changes in neural connectivity interact or perhaps even reflect two sides of the same coin.

Acknowledgments and Disclosures

This work was supported by the Netherlands Organisation for Scientific Research (Nederlandse Organisatie voor Wetenschappelijk Onderzoek) Innovational Research Incentives Scheme Veni grant (Grant No. 451-12-001 to MPvdH). The funding agency did not have any influence on the data acquisition, analysis, or report of the data. Human neuroimaging data (for part I of this study) was provided by the Human Connectome Project, WU-Minn Human Connectome Project Consortium (Principal Investigators: David Van Essen and Kamil Ugurbil; Grant No. 1U54MH091657) funded by the 16 National Institutes of Health Institutes and Centers that support the National Institutes of Health Blueprint for Neuroscience Research and by the McDonnell Center for Systems Neuroscience at Washington University. We thank Ruben Schmidt for

Chapter 3

helping out with the statistical analysis. The authors report no biomedical financial interests or potential conflicts of interest.

References

- Alexander DC, Hubbard PL, Hall MG, Moore EA, Ptito M, Parker GJ, Dyrby TB (2010) Orientationally invariant indices of axon diameter and density from diffusion mri. *Neuroimage* 52:1374–1389.
- Anderson K, Bones B, Robinson B, Hass C, Lee H, Ford K, Roberts TA, Jacobs B (2009) The morphology of supragranular pyramidal neurons in the human insular cortex: a quantitative golgi study. *Cereb Cortex* 19:2131–44.
- Betzel RF, Byrge L, He Y, Goni J, Zuo XN, Sporns O (2014) Changes in structural and functional connectivity among resting-state networks across the human lifespan. *Neuroimage* 102 Pt 2:345–57.
- Beul SF, Grant S, Hilgetag CC (2015) A predictive model of the cat cortical connectome based on cytoarchitecture and distance. *Brain Structure and Function* 220:3167–3184.
- Bullmore E, Sporns O (2009) Complex brain networks: graph theoretical analysis of structural and functional systems. *Nat Rev Neurosci* 10.
- Bullmore ET, Frangou S, Murray RM (1997) The dysplastic net hypothesis: an integration of developmental and dysconnectivity theories of schizophrenia. *Schizophr Res* 28:143–56.
- Catani M, ffytche DH (2005) The rises and falls of disconnection syndromes. *Brain* 128:2224–2239.
- Cole MW, Reynolds JR, Power JD, Repovs G, Anticevic A, Braver TS (2013) Multi-task connectivity reveals flexible hubs for adaptive task control. *Nature neuroscience* 16:1348–1355.
- Collin G, Sporns O, Mandl RCW, van den Heuvel MP (2013) Structural and functional aspects relating to cost and benefit of rich club organization in the human cerebral cortex. *Cerebral cortex (New York, N.Y. : 1991)* .
- Collin G, van den Heuvel MP (2013) The ontogeny of the human connectome: Development and dynamic changes of brain connectivity across the life span. *The Neuroscientist : a review journal bringing neurobiology, neurology and psychiatry* .
- Davidsson P, Gottfries J, Bogdanovic N, Ekman R, Karlsson I, Gottfries CG, Blennow K (1999) The synaptic-vesicle-specific proteins rab3a and synaptophysin are reduced in thalamus and related cortical brain regions in schizophrenic brains. *Schizophrenia Research* 40:23–29.
- Eastwood SL, Harrison PJ (1995) Decreased synaptophysin in the medial temporal lobe in schizophrenia demonstrated using immunautoradiography. *Neuroscience* 69:339–343.
- Eastwood SL, Harrison PJ, Cairns NJ (2000) Synaptophysin gene expression in schizophrenia:

- Investigation of synaptic pathology in the cerebral cortex. *The British Journal of Psychiatry* 176:236–242.
- Eastwood S, Burnet P, Harrison P (1995) Altered synaptophysin expression as a marker of synaptic pathology in schizophrenia. *Neuroscience* 66:309–319.
- Ellison-Wright I, Bullmore E (2009) Meta-analysis of diffusion tensor imaging studies in schizophrenia. *Schizophr Res* 108:3–10.
- Elston GN (2003) Cortex, cognition and the cell: New insights into the pyramidal neuron and prefrontal function. *Cerebral Cortex* 13:1124–1138.
- Elston GN, Okamoto T, Oga T, Dornan D, Fujita I (2010) Spinogenesis and pruning in the primary auditory cortex of the macaque monkey (*Macaca fascicularis*): an intracellular injection study of layer iii pyramidal cells. *Brain research* 1316:35–42.
- Fair DA, Cohen AL, Power JD, Dosenbach NU, Church JA, Miezin FM, Schlaggar BL, Petersen SE (2009) Functional brain networks develop from a "local to distributed" organization. *PLoS Comput Biol* 5:e1000381.
- Fornito A, Zalesky A, Breakspear M (2015) The connectomics of brain disorders. *Nat Rev Neurosci* 16:159–72.
- Fornito A, Zalesky A, Pantelis C, Bullmore ET (2012) Schizophrenia, neuroimaging and connectomics. *NeuroImage* 62:2296–2314.
- Garey LJ, Ong WY, Patel TS, Kanani M, Davis A, Mortimer AM, Barnes TRE, Hirsch SR (1998) Reduced dendritic spine density on cerebral cortical pyramidal neurons in schizophrenia. *Journal of Neurology, Neurosurgery & Psychiatry* 65:446–453.
- Glantz LA, Lewis DA (2000) Decreased dendritic spine density on prefrontal cortical pyramidal neurons in schizophrenia. *Arch Gen Psychiatry* 57:65–73.
- Glantz LA, Lewis DA (1997) Reduction of synaptophysin immunoreactivity in the prefrontal cortex of subjects with schizophrenia: regional and diagnostic specificity. *Archives of general psychiatry* 54:943–952.
- Glausier JR, Lewis DA (2013) Dendritic spine pathology in schizophrenia. *Neuroscience* 251:90–107.
- Grayson DS, Ray S, Carpenter S, Iyer S, Dias TGC, Stevens C, Nigg JT, Fair DA (2014) Structural and functional rich club organization of the brain in children and adults. *PLoS ONE* 9:e88297.
- Hagmann P, Cammoun L, Gigandet X (2008) Mapping the structural core of human cerebral cortex. *PLoS biology* 6:e159.

- Honer WG, Falkai P, Chen C, Arango V, Mann JJ, Dwork AJ (1999) Synaptic and plasticity-associated proteins in anterior frontal cortex in severe mental illness. *Neuroscience* 91:1247–1255.
- Honer WG, Falkai P, Young C, Wang T, Xie J, Bonner J, Hu L, Boulianne GL, Luo Z, Trimble WS (1997) Cingulate cortex synaptic terminal proteins and neural cell adhesion molecule in schizophrenia. *Neuroscience* 78:99–110.
- Hu W, MacDonald ML, Elswick DE, Sweet RA (2014) The glutamate hypothesis of schizophrenia: evidence from human brain tissue studies. *Annals of the New York Academy of Sciences* 1338:38–57.
- Hulshoff Pol HE, Schnack HG, Mandl RC, Cahn W, Collins DL, Evans AC, Kahn RS (2004) Focal white matter density changes in schizophrenia: reduced inter-hemispheric connectivity. *Neuroimage* 21:27–35.
- Hutsler JJ, Zhang H (2010) Increased dendritic spine densities on cortical projection neurons in autism spectrum disorders. *Brain Res* 1309:83–94.
- Huttenlocher PR, Dabholkar AS (1997) Regional differences in synaptogenesis in human cerebral cortex. *The Journal of Comparative Neurology* 387:167–178.
- Innocenti GM, Price DJ (2005) Exuberance in the development of cortical networks. *Nat Rev Neurosci* 6:955–65.
- Jacobs B, Driscoll L, Schall M (1997) Life-span dendritic and spine changes in areas 10 and 18 of human cortex: a quantitative golgi study. *J Comp Neurol* 386:661–80.
- Jacobs B, Schall M, Prather M, Kapler E, Driscoll L, Baca S, Jacobs J, Ford K, Wainwright M, Trembl M (2001) Regional dendritic and spine variation in human cerebral cortex: a quantitative golgi study. *Cerebral Cortex* 11:558–571.
- Jbabdi S, Johansen-Berg H (2011) Tractography: where do we go from here? *Brain Connect* 1:169–83.
- Jones DK (2008) Studying connections in the living human brain with diffusion mri. *Cortex* 44:936–52.
- Kalus P, Muller TJ, Zuschratter W, Senitz D (2000) The dendritic architecture of prefrontal pyramidal neurons in schizophrenic patients. *Neuroreport* 11:3621–5.
- Kanaan RA, Kim JS, Kaufmann WE, Pearlson GD, Barker GJ, McGuire PK (2005) Diffusion tensor imaging in schizophrenia. *Biol Psychiatry* 58:921–9.
- Karson CN, Mrak RE, Schluterman KO, Sturner WQ, Sheng JG, Griffin WS (1999) Alterations in synaptic proteins and their encoding mrnas in prefrontal cortex in schizophrenia: a possible

- neurochemical basis for 'hypofrontality'. *Mol Psychiatry* 4:39–45.
- Kolluri N, Sun Z, Sampson AR, Lewis DA (2005) Lamina-specific reductions in dendritic spine density in the prefrontal cortex of subjects with schizophrenia. *Am J Psychiatry* 162:1200–2.
- Konopaske GT, Lange N, Coyle JT, Benes FM (2014) Prefrontal cortical dendritic spine pathology in schizophrenia and bipolar disorder. *JAMA psychiatry* 71:1323–1331.
- Kubicki M, McCarley R, Westin CF, Park HJ, Maier S, Kikinis R, Jolesz FA, Shenton ME (2007) A review of diffusion tensor imaging studies in schizophrenia. *J Psychiatr Res* 41:15–30.
- Kuperberg GR, Broome MR, McGuire PK, David AS, Eddy M, Ozawa F, Goff D, West WC, Williams SC, van der Kouwe AJ, Salat DH, Dale AM, Fischl B (2003) Regionally localized thinning of the cerebral cortex in schizophrenia. *Arch Gen Psychiatry* 60:878–88.
- Landén M, Davidsson P, Gottfries CG, Månsson JE, Blennow K (2002) Reduction of the synaptophysin level but normal levels of glycerophospholipids in the gyrus cinguli in schizophrenia. *Schizophrenia Research* 55:83–88.
- Lewis DA, Glantz LA, Pierri JN, Sweet RA (2003) Altered cortical glutamate neurotransmission in schizophrenia. *Annals of the New York Academy of Sciences* 1003:102–112.
- Loughland C, Draganic D, McCabe K, Richards J, Nasir A, Allen J, Catts S, Jablensky A, Henskens F, Michie P (2010) Australian schizophrenia research bank: a database of comprehensive clinical, endophenotypic and genetic data for aetiological studies of schizophrenia. *Australian & New Zealand Journal of Psychiatry* 44:1029–1035.
- Lynall ME, Bassett DS, Kerwin R, McKenna PJ, Kitzbichler M, Muller U, Bullmore E (2010) Functional connectivity and brain networks in schizophrenia. *The Journal of Neuroscience* 30:9477–9487.
- McGlashan TH, Hoffman RE (2000) Schizophrenia as a disorder of developmentally reduced synaptic connectivity. *Archives of general psychiatry* 57:637–648.
- Mesulam MM (1998) From sensation to cognition. *Brain* 121:1013–1052.
- Moyer CE, Shelton MA, Sweet RA (2015) Dendritic spine alterations in schizophrenia. *Neuroscience letters* 601:46–53.
- Perrone-Bizzozero NI, Sower AC, Bird ED, Benowitz LI, Ivins KJ, Neve RL (1996) Levels of the growth-associated protein gap-43 are selectively increased in association cortices in schizophrenia. *Proc Natl Acad Sci U S A* 93:14182–7.
- Pierri JN, Volk CL, Auh S, Sampson A, Lewis DA (2001) Decreased somal size of deep layer 3 pyramidal neurons in the prefrontal cortex of subjects with schizophrenia. *Archives of general psychiatry* 58:466–473.

- Power JD, Schlaggar BL, Lessov-Schlaggar CN, Petersen SE (2013) Evidence for hubs in human functional brain networks. *Neuron* 79:798–813.
- Rajkowska G, Selemon LD, Goldman-Rakic PS (1998) Neuronal and glial somal size in the prefrontal cortex: a postmortem morphometric study of schizophrenia and huntington disease. *Arch Gen Psychiatry* 55:215–24.
- Rao JS, Kim HW, Harry GJ, Rapoport SI, Reese EA (2013) Increased neuroinflammatory and arachidonic acid cascade markers, and reduced synaptic proteins, in the postmortem frontal cortex from schizophrenia patients. *Schizophrenia Research* 147:24–31.
- Repovs G, Csernansky JG, Barch DM (2011) Brain network connectivity in individuals with schizophrenia and their siblings. *Biol Psychiatry* 69:967–73.
- Rubinov M (2013) Schizophrenia and abnormal brain network hubs. *Dialogues in clinical neuroscience* 15:339.
- Rubinov M, Sporns O (2010) Complex network measures of brain connectivity: uses and interpretations. *NeuroImage* 52:1059–69.
- Scholten LH, Schmidt R, de Reus MA, van den Heuvel MP (2014) Linking macroscale graph analytical organization to microscale neuroarchitectonics in the macaque connectome. *The Journal of Neuroscience* 34:12192–12205.
- Schüz A, Miller R (2002) *Cortical areas: unity and diversity* Conceptual advances in brain research. Taylor & Francis, London; New York.
- Somenarain L, Jones LB (2012) Dendritic and spine alterations in areas 9 and 17 in schizophrenia and huntington chorea and the role of neuroleptic exposure. *Open Journal of Psychiatry* 2:243–248.
- Stephan KE, Baldeweg T, Friston KJ (2006) Synaptic plasticity and dysconnection in schizophrenia. *Biological psychiatry* 59:929–939.
- Sweet RA, Henteleff RA, Zhang W, Sampson AR, Lewis DA (2009) Reduced dendritic spine density in auditory cortex of subjects with schizophrenia. *Neuropsychopharmacology* 34:374–389.
- Tomasi D, Volkow ND (2011) Association between functional connectivity hubs and brain networks. *Cerebral cortex* 21:2003–2013.
- van den Heuvel MP, Kahn RS, Goñi J, Sporns O (2012) High-cost, high-capacity backbone for global brain communication. *Proceedings of the National Academy of Sciences of the United States of America* 109:11372–11377.
- van den Heuvel MP, Mandl RCW, Stam CJ, Kahn RS, Hulshoff Pol HE (2010) Aberrant frontal and temporal complex network structure in schizophrenia: a graph theoretical analysis. *The Journal*

- of neuroscience : the official journal of the Society for Neuroscience* 30:15915–26.
- van den Heuvel MP, Scholtens LH, Feldman Barrett L, Hilgetag CC, de Reus MA (2015) Bridging cytoarchitectonics and connectomics in human cerebral cortex. *The Journal of Neuroscience* 35:13943–13948.
- van den Heuvel MP, Sporns O (2011) Rich-club organization of the human connectome. *The Journal of neuroscience : the official journal of the Society for Neuroscience* 31:15775–86.
- van den Heuvel MP, Sporns O (2013a) An anatomical substrate for integration among functional networks in human cortex. *The Journal of neuroscience : the official journal of the Society for Neuroscience* 33:14489–500.
- van den Heuvel MP, Sporns O (2013b) Network hubs in the human brain. *Trends in cognitive sciences* 17:683–696.
- van den Heuvel MP, Sporns O, Collin G, Scheewe T, Mandl RCW, Cahn W, Goñi J, Hulshoff Pol HE, Kahn RS (2013) Abnormal rich club organization and functional brain dynamics in schizophrenia. *JAMA psychiatry (Chicago, Ill.)* 70:783–92.
- van den Heuvel M, Fornito A (2014) Brain networks in schizophrenia. *Neuropsychology Review* pp. 1–17.
- Van Essen DC, Smith SM, Barch DM, Behrens TE, Yacoub E, Ugurbil K (2013) The wu-minn human connectome project: an overview. *Neuroimage* 80:62–79.
- van Haren NEM, Schnack HG, Cahn W, van den Heuvel MP, Lepage C, Collins L, Evans AC, Hulshoff Pol HE, Kahn RS (2011) Changes in cortical thickness during the course of illness in schizophrenia. *Archives of general psychiatry* 68:871–80.
- Zeba M, Jovanov-Milošević N, Petanjek Z (2008) Quantitative analysis of basal dendritic tree of layer iiic pyramidal neurons in different areas of adult human frontal cortex. *Collegium antropologicum* 32:161–169.
- Zhang H, Schneider T, Wheeler-Kingshott CA, Alexander DC (2012) Noddi: practical in vivo neurite orientation dispersion and density imaging of the human brain. *Neuroimage* 61:1000–1016.

Supplemental Information

of

Associated Microscale Spine Density and Macroscale Connectivity Disruptions in Schizophrenia

Supplemental Methods

Micro-Macro Relationship in the Healthy Brain

Microscale Data

Microscale data on regional variation in cortical neuroarchitectonics involved a collation of data of studies examining the dendritic complexity of layer 3 pyramidal neurons of cortical regions. Data included the collation of documented data across literature studies (Anderson et al., 2009; Garey et al., 1998; Hutsler and Zhang, 2010; Jacobs et al., 1997, 2001; Zeba et al., 2008) (see Table S1), describing data on a) dendritic tree complexity of layer 3 pyramidal neurons including information on 1) total length of the dendritic tree, 2) total number of dendritic segments and 3) total mean segment length of a dendritic branch and b) information on the number of synaptic contact points on these dendritic segments including information on 4) total estimated spine count and 5) density of spines per dendritic segment (Figure 1B). Data from literature was included when the original report included 1) measurements on spine-density (the primary research question), 2) a clear description of the examined cortical region was provided in the published paper (the original reports included a visual representation and/or a detailed textural description of the cortical patch examined) (see Table S1), 3) a clear mentioning of the examined cortical patch with respect to the Brodmann Atlas, meaning which Brodmann area (BA) a parcel was situated in, AND 4) when at least one of the reported regions overlapped with regions in one of the other studies. This latter information was used to scale each reported value to the metric scale of the reference dataset of (Jacobs et al., 2001), using the information on brain regions reported in multiple studies, correcting for potential differences in measurement and acquisition methodology across studies. In total, information of microscale data on pyramidal layer 3 dendritic tree complexity of 10 regions, spine count of 10, and spine density of 14 regions (Table S1, Figure 1C-left panel) was collated across studies, with regions spread over all lobes of the cortex (see Figures 1 and 3). Given that each report included a

definition of the examined cortical patch(es) as BAs, each cortical patch was taken as a representative of the mentioned particular BA (Table S1).

Spine Density.

We focussed on spine density as a metric of microscale connectivity as this aspect of microscale connectivity is argued to be predominantly reported to be affected in schizophrenia (see part II of this study below) (Kolluri et al., 2005; Pierri et al., 2001; Rajkowska et al., 1998). Studies reporting on layer 3 pyramidal complexity, but not specifically reporting on level of spine density and/or not reporting quantitative levels were thus not included in our study.

Data Normalization.

In the main text, we note that our collation involved data across studies of multiple research groups, with measurements resulting from different analysis techniques and subjective measurement settings. To be able to analyze aspects of microscale connectivity in relationship to macroscale magnetic resonance imaging (MRI) derived connectivity (i.e. the main goal of part I of our study), data of the different groups were scaled to one another to allow across-study comparison. With data of 10 cortical areas resulting from studies of the Jacobs group using the same Golgi staining technique (Anderson et al., 2009; Jacobs et al., 1997, 2001) and with data of 4 regions resulting from three other groups using different techniques (Hutsler and Zhang, 2010; Zeba et al., 2008), data of the Hutsler, Garey and Zeba studies were scaled to the Jacobs data. This scaling could be performed as the Hutsler (besides reporting on BA7 and BA9), Garey (besides reporting on BA38) and Zeba (besides reporting on BA9 and BA45) studies report on density measurements of an overlapping region as reported by the Jacobs study (region BA22, BA11, BA4 respectively). Based on this overlap, a study specific *scaling factor* was determined as the ratio of reported values between respectively the Hutsler (Hutsler and Zhang, 2010), Garey (Garey et al., 1998), and Zeba (Zeba et al., 2008) study and the Jacobs study (Jacobs et al., 1997, 2001), and these scaling factors were applied to the data of the other regions reported in these three studies (see Table S1, and see Table S7 and Table S8 for the original values and the computed scaling factors). Bringing the data of the Hutsler, Garey and Zeba studies into the same scale of the Jacobs studies allowed for a comparison of data across studies, and thus our aimed meta-regression type of analysis of comparing this data with data on macroscale connectivity. We note that excluding spine data of the Hutsler, Garey, and Zeba studies – performed in a post-hoc analysis to verify that the described scaling procedure did not in any way drive our main effect – still revealed in a significant positive micro-macro interaction (see Supplemental Results). Furthermore, we also note that due to the need of this scaling procedure, only data of studies that reported on at least one overlapping region with the Jacobs studies could be included in our analysis. Data on cortical spine density of studies that

reported on quantitative data on a single cortical area (for example, the Somnarain study (Somnarain and Jones, 2012) and/or the Konopaske study (Konopaske et al., 2014), see Table S3) could thus not be included, as no scaling-factor could be computed. In all, data involved a collation of the quantitative measurements on spine density of layer 3 pyramidal neurons across 14 cortical areas (Table S1).

Cortical Mapping.

Reported spatial locations of the cortical patches were mapped to corresponding cortical regions of the Desikan-Killiany atlas used for diffusion-weighted MRI (DWI) connectome reconstruction (see below) (Table S1): For each reported histologically examined cortical patch, the spatial location was manually mapped onto a surface rendering of the left hemisphere, using the anatomical information as provided in the original report (Table S1, see above). This location was overlapped with the $n = 57$ left hemisphere cortical parcels of the Desikan-Killiany atlas fitting the surface rendering. Figure 1C shows the one-to-one mapping of the 14 collated cortical patches onto the cortical surface, and their selected overlapping cortical parcel of the Desikan-Killiany atlas. Table S1 summarizes the one-to-one mapping of each of the reported cortical patches, their reported BA region, their overlapping region in the Desikan-Killiany atlas and the original description of the anatomical location as provided in the original reports.

Macroscale Connectome Reconstruction

A macroscale human cortical connectome map was reconstructed on the basis of high-resolution DWI data of the Human Connectome Project (Van Essen et al., 2013), including data of 215 subjects (Q3 release, voxel-size 1.25 mm isotropic, TR/TE 5520/89.5 ms, 3 runs of 90 diffusion directions with diffusion weighting 1000, 2000 and/or 3000 s/mm²). Preprocessing involved realignment, correction for eddy current and susceptibility distortions (see (Glasser et al., 2013) for details). Per individual dataset, tissue classification and cortical parcellation was performed on basis of a high-resolution T1 anatomical image (Q3, voxel size: 0.7 mm isotropic), dividing the cortex into 114 distinct regions (57 unique regions per hemisphere) using a subdivision of FreeSurfer's Desikan-Killiany atlas. White matter pathways were reconstructed using generalized Q-sampling imaging (GQI), allowing for the reconstruction of complex diffusion fiber configurations (i.e., crossing/kissing fibers), and streamline tractography (de Reus and van den Heuvel, 2014; Yeh et al., 2010). A streamline was started in each white matter voxel, following the most matching diffusion direction from voxel to voxel until a streamline reached the gray matter, exited the brain tissue, made a turn of > 45 degrees or reached a voxel with a low fractional anisotropy ($< .1$). In the HCP data a single streamline was seeded from each voxel, due to the high spatial resolution of the diffusion data (1.25 mm isotropic voxels versus typical (and also in our patient-control sample, see below) 2 mm isotropic voxels). A binary structural connectivity matrix of

size $N \times N$ was formed, selecting from the total collection of reconstructed tractography streamlines those that touched both regions i and j , for all pairs (i, j) of the $N = 1$. In addition, a weighted connectivity matrix was formed by taking the strength of reconstructed region-to-region connections as the number of tractography streamlines (NOS) between i and j . In addition, with regional volume of regions noted to have an effect on the probability and number of streamlines interconnecting regions i and j (Hagmann et al., 2008), we also assessed strength as streamline density, computed as the number of reconstructed streamlines between i and j , divided by the average volume of i and j . Next, a group-averaged structural connectivity (SC) matrix was formed by taking the non-zero mean of the individual matrices, including a connection between brain regions when it was found in at least two-thirds of the total group of 215 subjects (Figure 1B, left panel).

Macroscale Functional Connectivity

Functional connectivity between each of the 114 cortical regions was assessed by means of analysis of the resting-state fMRI data of the HCP (Q3 release, voxel-size 2 mm isotropic, TR/TE 720/33.1 ms, 1200 volumes, 14:33 minutes). Images were realigned, co-registered with the T1 image, filtered (0.03 - 0.12 Hz), corrected for global effects of motion (realignment parameters), global signal mean, ventricle and white matter signal by means of linear regression and “motion-scrubbed” for potential movement artifacts (Power et al., 2012). Average time-series of the cortical regions (being identical to the SC reconstruction) were computed by averaging the time-series of the voxels in each of the cortical regions, and functional connectivity between all region pairs was derived by means of correlation analysis. A group-averaged weighted functional connectivity (FC) matrix was formed by averaging the individual matrices (Figure 1B, right panel).

Macroscale Connectome Organization

Network Metrics. With the SC matrix reflecting a mathematical graph of nodes (i.e., the set of cortical regions) and edges (i.e., the reconstructed anatomical connections between regions), nodal degree k described the total number of undirected connections of a region, providing a metric of how well a node is connected to the rest of the network. In addition, nodal strength was computed as the sum of the total weight of the connections of a region (both NOS and SD were examined). Nodal clustering C was computed as the ratio between closed and possible number of triangles around a node, with higher levels of C reflecting a higher level of local connectedness. The metric of nodal shortest path length L described the average minimum number of steps needed to travel from a node to the other nodes in the network, and is often interpreted as an (inverse) metric of the global communication efficiency of a node (Rubinov and Sporns, 2010). C and L were computed on binary networks.

Functional Communities.

Functional communities were determined on the basis of modular decomposition of the FC matrix (Louvain method, 1,000 runs (Rubinov and Sporns, 2010)). A two-stage approach was used, in which each detected functional community was made subject to a second modular decomposition, identifying sub-communities (Scholtens et al., 2014). With communities describing functional subdomains and the SC matrix describing the structural connections between cortical brain areas, the structural-functional intermodular connectivity profile of a node was assessed by means of computation of the nodal participation coefficient P_i , reflecting the level of partitioning of the connections of a node across the set of modules (Rubinov and Sporns, 2010; van den Heuvel and Sporns, 2013).

Hub Formation.

Hub nodes were selected as the set of top 30% nodes with the highest degree (overlapping $k > 12$) (van den Heuvel et al., 2012). Peripheral non-hub regions were selected as the lowest 70% of nodes of the network. Rich club organization describing the phenomena of nodes of increasing degree to show a denser level of mutual connectivity than expected based on their degree alone was assessed for reference (van den Heuvel and Sporns, 2011). For this, for each level of degree k , the subgraph S_k was selected from the total graph, consisting of all nodes $N > k$ with a degree $> k$. The rich club coefficient $\Phi(k)$ was then computed as the ratio between the number of connections $E > k$ present in subgraph S_k and the total number of possibly occurring connections in S_k being $(N > k \times N > k - 1)$. For all levels of k , $\Phi(k)$ was compared to the rich club coefficient(s) $\Phi_{random}(k)$ computed for a (set of) randomly organized network(s) (Colizza et al., 2006). A set of 1,000 random graphs were formed, randomly rewiring the connections of the main graph, preserving the degree of each node in the network (Maslov and Sneppen, 2002). A network is said to display a rich club organization if $\Phi(k)$ exceeds $\Phi_{random}(k)$ (or equally $\Phi(k)/\Phi_{random}(k) > 1$) for a range of k . A detailed formal description of the computation of a rich club organization is given in (Colizza et al., 2006; van den Heuvel and Sporns, 2011).

Statistical Analysis

Associations between macroscale connectome organization and microscale pyramidal complexity were examined by means of correlation analysis. Given that our study was to examine micro-to-macro relationships, analysis included the assessment of correlations between 5 microscale and 4 macroscale metrics, describing a total set of 20 possible micro-to-macrometric associations (Figure 1D). This yielded the need for proper correction for multiple testing (Scholtens et al., 2014). Considering the presence of high intra-class correlations (correlation coefficients microscale mean/std: .62/.23; macroscale: .51/.16) a correction method controlling for type I errors whilst avoiding

the inflation of type II error (i.e., avoiding missing true positive effects) is needed. A false discovery rate (FDR) corrected alpha level ($q = .05$) taking into account intra-class correlations was computed, yielding an FDR threshold of $p = .033$. To achieve family-wise error control across the study, also a more strict partial Bonferroni correction threshold was determined based on the number of effective tests (M_{eff}) performed, computed on the basis of a principal component analysis (PCA) of the data (Gao et al., 2008). Determination of the number of PCA components together explaining $> 95\%$ of the variance within each metric class resulted in respectively 3 components for the class of microscale and 2 components for the class of macroscale metrics, and M_{eff} was computed as the product of these numbers, resulting in a partial Bonferroni corrected alpha level of $.05/(3 \times 2) = .0083$. Effects reaching the more strict partial Bonferroni corrected alpha were taken as statistically significant; correlations reaching FDR were taken as trend-level effects.

Part II: Relationship Between Disease Related Changes in Spine Density and Changes in Macroscale Connectivity in Schizophrenia

Microscale Spine Density Data

Layer 3 Pyramidal Spine Density Reductions.

Data on cortical spine density measurements in schizophrenia were collated from literature. A PubMed search revealed in total 5 studies reporting on pyramidal layer 3 spine density reductions in schizophrenia (Garey et al., 1998; Glantz and Lewis, 2000; Konopaske et al., 2014; Somenarain and Jones, 2012; Sweet et al., 2009) (Table S3). Supragranular layer 3 is a major target and source layer of cortico-cortical white matter pathways (Kandel et al., 2000; Schüz and Miller, 2002), forming one of the primary layers for cortico-cortical communication, and therefore a primary target for studies examining spine density alterations in schizophrenia (see also discussion on potential specificity of pyramidal spine density reductions to this layer). From these 5 patient-control studies, of in total 7 Brodmann areas the percentage of change in layer 3 spine density between patients and healthy matched controls was collated. All studies provided a description of the anatomical locations of the examined cortical patches in text and/or visual representation, as well as reporting the corresponding Brodmann area according to the Brodmann's cytoarchitectonic atlas (Brodmann, 1909). Reported anatomical locations were mapped to the DK atlas. In cases a reported Brodmann area overlapped multiple DK regions (as listed in Table S3), this point was still taken as a single observation, with the level of macroscale connectivity across these DK regions was averaged in the micro-macro cross-scale regression analysis. Data was collated of cortical areas – as documented by these studies – BA 9, 10 and 46 in the frontal lobe, BA 17 in the occipital lobe and 38, 41 and 42 in the temporal lobe (Table S3). Of these

5 studies, 1 study used Golgi-Cox staining, 4 used rapid Golgi staining and 1 study used immunohistochemistry. Table S3 summarizes the information of the examined postmortem cortical tissue samples, their reported BA location, their reported group effect size in percentage of change, the number of included subjects, and the original literature source.

Part II: Layer Non-Specific Microscale Alterations

Besides techniques for the specific examination of spine effects of layer 3 pyramidal neurons, changes in microscale connectivity in schizophrenia have also been reported by studies using synaptophysin immunostaining techniques examining spine effects across all six layers of cortex combined. Synaptophysin is a protein that is present in virtually all presynaptic terminals of the central nervous system and this ubiquity at the synapse makes the measurement of synaptophysin a fast quantification method for the measurement of synapse density in postmortem tissue (see for review (Calhoun et al., 1996)). As such, the majority of synaptophysin immunostaining studies have reported on synapse reductions across entire examined volumes, that is, of reductions in estimated synapse effects across all layers of the cortex combined. In a PubMed search we found 11 additional studies reporting on synapse levels in cortical regions by means of synaptophysin immunostaining of postmortem brain material (listing (Davidsson et al., 1999; Eastwood and Harrison, 1995; Eastwood et al., 2000, 1995; Glantz and Lewis, 1997; Honer et al., 1997; Karson et al., 1999; Landén et al., 2002; Perrone-Bizzozero et al., 1996; Rao et al., 2013)). In a second analysis, we collated the results of these studies (summarized in Table S5), again collating information on between-group differences in synapse levels in patients compared to controls, measured by the reported percentage of change in patients as compared to the population of control participants. Disease-related percentage of synapse reduction of 12 BA regions of human cortex could be extracted across these studies (see Table S5). The cortical locations as reported in the original papers were mapped to cortical parcels of the Desikan-Killiany atlas using the same procedure as described above (Figure 7-A shows the mapping of the regions). Next, similar to in the layer 3 specific analysis, spine data was cross-referenced with between-group differences in macroscale connectivity as derived from the DWI data (see below).

Magnetic Resonance Imaging Data

Participants.

MRI data was acquired of 61 patients with schizophrenia and 55 age and gender matched healthy controls, involving a (partly overlapping) MR dataset described and examined in context of affected hub connectivity in schizophrenia by Van den Heuvel et al. (van den Heuvel et al., 2013). Table S6 summarizes the demographics of the patients and healthy control subjects. Patients underwent psychiatric assessment

procedures using the Comprehensive Assessment of Symptoms and History at the University Medical Center Utrecht. Diagnostic consensus of patients was achieved in the presence of a psychiatrist with the DSM-IV criteria for schizophrenia. All patients and controls provided written informed consent before study participation (van den Heuvel et al., 2013). Using the exact same dataset as in (van den Heuvel et al., 2013) resulted in similar findings.

MR Acquisition.

MRI data was acquired on a 3 Tesla Philips Achieva scanner with an eight-element SENSE receiver head-coil. Data acquisition included the acquisition of a T1 scan (3D FFE using parallel imaging, TR/TE 10 ms/4.6 ms, 200 slices, 0.75 mm voxel size) and a DWI scan (2 sets each consisting of 5 diffusion unweighted B=0 volumes (b-factor = 0 s/mm²) and 30 diffusion weighted volumes (b-factor = 1000 s/mm²) (parallel imaging SENSE p-reduction 3; TR/TE = 7035/68 ms, 2 mm isotropic voxel size, 75 slices, second set with reversed k-space read-out) (van den Heuvel et al., 2013).

Macro-Scale Anatomical Connectivity.

Individual white matter connectivity maps were derived from the DWI data (van den Heuvel et al., 2012), combined with the 114 region Desikan-Killiany atlas (see above). For each individual dataset, DWI images were corrected for small head movements, corrected for susceptibility distortions (by computing a field distortion map based on the two unweighted B0 images (Anderson et al., 2009)) and realigned with the averaged B=0 image. The T1 and individual parcellation atlas were registered to the B=0 image for anatomical reference (see (van den Heuvel et al., 2012) for a detailed description of the DWI protocol and preprocessing). Next, using the DWI data, white matter pathways were traced by reconstructing the diffusion orientation in each voxel using compressed sensing for DWI (Landman et al., 2012) (enabling the reconstruction of complex diffusion fiber configurations), followed by a variant of deterministic streamline tractography allowing for multiple fiber configurations (de Reus and van den Heuvel, 2014). For each individual dataset a total collection of streamlines was formed, starting 8 streamlines in each white matter voxel and following the most matching diffusion direction from voxel to voxel until one of the stopping criteria was reached: 1) streamline reached the gray matter, 2) exited brain tissue, 3) made a turn of > 45 degrees and/or 4) reached a voxel with a low fractional anisotropy ($< .1$). Next, for all pairs of cortical regions i and j of the parcellation atlas, from the total collection of reconstructed streamlines those streamlines that touched both region i and region j were selected and the streamline count (NOS) and density (SD computed as the number of streamlines divided by the average cortical volume of region i and j) were computed and stored in cell entry (i, j) of the connectivity matrix (SC) (Hagmann et al., 2008; van den Heuvel et al., 2012). Pathways of > 30 (other thresholds, e.g. 25

revealed similar findings) fiber streamlines were taken as a region-to-region connection in the SC matrix, minimizing the influence of potential false positive reconstructions (de Reus and van den Heuvel, 2013; Hagmann et al., 2008). Next, from these individual SC matrices, for each subject the average level of connectivity strength per cortical region was computed as the non-zero mean of NOS and SD of the reconstructed cortico-cortical pathways of a region.

Statistical Analysis.

Patient-to-control between-group analysis involved the computation of the group average effect sizes in regional connectivity strength in percentage of changes as compared to the group of controls.

Cortical Mapping

Similar to part I, anatomical overlap between the locations on the cortex examined in the histological studies (Table S3 and Table S5) and the cortical atlas used for macroscale network reconstruction was enabled by a one-to-one mapping of the reported anatomical locations examined in the histological studies to the regions defined in the Desikan-Killiany atlas. Each of the histological studies included a detailed textual description and/or visual representation of the examined cortical regions across patients and controls, as well as described the examined regions in reference to Brodmann areas. These descriptions were used to pinpoint the examined locations on a surface representation of the cortex by two experts in brain anatomy (LHS and MPvdH) (see Figure 5 and Figure 7) and the matching region(s) of the $n = 114$ cortical patches were then selected as the corresponding region(s) in the Desikan-Killiany atlas.

Micro-to-Macro Cross-Scale Analysis

To assess a possible relationship between effect-sizes of between-group differences in micro- and macroscale values of connectivity, the region-wise between-group effect sizes of (layer 3 and layer non-specific) spine density levels were correlated with region-wise between-group effect sizes in macroscale connectivity (i.e., control-to-patient differences in NOS, SD values, averaged over left and right hemisphere regions) and between-group effect sizes in cortical thinning using Pearson's correlation.

Supplemental Results

Part I: Macroscale Connectome Organization

The healthy macroscale anatomical brain network, derived from high resolution HCP DWI data, showed a high level of local clustering (mean over the set of nodes/std: .48/.12; 4.71x higher than in random networks, 1,000 random networks, $p < .001$) and short communication paths (mean/std: 2.75/.29; 1.24x longer than in random

networks, $p < .001$). The reconstructed connectome further showed rich club formation (meaning that the level of connectivity between high degree nodes $\Phi(k)$ was higher than expected by chance level for a range of $10 < \text{degree } k < 16$ ($p < .0025$, Bonferroni corrected, 1,000 random networks). High degree rich club hub nodes overlapped subparts of the precuneus, posterior cingulate, rostral middle frontal, superior frontal, inferior and superior parietal, ventral superior temporal gyrus, isthmus cingulate, anterior ventral part of the precentral gyrus (overlapping regions FB and FCBm (Von Economo and Koskinas, 1925)) and insular cortex (see Figure S2), findings highly consistent with previous reports on hub formation of human cortex (e.g., (Hagmann et al., 2008; van den Heuvel et al., 2012; Zalesky et al., 2010)). FC analysis revealed a pronounced hierarchical modular organization, comprising 3 main functional communities (first stage) and respectively 5, 4 and 4 sub-communities (second stage community structure). Taking these functional subsystems as a modular partitioning of the brain, hub nodes showed a significantly higher intermodular connectivity profile P_i (1.69x higher, $p < .001$, based on second-stage modules) and a significantly shorter path length L_i (.85x shorter, $p < .001$) than sparsely connected peripheral nodes.

Part I: Partial Least Squares Regression

Post-hoc partial least squares regression (PLS) with the total set of microscale metrics (5 metrics) set as predictors and macroscale metrics (4 metrics) set as responses also revealed a significant micro-macro association. Fitting 2 PLS components of microscale metrics explained 73.29% of the variance in macroscale metrics ($p = 1.0265 \times 10^{-10}$). Fitting of other number of components revealed similar findings (1 component: 59.29%, 1.121×10^{-10} ; 3 components: 80.82%, 1.3675×10^{-11} ; 4 components: 85.91%, 5.884×10^{-15}).

Part I: Analysis With Other Group Thresholds

A group-averaged consensus connectivity matrix was formed by taking the non-zero mean over the 215 individual connectivity matrices of the HCP data, with pathways included that were observed in two-thirds of the total population, yielding a group-threshold G of 66%. Using different group-thresholds revealed similar micro-macro correlations. For example, setting G to 20% (density of consensus matrix of 21.29%) also showed (some trend-level) correlations between macroscale degree microscale spine count ($r = .46$, $p = .0958$), spine density ($r = .69$, $p = .0273$), dendritic tree length ($r = .65$, $p = .0419$) and segment length ($r = .67$, $p = .0345$ trend-level). Setting G to 80% (density of consensus matrix of 7.5%) also showed (some trend-level) correlations between macroscale degree microscale spine count ($r = .46$, $p = .0960$), spine density ($r = .59$, $p = .0693$), dendritic tree length ($r = .70$, $p = .025$ trend-level), segment count ($r = .65$, $p = .0431$) and segment length ($r = .55$, $p = .0964$).

Part I: Analysis With the Control Data of Patient-Control Study

HCP data and matching reconstruction methodology was used to assess regional macroscale connectivity of the healthy brain in part I of our study, with the high-resolution HCP data providing a large (215 subjects) and high-quality dataset for connectome reconstruction. In a post-hoc analysis we examined the observed micro-macro associations using the DWI data of the healthy control group as included in part II of our study (55 healthy controls). Using this alternative dataset the same micro-macro correlations could be observed. Network degree across the two datasets correlated strongly ($r = .75, p < .0001$) and as a result regional degree as derived from the group-averaged SC matrix (20% group threshold, matrix density 19%) of the healthy control dataset correlated significantly with microscale spine count ($r = .79, p = .0065$), spine density ($r = .61, p = .0204$), dendritic tree length ($r = .62, p = .0549$ trend-level) and segment length ($r = .68, p = .031$ trend-level).

Part I: Analysis With Only Data of the Jacobs Group (Excluding the Hutsler, Garey and Zeba Studies)

Collation of spine density data across literature involved the grouping of data across multiple studies. However, with different studies using different types of techniques, spine density values can vary widely across studies, with data being highly dependent on measurement technique. To still allow cross-study comparison a scaling-factor was computed based on the Hutsler (Hutsler and Zhang, 2010), Garey (Garey et al., 1998), and Zeba (Zeba et al., 2008) studies reporting on at least one overlapping region also examined in the Jacobs studies (Anderson et al., 2009) (see main text, and Table S7 and S8 for this scaling factor, and Table S1 for the different types of measurement techniques used). After this scaling, spine-density values of the other BA regions examined by the Hutsler (Hutsler and Zhang, 2010), Garey (Garey et al., 1998), and Zeba (Zeba et al., 2008) studies indeed well fitted within the range of the reported values of the Jacobs group. Nevertheless, to verify that this scaling effect did not influence our main finding of an association between regional variation in layer 3 pyramidal spine density and DWI derived macroscale connectivity (part I of our study), post-hoc analysis was performed in which data of the Hutsler (Hutsler and Zhang, 2010), Garey (Garey et al., 1998), and Zeba (Zeba et al., 2008) were excluded. A leave-out-study analysis in which we excluded the data of the Hutsler (Hutsler and Zhang, 2010), Garey (Garey et al., 1998), and Zeba (Zeba et al., 2008) study one by one was performed. In all three cases ($p = .0157, r = .67$; $p = .0076, r = .70$; $p = .0054, r = .72$ respectively) the main effect of an association between layer 3 pyramidal spine density and macroscale connectivity remained. Excluding data of all three studies altogether (and thus including only data of the Jacobs group) still revealed a micro- macro correlation at trend-level ($p = .0135, r = .75$, only 10 of the 14 cortical regions remaining).

Part II: Analysis Excluding the Somenarain (2012) and/or Sweet (2009) Study

The Somenarain (Somenarain and Jones, 2012) and Sweet (Sweet et al., 2009) studies used different techniques (Golgi-Cox staining, and spinophilin immunoreactivity, respectively, see Table S4) as compared to the other studies (using Golgi). To verify that this could not have driven our results, in a post-hoc analysis the data of the Somenarain (Somenarain and Jones, 2012) and Sweet (Sweet et al., 2009) studies were excluded. First, a leave-one-study-out analysis was performed. Excluding the data of the Somenarain study again revealed a positive correlation between between-group differences in spine density reduction and macroscale connectivity in schizophrenia (NOS: $r = .92$, $p = .0264$; SD: $r = .89$, $p = .0448$). Excluding the data of the Sweet study (2009) revealed similar findings (NOS: $r = .93$, $p = .0074$; SD: $r = .91$, $p = .0114$). Excluding data of both studies still revealed a positive relationship (but now at trend-level p -values, as only 4 data points could be included) between between-group differences in spine-density reductions in schizophrenia and between-group differences in DWI derived macroscale connectivity (NOS: $r = .91$, $p = .083$; SD: $r = .93$, $p = .074$).

Part II: Analysis of Medication Effects

All schizophrenia patients used medication. With medication dose having potential effects on brain connectivity (potentially on both the micro- and macroscale level), this could constitute a confound in our observed micro-macro observations. To examine such an effect, we performed a post-hoc analysis in which the patient macroscale connectivity data was corrected for haloperidol equivalent dose (HEQ). Note that, due to the meta-analysis nature of the microscale data (with data on regional patient-control differences collated across reports in literature) no correction on medication was possible. Table S6 lists an overview of type of medication used and the dose in HEQ of the (as compared to the microdata separately) 61 patients of by whom T1 and DWI data was acquired. Correction for medication was performed by regressing out HEQ out of the regional levels of macroscale connectivity (NOS and SD) across the group of patients by means of regression analysis, before computing group-differences in regional macroscale connectivity as percentage of change of the patient population as compared to the healthy control population. No clear associations between HEQ and regional macroscale connectivity was observed (4 regions showed a potential effect showing an association with a liberal p -value $< .05$ (FDR correction)). As a result, after correction for HEQ all micro-macro associations remained significant: The association between group-differences in layer 3 spine density and macroscale DWI connectivity remained significant (NOS: $p = .0032$; SD: $p = .0033$). Similarly, the reported correlation between group-differences in layer non-specific effects and macroscale DWI connectivity also remained significant (NOS: $p = .0002$; SD: $p = .0018$), suggesting

that the reported micro-macro associations are likely not driven by medication effects.

Part II: Post-hoc Comparison Between Regional Changes in Dendritic Tree Size and Macroscale Connectivity in Schizophrenia

Besides effects in spine density, a few studies have reported significant reductions in the size of the dendritic trees of layer 3 pyramidal neurons in patients as compared to controls. A PubMed search revealed 3 studies reporting on dendritic tree alterations across 3 cortical regions (BA 46, 11 and 17) (Glantz and Lewis, 2000; Kalus et al., 2000; Konopaske et al., 2014), and interestingly, cross-referencing these reduction levels with level of macroscale DWI connectivity indeed revealed a positive staircase pattern, suggesting larger alterations in dendritic tree size to go possibly hand in hand with larger changes in macroscale connectivity (Figure S3). General caution is of course needed because of the sparse cortical sampling, but our findings in part I of this study indeed suggest a general correlation between layer 3 pyramidal complexity and macroscale connectivity, an observation also made for the macaque cortex (Scholtens et al., 2014).

cortical mapping of layer 3 spine data in schizophrenia

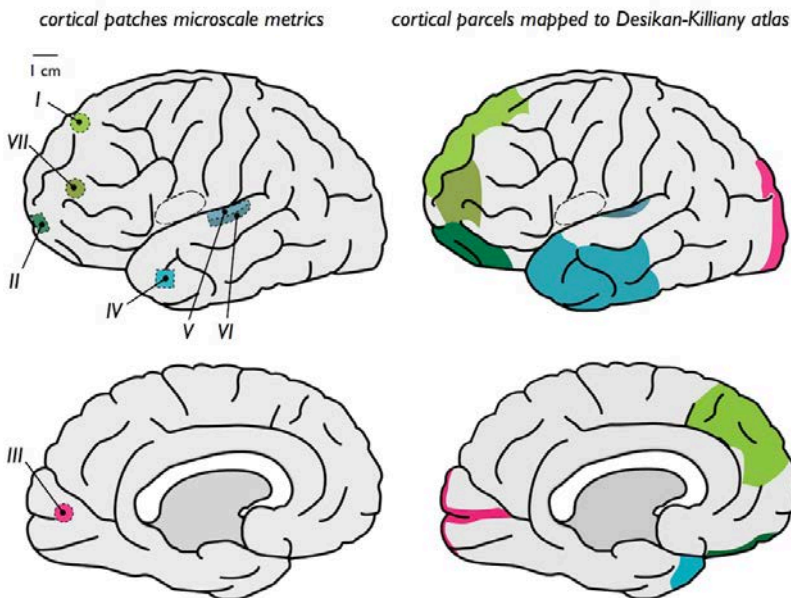


Figure S1. Figure illustrates the mapping of the cortical areas examined in the histological studies to regions of the Desikan-Killiany atlas. Cortical areas of which layer 3 pyramidal spine density was examined are shown in the left panel, their overlapping cortical regions in the Desikan-Killiany atlas are depicted in the right panel. Roman numbers correspond to the region descriptions in Table S3.

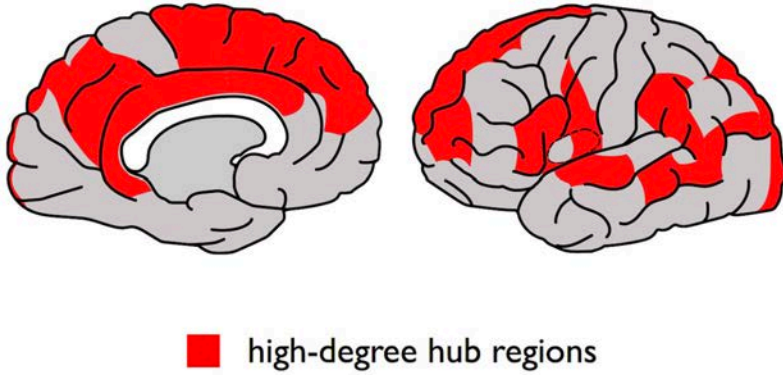


Figure S2. Hub regions of the human cortex as derived from the HCP DWI data of the total Desikan-Killiany 114 cortical area parcellation, depicted on the left hemisphere.

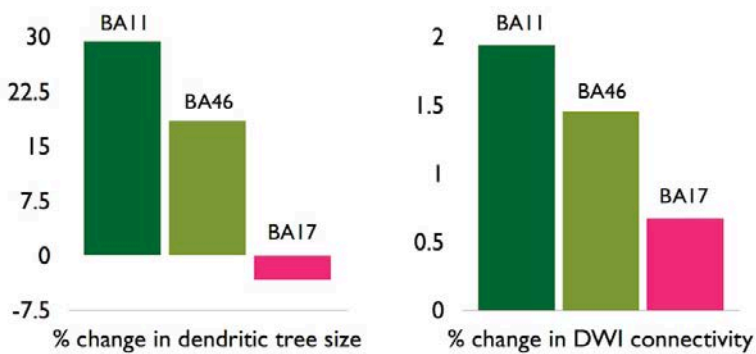


Figure S3. Between-group differences in dendritic tree size (left panel) of cortical regions BA 46, 11 (frontal cortex) and 17 (visual cortex) as reported by literature and between-group differences in macroscale connectivity strength of these regions (right panel) as derived from diffusion MR imaging.

Table S1. Microscale regions and mapping to the MRI Desikan-Killiany atlas.

Region	Brodman Area	MRI Cortical Region of Desikan-Killiany Atlas	Spine Density (per 10 μm)	Dendritic Length (x 1000 μm)	Mean Segment Length	Segment Count	Spine Number (x1000)	Source	Location Description
I	3-1-2	postcentral gyrus	1.9000	3.1914	63.5300	50.5400	0.8158	Jacobs (2001)	Postcentral gyrus 2-3 cm from midline along dorsolateral convexity
II	4	precentral gyrus	2.1000	3.5759	68.3300	52.6200	0.9039	Jacobs (2001)	Precentral gyrus 2-3 cm from midline along the dorsolateral convexity
III	6	superior frontal gyrus (DK superior frontal 3 and 4)	2.2000	4.1247	72.6500	57.6700	1.1253	Jacobs (2001)	Superior frontal gyrus anterior to the paracentral lobule on the medial surface of the hemisphere
IV	7	anterior superior parietal gyrus	1.9740	nr	nr	nr	nr	Hutsler (2010) ^a	Superior parietal lobule, posterior but not adjacent to the primary sensory cortex and lateral from the longitudinal fissure by 5 cm
V	9	rostral middle frontal gyrus	1.9683 ^d	nr	nr	nr	nr	Hutsler (2010) ^a and Zeba (2008) ^a	Hutsler: Anterior portion of the first frontal convolution, anterior to the premotor cortex and lateral front the longitudinal fissure by 5 cm; Zeba: Left superior frontal gyrus
VI	10	anterior superior frontal gyrus	2.5000	4.1847	69.6850	60.3750	1.3198	Jacobs (2001), Jacobs (1997) ^c	Superiorly from the frontal pole, 1.5 cm from midline and 3-4 cm superior to the orbitomedial surface
VII	11	anterior rostral middle frontal gyrus	2.2000	3.9901	70.5400	57.1600	1.1378	Jacobs (2001)	1.5 cm lateral from midline and along the anterior-most portion of the lateral orbital gyrus
VIII	13	posterior insular cortex	2.5333	3.7463	72.2000	52.8667	1.2537	Anderson (2009) ^b	Secondary gyrus brevis and pre/posterior insular gyrus
IX	18	middle occipital gyrus	2.1000	3.5633	64.8900	55.6400	0.9333	Jacobs (1997)	1.5 cm to the inferior surface of the occipital lobe and 2 cm from the midline
X	22	posterior superior temporal gyrus	2.1000	3.3027	68.1400	49.0300	0.9039	Jacobs (2001)	Adjacent with the posterior edge of the antero-lateral tip of the primary transverse gyrus of Heschl
XI	38	temporal pole	2.1338	nr	nr	nr	nr	Garey (1998) ^a	Temporal pole
XII	39	posterior supramarginal gyrus	2.2000	4.0821	71.5300	57.5300	1.1772	Jacobs (2001)	Angular gyrus, lobule surrounding the ascending posterior segment of the parallel sulcus
XIII	44	parsopercularis	2.0000	3.919	71.0500	56.0100	1.0205	Jacobs (2001)	Opercular portion of the inferior frontal cortex
XIV	45	parsorbitalis	2.1	nr	nr	nr	nr	Zeba (2008) ^{a,c}	Triangular part of inferior frontal gyrus from both hemispheres

^a Layer 3 pyramidal complexity values scaled to metric scale used by Jacobs et al. (1997, 2001) (see methods and Tables S7 and 7).

^b Anderson et al. (2009) report on three small subregions of the insula, of which data was averaged into a single regional average for analysis.

^c Average over the reports in the two studies was taken.

^d Zeba (2008) studied pyramidal neurons in the deeper layer 3c specifically, with the other studies reporting on pyramidal neurons in the upper layer 3 (Anderson et al., 2009), or not otherwise specified (Garey et al., 1998; Hutsler and Zhang, 2010). Deep layer 3c are noted to include generally larger pyramidal cells than upper layers (50) and for this, information on spine density only (as it is normalized to unit size) of (Zeba et al., 2008) could be included in our analysis. Excluding data from the Zeba study all together revealed similar findings.

nr, not reported.

Table S2. Demographics of included studies on healthy layer 3 pyramidal spine density.

Source	<i>N</i>	Age, Mean (SD)	Gender, M/F	Hemisphere, Left/Right	Technique
Anderson (2009)	20	39 (10)	10/10	20/0	modified rapid Golgi (Scheibel and Scheibel, 1978)
Garey (1998)	11	64 (9)	9/2	–	rapid Golgi
Hutsler (2010)	15	32 (15)	15/0	6/9	Golgi-Kopsch technique (Riley, 1979)
Jacobs (1997)	26	57 (22)	13/13	26/0	modified rapid Golgi (Scheibel and Scheibel, 1978)
Jacobs (2001)	10	30 (17)	5/5	10/0	modified rapid Golgi (Scheibel and Scheibel, 1978)
Zeba (2008)	3	41 (4)	2/1	left: BA4, BA9; left & right: BA45	Golgi-Cox

Table S3. Patient-control differences in layer 3 spine density reductions in schizophrenia and mapping to Desikan-Killiany atlas.

Region	Brodmann Area (BA)	Region Desikan-Killiany Atlas	No Participants Examined (Patients/Controls)	% Layer 3 Pyramidal Spine Reduction in Patients	Source	Location Description
I	BA9	rostral superior frontal gyrus	5/5	37.3	Somenarain (2012) ^a	Dorsolateral extent of area 9, on the middle third of the superior frontal gyrus
II	BA10&11	lateral orbital frontal gyrus	3/5	66.2	Garey (1998)	Frontal association cortex
III	BA17	pericalcarine gyrus, lateral occipital gyrus	15/15	13.8, ns	Glantz (2000)	Standardized locations in the primary visual cortex
IV	BA38	temporal pole, rostral middle frontal gyrus, rostral inferior gyrus, rostral inferior temporal gyrus	8/9	54.7	Garey (1998)	Temporal association cortex
V	BA41	transverse temporal gyrus	15/15	27.2	Sweet (2009)	Tissue blocks caudal to the level of the mammillary bodies and rostral to the crux of the fornix
VI	BA42	transverse temporal gyrus	15/15	22.2	Sweet (2009)	Tissue blocks caudal to the level of the mammillary bodies and rostral to the crux of the fornix
VII	BA46	rostral middle frontal gyrus	15/15	21.2	Glantz (2000)	Standardized locations in the DLPFC cortex
			14/19	6.5, ns	Konopaske (2014)	Dorsolateral prefrontal cortex (Brodmann area 46)

Region numbers (Roman numbers) correspond to those shown in Figure 5.

^a study reports on spine count, not spine density. Omitting the data of this study did not change the nature of our findings (see Supplemental Results for this post-hoc analysis).

Table S4. Demographics of included studies on layer 3 spine density reductions in schizophrenia.

Source	N (Schizophrenia Patients / Controls)	Technique	Age, Mean (SD)		Gender, M/F		Hemisphere	
			Schizophrenia Patients	Controls	Schizophrenia Patients	Controls	Schizophrenia Patients	Controls
Garey (1998)	3/5	Golgi	70.7 (5.5)	60.6 (10.9)	3/0	5/0	–	–
	8/9		65.8 (12.2)	63.8 (7.6)	7/1	7/2	–	–
Glantz (2000)	15/15	Golgi	47.7 (10.5)	50.9 (16.2)	7/8	9/6	15/0	15/0
Kolluri (2005) ^b	15/15	Golgi	47.6 (10.5)	50.9 (16.2)	6/8	9/6	–	–
Konopaske (2014)	14/9	Golgi	58.9 (12.6)	56.8 (13.6)	9/5	13/6	5/9	8/11
Somenarain (2012)	5/5	Golgi- Cox	62.2 (7.5)	64.5 (3.5) ^a	2/3	2/0*	–	–
Sweet (2009)	15/15	spinophilin immuno- reactivity	47.5 (6.4)	46.8 (8.3)	9/6	9/6	15/0	15/0

^a Of 3 controls no medical record was reported.

^b This study examined layer 5 pyramidal neurons, of which data was included in the discussion of the manuscript. This study was thus not included in the main analysis of the paper (discussing layer 3 pyramidal spine effects).

Table S5. Patient-control differences in (layer non-specific) spine density alterations as reported by studies using synaptophysin immunostaining.

Region	Brodman Area (BA)	Region Killiany Atlas	Desikan-Killiany Atlas	No Participants Examined (Patients/Controls)	% Synaptophysin Reduction	Source
I	9	rostral superior frontal gyrus		5/4	23.2	Perrone-Bizzozero (1996)
				10/10	15	Glantz (1997)
				10-11 / 9-11	3.5, ns	
II	10/11	superior frontal gyrus		7/10	17.3	Eastwood (2000) Honer (1999)
				6/6	43.7	Perrone-Bizzozero (1996)
				14/12	25	Karson (1999)
				10/10	34	Rao (2013)
III	17	pericalcarine gyrus, lateral occipital gyrus		10/6	35.7	Perrone-Bizzozero (1996)
				10-11 / 9-11	13.9, ns	Eastwood (2000)
IV	20	inferior temporal gyrus		6/4	26.4	Perrone-Bizzozero (1996)
V	21/22	middle temporal gyrus, superior temporal gyrus		13/9	12	Davidsson (1999)
	22/22			13/9	12	Davidsson (1999)
	22			10-11 / 9-11	4.5	Eastwood (2000)
VI	24	caudal anterior cingulate gyrus		18/24	12	Honer (2000)
				10-11 / 9-11	4.04, ns	Eastwood (2000)
VII	32/33	rostral anterior cingulate gyrus		18/12	33	Davissson (1999)
				11/13	28.4	Landn (2002)
VII	39	supramarginal gyrus		15/10	16, trend	Davidsson (1999)
IX	40	inferior parietal gyrus		15/10	16, trend	Davidsson (1999)
X	45	pars triangularis		5/6	19, trend	Davidsson (1999)
XI	45/46	rostral middle frontal		5/6	19, trend	Davidsson (1999)
				10/10	15	Glantz (1997)
				10-11 / 9-11	3.5, ns	Eastwood (2000)
XII	parahippocampal gyrus	parahippocampal gyrus		11/14	19	Eastwood (1995)
				7/13	20, ns	Eastwood (1995)

Table reports the reported location, the mapped region to the Desikan-Killiany MRI atlas, and the reported percentage of change between the patient population and the healthy control. Region numbers (roman numbers) correspond to those shown in Figure 7.

Table S6. Demographics and clinical characteristics of patient and control population.

	Patients (<i>n</i> = 61)	Controls (<i>n</i> = 55)	<i>P</i>
Age in years, mean (SD) [range]	29.4 (7.2) [19.6-47.8]	29.3 (7.7) [19.7-44.8]	.96 ^c
Gender, M/F	46/15	36/19	.24 ^d
Parental education ^a , mean (SD) [range]	5.0 (1.4) [1-7]	5.6 (1.1) [2-7]	.02 ^c
Diagnosis, <i>n</i> (%)			
Schizophrenia	44 (72.1)		
Schizophreniform disorder	3 (4.9)		
Schizoaffective disorder	14 (23.0)		
Duration of illness in years, mean (SD) [range]	6.6 (5.9) [0.1-23.2]		
PANSS total score, mean (SD) [range]	63.0 (11.1) [37-99]		
Antipsychotic medication, <i>n</i> (%) ^b			
Type			
aripiprazole, <i>n</i> (%)	6 (9.8)		
clozapine, <i>n</i> (%)	9 (14.8)		
haloperidol, <i>n</i> (%)	1 (1.6)		
olanzapine, <i>n</i> (%)	16 (26.2)		
penfluridol, <i>n</i> (%)	2 (3.3)		
pimozide, <i>n</i> (%)	1 (1.6)		
quetiapine, <i>n</i> (%)	3 (4.9)		
risperidone, <i>n</i> (%)	7 (11.5)		
zuclopentixol, <i>n</i> (%)	2 (3.3)		
combination of two APs, <i>n</i> (%)	10 (16.4)		
none or unknown, <i>n</i> (%)	4 (6.6)		
Dose			
Total HEQ daily dose, mean (SD) [range]	8.4 (5.6) [2-30]		

^a Parental education: highest education of father or mother, ranging from primary school (1) to university (7).

^b Medication data missing for 4 subjects.

Statistical comparison was performed using ^c analysis of variance and ^d χ^2 test.

^e Combinations include: aripiprazole/haloperidol (*n* = 1), aripiprazole/olanzapine (*n* = 1), aripiprazole/clozapine (*n* = 1), aripiprazole/risperidone, clozapine/haloperidol (*n* = 1), clozapine/olanzapine (*n* = 1), clozapine/quetiapine (*n* = 1), clozapine/risperidone (*n* = 1), olanzapine/risperidone (*n* = 1), quetiapine/pimozide (*n* = 1).

APs, antipsychotics; HEQ, haloperidol equivalent.

Table S7. Computation of scaling factor.

Source	Brodmann Area in Source Study	Spine Reported Source (Spines/10 μ m)	Density in Study (μ m)	Brodmann Area in Jacobs (1997, 2001)	Spine Reported by Jacobs (Spines/10 μ m)	Density Jacobs	Scaling Factor to Jacobs [Ratio: Source/Jacobs]
Hutsler (2010)	22	10		22	2.1		0.21
Zeba (2008)	4	4.4		4	2.2		0.477272727
Garey (1998)	11	29.9		11	2.2		0.073578595

For the Hutsler, Zeba and Garey studies a scaling factor was computed based on an overlapping region with the Jacobs study. Table lists the BA regions and data on which these study scaling factors was computed.

Table S8. Raw and scaled spine density data.

Source	Brodmann Area	Original Spine Density (Spines/10 μ m)	Reported Density (μ m)	Adjusted Spine Density (Spines/10 μ m)	Reported Density (μ m)	Scaling Factor as Based on Overlapping Area as Also Reported in Jacobs (1997, 2001)
Hutsler (2010)	7	9.4		1.9740		0.21
Hutsler (2010)	9	9.2		1.9320		0.21
Zeba (2008)	9	4.2		2.0045		0.50
Garey (1998)	38	29		2.1338		0.07
Zeba (2008)	45	4.3		2.1000		0.50

Table lists the raw and scaled spine density values of the Hutsler, Zeba and Garey studies.

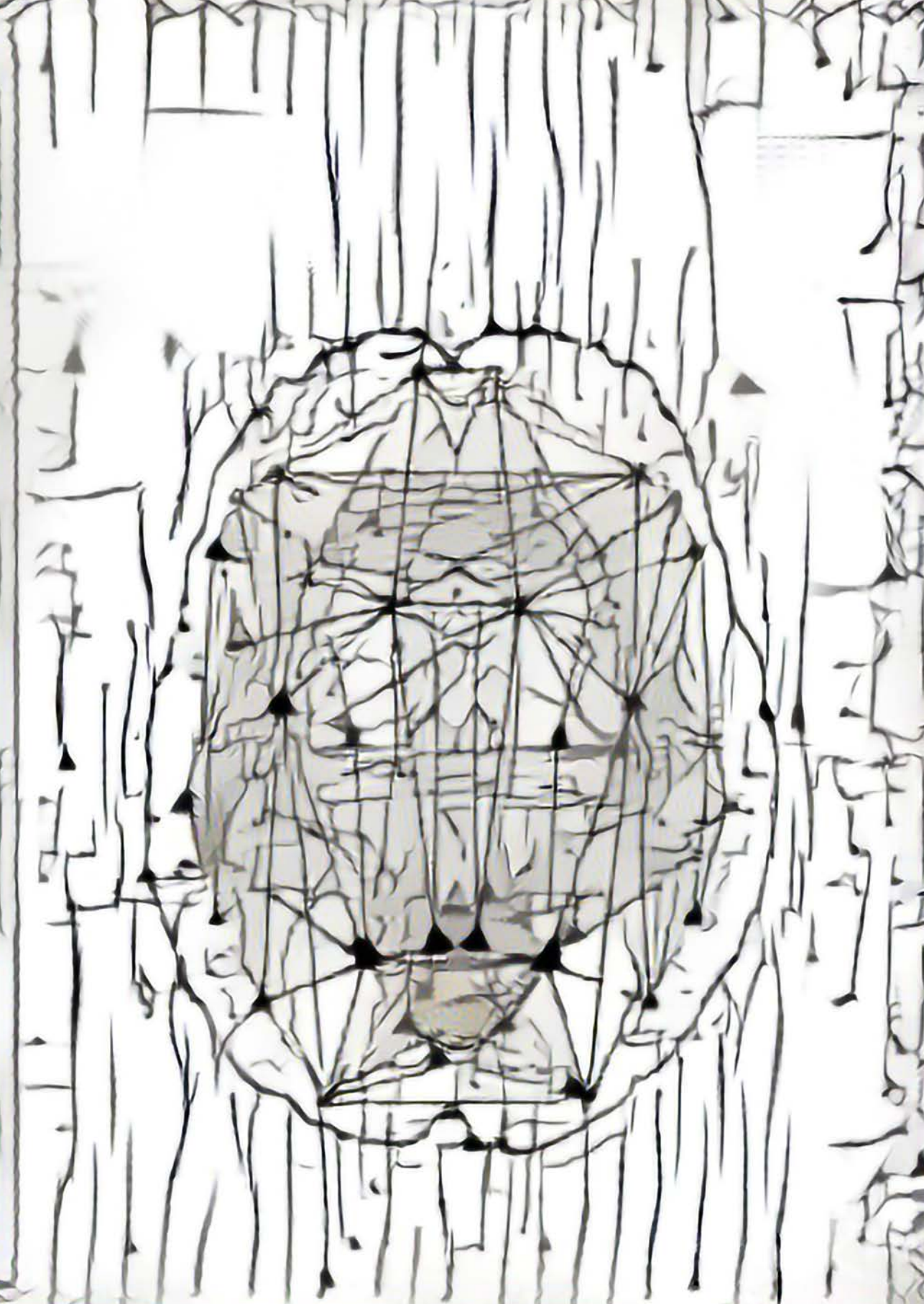
References

- Anderson K, Bones B, Robinson B, Hass C, Lee H, Ford K, Roberts TA, Jacobs B (2009) The morphology of supragranular pyramidal neurons in the human insular cortex: a quantitative golgi study. *Cereb Cortex* 19:2131–44.
- Brodmann K (1909) *Vergleichende Lokalisationslehre der Grosshirnrinde in ihren Prinzipien dargestellt auf Grund des Zellenbaues* Barth.
- Calhoun ME, Jucker M, Martin LJ, Thinakaran G, Price DL, Mouton PR (1996) Comparative evaluation of synaptophysin-based methods for quantification of synapses. *Journal of neurocytology* 25:821–828.
- Colizza V, Flammini A, Serrano M, Vespignani A (2006) Detecting rich-club ordering in complex networks. *Nat Phys* 2:110–115.
- Davidsson P, Gottfries J, Bogdanovic N, Ekman R, Karlsson I, Gottfries CG, Blennow K (1999) The synaptic-vesicle-specific proteins rab3a and synaptophysin are reduced in thalamus and related cortical brain regions in schizophrenic brains. *Schizophrenia Research* 40:23–29.
- de Reus M, van den Heuvel M (2013) Estimating false positives and negatives in brain networks. *Neuroimage* 70:402–9.
- de Reus MA, van den Heuvel MP (2014) Simulated rich club lesioning in brain networks: a scaffold for communication and integration? *Frontiers in Human Neuroscience* 8.
- Eastwood SL, Harrison PJ (1995) Decreased synaptophysin in the medial temporal lobe in schizophrenia demonstrated using immunoautoradiography. *Neuroscience* 69:339–343.
- Eastwood SL, Harrison PJ, Cairns NJ (2000) Synaptophysin gene expression in schizophrenia: Investigation of synaptic pathology in the cerebral cortex. *The British Journal of Psychiatry* 176:236–242.
- Eastwood S, Burnet P, Harrison P (1995) Altered synaptophysin expression as a marker of synaptic pathology in schizophrenia. *Neuroscience* 66:309–319.
- Gao X, Starmer J, Martin ER (2008) A multiple testing correction method for genetic association studies using correlated single nucleotide polymorphisms. *Genetic epidemiology* 32:361–369.
- Garey LJ, Ong WY, Patel TS, Kanani M, Davis A, Mortimer AM, Barnes TRE, Hirsch SR (1998) Reduced dendritic spine density on cerebral cortical pyramidal neurons in schizophrenia. *Journal of Neurology, Neurosurgery & Psychiatry* 65:446–453.
- Glantz LA, Lewis DA (2000) Decreased dendritic spine density on prefrontal cortical pyramidal neurons in schizophrenia. *Arch Gen Psychiatry* 57:65–73.

- Glantz LA, Lewis DA (1997) Reduction of synaptophysin immunoreactivity in the prefrontal cortex of subjects with schizophrenia: regional and diagnostic specificity. *Archives of general psychiatry* 54:943–952.
- Glasser MF, Sotiropoulos SN, Wilson JA, Coalson TS, Fischl B, Andersson JL, Xu J, Jbabdi S, Webster M, Polimeni JR, Van Essen DC, Jenkinson M, for the WUMHCPC (2013) The minimal preprocessing pipelines for the human connectome project. *NeuroImage* 80:105–124.
- Hagmann P, Cammoun L, Gigandet X (2008) Mapping the structural core of human cerebral cortex. *PLoS biology* 6:e159.
- Honer WG, Falkai P, Young C, Wang T, Xie J, Bonner J, Hu L, Boulianne GL, Luo Z, Trimble WS (1997) Cingulate cortex synaptic terminal proteins and neural cell adhesion molecule in schizophrenia. *Neuroscience* 78:99–110.
- Hutsler JJ, Zhang H (2010) Increased dendritic spine densities on cortical projection neurons in autism spectrum disorders. *Brain Res* 1309:83–94.
- Jacobs B, Driscoll L, Schall M (1997) Life-span dendritic and spine changes in areas 10 and 18 of human cortex: a quantitative golgi study. *J Comp Neurol* 386:661–80.
- Jacobs B, Schall M, Prather M, Kapler E, Driscoll L, Baca S, Jacobs J, Ford K, Wainwright M, Trembl M (2001) Regional dendritic and spine variation in human cerebral cortex: a quantitative golgi study. *Cerebral Cortex* 11:558–571.
- Kalus P, Muller TJ, Zuschratter W, Senitz D (2000) The dendritic architecture of prefrontal pyramidal neurons in schizophrenic patients. *Neuroreport* 11:3621–5.
- Kandel ER, Schwartz JH, Jessell TM (2000) *Principles of neural science*, Vol. 4 McGraw-hill New York.
- Karson CN, Mrak RE, Schluterman KO, Sturner WQ, Sheng JG, Griffin WS (1999) Alterations in synaptic proteins and their encoding mrnas in prefrontal cortex in schizophrenia: a possible neurochemical basis for 'hypofrontality'. *Mol Psychiatry* 4:39–45.
- Kolluri N, Sun Z, Sampson AR, Lewis DA (2005) Lamina-specific reductions in dendritic spine density in the prefrontal cortex of subjects with schizophrenia. *Am J Psychiatry* 162:1200–2.
- Konopaske GT, Lange N, Coyle JT, Benes FM (2014) Prefrontal cortical dendritic spine pathology in schizophrenia and bipolar disorder. *JAMA psychiatry* 71:1323–1331.
- Landén M, Davidsson P, Gottfries CG, Månsson JE, Blennow K (2002) Reduction of the synaptophysin level but normal levels of glycerophospholipids in the gyrus cinguli in schizophrenia. *Schizophrenia Research* 55:83–88.
- Landman BA, Bogovic JA, Wan H, ElShahaby FEZ, Bazin PL, Prince JL (2012) Resolution

- of crossing fibers with constrained compressed sensing using diffusion tensor mri. *NeuroImage* 59:2175–2186.
- Maslov S, Sneppen K (2002) Specificity and stability in topology of protein networks. *Science* 296:910–913.
- Perrone-Bizzozero NI, Sower AC, Bird ED, Benowitz LI, Ivins KJ, Neve RL (1996) Levels of the growth-associated protein gap-43 are selectively increased in association cortices in schizophrenia. *Proc Natl Acad Sci U S A* 93:14182–7.
- Pierri JN, Volk CL, Auh S, Sampson A, Lewis DA (2001) Decreased somal size of deep layer 3 pyramidal neurons in the prefrontal cortex of subjects with schizophrenia. *Archives of general psychiatry* 58:466–473.
- Power JD, Barnes KA, Snyder AZ, Schlaggar BL, Petersen SE (2012) Spurious but systematic correlations in functional connectivity mri networks arise from subject motion. *NeuroImage* 59:2142–2154.
- Rajkowska G, Selemon LD, Goldman-Rakic PS (1998) Neuronal and glial somal size in the prefrontal cortex: a postmortem morphometric study of schizophrenia and huntington disease. *Arch Gen Psychiatry* 55:215–24.
- Rao JS, Kim HW, Harry GJ, Rapoport SI, Reese EA (2013) Increased neuroinflammatory and arachidonic acid cascade markers, and reduced synaptic proteins, in the postmortem frontal cortex from schizophrenia patients. *Schizophrenia Research* 147:24–31.
- Riley JN (1979) A reliable golgi-kopsch modification. *Brain research bulletin* 4:127–129.
- Rubinov M, Sporns O (2010) Complex network measures of brain connectivity: uses and interpretations. *NeuroImage* 52:1059–69.
- Scheibel ME, Scheibel AB (1978) The methods of golgi. *Neuroanatomical research techniques* 89:114.
- Scholtens LH, Schmidt R, de Reus MA, van den Heuvel MP (2014) Linking macroscale graph analytical organization to microscale neuroarchitectonics in the macaque connectome. *The Journal of Neuroscience* 34:12192–12205.
- Schüz A, Miller R (2002) *Cortical areas: unity and diversity* Conceptual advances in brain research. Taylor & Francis, London; New York.
- Somenarain L, Jones LB (2012) Dendritic and spine alterations in areas 9 and 17 in schizophrenia and huntington chorea and the role of neuroleptic exposure. *Open Journal of Psychiatry* 2:243–248.
- Sweet RA, Henteleff RA, Zhang W, Sampson AR, Lewis DA (2009) Reduced dendritic spine density

- in auditory cortex of subjects with schizophrenia. *Neuropsychopharmacology* 34:374–389.
- van den Heuvel MP, Kahn RS, Goñi J, Sporns O (2012) High-cost, high-capacity backbone for global brain communication. *Proceedings of the National Academy of Sciences of the United States of America* 109:11372–11377.
- van den Heuvel MP, Sporns O (2011) Rich-club organization of the human connectome. *The Journal of neuroscience : the official journal of the Society for Neuroscience* 31:15775–86.
- van den Heuvel MP, Sporns O (2013) An anatomical substrate for integration among functional networks in human cortex. *The Journal of neuroscience : the official journal of the Society for Neuroscience* 33:14489–500.
- van den Heuvel MP, Sporns O, Collin G, Scheewe T, Mandl RCW, Cahn W, Goñi J, Hulshoff Pol HE, Kahn RS (2013) Abnormal rich club organization and functional brain dynamics in schizophrenia. *JAMA psychiatry (Chicago, Ill.)* 70:783–92.
- Van Essen DC, Smith SM, Barch DM, Behrens TE, Yacoub E, Ugurbil K (2013) The wu-minn human connectome project: an overview. *Neuroimage* 80:62–79.
- Von Economo CF, Koskinas GN (1925) *Die cytoarchitektonik der hirnrinde des erwachsenen menschen* J. Springer.
- Yeh FC, Wedeen VJ, Tseng WYI (2010) Generalized q-sampling imaging. *IEEE transactions on medical imaging* 29:1626–1635.
- Zalesky A, Fornito A, Harding IH, Cocchi L, Yücel M, Pantelis C, Bullmore ET (2010) Whole-brain anatomical networks: does the choice of nodes matter? *Neuroimage* 50:970–983.
- Zeba M, Jovanov-Milošević N, Petanjek Z (2008) Quantitative analysis of basal dendritic tree of layer iii pyramidal neurons in different areas of adult human frontal cortex. *Collegium antropologicum* 32:161–169.



Chapter 4

Bridging cytoarchitectonics and connectomics in human cerebral cortex

Martijn P. van den Heuvel, Lianne H. Scholtens, Lisa Feldman Barrett, Claus C. Hilgetag, Marcel A. de Reus

Journal of Neuroscience 2015; 35 (41): 13943-13948

The rich variation in cytoarchitectonics of the human cortex is well known to play an important role in the differentiation of cortical information processing, with functional multimodal areas noted to display more branched, more spinous, and an overall more complex cytoarchitecture. In parallel, connectome studies have suggested that also the macroscale wiring profile of brain areas may have an important contribution in shaping neural processes; for example, multimodal areas have been noted to display an elaborate macroscale connectivity profile. However, how these two scales of brain connectivity are related – and perhaps interact – remains poorly understood. In this communication, we combined data from the detailed mappings of early twentieth century cytoarchitectonic pioneers Von Economo and Koskinas (1925) on the microscale cellular structure of the human cortex with data on macroscale connectome wiring as derived from high-resolution diffusion imaging data from the Human Connectome Project. In a cross-scale examination, we show evidence of a significant association between cytoarchitectonic features of human cortical organization – in particular the size of layer 3 neurons – and whole-brain cortico-cortical connectivity. Our findings suggest that aspects of microscale cytoarchitectonics and macroscale connectomics are related.

Introduction

The human brain comprises a complex network of neural connections known as the human connectome. At the microscale, neurons are linked by dendrites, axons, and synapses, ensuring transmission, dissemination, and integration of neural information. In parallel, at the macroscale level of brain organization, cortical and subcortical regions are connected by long-distance white matter projections, enabling neural communication and integration of information across different parts of the brain. However, how these two scales of brain organization relate – or perhaps interact – remains poorly understood.

Evidently, organizational features at both the microscale and macroscale are of crucial importance to brain functioning. Work of neuroanatomists such as Brodmann 1909; Vogt and Vogt 1903, and Von Economo and Koskinas 1925 revealed a rich variety in cytoarchitecture of the human cortex and, expanding the thoughts of these early pioneers, contemporary neuroanatomy studies have suggested that cytoarchitectonic differentiation may play a fundamental role in the type of information processed by cortical areas (Barbas, 2015; Sanides, 1970; Zilles et al., 2015). Additional support for such theories may come from studies examining the organization of neurons by means of Golgi staining techniques showing that associative frontal areas of the human and macaque cortex (e.g., BA 46/10/11) display elaborate neuronal architectures with larger, more branched, and more spinous pyramidal neurons compared with unimodal primary regions (e.g., BA 17/41/42) (Elston, 2003; Jacobs et al., 2001; Yuste, 2011). Together, these observations have led to influential theories on regional differences in cytoarchitecture and the associated degree of laminar differentiation to play a pivotal role in shaping the dynamics of neural processing and cortico-cortical communication (Barbas, 2015; Mesulam, 1998; Zilles et al., 2015).

In parallel, studies examining connectivity at the macroscale level of brain organization have suggested that the brain's global network structure of large-scale white matter projections may play an important role in neural processing. For example, macroscale connectome studies have suggested large variation in the connectivity profiles of cortical regions, with some regions showing predominantly local short-range projections and other regions displaying more elaborate connectivity profiles suitable for sending and receiving neural information across different parts of the cortex. Somewhat analogous to the microscale, regional variation in macroscale connectivity profile has been directly related to the type of information processed by cortical regions, with densely wired “brain hubs” noted to show high spatial overlap with functional multimodal association areas and, accordingly, being thought to act as central integration zones of the cortex (for review, see van den Heuvel and Sporns (2013)).

While it is thus apparent that features of connectivity at both the microscale and macroscale play a pivotal role in brain functioning, it is much less clear how these two scales of neural connectivity are related. In this brief communication, we show evidence of a putative microscale–macroscale relationship across the human cortical mantle by combining data from the cortical mappings of cytoarchitectonic pioneers Von Economo and Koskinas (1925) with data on macroscale connectome organization as derived from high-resolution diffusion MRI data from the Human Connectome Project (HCP) (Van Essen et al., 2013).

Materials and Methods

Von Economo and Koskinas cytoarchitectonic metrics

Cytoarchitectonic mappings of the human cortex were taken from the 1925 Von Economo and Koskinas work *Die Cytoarchitektonik der Hirnrinde des erwachsenen Menschen* (Von Economo and Koskinas, 1925) [translated as *Cytoarchitectonics of the Adult Human Cerebral Cortex* (Von Economo et al., 2008)]. As described in their accompanying 1925 writings and in Von Economo’s 1927 writings, *Zellaufbau der Grosshirnrinde des Menschen*, based on a series of his teaching lectures (Von Economo, 1927) and translated as *Cellular Structure of the Human Cerebral Cortex* (Von Economo, 2009), Von Economo and Koskinas described a parcellation of the whole human cortex into 48 “Grundareae” regions (“ground” areas), with a finer parcellation into 76 smaller “Varianten” (“variants”). For 51 regions (40 ground areas and 8 variants covering the whole cortex, together with three hippocampal areas), Von Economo and Koskinas listed detailed tables including layer-specific information on (1) neuronal count per cubic millimeter, (2) layer width, and (3) neuron width and length defining neuron size (taken here as an ellipse multiplication of the reported cell width and length; Von Economo and Koskinas (1925)). The 48 cortical regions were manually mapped to a 57-region subdivision of the FreeSurfer Desikan-Killiany atlas (describing 57 regions in each hemisphere; Figure 1; Fischl et al. (2004); Hagmann et al. (2008)) using the original 1925 and 1927 text and drawings. The drawings were overlaid and manually projected onto a 3D cortical surface reconstruction of the FreeSurfer average brain (Fischl et al., 2004) from which the overlap with the DK-57 atlas was determined. A complete textual and visual description of this mapping (together with a validation for the DK-57 atlas, as well as for atlases with other resolutions) was performed as part of a recent study in which we examined the validity of MRI T1-based estimates of cortical thickness by means of ground-truth histological examinations of cortical mantle width by Von Economo and Koskinas (Scholtens et al., 2015). Mapping resulted in a listing of cytoarchitectonic values for each of the DK-57 regions, describing 18 [3 (neuron count, layer thickness, and neuron size) × 6 (cortical layers)] metrics of

cytoarchitectonic organization for each cortical area.

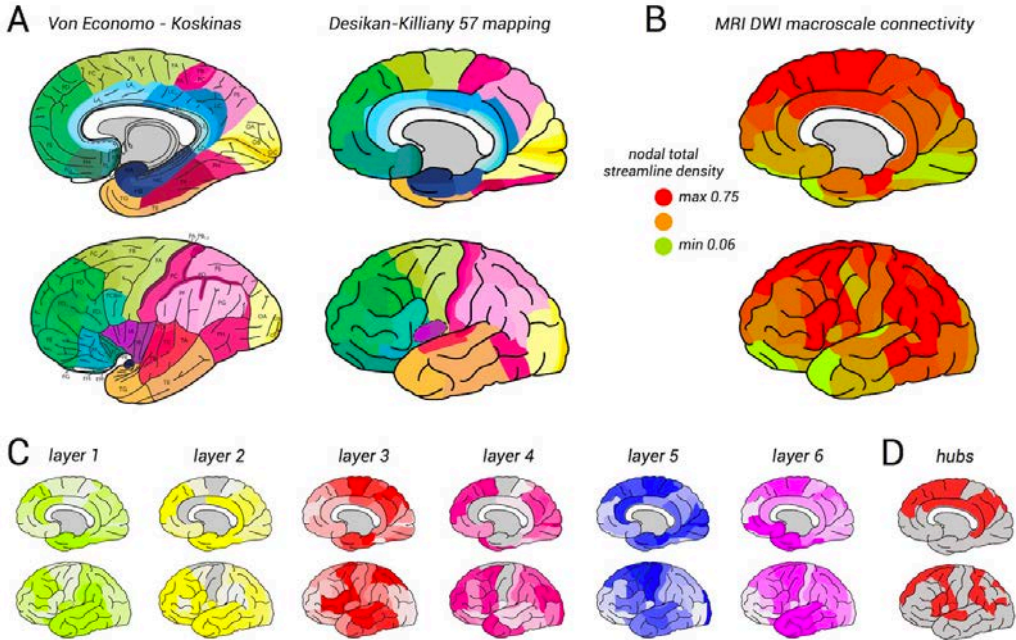


Figure 1. A, Digital version of the cytoarchitectonic Von Economo and Koskinas (1925) parcellation (left) and the mapped subregions of the Desikan-Killiany (DK-57) atlas (right). B, Nodal strength of macroscale connectivity for the DK-57 regions (left hemisphere). C, Derived Von Economo-Koskinas values of neuron size for the six layers mapped on the DK-57 areas. D, Regions considered as connectome hubs based on their macroscale projections.

Supragranular architecture.

In addition to layer specific neuron count, the degree of supragranular differentiation of cortical regions was computed. The relative number of originating supragranular neurons (SGN%) is often used as a metric of the degree of laminar differentiation and has been noted to form an important marker for the distribution of cortico-cortical projections (Hilgetag and Grant, 2010). Following the definition of Barbas and coworkers (Barbas and Rempel-Clower, 1997; Hilgetag and Grant, 2010), the degree of laminar differentiation SGN% was computed as the balance between SGN and infragranular neurons (IGN) as $SGN / (SGN + IGN)$, with SGN the number of neurons in supragranular layers 2 and 3, computed as the Von Economo and Koskinas reported neuron count per cubic millimeter multiplied by regional layer thickness and cortical surface area, and IGN the total number of neurons in infragranular layers 5 and 6.

Macroscale MRI connectome reconstruction and analysis

Connectome reconstruction.

High-resolution diffusion-weighted data from the HCP (Van Essen et al., 2013); Q3 release; $n = 215$ subjects, males and females mixed, age 22–35 years; imaging parameters: voxel size 1.25 mm isotropic, TR/TE 5520/89.5 ms, 270 diffusion directions with diffusion weighting 1000, 2000, or 3000 s/mm²) was used to reconstruct a macroscale human connectome map. Diffusion weighted imaging data processing included the following: (1) eddy current and susceptibility distortion correction, (2) reconstruction of the voxelwise diffusion profile using generalized q-sampling imaging, and (3) whole-brain streamline tractography (for details on HCP connectome reconstruction, see also de Reus and van den Heuvel (2014)). Cortical segmentation and parcellation was performed on the basis of a high-resolution T1-weighted image (voxel size: 0.7 mm isotropic) of each subject using FreeSurfer (Fischl et al., 2004), automatically parcellating the complete cortical sheet into 114 distinct regions (57 per hemisphere) using the DK-57 atlas (Cammoun et al., 2012). For each individual subject, a 114×114 connectivity matrix was formed, representing for each pair of regions their reconstructed pathways. The strength of the reconstructed connections was measured using the notion of streamline density, computed as the number of tractography streamlines that touched both cortical regions divided by their average cortical surface area (Hagmann et al., 2008). A group-level human connectome map was formed by taking the nonzero mean across the individual connectivity matrices, including connections that were observed in at least 60% of the subjects (van den Heuvel and Sporns, 2011).

Connectome analysis.

With the connectome map describing a mathematical graph for each cortical region, the level of nodal degree was computed as the number of binary connections of a region and the level of nodal strength was computed as the total sum of connectivity strength across all reconstructed projections of a region. Because the Von Economo and Koskinas mappings did not distinguish between hemispheres, nodal connectivity properties of the left hemispheric regions were taken for analysis.

Statistical analysis

Associations between regional variation in cytoarchitectonic features and macroscale connectome properties were examined by means of Pearson correlation analysis. Correlations reaching a partial Bonferroni α of .0083 [$.05/(3 \times 2)$] were taken as significant, corresponding to 3 microscale factors derived from a principal component analysis on the 18 micrometrics, with the 3 components describing 99% of the variance and the 2 macrometrics (nodal degree and strength). For additional tests, a Bonferroni threshold of $.05/4 = .0125$ was taken.

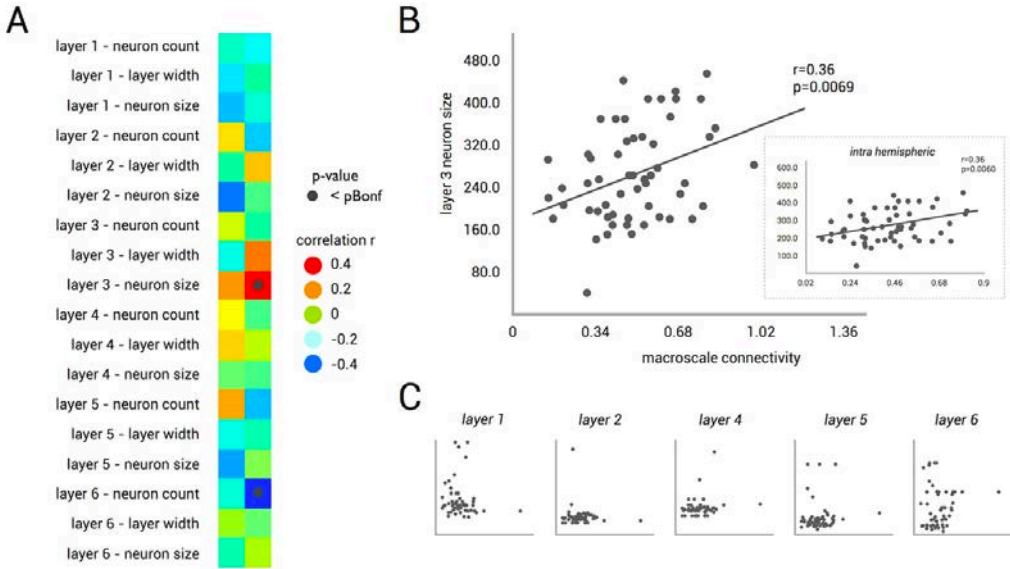


Figure 2. A, Correlation matrix between all 18 microscale cytoarchitectonic metrics (6 layers \times 3 metrics) and the two examined macroscale connectome values (degree and strength). B, Positive association between layer 3 neuron size (y -axis) and macroscale connectivity strength of cortical regions (i.e., nodal strength, x -axis). Insert shows the association between layer 3 neuron size (y -axis) and intrahemispheric nodal strength (x -axis, left hemisphere). C, Panels illustrate an absence of a micro–macro association for the other layers.

Results

Figure 2A shows the full matrix of correlation values between the examined microscale and macroscale metrics. Layer 3 neuron size significantly correlated to the regional connectivity strength of macroscale connectome pathways ($r = .37$, $p = .0039$; Figure 2B; effect reaching partial Bonferroni correction). Examining nodal strength across intrahemispheric connections (i.e., thus taking the strength of a node as the sum over its intrahemispheric cortico-cortical connections) revealed a similar positive association with layer 3 neuron size ($r = .39$, $p = .0027$; Figure 2B, insert). Other layers (layer 1, 2, 4, 5, and 6) showed no clear link between nodal strength and neuron size (Figure 2C, all $p < .05$).

Looking into the layer 3 cortical association in more detail, no effect was found with total neuron count ($r = .034$, $p = .79$; Figure 2A). Partial correlation of nodal connectivity strength with layer 3 neuron size (regressing out the effects of neuron count by including it as a covariate) thus similarly resulted in a significant association between macroscale connectivity strength and layer 3 neuron size ($p = .0040$). Further regressing out the effect of the thickness of layer 3 (with layer 3 thickness and neuron size correlating, $r =$

.32) again revealed a relation (that was somewhat attenuated) between layer 3 neuron size and macroscale connectivity ($p = .0186$). In addition, a negative correlation was observed between layer 6 neuron count and regional macroscale connectivity ($p = .0027$; Figure 2A), but this effect was attenuated when examining intrahemispheric connectivity only ($p = .0147$).

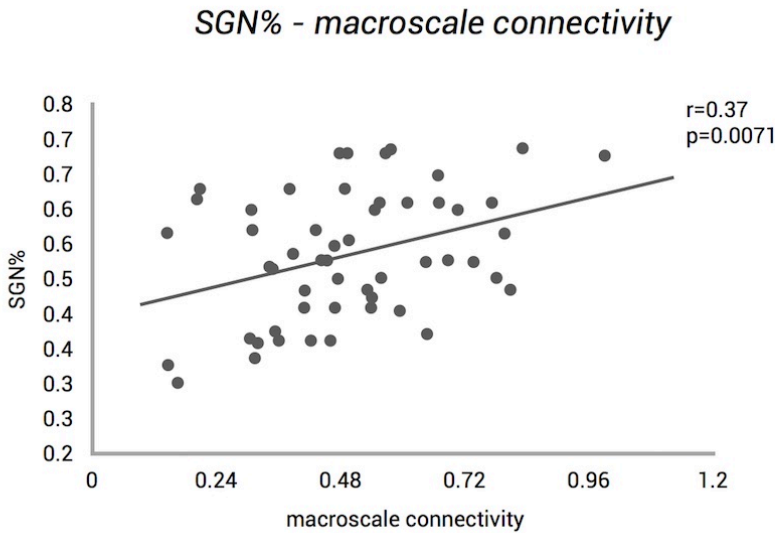


Figure 3. Association between cortical variation in macroscale connectivity (nodal strength, x -axis) and the microscale level of supragranular organization (SGN%, y -axis).

Laminar differentiation

SGN% was found to be significantly correlated to regional variation in macroscale connectivity strength ($r = .38$, $p = .0045$; Figure 3), with more densely connected cortical areas showing an overall more developed supragranular structure.

Hubs, communities, and cytoarchitectural overlap

Hub regions – selected as the top 20% highest degree nodes in the network (van den Heuvel and Sporns, 2011) – included subregions of the caudal middle frontal cortex, inferior and superior parietal cortex, middle and superior temporal cortex, subparts of the inferior (parsopercularis) and superior frontal gyrus, precuneus, as well as the most inferior subpart of the precentral gyrus (Von Economo–Koskinas region FB/FBop, inferior part of Brodmann Area 6) and subparts of the supramarginal gyrus and insular cortex, regions highly consistent with those described previously (Hagmann et al., 2008; van den Heuvel and Sporns, 2011), Figure 1D). This set of network hubs showed, on average, larger layer 3 neurons (1.29 times larger, $p = .0112$, permutation testing,

10,000 permutations) compared with peripheral nodes (meaning low-degree regions). [Hub selection thresholds of 10% ($1.33\times$, $p = .0226$, not reaching Bonferroni correction) and 30% ($1.25\times$, $p = .0122$) revealed similar findings.]

Next, we examined regional involvement in connectome communities and overlap in the cytoarchitectonic profile of cortical regions. Between all pairs of cortical areas, region-to-region correspondence in the cytoarchitectonic profile was computed by correlating profiles of regions (before computing the correlation coefficients each microscale factor was normalized by dividing by the mean and redistributing the values to a Gaussian distribution). Cortical regions belonging to the same structural network community (module detection using Newman's modularity algorithm identified 5 anatomical communities) showed a significantly higher cytoarchitectural correspondence than region pairs belonging to communities (1.25 times higher, $p = .0028$, permutation testing 10,000 permutations).

Discussion

Our findings provide evidence of a correlation between microscale cytoarchitectonics and macroscale connectomics of human cortex. We show that macroscale connectivity of cortical regions is not directly related to neuronal count and/or layer thickness of the cortical mantle [noted to correspond well to MRI-derived estimates of cortical thickness (Scholtens et al., 2015)]. Rather, our findings show that the organization of macroscale projections correlates with cortical variation in neuron size, in particular the size of neurons in cortical layer 3. Furthermore, more developed supragranular structure of cortical areas was found to be associated to stronger cortico-cortical macroscale connectivity. Supragranular layers (and in particular layer 3) of the mammalian cortex are known to form a primary layer for long-range cortico-cortical communication (for overview, see Barbas (2015); Jacobs et al. (1997, 2001); Schüz and Miller (2002)), supporting our observation that macroscale connectivity is related to microscale cytoarchitectonic properties.

The monumental – but perhaps by today's neuroscientists sometimes forgotten – 1925 work of Von Economo and Koskinas is arguably one of the most detailed and most complete listings of cytoarchitectonic features of the human cortical mantle, but it is of course inherently limited by the technology and methodology of that time (for discussion, see Amunts and Zilles (2012); Von Economo (2009)). The writings of Von Economo and Koskinas (1925) do not mention the exact number of samples, making the study power perhaps less than we are used to in modern day examinations. Von Economo and Koskinas nevertheless explicitly state that every region was

consistently observed in all investigated samples, with recordings based on histological examinations of – as they emphasize – “zahlreichen Gehirnen” (“numerous brains”; Von Economo and Koskinas (1925)) of healthy subjects (i.e., no reported history of neurological and/or psychiatric disorders). Furthermore, it should be noted that the from the work of Von Economo and Koskinas (1925) derived metric of cell size – derived from their at that time newly adopted notation of “Schlankheit” (slenderness) of a neuron (Von Economo and Koskinas, 1925) – includes a simplified metric of neuronal organization compared with metrics provided by modern day 3D techniques that allow for complete reconstructions of neuron dendritic trees and detailed measurements of spine count, spine type, and so forth (Jacobs et al., 2001; Lichtman and Sanes, 2008). To provide some insight into this matter, we examined the value of layer 3 neuron size as an indicator for neuronal complexity in a post hoc analysis. Examining layer 3 pyramidal neuron size in a recently collated dataset on layer 3 neuronal and dendritic organization of cortical regions in the macaque cortex (Elston, 2003; Scholtens et al., 2014), we observed pyramidal soma size to be highly correlated to measurements of dendritic tree size ($r = .67, p = .0013$), spine count ($r = .71, p = .0004$), and spine density (number of spines per unit of tree length, $r = .72, p = .0005$), suggesting that neuron soma size is a simplistic but nevertheless useful marker for neuronal organization.

With neurons most often interpreted as being biological accumulators and integrators of neural information, larger neuron size and accompanying higher complexity of dendritic branching has been related to a higher neural processing and integration capacity of cortical areas (Elston et al., 2001; Yuste, 2011). In their work on morphological aspects of pyramidal neurons in the macaque cortex, Elston and colleagues noted a gradient of pyramidal complexity from posterior to anterior regions, with association regions showing more elaborate pyramidal organization (Elston, 2003; Scholtens et al., 2014). From a functional perspective on brain processes, the “global workspace hypothesis” (Dehaene et al., 1998) describes the existence of a functional system in which information can be integrated through means of abundant communication and interaction, a system that is hypothesized as a distributed set of cortical regions with dense levels of mutual and bidirectional projections and, to be able to process high amounts of neuronal information, a system of multimodal regions with an elaborate cytoarchitectonic organization (Dehaene and Naccache, 2001). Studies have identified hub regions in the mammalian cortex to constitute a widespread anatomical “rich club” system with an above average level of mutual and mostly reciprocal interregional connectivity (van den Heuvel and Sporns, 2013) and, from this, we and others have hypothesized the neural rich club to form an ideal candidate for an anatomical substrate of a global workspace in the mammalian brain (for review, see

van den Heuvel and Sporns (2013). We argue that our current findings add another piece to this puzzle, confirming macroscale high-degree hub areas of the human cortex to indeed, as hypothesized, display an intricate neuronal organization on the microscale.

The notion of an association between microscale and macroscale properties of neural connectivity and complexity is consistent with recent observations from animal studies. Beul et al. (2015) reported that cytoarchitectonic classes of areas of cat cortex overlap with patterns of macroscale connectivity as derived from tract-tracing experiments. We previously reported the neural complexity (e.g., spine density, dendritic branching) of layer 3 pyramidal neurons of a subset of areas of macaque cortex to be related to macroscale connectivity of cortical regions (Scholtens et al., 2014). Extending such observations now to the whole human cortex, our findings converge on the notion of architectonic aspects of connectivity at the microscale and macroscale level of brain organization to be associated – and to possibly interact – to shape the flow of cortico-cortical communication (Barbas, 2015; van den Heuvel et al., 2012).

Our study shows encouraging findings of an association between microscale cytoarchitectonics and macroscale connectomics of the human cortex, but several aspects have to be taken into account when interpreting the results. It has to be noted that, in addition to limitations concerning the dimensionality of the Von Economo and Koskinas cytoarchitectonic mappings (see above), the reconstructions of macroscale connectome maps are also inherently limited by the techniques used. Even though the data of the HCP is of very high quality, diffusion tractography remains a technique that depends on indirect information (the hindered diffusion of water molecules by fiber structure) for the reconstruction of anatomical pathways. As a result, diffusion tractography is known to have limitations with respect to the reconstruction of white matter projections in areas with a complicated pathway layout and has been argued to involve both overrepresentations and underrepresentations of connectivity (Jbabdi and Johansen-Berg, 2011) compared with animal tract tracing-based connectome maps (Markov et al., 2013).

Our findings converge on the notion that aspects of the brain's smallest and largest organizational features of neural connectivity are associated (Oh et al., 2014). Studying the fundamental interplay between microscale and macroscale properties of human brain connectivity might form a fruitful new framework for the examination of dysconnectivity effects in neurological and psychiatric brain disorders because many are reported to involve affected connectivity on both ends of the organizational scale.

References

- Amunts K, Zilles K (2012) Architecture and organizational principles of broca's region. *Trends in cognitive sciences* 16:418–426.
- Barbas H (2015) General cortical and special prefrontal connections: Principles from structure to function. *Annual Review of Neuroscience* 38:269–289.
- Barbas H, Rempel-Clower N (1997) Cortical structure predicts the pattern of corticocortical connections. *Cerebral cortex (New York, NY: 1991)* 7:635–646.
- Beul SF, Grant S, Hilgetag CC (2015) A predictive model of the cat cortical connectome based on cytoarchitecture and distance. *Brain Structure and Function* 220:3167–3184.
- Brodmann K (1909) *Vergleichende Lokalisationslehre der Grosshirnrinde in ihren Prinzipien dargestellt auf Grund des Zellenbaues* Barth.
- Cammoun L, Gigandet X, Meskaldji D, Thiran JP, Sporns O, Do KQ, Maeder P, Meuli R, Hagmann P (2012) Mapping the human connectome at multiple scales with diffusion spectrum mri. *Journal of neuroscience methods* 203:386–97.
- de Reus MA, van den Heuvel MP (2014) Simulated rich club lesioning in brain networks: a scaffold for communication and integration? *Frontiers in Human Neuroscience* 8.
- Dehaene S, Kerszberg M, Changeux JP (1998) A neuronal model of a global workspace in effortful cognitive tasks. *Proceedings of the National Academy of Sciences* 95:14529–14534.
- Dehaene S, Naccache L (2001) Towards a cognitive neuroscience of consciousness: basic evidence and a workspace framework. *Cognition* 79:1–37.
- Elston GN (2003) Cortex, cognition and the cell: New insights into the pyramidal neuron and prefrontal function. *Cerebral Cortex* 13:1124–1138.
- Elston GN, Benavides-Piccione R, DeFelipe J (2001) The pyramidal cell in cognition: a comparative study in human and monkey. *The Journal of neuroscience : the official journal of the Society for Neuroscience* 21:RC163.
- Fischl B, van der Kouwe A, Destrieux C, Halgren E, Segonne F, Salat DH, Busa E, Seidman LJ, Goldstein J, Kennedy D, Caviness V, Makris N, Rosen B, Dale AM (2004) Automatically parcellating the human cerebral cortex. *Cereb Cortex* 14:11–22.
- Hagmann P, Cammoun L, Gigandet X (2008) Mapping the structural core of human cerebral cortex. *PLoS biology* 6:e159.
- Hilgetag CC, Grant S (2010) Cytoarchitectural differences are a key determinant of laminar

- projection origins in the visual cortex. *Neuroimage* 51:1006–17.
- Jacobs B, Driscoll L, Schall M (1997) Life-span dendritic and spine changes in areas 10 and 18 of human cortex: a quantitative golgi study. *J Comp Neurol* 386:661–80.
- Jacobs B, Schall M, Prather M, Kapler E, Driscoll L, Baca S, Jacobs J, Ford K, Wainwright M, Trembl M (2001) Regional dendritic and spine variation in human cerebral cortex: a quantitative golgi study. *Cerebral Cortex* 11:558–571.
- Jbabdi S, Johansen-Berg H (2011) Tractography: where do we go from here? *Brain Connect* 1:169–83.
- Lichtman JW, Sanes JR (2008) Ome sweet ome: what can the genome tell us about the connectome? *Current opinion in neurobiology* 18:346–353.
- Markov NT, Ercsey-Ravasz M, Van Essen DC, Knoblauch K, Toroczkai Z, Kennedy H (2013) Cortical high-density counterstream architectures. *Science* 342:1238406–1238406.
- Mesulam MM (1998) From sensation to cognition. *Brain* 121:1013–1052.
- Oh SW, Harris JA, Ng L, Winslow B, Cain N, Mihalas S, Wang Q, Lau C, Kuan L, Henry AM, Mortrud MT, Ouellette B, Nguyen TN, Sorensen SA, Slaughterbeck CR, Wakeman W, Li Y, Feng D, Ho A, Nicholas E, Hirokawa KE, Bohn P, Joines KM, Peng H, Hawrylycz MJ, Phillips JW, Hohmann JG, Wohnoutka P, Gerfen CR, Koch C, Bernard A, Dang C, Jones AR, Zeng H (2014) A mesoscale connectome of the mouse brain. *Nature* 508:207–214.
- Sanides F (1970) *Functional architecture of motor and sensory cortices in primates in the light of a new concept of neocortex evolution* Appleton, New York.
- Scholtens LH, de Reus MA, van den Heuvel MP (2015) Linking contemporary high resolution magnetic resonance imaging to the von economo legacy: A study on the comparison of mri cortical thickness and histological measurements of cortical structure. *Human Brain Mapping* 36:3038–3046.
- Scholtens LH, Schmidt R, de Reus MA, van den Heuvel MP (2014) Linking macroscale graph analytical organization to microscale neuroarchitectonics in the macaque connectome. *The Journal of Neuroscience* 34:12192–12205.
- Schüz A, Miller R (2002) *Cortical areas: unity and diversity* Conceptual advances in brain research. Taylor & Francis, London; New York.
- van den Heuvel MP, Kahn RS, Goñi J, Sporns O (2012) High-cost, high-capacity backbone for global brain communication. *Proceedings of the National Academy of Sciences of the United States of America* 109:11372–11377.
- van den Heuvel MP, Sporns O (2011) Rich-club organization of the human connectome. *The*

- Journal of neuroscience : the official journal of the Society for Neuroscience* 31:15775–86.
- van den Heuvel MP, Sporns O (2013) Network hubs in the human brain. *Trends in cognitive sciences* 17:683–696.
- Van Essen DC, Smith SM, Barch DM, Behrens TE, Yacoub E, Ugurbil K (2013) The wu-minn human connectome project: an overview. *Neuroimage* 80:62–79.
- Vogt O, Vogt C (1903) Zur anatomischen gliederung des cortex cerebri. *J Psychol Neurol* 2:160–180.
- Von Economo C (1927) *Zellaufbau der Grosshirnrinde des Menschen* Springer, Berlin.
- Von Economo C (2009) *Cellular structure of the human cerebral cortex* Karger Medical and Scientific Publishers, Basel.
- Von Economo CF, Koskinas GN (1925) *Die cytoarchitektonik der hirnrinde des erwachsenen menschen* J. Springer.
- Von Economo CF, Koskinas GN, Triarhou LC (2008) *Atlas of cytoarchitectonics of the adult human cerebral cortex* Karger Basel.
- Yuste R (2011) Dendritic spines and distributed circuits. *Neuron* 71:772–781.
- Zilles K, Mohlberg H, Amunts K, Palomero-Gallagher N, Bludau S (2015) *Cytoarchitecture and maps of the human cerebral cortex*, pp. 137–156 Academic Press.

Supplemental Information
of
Bridging Cytoarchitectonics and Connectomics in Human
Cerebral Cortex

Table S1. Mapping Von Economo atlas to Desikan-Killiany atlas.

region code	Von Economo - Koskinas atlas region name	Desikan - Killiany atlas region number(s) & region name(s)*
Frontal pole		
FA	precentral gyrus	precentral_1, precentral_2, precentral_3, superiorfrontal_4
FB	granular frontal area	precentral_4, superiorfrontal_4, caudalmiddlefrontal_1
FC	intermediate frontal area	superiorfrontal_3, caudalmiddlefrontal_1
FCBm	magnocellular agranular intermediated frontal	parsopercularis_1
FD	granular frontal area	superiorfrontal_2, rostralmiddlefrontal_1
FDdelta	middle granular frontal area	rostralmiddlefrontal_2
FDT	triangular granular frontal area	parstriangularis_1
FE	frontalpolar area	parsorbitalis_1, rostralmiddlefrontal_3, superiorfrontal_1, frontalpole_1
FF	orbital area (agranular orbital area FFalpha)	parsorbitalis_1, lateralorbitofrontal_1, lateralorbitofrontal_2
FG	straight area	lateralorbitofrontal_2
FH	prefrontal area	medialorbitofrontal_1
FI	frontoinsular area	lateralorbitofrontal_1
FK	frontal piriform area	lateralorbitofrontal_1
FL	parolfactory area	medialorbitofrontal_1
FM	geniculate area	medialorbitofrontal_1
FN	precommissural	medialorbitofrontal_1
Parietal lobe		
PA	postcentral giant pyramidal area PA1 and postparacentral giant pyramidal area PA2	postcentral_1, postcentral_2, postcentral_3, paracentral_1
PB1	oral postcentral area granulosa	postcentral_1, postcentral_2, postcentral_3
PB2	oral postcentral area simplex	postcentral_1, postcentral_2, postcentral_3
PC	intermediate postcentral area	postcentral_1, postcentral_2, postcentral_3
PD	caudal postcentral area	postcentral_1, postcentral_2, postcentral_3
PE	superior parietal area	superiorparietal_1, superiorparietal_2, superiorparietal_3, precuneus_2, precuneus_1
PF	supramarginal area	supramarginal_2, supramarginal_1
PG	angular area	inferiorparietal_1, inferiorparietal_2
PH	basal temporo-occipital parietal area	inferiortemporal_2, middletemporal_1, bankssts_1, fusiform_1, lingual_1
Insular cortex		
IA	precentral insular area	insula_2
IB	postcentral insular area	insula_1
Occipital lobe		
OA	peristriate area	lateraloccipital_2, inferiorparietal_1, superiorparietal_3, cuneus_1, lingual_1, lingual_2
OB	parastriate area	cuneus_1, lingual_1, lingual_2, lateraloccipital_1
OC	striate area	lateraloccipital_1, pericalcarine_1

* region subnumbers are study specific.

Table S1 – continued.

region code	Von Economo - Koskinas atlas region name	Desikan - Killiany atlas region number(s) & region name(s)*
Temporal lobe		
TA	superior temporal area	transversetemporal_1, superiortemporal_2
TB	supratemporal area simplex	transversetemporal_1
TC	supratemporal area granulosa	transversetemporal_1
TD	intercalated supratemporal area	transversetemporal_1
TE	temporal area proper	inferiortemporal_2, middletemporal_1, superiortemporal_2, middletemporal_2, inferiortemporal_1, superiortemporal_1
TF	fusiform area	fusiform_2
TG	temporopolar area	temporalpole_1, inferiortemporal_1
Cingulate cortex		
LA1	precingulate agranular anterior limbic area	rostralanteriorcingulate_1, caudalanteriorcingulate_1
LA2	precingulate agranular anterior limbic area	rostralanteriorcingulate_1, caudalanteriorcingulate_1
LC1	dorsal posterior cingulate area	precuneus_2
LC2	ventral posterior cingulate area	posteriorcingulate_1, isthmuscingulate_1
LC3	precingulate agranular anterior limbic area	posteriorcingulate_1
LD	angranular retrosplenial area	isthmuscingulate_1
LE1	superior retrosplenial area granulosa	isthmuscingulate_1
LE2	inferior retrosplenial area granulosa	isthmuscingulate_1
Hippocampal lobe		
HA	uncinate area	entorhinal_1
HB	parauncinate area	entorhinal_1
HC	rhinal area limitans	parahippocampal_1

* region subnumbers are study specific.



Chapter 5

Converging evidence of interplay between neural connectivity at the micro- and macroscale of connectome organization in human, mouse and rat brain

Lianne H. Scholtens, Lisa Feldman Barrett and Martijn P. van den Heuvel

Cerebral Cortex; submitted for review

The mammalian brain describes a multi-scale system. At the microscale, axonal, dendritic and synaptic elements ensure neuron-to-neuron communication, and at the macroscale, large-scale projections form the anatomical wiring for communication between cortical areas. While it is clear that both levels of neural organization play a crucial role in brain functioning, their interaction is not well understood. Connectome studies of the mammalian brain in cat, macaque and human have recently shown regions with larger and more complex pyramidal cells to have more macroscale corticocortical connections. The aim of this report is to replicate reported cross-scale findings in the human and to further validate these observations in the mouse and rat brain. Information from neuron reconstructions from the NeuroMorpho.org neuroarchitecture database was combined with macroscale connectivity data derived from connectome mapping by means of tract-tracing (rat, mouse) and in vivo diffusion MRI (human). Comparison across three mammalian species shows cortical variation in neural organization to be related to features of macroscale connectivity, with cortical variation in neuronal complexity explaining significant proportions of cortical variation in the number of white matter projections of cortical areas. These findings converge on

the notion of a relationship between features of micro- and macroscale neural connectivity to form a central aspect of mammalian neural architecture.

Introduction

Connectome studies of the mammalian brain in cat, macaque and human have shown regional variation in microscale structural type (Beul et al., 2015) and layer III pyramidal cell complexity (Scholtens et al., 2014; van den Heuvel et al., 2016) to be related to a region's macroscale projection pattern, with regions with larger and more complex pyramidal shown to have more macroscale corticocortical connections. Here, we further investigated this relationship in the human brain, and extend the observed micro-macro relationship of neural connectivity organization to the rodent brain.

Cytoarchitectonic variation is one of the cornerstones of mammalian cortex organization (Brodmann, 1909; Campbell, 1905; Hammarberg, 1895; Von Economo and Koskinas, 1925). This profuse cytoarchitectural variation across cortical areas is thought to play a crucial role in the physiological properties of cortical areas (Mesulam, 1998). Golgi staining studies of macaque and human cortex have shown a posterior to anterior gradient in cortical pyramidal complexity, with frontal association areas noted to display larger, more branched and more spinous pyramidal neurons as compared to unimodal primary motor, visual and/or auditory cortex (Elston et al., 2010; Jacobs et al., 2001) and have accordingly led to the suggestion of frontal regions to be involved in more complex neural processing (Elston, 2003). This posterior-anterior gradient in neuron size has since been reported in different primate and rodent species (Charvet et al., 2015), showing an increasingly strong gradient with larger brain volume (Finlay and Uchiyama, 2015).

At the macroscale level of brain organization, network studies of large-scale white matter corticocortical projections have revealed the mammalian macroscale connectome – the comprehensive network of neural projections of a species' neural system (Sporns et al., 2005) – to display features of an efficient cost-effective communication network (Bullmore and Sporns, 2009, 2012; van den Heuvel et al., 2016; van den Heuvel and Sporns, 2013). These studies have – in particular in humans – argued that macroscale network attributes play a role in brain function and behavior (Adelstein et al., 2011; Li et al., 2009; Park and Friston, 2013; Pessoa, 2012; Shanahan, 2012). Moreover, the number of projections of cortical areas has been suggested to display a non-uniform distribution across the cortex, with unimodal areas showing a relatively sparse connectivity profile dominated by projections to areas with a similar function, while multimodal association areas display a much richer macroscale

connectivity profile, receiving and projecting connections from and to areas of multiple functional domains (Tomasi and Volkow, 2011; van den Heuvel and Sporns, 2013; Zamora-López et al., 2010).

It is thus evident that properties at both the microscale and macroscale level of mammalian cortex organization plays a critical role in brain functioning and recent studies argue for a potential interplay between these two organizational scales (Beul et al., 2015; Hilgetag and Grant, 2010; Scholtens et al., 2014; van den Heuvel et al., 2016, 2015b), including an association between microscale layer 3 pyramidal morphology and the number of corticocortical projections of macaque cortex (Scholtens et al., 2014); as well as associations between region-wise cytoarchitecture and macroscale connectedness of the human cortex (van den Heuvel et al., 2016c). A study investigating the same relationship in the rat cortical connectome confirmed regional microscale structural type to be an important predictor of macroscale connectivity patterns (Goulas et al., 2017).

In the current study, we further explore a possible micro-macro relationship by validation of this phenomenon in the human brain and by investigations of the mouse and rat rodent brain. Technological advances have enabled spatially highly detailed tract-tracing mappings of the mouse (Oh et al., 2014) and rat connectome (Bota et al., 2012, 2015; Bota and Swanson, 2007) and high-resolution *in vivo* neuroimaging (Van Essen et al., 2013) has enabled detailed connectome reconstructions of human macroscale brain wiring. This, combined with important undertakings in large-scale collation of detailed neuron morphology data across published studies such as in the NeuroMorpho.org database (Ascoli et al., 2007) allows for a further exploration of a micro-to-macro relationship in neural connectivity organization across mammalian species.

Materials and Methods

Microscale neuronal data

Data on neuron morphology from the human, rat and mouse cortex were extracted from the comprehensive NeuroMorpho.org database (<http://neuromorpho.org>, version 6.1) (Ascoli, 1999), curated by Ascoli and coworkers (Ascoli, 2006; Ascoli et al., 2001). The NeuroMorpho.org database includes a collection of a large number of individual neuron reconstructions as grouped together across multiple experiments presented in literature. The database includes standardized digital reconstructions of the original reported reconstructed neurons from which morphological properties can be derived (as provided at neuromorpho.org) (Ascoli et al., 2001), as well as detailed meta information

on the original literature source, staining procedures, and the examined cortical areas and layers. In our study, data from healthy control individuals of experiments examining adult human, rat and mouse cortical areas was extracted. To exclude effects resulting from differences in reconstruction methods, only neuron reconstructions made using NeuroLucida software were included for analysis. Extracted neuron cytoarchitectonic properties as examined here included metrics of total neuron length, number of dendritic branches and soma surface.

Human neuron morphology. NeuroMorpho.org extraction from studies on human cortex included experiments using Golgi, rapid-Golgi and Golgi-Scheibel staining procedures, and described a total of 1916 neuron recordings across 10 cortical areas. Information on neuronal cytoarchitectonic properties was extracted from these recordings, and averaged for each cortical area. Next, the reported regions were manually mapped to a 2×57 regions subdivision of the Desikan-Killiany cortical atlas of the FreeSurfer software suite (Cammoun et al., 2012; Desikan et al., 2006; Fischl, 2012; van den Heuvel et al., 2016, 2015b) (DK-57, describing 57 distinct cortical areas per hemisphere) for comparison to macroscale connectivity (Figure 1A shows the mapping of the included cortical regions). This resulted in morphological data of in total 10 areas of the human cortex (mean number recordings per area 185, std 147 (range: 70-594)), including left-hemispheric sub areas of lateral occipital cortex, pars opercularis, postcentral, precentral, rostral middle frontal, superior frontal (2 sub areas), superior temporal, supramarginal and insular cortex. Regions and their mappings are shown in Figure 1A .

Rat neuron morphology. NeuroMorpho.org extraction from studies on the rat brain included experiments using Golgi, Golgi-Cox, Biocytin, Lucifer Yellow, Neurobiotin, biotinylated dextran amine (BDA), and horseradish peroxidase (HRP) staining procedures, and described 875 neuron recordings across 10 different cortical sites. Similar to the human extraction, data on primary and secondary metrics was extracted from the NeuroMorpho.org recordings and averaged for each cortical area. Regions included areas MOp, MOs, SSp, AON, PL, AIId, PERI, CA1, CA2 and AUDp (mean/std: 83/97 (range: 1-283) recordings per cortical area)(Figure 1). Using the Swanson rat cortical atlas (Swanson, 1992), these areas were mapped to regions of which macroscale connectivity was available in the mesoscale BAMS-II rat cortical connectome map as presented by Swanson and Bota (Bota et al., 2015).

Mouse neuron morphology. NeuroMorpho.org extraction on the mouse brain included experiments using Golgi, Golgi-Cox and rapid-Golgi staining procedures, and described a total of 408 neuron recordings across 7 brain areas. Similar as in the human and rat dataset, morphological data of the reconstructed neurons in the database were extracted, with values subsequently averaged across cortical areas. Using the Allen

Mouse Brain Atlas (<http://mouse.brain-map.org>), these cortical areas were manually mapped to cortical areas included in the connectome map of Oh and coworkers (Oh et al., 2014) (see Figure 1A for a visual representation of the included regions), resulting in neuron information for 7 brain regions (mean/std: 58/58 (range: 1-167) recordings per cortical area): AON, BLA, CA1, CA3, MOs, SSP-bfd and VISp.

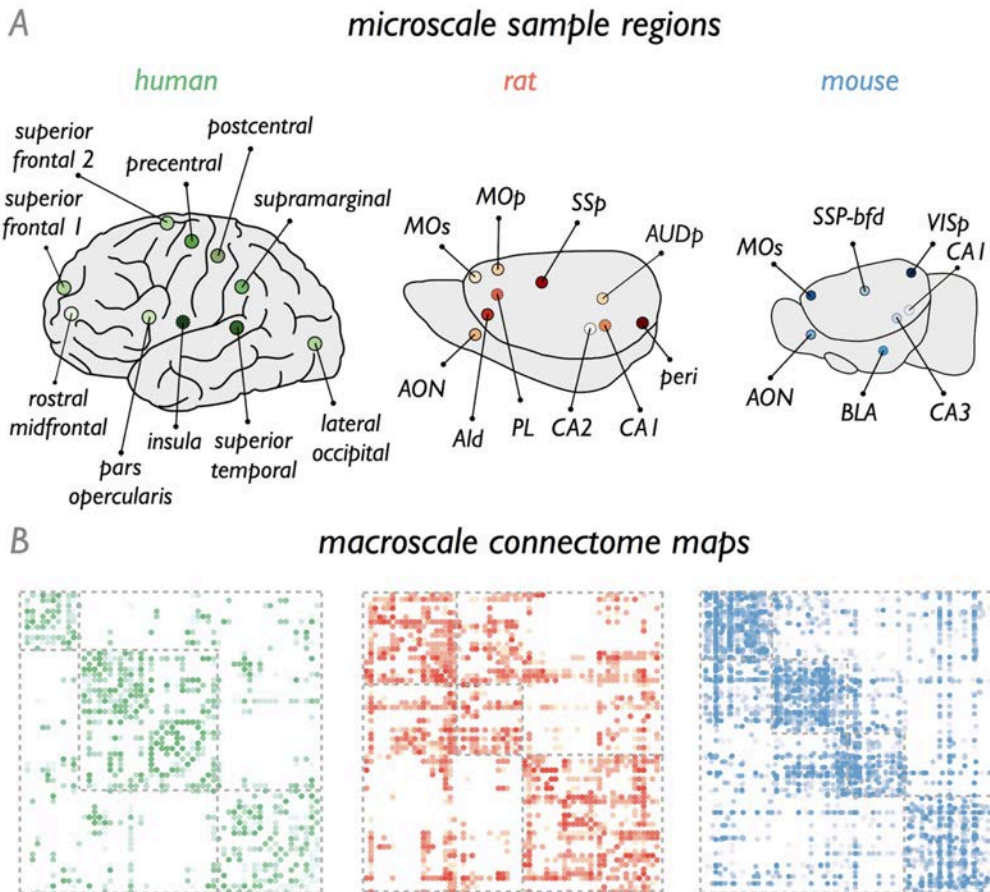


Figure 1. **A.** Schematic representation of cortical areas reported in the NeuroMorpho.org data mapped to regions of the adopted human (DK-57 atlas), rat (Swanson atlas (Swanson, 1992)) and mouse (Allen Mouse Brain Atlas) brain atlases. Figures highlight the regions for which neuronal morphological data could be extracted from the NeuroMorpho.org database, approximate location of medial regions depicted with a dotted outline. From left to right: human, rat and mouse data. **B.** Extracted connectivity matrices of the human (as derived from in vivo DWI data from the Human Connectome Project), rat (as derived from the BAMS-II rat connectome database (Bota and Swanson, 2007)) and mouse (as derived from the Allen Mouse Brain Connectivity Atlas (Oh et al., 2014)) connectome.

Macroscale connectome data

Human connectome. Data on macroscale connectivity of the human brain was derived

from the high-resolution Diffusion Weighted Imaging (DWI) data from the Human Connectome Project (Van Essen et al., 2013), including data of 215 subjects (Q3 release, voxel size 1.25 mm isotropic, TR/TE 5520/89.5 ms, 3×90 diffusion directions with diffusion weighting 1000, 2000 and 3000 s/mm^2). Preprocessing involved correction for eddy current and susceptibility distortions and realignment of the diffusion-weighted and B=0 images (Glasser et al., 2013). Next, for each individual dataset, white matter, grey matter, and cortical spinal fluid (CSF) classification was performed based on the T1 anatomical image (Q3, voxel size .7 mm isotropic) using FreeSurfer (Fischl, 2012), followed by a 3D reconstruction of the cortical mantle and parcellation of the cortex into 114 distinct cortical areas (57 unique regions per hemisphere) using a subdivision of FreeSurfer's Desikan-Killiany atlas (Cammoun et al., 2012; Desikan et al., 2006; Scholtens et al., 2015), providing the 57 cortical areas to which the reported cortical regions of the NeuroMorpho.org dataset were mapped (see Figure 1A). Subsequently, for each voxel, the diffusion profile was computed by applying generalized q-sampling imaging (GQI) to the DWI data, allowing for the reconstruction of complex fiber configurations (e.g. crossing fibers) (de Reus and van den Heuvel, 2014; Romme et al., 2017; Yeh et al., 2010). Streamline tractography was then used to reconstruct white matter pathways, starting 8 streamlines in each white matter voxel, following the best matching diffusion direction from voxel to voxel. A streamline was stopped when it exited the brain tissue mask, made a sharp turn of 45 degrees or more, or reached a voxel with a low fractional anisotropy (a threshold of .1 was used). Combination of the 114 parcellated cortical regions and the tractography streamlines resulted in the formation of a weighted structural connectivity matrix of size $N \times N$ by selecting the subsets of reconstructed tractography streamlines that touched both region i and j , for all pairs (i, j) of the $N = 114$ cortical regions. To reduce potential false positive reconstructions, pathways consisting of > 5 streamlines were included for further analysis (Verstraete et al., 2013). Next, the resulting individual connectivity matrices of the 215 subjects were combined into a group-averaged structural connectivity matrix (SC, Figure 1B) by taking the non-zero mean of the individual matrices, including a region-to-region connection when a pathway was found in at least 71 of the 215 subjects (i.e., 33%) (de Reus and van den Heuvel, 2013a; Verstraete et al., 2013). Graph theoretical analysis was used to compute the number of pathways (in DWI, due to the absence of information on projection directionality, data on efferent and afferent pathways was combined) of each of the cortical areas, reflecting a region's network degree. To match the single hemisphere datasets of the mouse and rat connectome (see below), for the human dataset nodal degree values of regions from the left hemisphere were taken for further analysis. [Taking nodal degree data from the right hemisphere revealed similar findings].

Rat connectome. Data on macroscale connectivity of the rat brain was obtained from the recent rat connectome mapping of the BAMS-II database by Swanson and Bota and colleagues, providing a comprehensive collation of data from multiple tract-tracing experiments in the rat brain. The BAMS-II database of Swanson and Bota (<http://brancusi1.usc.edu/connectome/>; (Bota et al., 2015; Bota and Swanson, 2007)) describes macroscale connectivity between 67 regions of the rat brain (described and analyzed in (Bota et al., 2015)). For 1662 region pairs (37.6% of total number of pairs), information on the non-existence, existence, and/or strength (1424 of 1487 projections) of region-to-region macroscale pathways was extracted. In total, this dataset described a single hemisphere connectome of 67 regions and 1487 pathways, represented as a directed 67×67 connectivity matrix. Region pairs for which no information on connectivity was present (i.e., NaNs in the matrix) were taken as non-connected regions (i.e., represented as a 0) (Bota et al., 2015; van den Heuvel et al., 2015), resulting in a connectivity matrix with a density of 31.6% (Figure 1B). For each of the cortical regions of the rat brain, the network degree was computed as the total number of combined efferent and afferent pathways of a cortical area.

Mouse connectome. Data on macroscale connectivity of the mouse brain was taken from the recently mapped mesoscale mouse connectome from the Allen Institute for Brain Science (<http://connectivity.brain-map.org> (Oh et al., 2014)). This connectome dataset comprises a fully mapped mesoscale connectome of 213 regions describing a single hemisphere of the mouse brain, including an initial weighted and directed connectivity matrix of 213 regions with 16954 inter-areal pathways and 37.5% density. To eliminate very weak projections (reflecting potential false positive mappings (Oh et al., 2014)), a strength threshold of .75 was applied, resulting in a directed connectivity matrix of 3433 pathways and 7.6% density (depicted in Figure 1B). For each of the cortical and subcortical areas, the network degree was computed, taken as the total number of efferent and afferent pathways of each area.

Micro-macro cross-scale analysis

For the three datasets, data on regional microscale neuron morphology (describing 3 micrometrics, of in total 10 cortical regions for the human dataset, 10 for the rat, and 7 regions for the mouse brain) were examined in the context of levels of regional variation in macroscale connectivity (i.e. nodal network degree) by means of Pearson's correlation analyses. With the individual microscale (3 metrics) and macroscale metrics (2 metrics) correlated, correction for multiple testing was performed by computing the actual number of independent tests performed via Principal Component Analysis (PCA) (Scholtens et al., 2014). A significance threshold of $p < .01$ was used, with effects of $p < .05$ taken as trend-level effects.

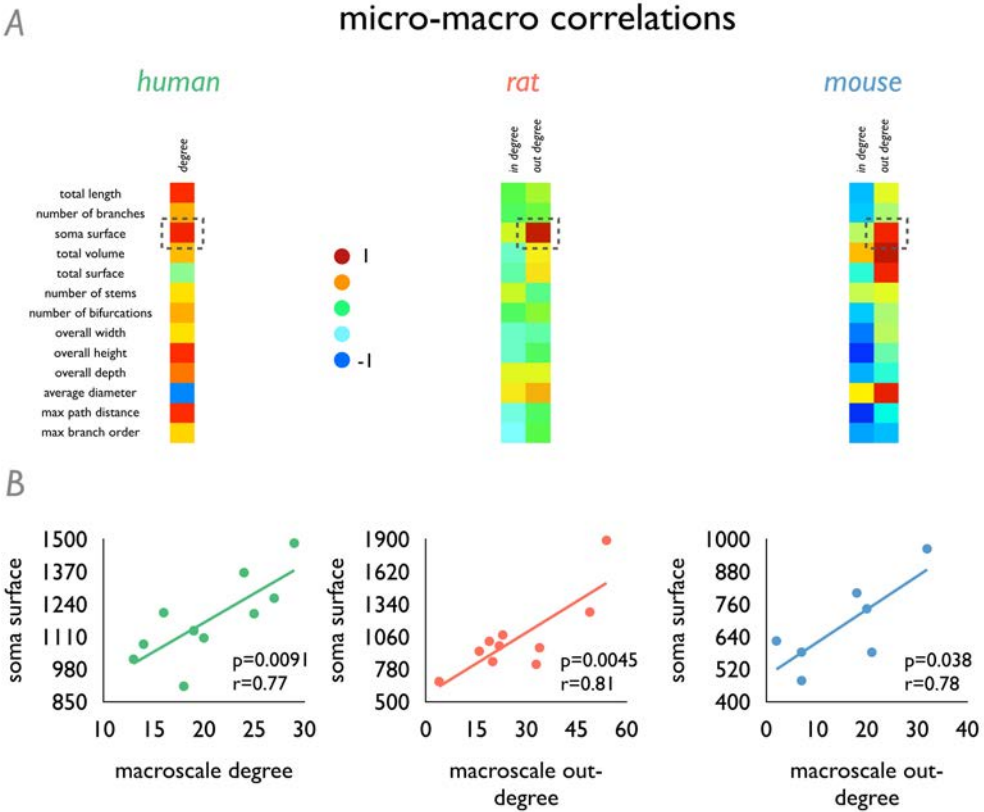


Figure 2. A. Panels show the correlation vectors between regional levels of the 13 extracted microscale metrics (as extracted from the NeuroMorpho.org database) and regional macroscale connectivity (described by network degree in the human, and network in-degree and out-degree in the rat and mouse). From left to right: human, rat and mouse data. B. Panels show cross-scale correlation plots of regional variation in neuron morphology and macroscale connectivity. Left panel shows the association between regional variation in neuron soma surface and macroscale connectivity in the human dataset (correlation over 10 cortical regions of which data in the NeuroMorpho.org database was present). Middle panel shows the association between regional variation in total soma surface and number of efferent pathways (i.e. network out-degree) in the rat brain. Right panel shows the association between regional variation in soma surface and number of efferent pathways (out-degree) in the mouse dataset.

Results

Micro-macro correlations Human. In the human dataset, regional variation in soma surface ($r = .7706$, $p = .0091$) correlated significantly to regional variation in the total number of reconstructed white matter pathways, with regions displaying a dense macroscale connectivity profile overlapping with those cortical areas showing larger neurons. A trend level effect was observed between macroscale degree and total neuron length ($r = .7015$, $p = .0238$). No clear association was observed between macroscale degree and dendritic branching ($p = .2290$, Figure 2A). *Rat.* Cortical variation in soma

surface showed to be related to regional variation in the number of efferent macroscale pathways (i.e. out-degree, $r = .8102$, $p = .0045$, Figure 2). This effect was observed to be specific to out-degree, with no such effect observed with in-degree ($p = .1864$). *Mouse.* Cross-scale analysis in the mouse revealed a trend-level relationship of microscale soma surface ($r = .7794$, $p = .0388$, Figure 2B). A significant relationship between out-degree and total neuron volume was observed ($r = .8754$, $p = .0059$, Figure 2A). No correlations were observed with network in-degree.

Discussion

Cross-scale analysis on neuron morphology and meso- and macroscale connectivity provides further evidence of aspects of neural connectivity across different scales of mammalian cortical organization to be related.

Findings of an association between micro- and macroscale features of brain connectivity in the cat, macaque and human cortex include observations of a predictive role of cytoarchitectonic classes on the existence of corticocortical axonal pathways (Barbas, 2015; Beul et al., 2015; Hilgetag and Grant, 2010; Hilgetag, 2000), an association recently confirmed in the rat connectome (Goulas et al., 2017). A similar association has previously been reported between macroscale connectivity and layer 3 pyramidal complexity (Scholtens et al., 2014; van den Heuvel et al., 2016, 2015b). We now further confirm findings in the rodent brain, providing evidence of a micro-macro association in two of the most highly detailed tract-tracing connectome mappings present for mammalian species. Our findings also confer on recent observations showing granular structure of the cortex to be related to the level of between-network functional connectivity (Wylie et al., 2015). Findings in the human, mouse and rat thus converge on an association and potential interplay between architectonic features of neural connectivity at the micro- and macroscale of brain organization in mammalian neural systems.

What may be the etiology of such a potential micro-macro relationship? Our observations – and those of the mentioned previous studies – are inferential of nature, meaning they show a correlation between microscale and macroscale variables of brain organization. Such correlation analyses cannot answer the important question of whether one effect is driving the other. Whether neuronal morphological or cytoarchitectonic structure allow for the existence of large-scale macroscale pathways and connectivity profiles, or whether the cytoarchitectonic organization of a cortical region is shaped by the amount and type of neural information from large-scale macroscale axonal projections remains unknown. Cortical development may form a

strong influential factor on this relationship, with both organizational scales of connectivity simultaneously shaped by developmental processes. Post-mortem observations in young developing animals have suggested initial widespread axonal growth followed by a long period of pruning and local specialization of long-range axonal projections (Innocenti and Price, 2005; LaMantia and Rakic, 1994), thus suggesting a potential interaction between local neuronal activation and the formation and tuning of inter-areal communication patterns (Innocenti and Price, 2005). As such, with a reductionist view, one could argue that processes of dendritic specialization and synaptic pruning may lead to the formation and pruning of long-range axonal pathways that connect to these pruned synapses. Vice versa, variation in axonal pathways of cortical regions has also been suggested to have direct consequences for regional differentiation in cytoarchitecture (Schüz and Miller, 2002), from which one could speculate on the notion of macroscale anatomical and functional patterns to play a role in developmental patterns in the formation, growth and pruning of dendritic branches and synapses. Interestingly, a recent report on macaque developmental gene expression and cytoarchitecture showed a late formation of adult-like cortical regional and laminar molecular phenotypes, pointing towards an important role of functional cell-cell interaction in forming mature cellular phenotypes (Bakken et al., 2016). From the presented micro-macro findings we speculate on a similar – and intertwined – developmental pattern of macroscale connectivity. In humans, studies have shown clear developmental change of large-scale patterns of anatomical and functional connectivity (Betz et al., 2014; Fair et al., 2009; Hagmann et al., 2010; van den Heuvel et al., 2014). Furthermore, previous observations have shown differential developmental time windows between cortical regions on both the microscale (e.g. cellular proliferation, migration and elimination (Dombrowski et al., 2001)) as well as on the macroscale (e.g. myelination of large axonal pathways as observed by (Flechsig, 1920)), suggesting that the timing of the different interacting processes may serve as an important modulator in establishing the observed adult region-wise micro-macro associations.

Studies have reported both overlap (e.g. (Brodmann, 1909; Campbell, 1905; Goulas et al., 2014)) and cross-species differences in pyramidal and cytoarchitectonic organization of cortical regions (Elston et al., 2001, 2011) and macroscopic connectome formation (Li et al., 2013; Miranda-Dominguez et al., 2014). Contrasts in pyramidal complexity between unimodal and multimodal association cortex have been suggested to be significantly different across primate species, arguing for both an absolute as well as a relative increase in neuronal organization of pyramidal neurons from unimodal regions to higher-order association cortex in humans as compared to primates (Elston et al., 2001, 2011). Interestingly, in parallel, studies examining cross-species differences in macroscale connectivity of cortical areas have shown evidence of frontal cortical areas

to display differences in macroscale connectivity patterns from primates to humans (Sallet et al., 2013). The frontal cortex is among those brain regions showing the largest evolutionary differences in developmental timing, with an extended developmental period in humans compared to other primates on both the microscale (e.g. synaptogenesis (Petanjek et al., 2011)) and the macroscale (myelination (Miller et al., 2012)). Future studies could examine whether, and if so how, such cross-species differences in micro- and macroscale connectivity are related.

Several points need to be taken into account when interpreting the reported findings. First, as a direct result of our study design, our examination is limited by the amount of microscale data (and in particular the number of areas) available in the NeuroMorpho.org database. Due to the highly labor intensive nature of microscale measurements, our analysis is limited to a small number of regions. However, the observation of effects to be consistent across three different species provides strong validation of the reported micro-macro relationship. Second, it should be noted that the examined microscale data involves a collation of data across multiple experiments and across different studies of different groups, and thus involves a collation of data acquired across multiple research conditions, study designs, specimens with varying age and gender, varying mouse/rat strains, as well as data obtained across different measurement methodologies. Different staining and neuron reconstruction methods can have for example different sensitivity profiles, potentially leading to subjective measurements across research groups. To overcome these differences, the NeuroMorpho.org database contains detailed information on the original source and applied experimental procedures and, importantly, includes standardized 3D reconstructions of the individual neurons examined in the reported studies, which allows for a standardized extraction of morphological metrics. Third, even though the mouse and rat connectome datasets contain highly detailed information on mesoscale connectivity, the included connectome datasets are formed by collating data from a large number of specimens (Bota et al., 2015; Oh et al., 2014), involving a group-averaged consensus connectome map (de Reus and van den Heuvel, 2013b). Concerning the reconstructed human connectome map, diffusion weighted MR imaging depends on the estimation of the diffusion profile of water molecules and thus involves an indirect measurement of axonal pathways. As a result, diffusion MRI is known to include several limitations and caveats, with in particular a difficulty in resolving pathway orientation in white matter areas with complex fiber architecture, leading to argued over- and underestimations of classes of white matter pathways (Jones, 2008; van den Heuvel et al., 2015a). As a fourth remark, we once again stress that our study involves a meta-regression type of analysis in which data of several histology reports and data on tract reconstruction of multiple specimens are collated into one single

dataset. The micro- and macroscale data is thus acquired across different specimens and we note that this means that we could only examine variation across different areas of the cortex, but not across individual specimens. A dataset including data on micro- and macroscale connectivity of single specimens would allow for a much more detailed examination. In particular, such studies would allow for the examination of influences of external factors on a micro-macro interplay of connectivity and as such could provide new insights into how brain properties like learning or complex cognitive behavior can emerge from the smallest and largest aspects of neural organization.

Taken together, our findings across the human, rat and mouse cortex provide converging evidence for a relationship between aspects of neural organization at the smallest and largest organizational scales of the mammalian brain. Examining this micro-macro interplay, and a possible disruption therein, may provide new ways to better comprehend the etiology of neurodegenerative and neurodevelopmental brain disorders (van den Heuvel et al., 2016) as many neurological and psychiatric brain disorders have been noted to display affected neural connectivity and disrupted connectome formation at both the micro- and macroscale level of organization.

References

- Adelstein JS, Shehzad Z, Mennes M, DeYoung CG, Zuo XN, Kelly C, Margulies DS, Bloomfield A, Gray JR, Castellanos FX (2011) Personality is reflected in the brain's intrinsic functional architecture. *PLoS one* 6:e27633.
- Ascoli GA (1999) Progress and perspectives in computational neuroanatomy. *Anat Rec* 257:195–207.
- Ascoli GA (2006) Mobilizing the base of neuroscience data: the case of neuronal morphologies. *Nature reviews. Neuroscience* 7:318.
- Ascoli GA, Donohue DE, Halavi M (2007) Neuromorpho. org: a central resource for neuronal morphologies. *Journal of Neuroscience* 27:9247–9251.
- Ascoli GA, Krichmar JL, Nasuto SJ, Senft SL (2001) Generation, description and storage of dendritic morphology data. *Philosophical Transactions of the Royal Society of London B: Biological Sciences* 356:1131–1145.
- Bakken TE, Miller JA, Ding SL, Sunkin SM, Smith KA, Ng L, Szafer A, Dalley RA, Royall JJ, Lemon T, Shapouri S, Aiona K, Arnold J, Bennett JL, Bertagnolli D, Bickley K, Boe A, Brouner K, Butler S, Byrnes E, Caldejon S, Carey A, Cate S, Chapin M, Chen J, Dee N, Desta T, Dolbear TA, Dotson N, Ebbert A, Fulfs E, Gee G, Gilbert TL, Goldy J, Gourley L, Gregor B, Gu G, Hall J, Haradon Z, Haynor DR, Hejazinia N, Hoerder-Suabedissen A, Howard R, Jochim J, Kinnunen M, Kriedberg A, Kuan CL, Lau C, Lee CK, Lee F, Luong L, Mastan N, May R, Melchor J, Mosqueda N, Mott E, Ngo K, Nyhus J, Oldre A, Olson E, Parente J, Parker PD, Parry S, Pendergraft J, Potekhina L, Reding M, Riley ZL, Roberts T, Rogers B, Roll K, Rosen D, Sandman D, Sarreal M, Shapovalova N, Shi S, Sjoquist N, Sodt AJ, Townsend R, Velasquez L, Wagley U, Wakeman WB, White C, Bennett C, Wu J, Young R, Youngstrom BL, Wohnoutka P, Gibbs RA, Rogers J, Hohmann JG, Hawrylycz MJ, Hevner RF, Molnar Z, Phillips JW, Dang C, Jones AR, Amaral DG, Bernard A, Lein ES (2016) A comprehensive transcriptional map of primate brain development. *Nature* 535:367–75.
- Barbas H (2015) General cortical and special prefrontal connections: Principles from structure to function. *Annual Review of Neuroscience* 38:269–289.
- Betzl RF, Byrge L, He Y, Goni J, Zuo XN, Sporns O (2014) Changes in structural and functional connectivity among resting-state networks across the human lifespan. *Neuroimage* 102 Pt 2:345–57.
- Beul SF, Grant S, Hilgetag CC (2015) A predictive model of the cat cortical connectome based on cytoarchitecture and distance. *Brain Structure and Function* 220:3167–3184.
- Bota M, Dong HW, Swanson LW (2012) Combining collation and annotation efforts toward completion of the rat and mouse connectomes in bams. *Frontiers in neuroinformatics* 6.

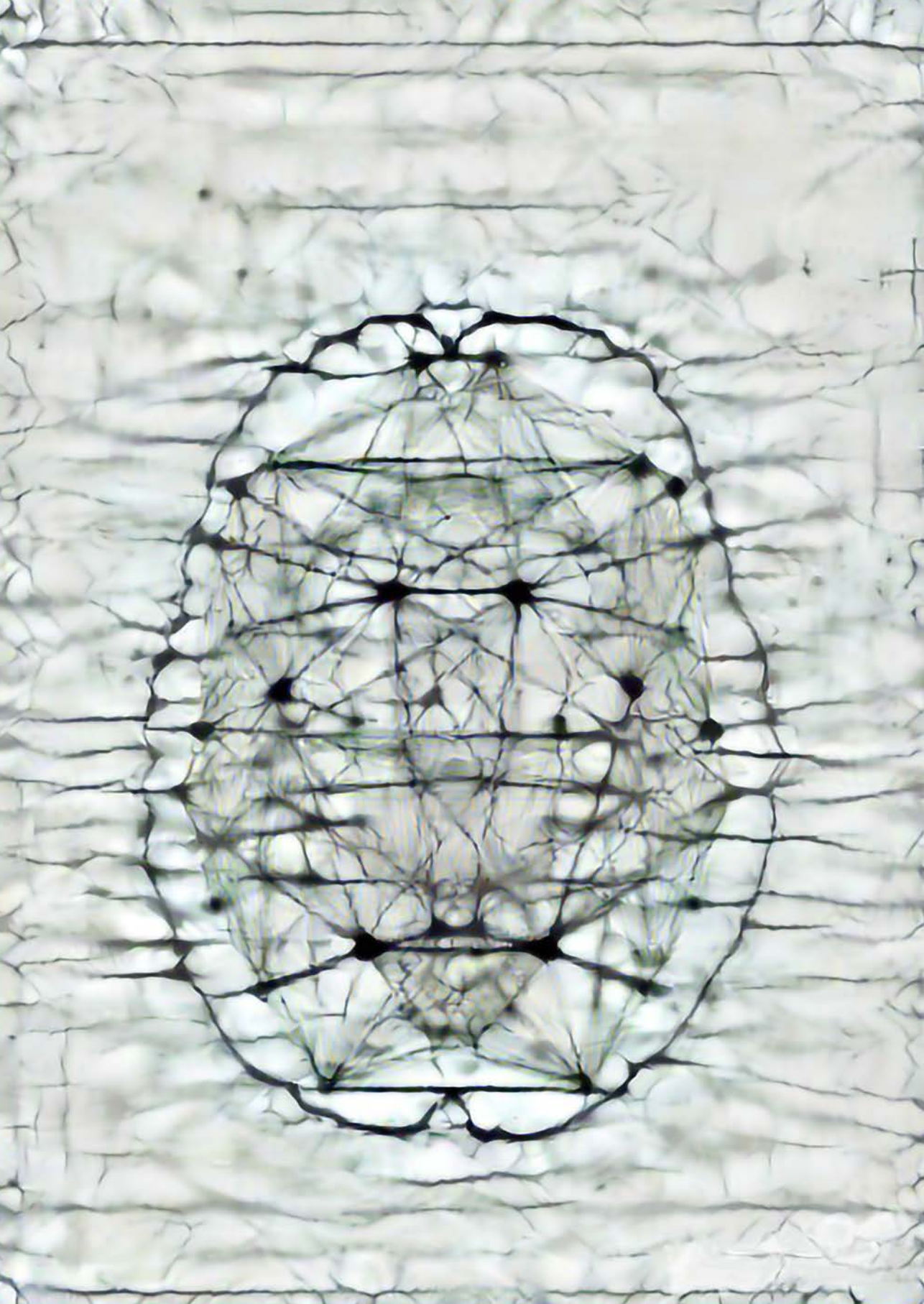
- Bota M, Sporns O, Swanson LW (2015) Architecture of the cerebral cortical association connectome underlying cognition. *Proceedings of the National Academy of Sciences* .
- Bota M, Swanson LW (2007) Online workbenches for neural network connections. *Journal of Comparative Neurology* 500:807–814.
- Brodmann K (1909) *Vergleichende Lokalisationslehre der Grosshirnrinde in ihren Prinzipien dargestellt auf Grund des Zellenbaues* Barth.
- Bullmore E, Sporns O (2009) Complex brain networks: graph theoretical analysis of structural and functional systems. *Nat Rev Neurosci* 10.
- Bullmore E, Sporns O (2012) The economy of brain network organization. *Nature reviews. Neuroscience* 13:336–49.
- Cammoun L, Gigandet X, Meskaldji D, Thiran JP, Sporns O, Do KQ, Maeder P, Meuli R, Hagmann P (2012) Mapping the human connectome at multiple scales with diffusion spectrum mri. *Journal of neuroscience methods* 203:386–97.
- Campbell AW (1905) *Histological studies on the localisation of cerebral function* University Press.
- Charvet CJ, Cahalane DJ, Finlay BL (2015) Systematic, cross-cortex variation in neuron numbers in rodents and primates. *Cerebral Cortex* 25:147–160.
- de Reus M, van den Heuvel M (2013a) Estimating false positives and negatives in brain networks. *Neuroimage* 70:402–9.
- de Reus M, van den Heuvel M (2013b) The parcellation-based connectome: Limitations and extensions. *NeuroImage* 80:397–404.
- de Reus MA, van den Heuvel MP (2014) Simulated rich club lesioning in brain networks: a scaffold for communication and integration? *Frontiers in Human Neuroscience* 8.
- Desikan RS, Segonne F, Fischl B, Quinn BT, Dickerson BC, Blacker D, Buckner RL, Dale AM, Maguire RP, Hyman BT, Albert MS, Killiany RJ (2006) An automated labeling system for subdividing the human cerebral cortex on mri scans into gyral based regions of interest. *Neuroimage* 31:968–80.
- Dombrowski SM, Hilgetag CC, Barbas H (2001) Quantitative architecture distinguishes prefrontal cortical systems in the rhesus monkey. *Cereb Cortex* 11:975–88.
- Elston GN (2003) Cortex, cognition and the cell: New insights into the pyramidal neuron and prefrontal function. *Cerebral Cortex* 13:1124–1138.
- Elston GN, Benavides-Piccione R, DeFelipe J (2001) The pyramidal cell in cognition: a comparative study in human and monkey. *The Journal of neuroscience : the official journal of the Society for*

- Neuroscience* 21:RC163.
- Elston GN, Benavides-Piccione R, Elston A, Manger PR, Defelipe J (2011) Pyramidal cells in prefrontal cortex of primates: marked differences in neuronal structure among species. *Frontiers in neuroanatomy* 5:2.
- Elston GN, Okamoto T, Oga T, Dornan D, Fujita I (2010) Spinogenesis and pruning in the primary auditory cortex of the macaque monkey (*macaca fascicularis*): an intracellular injection study of layer iii pyramidal cells. *Brain research* 1316:35–42.
- Fair DA, Cohen AL, Power JD, Dosenbach NU, Church JA, Miezin FM, Schlaggar BL, Petersen SE (2009) Functional brain networks develop from a "local to distributed" organization. *PLoS Comput Biol* 5:e1000381.
- Finlay BL, Uchiyama R (2015) Developmental mechanisms channeling cortical evolution. *Trends Neurosci* 38:69–76.
- Fischl B (2012) Freesurfer. *NeuroImage* 62:774–781.
- Flechsig P (1920) *Anatomie des menschlichen Gehirns und Rückenmarks auf myelogenetischer Grundlage* G. Thieme.
- Glasser MF, Sotiropoulos SN, Wilson JA, Coalson TS, Fischl B, Andersson JL, Xu J, Jbabdi S, Webster M, Polimeni JR, Van Essen DC, Jenkinson M, for the WUMHCPC (2013) The minimal preprocessing pipelines for the human connectome project. *NeuroImage* 80:105–124.
- Goulas A, Bastiani M, Bezgin G, Uylings HB, Roebroek A, Stiers P (2014) Comparative analysis of the macroscale structural connectivity in the macaque and human brain. *PLoS Comput Biol* 10:e1003529.
- Goulas A, Uylings HB, Hilgetag CC (2017) Principles of ipsilateral and contralateral cortico-cortical connectivity in the mouse. *Brain Structure and Function* 222:1281–1295.
- Hagmann P, Sporns O, Madan N, Cammoun L, Pienaar R, Wedeen VJ, Meuli R, Thiran JP, Grant PE (2010) White matter maturation reshapes structural connectivity in the late developing human brain. *Proc Natl Acad Sci U S A* 107:19067–72.
- Hammarberg C (1895) *Studien über Klinik und Pathologie der Idiotie, nebst untersuchungen über die normale Anatomie der Hirnrinde* Druck der Edv. Berling.
- Hilgetag CC, Grant S (2010) Cytoarchitectural differences are a key determinant of laminar projection origins in the visual cortex. *Neuroimage* 51:1006–17.
- Hilgetag C (2000) Hierarchical organization of macaque and cat cortical sensory systems explored with a novel network processor. *Philos Trans R Soc Lond B Biol Sci* 355:71–89.

- Innocenti GM, Price DJ (2005) Exuberance in the development of cortical networks. *Nat Rev Neurosci* 6:955–65.
- Jacobs B, Schall M, Prather M, Kapler E, Driscoll L, Baca S, Jacobs J, Ford K, Wainwright M, Tremblay M (2001) Regional dendritic and spine variation in human cerebral cortex: a quantitative golgi study. *Cerebral Cortex* 11:558–571.
- Jones DK (2008) Studying connections in the living human brain with diffusion mri. *Cortex* 44:936–52.
- LaMantia AS, Rakic P (1994) Axon overproduction and elimination in the anterior commissure of the developing rhesus monkey. *J Comp Neurol* 340:328–36.
- Li L, Hu X, Preuss TM, Glasser MF, Damen FW, Qiu Y, Rilling J (2013) Mapping putative hubs in human, chimpanzee and rhesus macaque connectomes via diffusion tractography. *Neuroimage* 80:462–74.
- Li Y, Liu Y, Li J, Qin W, Li K, Yu C, Jiang T (2009) Brain anatomical network and intelligence. *PLoS computational biology* 5:e1000395.
- Mesulam MM (1998) From sensation to cognition. *Brain* 121:1013–1052.
- Miller DJ, Duka T, Stimpson CD, Schapiro SJ, Baze WB, McArthur MJ, Fobbs AJ, Sousa AMM, Šestan N, Wildman DE, Lipovich L, Kuzawa CW, Hof PR, Sherwood CC (2012) Prolonged myelination in human neocortical evolution. *Proceedings of the National Academy of Sciences* 109:16480–16485.
- Miranda-Dominguez O, Mills BD, Grayson D, Woodall A, Grant KA, Kroenke CD, Fair DA (2014) Bridging the gap between the human and macaque connectome: a quantitative comparison of global interspecies structure-function relationships and network topology. *J Neurosci* 34:5552–63.
- Oh SW, Harris JA, Ng L, Winslow B, Cain N, Mihalas S, Wang Q, Lau C, Kuan L, Henry AM, Mortrud MT, Ouellette B, Nguyen TN, Sorensen SA, Slaughterbeck CR, Wakeman W, Li Y, Feng D, Ho A, Nicholas E, Hirokawa KE, Bohn P, Joines KM, Peng H, Hawrylycz MJ, Phillips JW, Hohmann JG, Wahnoutka P, Gerfen CR, Koch C, Bernard A, Dang C, Jones AR, Zeng H (2014) A mesoscale connectome of the mouse brain. *Nature* 508:207–214.
- Park HJ, Friston K (2013) Structural and functional brain networks: from connections to cognition. *Science* 342:1238411.
- Pessoa L (2012) Beyond brain regions: Network perspective of cognition–emotion interactions. *Behavioral and Brain Sciences* 35:158–159.
- Petanjek Z, Judaš M, Šimić G, Rašin MR, Uylings HBM, Rakic P, Kostović I (2011) Extraordinary

- neoteny of synaptic spines in the human prefrontal cortex. *Proceedings of the National Academy of Sciences* 108:13281–13286.
- Romme IAC, de Reus MA, Ophoff RA, Kahn RS, van den Heuvel MP (2017) Connectome disconnectivity and cortical gene expression in patients with schizophrenia. *Biological Psychiatry* 81:495–502.
- Sallet J, Mars RB, Noonan MP, Neubert FX, Jbabdi S, O'Reilly JX, Filippini N, Thomas AG, Rushworth MF (2013) The organization of dorsal frontal cortex in humans and macaques. *J Neurosci* 33:12255–74.
- Scholtens LH, de Reus MA, van den Heuvel MP (2015) Linking contemporary high resolution magnetic resonance imaging to the von Economo legacy: A study on the comparison of MRI cortical thickness and histological measurements of cortical structure. *Human Brain Mapping* 36:3038–3046.
- Scholtens LH, Schmidt R, de Reus MA, van den Heuvel MP (2014) Linking macroscale graph analytical organization to microscale neuroarchitectonics in the macaque connectome. *The Journal of Neuroscience* 34:12192–12205.
- Schüz A, Miller R (2002) *Cortical areas: unity and diversity* Conceptual advances in brain research. Taylor & Francis, London; New York.
- Shanahan M (2012) The brain's connective core and its role in animal cognition. *Philosophical Transactions of the Royal Society B: Biological Sciences* 367:2704–2714.
- Sporns O, Tononi G, Kötter R (2005) The human connectome: a structural description of the human brain. *PLoS computational biology* 1:e42.
- Swanson L (1992) *Brain maps: structure of the rat brain* Elsevier, Amsterdam.
- Tomasi D, Volkow ND (2011) Association between functional connectivity hubs and brain networks. *Cerebral cortex* 21:2003–2013.
- van den Heuvel MP, Kersbergen KJ, de Reus MA, Keunen K, Kahn RS, Groenendaal F, de Vries LS, Benders MJ (2014) The neonatal connectome during preterm brain development. *Cereb Cortex* 25:3000–3013.
- van den Heuvel MP, Scholtens LH, de Reus MA, Kahn RS (2016) Associated microscale spine density and macroscale connectivity disruptions in schizophrenia. *Biol Psychiatry* 80:293–301.
- van den Heuvel MP, de Reus MA, Feldman Barrett L, Scholtens LH, Coopmans FMT, Schmidt R, Preuss TM, Rilling JK, Li L (2015a) Comparison of diffusion tractography and tract-tracing measures of connectivity strength in rhesus macaque connectome. *Human Brain Mapping* 36:3064–3075.

- van den Heuvel MP, Scholtens LH, Feldman Barrett L, Hilgetag CC, de Reus MA (2015b) Bridging cytoarchitectonics and connectomics in human cerebral cortex. *The Journal of Neuroscience* 35:13943–13948.
- van den Heuvel MP, Scholtens LH, Turk E, Mantini D, Vanduffel W, Feldman Barrett L (2016) Multimodal analysis of cortical chemoarchitecture and macroscale fmri resting-state functional connectivity. *Human brain mapping* 37:3103–3113.
- van den Heuvel MP, Sporns O (2013) Network hubs in the human brain. *Trends in cognitive sciences* 17:683–696.
- van den Heuvel M, Scholtens L, de Reus M (2015) Topological organization of connectivity strength in the rat connectome. *Brain Structure and Function* pp. 1–18.
- Van Essen DC, Smith SM, Barch DM, Behrens TE, Yacoub E, Ugurbil K (2013) The wu-minn human connectome project: an overview. *Neuroimage* 80:62–79.
- Verstraete E, Veldink JH, van den Berg LH, van den Heuvel MP (2013) Structural brain network imaging shows expanding disconnection of the motor system in amyotrophic lateral sclerosis. *Human brain mapping* 00:1–11.
- Von Economo CF, Koskinas GN (1925) *Die Cytoarchitektonik der Hirnrinde des erwachsenen Menschen* J. Springer.
- Wylie KP, Kronberg E, Maharajh K, Smucny J, Cornier MA, Tregellas JR (2015) Between-network connectivity occurs in brain regions lacking layer iv input. *NeuroImage* 116:50–58.
- Yeh FC, Wedeen VJ, Tseng WYI (2010) Generalized q-sampling imaging. *IEEE transactions on medical imaging* 29:1626–1635.
- Zamora-López G, Zhou C, Kurths J (2010) Cortical hubs form a module for multisensory integration on top of the hierarchy of cortical networks. *Frontiers in Neuroinformatics* 4.



Rich layer III pyramidal morphology of highly connected macroscale regions: a pilot study

Lianne H. Scholtens, Rory Pijnenburg and Martijn P. van den Heuvel

In preparation

The human brain consists of a large variety of microscale cellular morphologies and macroscale global properties. Together, these multiscale properties of the brain form a network system supportive of efficient information processing and integration. Highly connected hub regions of the macroscale connectome have been proposed to play a crucial role in these integrative processes, and to have a microscale architecture supportive of such a computationally demanding role in the brain. Here, we present the first observations of a pilot study employing the classic Golgi method to in more detail quantify the microscale character of known hub and non-hub regions of the human cerebral cortex.

Introduction

The mammalian brain is a complex system, with a micro and macroscale cortical organization supportive of integration of information from a wide variety of sources. Highly connected regions in the brain – also known as hub regions – have been described to be crucial for the integrative capacity of the brain (van den Heuvel et al., 2012). Recent studies have shown that microscale cytoarchitectural properties of cortical regions are associated to a region's macroscale connectivity profile, with hub

regions having a more agranular cortical type, and larger and more spinous layer III pyramidal cells than non-hub regions (see for review (van den Heuvel et al., 2016)). For example, studies investigating the relation between cortical type and macroscale connectivity in rodent, cat, macaque and human cortex have shown regions with similar cortical type to have a larger probability to be interconnected, and regions with a more agranular cortical type to have more cortical connections than others (Beul et al., 2015; Beul and Hilgetag, 2017; Goulas et al., 2017, 2016). In previous work of our group, we have reported on similar associations between a region's layer III pyramidal cell complexity and its number of corticocortical connections. In the macaque cortex, regions with larger, more branched and more spinous pyramidal cells in layer III – known to be an important layer for long-range corticocortical connectivity – were shown to have more and longer projections to other cortical regions (Scholtens et al., 2014). Similarly, in the human brain, combining microscale pyramidal cell complexity data from literature involving quantifications of Golgi-stained brain tissue showed regions with larger, more branched layer III pyramidal cells with more dendritic spines to have more and stronger macroscale corticocortical connectivity (van den Heuvel et al., 2016, 2015). Further extending these comparisons to schizophrenia, a disorder long hypothesized to be one of brain disconnectivity (e.g. (Friston and Frith, 1995; Stephan et al., 2006)), showed larger reductions in layer III pyramidal spine density as obtained from literature to be associated with larger macroscale disconnectivity (van den Heuvel et al., 2016). These previously mentioned micro-macro comparisons all incorporated collated data across many literature sources with differing staining and reconstruction methods, and although valuable were only able to give a partial view of the putative micro-macro association.

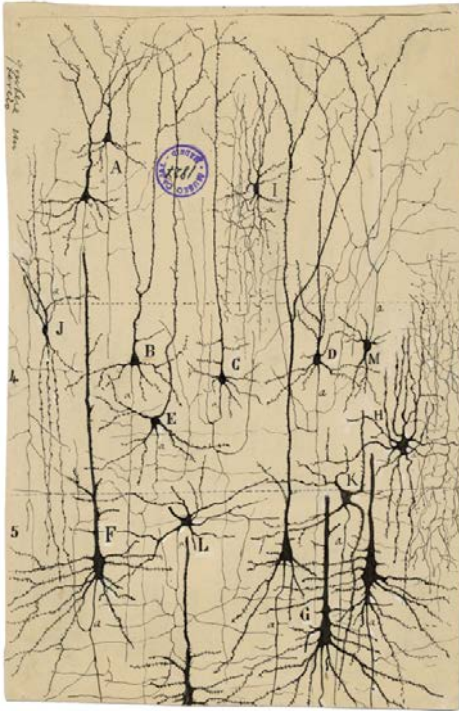
Here, we describe a pilot study in which we performed Golgi-Cox staining in 7 cortical locations overlapping with established cortical hub and non-hub regions described in literature and reconstructed layer III pyramidal cell morphology in each of these regions. We first confirm a micro – macro association previously observed in collated data from literature. Next, we combine our newly obtained information with data from literature sources (as collated in (van den Heuvel et al., 2016)), to enable a more complete micro-macro comparison of pyramidal complexity and hub connectivity in the human brain.

Methods

Microscale Golgi-Cox staining procedure and data acquisition

The famous “black reaction” developed by Camillo Golgi in 1873 (Golgi, 1873) lies at the foundation of modern neuroscience. Since the Golgi method only stains a sparse subset of all neurons, it enabled scientists to for the first time obtain a relatively

A



B



Figure 1. Historical and modern examples of Golgi-stained brain tissue. A) Legacy illustration by Ramón y Cajal (Ramón y Cajal, 1904) based on histological preparations of the cat cortex using the Golgi silver impregnation method. The illustration gives an overview of the size, shape and distribution of different cell types in the cerebral cortex as observed by Cajal. B) Photo of a Golgi-Cox preparation made by the authors, aiming to capture an overview of cortical cell types similar to that depicted in the illustration by Ramón y Cajal included in part A of this figure.

complete overview of brain morphology. Ramón y Cajal used an adapted version of Golgi's silver staining for his experiments that would lead to his world-famous schematic illustrations of black neurons (Figure 1A). Since its inception, many different adaptations to the original silver impregnation method have been developed. To name a few commonly used variants, Golgi-Kopsch (Kopsch, 1896; Riley, 1979), (modified) rapid Golgi (e.g. (Scheibel and Scheibel, 1978)) and Golgi-Cox (Cox, 1891). For our pilot study, we used the Golgi-Cox protocol as described by van der Loos (van der Loos, 1959) (Figure 1B), which has been noted to reliably yield well defined dendritic arborization with low background staining, and to have relatively low sensitivity to post mortem delay compared to other Golgi techniques (Buell, 1982; Swaab and Uylings,

Tissue sample location	Desikan-Killiany parcel
gyrus precentralis	precentral gyrus
gyrus postcentralis	postcentral gyrus
gyrus frontalis superior	superior frontal gyrus
gyrus frontalis medius	rostral middle frontal gyrus
gyrus occipitalis superior	lateral occipital gyrus
gyrus cingula anterior	rostral anterior cingulate gyrus
medial gyrus parietalis superior	precuneus

Table 1. Mapping of pilot tissue sample locations to Desikan-Killiany FreeSurfer parcellation atlas. The left column describes the locations of tissue samples as obtained from the NBB, the right column lists the labels of the FreeSurfer Desikan-Killiany atlas (Desikan et al., 2006) to which the locations of the tissue samples were mapped. All regions were sampled from the left hemisphere.

1987).

Tissue samples

Tissue was obtained from a clinical control subject (female, 81 years of age) of the Netherlands Brain Bank (NBB) in Amsterdam. Post mortem delay of this subject was 5 hours and 15 minutes. Tissue blocks were obtained from 7 cortical locations in the left hemisphere of the brain, while taking care to not apply too much pressure to avoid staining artifacts. The fresh brain tissue was moved directly into light-proof jars containing Golgi-Cox solution, for simultaneous fixation and impregnation (van der Loos, 1959). Thin tissue blocks (0.5 cm), were cut perpendicular to the gyral surface, spanning the complete width of the gyrus of interest. Regions included in this pilot study were selected to overlap with both known macroscale highly connected hub regions and non-hub regions. In order to allow for comparisons to previous studies of other groups reported in literature, some selected regions were overlapping with those reported in literature. The selected cortical locations included: 1) gyrus precentralis; 2) gyrus postcentralis; 3) gyrus frontalis superior; 4) gyrus frontalis medius; 5) gyrus occipitalis superior; 6) gyrus cingula anterior; 7) medial gyrus parietalis superior (precuneus).

Tissue processing

Golgi-Cox impregnation. After 48 hours of impregnation, the Golgi-Cox solution was replaced with fresh stock Golgi-Cox solution to reduce tissue precipitate. After 2.5 to 3 weeks of Golgi-Cox impregnation, the quality and progression of the Golgi-Cox impregnation was assessed. Criteria for Golgi-Cox impregnation quality assessment were 1) complete impregnation of the dendritic branches (including the tips both basal and apical dendrites) of cells throughout the section; 2) clearly visible dendritic spines on all most distal branches; while 3) avoiding overimpregnation of the tissue. Next, the tissue blocks were removed from the Golgi-Cox solution, rinsed briefly in tap water and moved to the next tissue processing step.

Dehydration and celloidin embedding. The tissue was dehydrated over the course of 2 days in a grading ethanol series (ethanol 70%-96%-100%), followed by 24 hours in a mixture of 100% ethanol – (di)Ethyl ether (1:2). After dehydration, the tissue was placed in a graded series of celloidin in 100% ethanol – (di)Ethyl ether (1:2).

For the final embedding step, each tissue block was placed in an uncoated paper box made to size. The bottom of each box was filled with a thin layer of 10% celloidin, which was allowed some time to dry in order to form a thin membrane before carefully placing the tissue on top. The tissue was oriented to later facilitate the preferred plane of cutting in the sectioning step. Afterwards the box was filled with more 10% celloidin and allowed to dry for 30 minutes. Next, the boxes were placed in a glass desiccator, weighted down and submerged in chloroform. After hardening in the chloroform for 24 hours, the boxes were moved to ethanol 70% for storage.

Sectioning. Before sectioning, tissue blocks were removed from their paper box, mounted onto a block using 10% celloidin and placed in ethanol 70% until fixed. Tissue blocks were sectioned perpendicular to the cortical layering, and parallel to the apical dendrites of the pyramidal cells. The tissue was sectioned into 180 μ m thick sections using a sledge microtome (Leica / Reichert-Jung Polycut S) and transferred to ethanol 70% in individual compartments of a Teflon disk. The disk was used during the entire free-floating development and dehydration process.

The sections were rinsed in demineralized water, after which the staining was developed by placing them in a 16% ammonium solution (NH₄OH; 15 minutes), followed by rinsing and further development in 1% sodium thiosulfate (Na₂S₂O₃; 7 minutes). Next, the sections were again thoroughly rinsed, after which the sections for Nissl counter staining were moved to the cresyl violet solution, while the rest was moved through 5 minutes each of ethanol 70%, ethanol 90% and butanol for dehydration. Finally, the sections were placed in HistoClear (National Diagnostics, Atlanta USA) for 5 minutes, after which they were mounted in Histomount (National Diagnostics, Atlanta USA) on microscopic slides and coverslipped. Weights were placed on the cover slips in order to flatten the sections, and the slides were placed in the dark at 4°C to dry. After drying, the weights were removed, the slides cleaned of excess mounting medium and stored horizontally in the dark at 4°C.

Nissl counter staining of non-impregnated neurons. In every sixth section, non-impregnated neurons were counterstained using a solution of 2.5% cresyl violet, in order to provide some assessment of the cytoarchitecture of the cortical region. The sections were submerged in the cresyl violet solution for 10 minutes, at which point the tissue was stained completely purple. After rinsing off the excess dye in demineralized

water, the sections were rinsed in 70% ethanol until all background staining had been cleared, after which the sections were dehydrated and further processed according to the main protocol (see above paragraph).

Cell selection and quantification

Pyramidal cells for Neurolucida reconstruction were selected from the set of neurons with their soma located in deep supragranular layer III. A neuron was included when 1) the cell was located in the center of the tissue section; 2) it had at least two basal dendrites that each branched at least twice; 3) no branches were occluded by staining artifacts or other cells. We did not exclude neurons with cut branches, to avoid a selection bias towards smaller neurons (Uylings et al., 1986). Neurons were reconstructed with Neurolucida software (MicroBrightfield, Williston), using a 40x oil-immersion objective (Carl Zeiss Axioskop microscope). Pyramidal cells were manually traced using the neuron tracing tools included in Neurolucida, automatically registering the 3D dimensions and branch order of each reconstructed neuron part. Tracing started at the axon, followed by the soma of the neuron, after which the main branch of the apical dendrite was reconstructed for orientation purposes. Finally, the basal dendrites including all branches were traced. Neuron reconstruction was performed by two observers (LHS and RP). After an initial training phase both observers quantified a set of 10 pyramidal cells and the resulting data was used to calibrate future reconstructions of both observers to each other.

For this pilot, 8 neurons per cortical region were reconstructed. After reconstruction was completed, screenshots of the section at multiple magnifications were saved to note the specific location of each individual neuron (thus preventing the same neuron from being included multiple times), and neuron morphometric information was exported using Neurolucida Explorer (MicroBrightfield, Williston). For the purpose of this pilot study, in which we aimed to make a first assessment of the variation in our sample of reconstructed neurons, we chose to focus our analyses on the total length of the basal dendrites since we considered this to be one of the most basic measures, which has consistently been reported to be associated to macroscale connectivity (Scholtens et al., 2014; van den Heuvel et al., 2016).

Macroscale diffusion-weighted connectome reconstruction

High resolution diffusion-weighted scans of 500 subjects of the Human Connectome Project (HCP; (Van Essen et al., 2013); S500 release; $n = 487$ subjects, age 22-35 years, male and female combined) were used to reconstruct a macroscale human connectome map. Imaging parameters included 1.25 mm isotropic voxel size, TR/TE 5520/89.5 ms, 270 diffusion directions with diffusion weighting 1000, 2000, or 3000 s/mm². For each individual, preprocessing of the diffusion-weighted images included realignment, eddy

Brodmann Area	Desikan-Killiany parcel
3-1-2	postcentral gyrus
4	precentral gyrus
6	superior frontal gyrus
10	superior frontal gyrus
11	rostral middle frontal gyrus
13	insular cortex
18	lateral occipital gyrus
22	superior temporal gyrus
39	supramarginal gyrus
44	pars opercularis

Table 2. Mapping of literature tissue sample locations to Desikan-Killiany FreeSurfer parcellation atlas. The left column describes the locations (Brodmann Areas) of the tissue samples as described in literature, the right column lists the labels of the FreeSurfer Desikan-Killiany atlas (Desikan et al., 2006) to which the locations of the tissue samples were mapped.

current and susceptibility distortion correction, followed by a voxel-wise reconstruction of diffusion profiles using generalized q-sampling imaging, and whole-brain streamline tractography (see (de Reus and van den Heuvel, 2014) for more details on this method of HCP connectome reconstruction). High resolution anatomical T1 scans (voxel-size .7 mm isotropic) were used for cortical segmentation and FreeSurfer (Fischl et al., 2004) parcellation of the cortical sheet of each individual subject into 68 distinct regions (34 regions per hemisphere) using the Desikan-Killiany atlas (Desikan et al., 2006; Hagmann et al., 2008). The resulting individual cortical parcellation was overlaid with the subject's whole-brain tractography to form a 68×68 connectivity matrix, describing each pair of regions and their reconstructed pathways. The strength of a connection between regions was computed as number of streamlines, measured as the number of tractography streamlines touching both cortical regions. A group-level threshold of 60% was applied, including for analysis those connections that have been consistently reconstructed in at least 60% of the subjects (van den Heuvel and Sporns, 2011).

Statistical analysis and scaling to literature data

The cortical locations of the obtained samples were mapped to the regions included in the Desikan-Killiany parcellation atlas (Table 1). The putative association between regional total basal dendritic length of layer III pyramidal neurons and macroscale connectivity (computed as the number of corticocortical connections between regions) was assessed by means of Pearson correlation analysis. Collated information on layer III pyramidal cell morphometry, as previously used in (van den Heuvel et al., 2016) was also mapped to the Desikan-Killiany atlas (Table 2; including data from (Anderson et al., 2009; Garey et al., 1998; Hutsler and Zhang, 2010; Jacobs et al., 1997, 2001; Zeba et al., 2008)). Since differences in experimental protocols can result in differences in absolute measures of pyramidal cell morphology, pilot-literature overlapping regions in the precentral and postcentral gyrus were used to compute a scaling factor between our pilot data and data from literature sources. Next, this scaling factor was applied to the pilot regions to bring

the data into the same range to allow for direct comparison of our pilot data to layer III pyramidal neuron morphology reported in literature (for a similar approach see (van den Heuvel et al., 2016)).

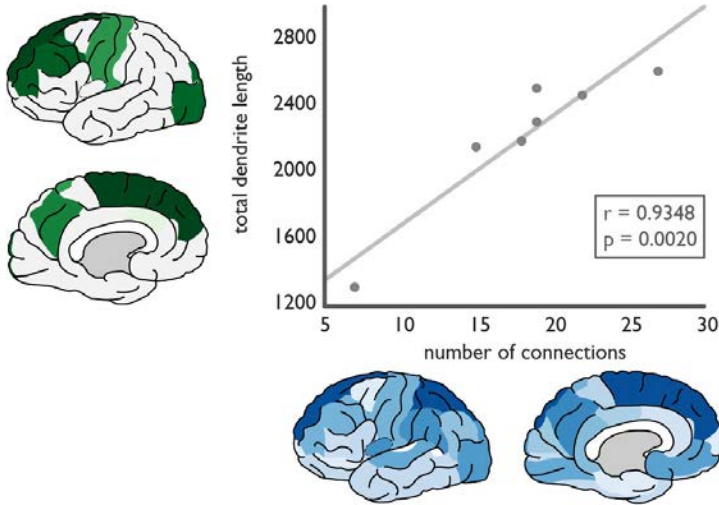


Figure 2. Association between microscale basal dendritic length pilot data and macroscale connectivity. Scatter plot shows an association between regional microscale total basal dendritic length of layer III pyramidal cells (y -axis) and macroscale connectivity (x -axis, number of corticocortical connections; $r = .9348$, $p = .0020$). The schematic surface representations next to the axes show the regional number of connections in blue and the total basal dendrite length in green (darker colors represent higher values). Microscale pilot data based on measurements in 7 cortical regions of a single individual.

Results

Preliminary micro-macro association in pilot data

Cross-correlation between regional microscale data on layer III pyramidal complexity in our pilot data and macroscale connectivity revealed a significant micro – macro association. In line with previous findings (Scholtens et al., 2014; van den Heuvel et al., 2016) the number of macroscale connections (i.e., network nodal degree) of cortical regions revealed a positive correlation with layer III pyramidal total basal dendrite length ($r = .9348$, $p = .0020$, Figure 2).

Combined analysis with literature data

A similar, but trend-level correlation was observed when merging our pilot data on dendritic length with data from literature sources ($r = .6094$, $p = .0614$). The insular cortex appears to be an outlier to the observed association, showing a large number of macroscale connections although it has relatively small layer III dendritic tree length. Removing the insular region, from the comparison results in a much stronger micro –

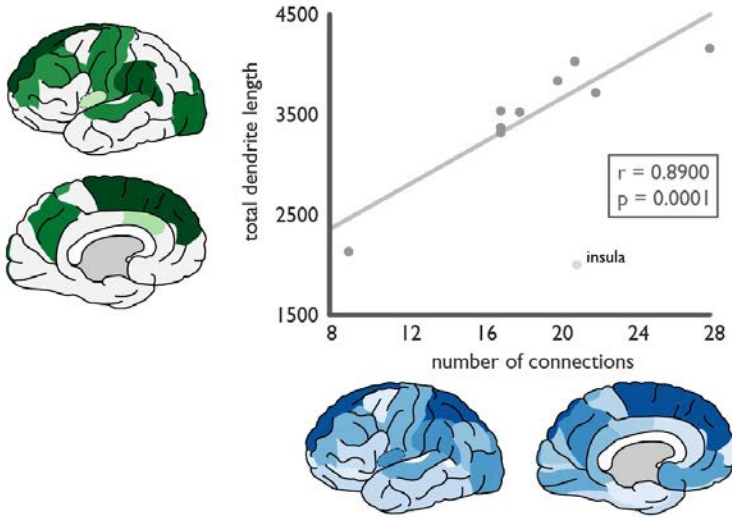


Figure 3. Association between combined pilot and literature data of basal dendritic tree length and macroscale connectivity. Scatter plot shows a trend level association between combined literature and pilot data on microscale total basal dendritic tree length of layer III pyramidal cells (y -axis) and the number of macroscale corticocortical connections of a cortical region (x -axis; $r = .6094$, $p = .0614$). The insular cortex appears to form an outlier to the association, excluding this region from the comparison results in a stronger micro-macro association ($r = .8900$, $p = .0001$).

macro correlation ($r = .8900$, $p = .0001$; Figure 3). Taken together, this indicates that our pilot data presented here shows a very similar relation to macroscale connectivity as data previously collated in literature. This supports the notion of the micro and macroscale of brain organization to be intertwined.

Discussion

In this pilot study, we report on a micro-macro association between newly acquired microscale data on layer III pyramidal basal dendritic tree length in 7 established hub and non-hub regions and macroscale connectivity. We show that our preliminary results are in line with the micro-macro associations previously observed based on literature data, and that larger basal dendritic tree length in layer III pyramidal cells is associated with increased macroscale corticocortical connectivity.

Some important points should be kept in mind when interpreting the results of this pilot study. First, the preliminary data presented in this manuscript is based on pyramidal cell morphology measurements acquired in 7 cortical regions of a single subject. This subject, although included as a clinical control of the NBB, is with 81 years of age significantly older than the HCP subjects of which high-resolution diffusion weighted images were

included into the connectome analysis. Nevertheless, the observed relation between microscale dendritic tree length and macroscale connectivity *across regions* in our pilot data is in line with observations previously reported in literature (Figure 3; (Scholtens et al., 2014; van den Heuvel et al., 2016, 2015)). Furthermore, dendritic tree length of layer III pyramidal cells has been shown to be less susceptible to ageing effects than those of pyramidal cells of infragranular layers (de Brabander et al., 1998; Uylings and de Brabander, 2002).

Second, in our analysis combining pilot and literature data, the insular cortex appears to be an outlier to the general observation. A possible explanation may be related to the relative coarseness of the Desikan-Killiany atlas used in this comparison, especially when considering that the insular cortex can be divided into subregions with distinct functions and connectivity patterns in the brain (e.g. (Barbas, 2015)). Using a higher resolution atlas that allows for a more precise mapping of microscale data to a specific portion of the insula would be of interest, also for all other microscale data available. Alternatively, the fact that the insular cortex appears to be an outlier could be related to the limited number of regions in our analyses. Including other limbic regions could provide more insight into whether these follow the pattern observed in the rest of the cortex.

Third, the specificity of Golgi-type stainings is a long-standing topic of discussion in the field (e.g. (Buell, 1982; Ramon-Moliner, 1970; Swaab and Uylings, 1987)). In Golgi-impregnated tissue, a seemingly random subset of neurons in the cortex is stained a dark saturated black, an “all or nothing” process leaving the vast majority of neurons unstained and transparent. While it is precisely this sparse staining that enables the tracing of individual neurons using this technique, the reason why some neurons are stained while most are not remains unclear (see e.g. (Ramon-Moliner, 1970; Swaab and Uylings, 1987)). Two hypotheses have been suggested regarding the underlying mechanisms. According to the first, the functional activity of a neuron in its last moments is an important factor, with neurons active at the moment of death being more likely to be stained (Bertram and Sheppard, 1964). This does however not account for the observation that other non-neuronal parts of impregnated tissue (e.g. blood vessels) can also be stained. A second hypothesis suggests that the Golgi-impregnated neurons were somehow more vulnerable to the staining procedure because they were already less healthy to start with or were previously damaged (i.e. Golgi-type stainings color damaged, unhealthy or even dying neurons). This argument has been countered to a certain extent by the observation that impregnation of more well-preserved tissue – with arguably more intact neurons – results in an improvement of the Golgi stain (Morest and Morest, 1966). A further counter argument against a preferential staining of damaged or diseased neurons could be made by the successful application of Golgi stainings to demonstrate neuronal proliferation or plasticity, for example in studies of

increased neuronal growth in rats reared in an enriched environment (Bose et al., 2010; Faherty et al., 2003; Uylings et al., 1978). Interestingly, the mechanisms underlying the seemingly random staining of neurons appear not to be identical between variants of the Golgi method. For example, it has been noted that Golgi-Cox seems to preferentially stain healthy neurons, while rapid Golgi and Golgi-Kopsch are more suited for studies of pathological tissue (Swaab and Uylings, 1987). Nevertheless, the unique capacity of the Golgi method to visualize a sparse subset of different neurons in the brain – showing the cortical morphology “as it really is” – ensures that even almost 150 years after its inception, the Golgi method still has added value next to other more targeted histological methods.

Building upon the pilot results presented here, we aim to expand our analyses of neuron morphometry using Golgi-Cox impregnated tissue to more individuals, and potentially to a wider range of cortical layers and regions. This would provide us with a more complete coverage of the cortical surface for comparison with macroscale connectivity. In addition to including more subjects and more regions to our analyses, other measures could be included, for instance quantifying synapses, glia cells, or the distribution of neurotransmitter receptors. Layer-wise, cell-type specific or even single-cell gene expression analyses could be of interest to assess in more detail how microscale measures are related to each other and to macroscale connectivity. Ultimately, future studies would combine high resolution neuroimaging and whole-brain microscale measurements in the same individual to directly assess the putative relation between both scales of organization in the brain.

Acknowledgments

This work was supported by the Netherlands Organization for Scientific Research VIDI grant (MPvdH, VIDI-452-16-015).

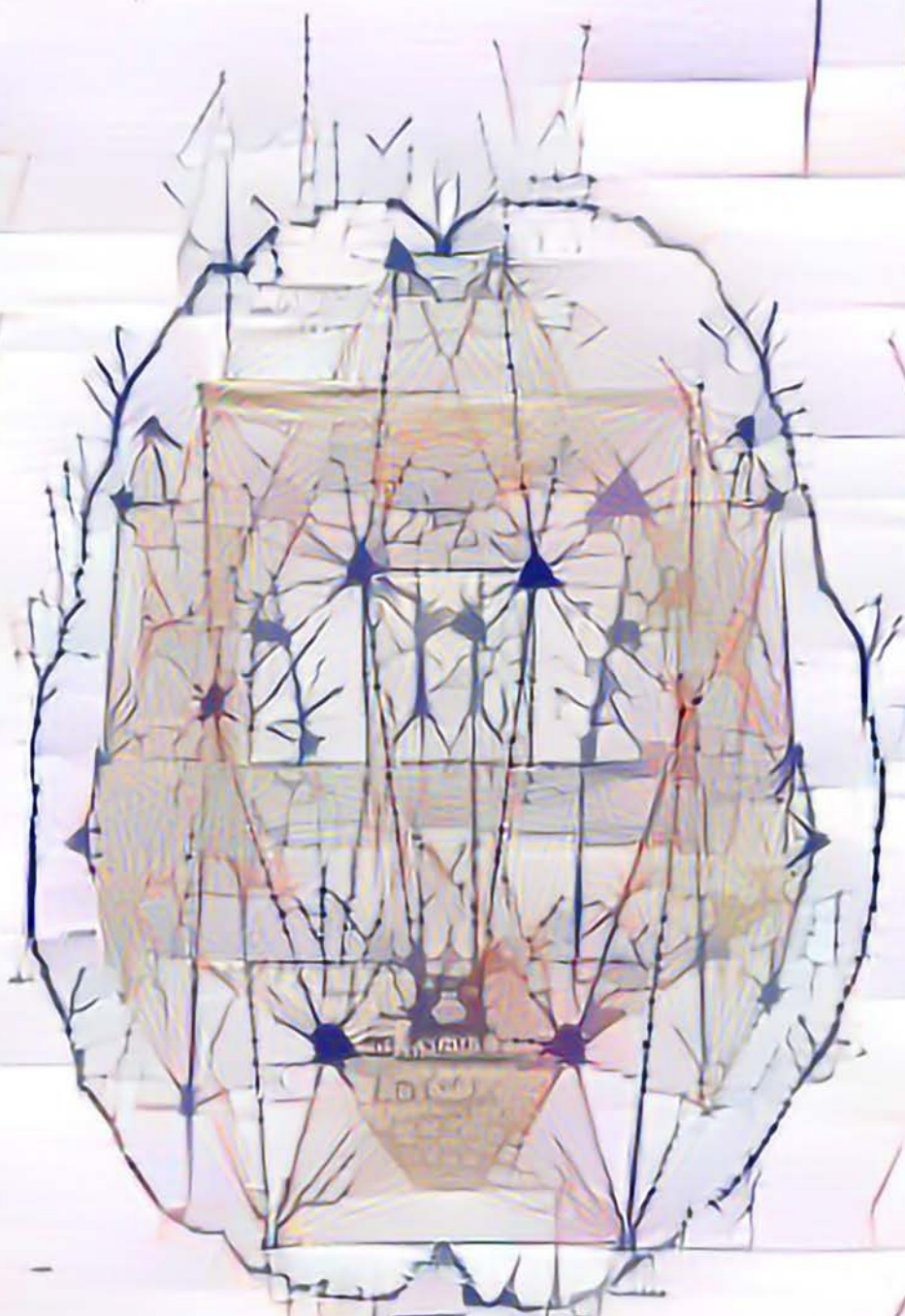
References

- Anderson K, Bones B, Robinson B, Hass C, Lee H, Ford K, Roberts TA, Jacobs B (2009) The morphology of supragranular pyramidal neurons in the human insular cortex: a quantitative golgi study. *Cereb Cortex* 19:2131–44.
- Barbas H (2015) General cortical and special prefrontal connections: Principles from structure to function. *Annual Review of Neuroscience* 38:269–289.
- Bertram E, Sheppard C (1964) Possible explanation for golgi impregnation of neurons. *Anatomical Record* 148:413.
- Beul SF, Grant S, Hilgetag CC (2015) A predictive model of the cat cortical connectome based on cytoarchitecture and distance. *Brain Structure and Function* 220:3167–3184.
- Beul SF, Hilgetag CC (2017) Neuron density is a fundamental determinant of structural connectivity in the primate cerebral cortex. *bioRxiv* p. 117051.
- Bose M, Muñoz-Llancao P, Roychowdhury S, Nichols JA, Jakkamsetti V, Porter B, Byrapureddy R, Salgado H, Kilgard MP, Aboitiz F, Dagnino-Subiabre A, Atzori M (2010) Effect of the environment on the dendritic morphology of the rat auditory cortex. *Synapse (New York, N.Y.)* 64:97–110.
- Buell SJ (1982) Golgi-cox and rapid golgi methods as applied to autopsied human brain tissue: widely disparate results. *Journal of Neuropathology & Experimental Neurology* 41:500–507.
- Cox WH (1891) Imprägnation des centralen nervensystems mit quecksilbersalzen. *Archiv für mikroskopische Anatomie* 37:16–21.
- de Brabander JM, Kramers RJK, Uylings HBM (1998) Layer-specific dendritic regression of pyramidal cells with ageing in the human prefrontal cortex. *European Journal of Neuroscience* 10:1261–1269.
- de Reus MA, van den Heuvel MP (2014) Simulated rich club lesioning in brain networks: a scaffold for communication and integration? *Frontiers in Human Neuroscience* 8.
- Desikan RS, Segonne F, Fischl B, Quinn BT, Dickerson BC, Blacker D, Buckner RL, Dale AM, Maguire RP, Hyman BT, Albert MS, Killiany RJ (2006) An automated labeling system for subdividing the human cerebral cortex on mri scans into gyral based regions of interest. *Neuroimage* 31:968–80.
- Faherty CJ, Kerley D, Smeyne RJ (2003) A golgi-cox morphological analysis of neuronal changes induced by environmental enrichment. *Developmental Brain Research* 141:55–61.
- Fischl B, van der Kouwe A, Destrieux C, Halgren E, Segonne F, Salat DH, Busa E, Seidman

- LJ, Goldstein J, Kennedy D, Caviness V, Makris N, Rosen B, Dale AM (2004) Automatically parcellating the human cerebral cortex. *Cereb Cortex* 14:11–22.
- Friston KJ, Frith CD (1995) Schizophrenia: a disconnection syndrome? *Clin Neurosci* 3:89–97.
- Garey LJ, Ong WY, Patel TS, Kanani M, Davis A, Mortimer AM, Barnes TRE, Hirsch SR (1998) Reduced dendritic spine density on cerebral cortical pyramidal neurons in schizophrenia. *Journal of Neurology, Neurosurgery & Psychiatry* 65:446–453.
- Golgi C (1873) Sulla struttura della sostanza grigia del cervello. *Gazzetta Medica Italiana. Lombardia* 33:244–246.
- Goulas A, Uylings HB, Hilgetag CC (2017) Principles of ipsilateral and contralateral cortico-cortical connectivity in the mouse. *Brain Structure and Function* 222:1281–1295.
- Goulas A, Werner R, Beul SF, Saering D, van den Heuvel M, Triarhou LC, Hilgetag CC (2016) Cytoarchitectonic similarity is a wiring principle of the human connectome. *bioRxiv* p. 068254.
- Hagmann P, Cammoun L, Gigandet X (2008) Mapping the structural core of human cerebral cortex. *PLoS biology* 6:e159.
- Hutsler JJ, Zhang H (2010) Increased dendritic spine densities on cortical projection neurons in autism spectrum disorders. *Brain Res* 1309:83–94.
- Jacobs B, Driscoll L, Schall M (1997) Life-span dendritic and spine changes in areas 10 and 18 of human cortex: a quantitative golgi study. *J Comp Neurol* 386:661–80.
- Jacobs B, Schall M, Prather M, Kapler E, Driscoll L, Baca S, Jacobs J, Ford K, Wainwright M, Trembl M (2001) Regional dendritic and spine variation in human cerebral cortex: a quantitative golgi study. *Cerebral Cortex* 11:558–571.
- Kopsch F (1896) Erfahrungen uber die verwendung des formaldehyds bei chromsilber-impregnation. *Anat. Anz.* 11:727.
- Morest DK, Morest R (1966) Perfusion-fixation of the brain with chrome-osmium solutions for the rapid golgi method. *Developmental Dynamics* 118:811–831.
- Ramon-Moliner E (1970) *The Golgi-Cox technique*, pp. 32–55 Springer.
- Ramón y Cajal S (1904) *Textura del sistema nervioso del hombre y los vertebrados. Madrid: Moya, N.*
- Riley JN (1979) A reliable golgi-kopsch modification. *Brain research bulletin* 4:127–129.
- Scheibel ME, Scheibel AB (1978) The methods of golgi. *Neuroanatomical research techniques* 89:114.

- Scholtens LH, Schmidt R, de Reus MA, van den Heuvel MP (2014) Linking macroscale graph analytical organization to microscale neuroarchitectonics in the macaque connectome. *The Journal of Neuroscience* 34:12192–12205.
- Stephan KE, Baldeweg T, Friston KJ (2006) Synaptic plasticity and dysconnection in schizophrenia. *Biological psychiatry* 59:929–939.
- Swaab D, Uylings H (1987) Potentialities and pitfalls in the use of human brain material in molecular neuroanatomy. *Manual ETP/ENA/IBRO practical course Molecular Neuroanatomy* pp. 549–566.
- Uylings HBM, de Brabander JM (2002) Neuronal changes in normal human aging and alzheimer's disease. *Brain and Cognition* 49:268–276.
- Uylings H, Kuypers K, Diamond MC, Veltman W (1978) Effects of differential environments on plasticity of dendrites of cortical pyramidal neurons in adult rats. *Experimental neurology* 62:658–677.
- Uylings H, Ruiz-Marcos A, Van Pelt J (1986) The metric analysis of three-dimensional dendritic tree patterns: a methodological review. *Journal of neuroscience methods* 18:127–151.
- van den Heuvel MP, Bullmore ET, Sporns O (2016) Comparative connectomics. *Trends Cogn Sci* 20:345–61.
- van den Heuvel MP, Scholtens LH, de Reus MA, Kahn RS (2016) Associated microscale spine density and macroscale connectivity disruptions in schizophrenia. *Biol Psychiatry* 80:293–301.
- van den Heuvel MP, Kahn RS, Goñi J, Sporns O (2012) High-cost, high-capacity backbone for global brain communication. *Proceedings of the National Academy of Sciences of the United States of America* 109:11372–11377.
- van den Heuvel MP, Scholtens LH, Feldman Barrett L, Hilgetag CC, de Reus MA (2015) Bridging cytoarchitectonics and connectomics in human cerebral cortex. *The Journal of Neuroscience* 35:13943–13948.
- van den Heuvel MP, Sporns O (2011) Rich-club organization of the human connectome. *The Journal of neuroscience : the official journal of the Society for Neuroscience* 31:15775–86.
- van der Loos H (1959) *Dendro-dendritische verbindingen in de schors de grote hersenen* H. Stam.
- Van Essen DC, Smith SM, Barch DM, Behrens TE, Yacoub E, Ugurbil K (2013) The wu-minn human connectome project: an overview. *Neuroimage* 80:62–79.
- Zeba M, Jovanov-Milošević N, Petanjek Z (2008) Quantitative analysis of basal dendritic tree of layer iiic pyramidal neurons in different areas of adult human frontal cortex. *Collegium antropologicum* 32:161–169.

Theme II – linking micro to macro scale in the functional connectome



Cortical chemoarchitecture shapes macroscale effective functional connectivity patterns in macaque cerebral cortex

Elise Turk, Lianne H. Scholtens*, Martijn P. van den Heuvel*

Human Brain Mapping 2016; 37 (5): 1856–1865

The mammalian cortex is a complex system of – at the microscale level – interconnected neurons and – at the macroscale level – interconnected areas, forming the infrastructure for local and global neural processing and information integration. While the effects of regional chemoarchitecture on local cortical activity are well known, the effect of local neurotransmitter receptor organization on the emergence of large scale region-to-region functional interactions remains poorly understood. Here, we examined reports of effective functional connectivity – as measured by the action of strychnine administration acting on the chemical balance of cortical areas – in relation to underlying regional variation in microscale neurotransmitter receptor density levels in the macaque cortex. Linking cortical variation in microscale receptor density levels to collated information on macroscale functional connectivity of the macaque cortex, we show macroscale patterns of effective cortico-cortical functional interactions – and in particular, the strength of connectivity of efferent macroscale pathways – to be related to the ratio of excitatory and inhibitory neurotransmitter receptor densities of cortical areas. Our findings provide evidence for the microscale chemoarchitecture of cortical areas to have a direct stimulating influence on the emergence of macroscale functional

connectivity patterns in the mammalian brain.

Introduction

Brain function emerges from neural interactions between individually connected neurons, as well as between globally interconnected areas (Passingham et al., 2002; Sporns et al., 2005; van den Heuvel and Sporns, 2013). At the microscale level of brain organization, functional organization entails signal transduction between neurons (Cossell et al., 2015; Ullo et al., 2014; Yuste, 2011). At the macroscale, functional connectivity of macroscale neuronal circuits describes interactions between large-scale cortical areas (Rubinov and Sporns, 2010; van den Heuvel et al., 2012) shaped by the underlying anatomical wiring infrastructure of the brain (Adachi et al., 2011; Honey et al., 2010; van den Heuvel and Sporns, 2013). Much is known about how signaling on the neuronal level depends on the local cyto-, myelo-, and chemoarchitecture of cortical areas (Amunts and von Cramon, 2006; Zilles et al., 2002, 1995). Functional activity of cortical areas on the microscale is shaped by local interactions between large numbers of neurons and their cortico-cortical interconnections with other brain regions (Kandel et al., 2000). A large proportion of these interactions is communicated through chemical transmission (Kandel et al., 2000). Whether a connected target area will fire depends on the summation of many factors, such as the neuronal types present in that region (Ullo et al., 2014), as well on their excitatory and inhibitory synaptic input (Kandel et al., 2000) and their excitatory and inhibitory balance (Duncan et al., 2014; Kapogiannis et al., 2013). However, how underlying microscale structural and chemical architecture of cortical regions shapes the emergence of macroscale brain-wide functional connectivity patterns is less well understood (Honey et al., 2010; Kötter, 2007; Passingham et al., 2002).

In this study, we set about to provide insight into this matter by examining a potential interplay between the chemoarchitecture of cortical areas and the formation of macroscale effective functional connectivity patterns in the macaque brain. Data on density of six common regional neurotransmitter receptors were collated from the pioneering autoradiography work of Kötter et al. (2001), reporting on regional neurotransmitter receptor densities of the macaque cortical surface. Induced functional connectivity of macaque cortical areas was derived from a collation of strychninization studies made by Stephan et al. (2000). Strychnine studies provide detailed information on a rather unique type of directed functional connectivity resulting from strychnine-induced regional cortical disinhibition. Targeted administration of strychnine on a cortical region leads to a temporary excitatory reaction at the local source region, and subsequently an increase in neural activity in remote cortical areas by means of

glutamate-mediated excitatory long-range projecting axons of the source region (a detailed description of strychnine functional connectivity is given in the section “Materials and Methods”). Combining chemoarchitectural receptor densities operating at the nano-scale of brain organization with measurements of macroscale strychnine-derived functional connectivity, we show the effective functional connectivity patterns of cortical areas to be modulated by regional variation in excitatory and inhibitory receptor density.

Materials and methods

Data on effective functional connectivity of the macaque cortex was derived from the strychnine-based functional connectivity dataset as collated by Stephan et al. (2000) in their seminal paper on strychnine-induced effective functional connectivity of the macaque cortex. Since the neuronographic studies from which the strychnine functional connectivity data was collated did not usually state in which hemisphere activity was recorded, Stephan et al. pooled connections across hemispheres, leaving a single monohemispheric connectivity matrix. Originally, the *in vivo* technique of strychninization has been designed to reveal functional relations between cortical areas and bodily movements by stimulation of motor regions of the macaque cerebral cortex (Dusser de Barenne, 1924). Later, local strychnine application was used to determine the boundaries between cortical areas based on their functional projections (Dusser de Barenne and Mcculloch, 1938). Functional interaction between cortical source and target areas was observed as alterations in electrocorticography activity of target areas following strychninization of source regions (Fig. 1A). Connectivity patterns similar to those observed after electrical stimulation of the same source region were demonstrated, labeling strychninization as an effective methodology for mapping cortico-cortical projections (Dusser de Barenne and Mcculloch, 1938). It is now known that strychnine acts as an antagonist for the neuronal glycine receptor (GlyR) and as a partial antagonist for the γ -aminobutyric acid type A receptor (GABA_A) (Curtis et al., 1971; Davidoff et al., 1969) partially blocking the function of inhibitory postsynaptic potentials (Fig. 1B). The resulting disinhibition of strychninized areas increases the chance of pyramidal neurons – in particular, layer 2 and 3 pyramidal neurons, neurons of which their projections are important for cortico-cortical signal transduction (Salling and Harrison, 2014) – to spike and to propagate action potentials along their long-range axons projecting to distinct cortical areas. At the macroscale level of brain organization, the net effect of strychnine administration is thus a strong stimulating action on target areas.

In their article, Stephan et al. (2000) collated functional connectivity data across 19

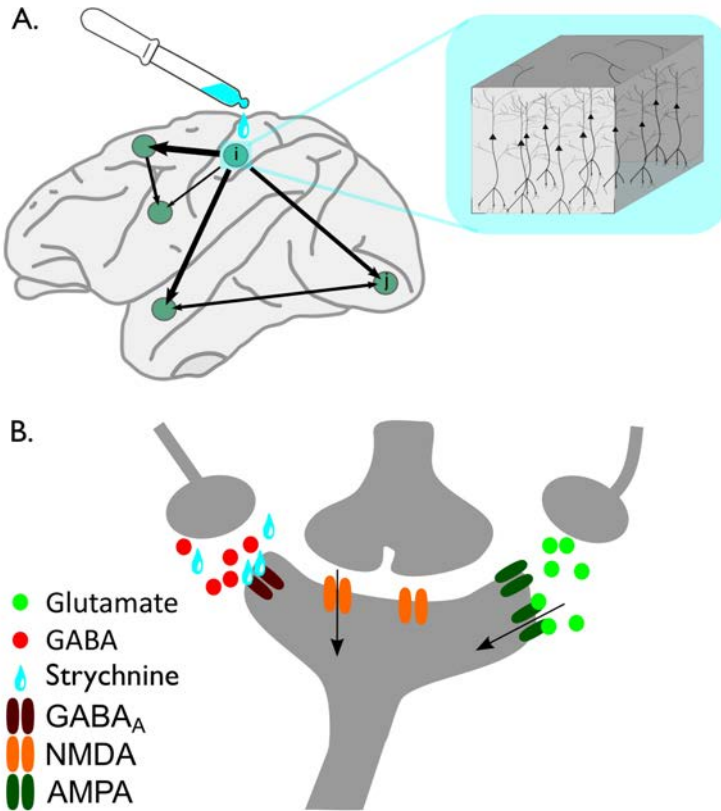


Figure 1. Schematic representation of workings of strychnine-induced functional connectivity. Figure shows the schematic presentation of the biological mechanism of the workings of strychninization (see also the main text). **(A)** During a strychnine experiment, strychnine (blue) is administered to a source region i . The schematic drawing (blue box) illustrates the strychnine to have an effect on the cortical column and to particularly act on layer 3 pyramidal cells. **(B)** At the nanoscale receptor level, local administration of strychnine (depicted by the blue drops) results in the blocking of inhibitory glycine receptors and partially blocking of the GABA_A receptors (dark red), therewith strongly reducing GABA-mediated influx (red dots) into the source neuron. The lack of GABAergic modulation increases the excitability of the source neuron and results in a strong sensitivity of the neuron to incoming glutamatergic-mediated excitatory activity (green dots) via – for example – AMPA receptors (dark green) and second messenger-dependent excitatory neurotransmission (orange receptor). At the microscale cellular level, this has the net effect of an overall increase in the excitability of the source neuron. Taken across the entire stimulated area (thus involving a large number of neurons), the source region’s macroscale net excitatory impulse on its short- and long-range connected cortical regions increases. This outgoing functional influence of source region i to these other regions j of the cortex is measured by means of electroencephalography recordings of an increase in cortical activity at the target regions j of the cortex.

strychnine studies for each cortical source region of the Walker-Von Bonin & Bailey atlas (WBB47). The WBB47 atlas is a combination of cortical areas of Von Bonin and Bailey’s 1947 atlas and frontal areas of Walker’s 1940 atlas and was first used by Stephan et al.

(2000) and later by others for the analysis of anatomical cortico-cortical connectivity (Scholtens et al., 2014). The WBB47 describes the whole (unihemispheric) surface of the macaque cortex in 39 non-overlapping areas (including 5 frontal, 10 prefrontal, 7 parietal, 9 temporal, 3 occipital, 2 insular, and 3 cingulate regions) (Stephan et al., 2000). Figure 2 shows the schematic illustration of the 39 WBB47 regions on the macaque cortical surface. Using the WBB47 atlas, Stephan et al. collated reports across literature on cortico-cortical strychnine functional connectivity (i.e., net excitatory effect) of the 39 WBB47 cortical regions with all other cortical regions in a 39×39 functional connectivity matrix. Information on the presence or absence and information on the strength of present connections was stored in the connectivity matrix as “0” (connection explicitly mentioned to be absent), “1” (connection present, strength: weak), “2” (connection present, strength: moderate), “3” (connection present, strength: strong), “X” (connection present, strength: unreported) or “2” when no information on a cortico-cortical connection could be found. Of the connections for which a specific strength was reported (64% of all 221 connections), the majority (52.7%) was reported to be weak ($s = 1$), 20.6% of connections was of moderate strength ($s = 2$), and 26.7% was strong ($s = 3$). For our analysis, connections of which clear presence but no information on strength was reported in literature (i.e., the “X” connections), were taken as connections with the strength most prevalent in our dataset ($s = 1$); connection pairs of which no information could be collated across literature (i.e., the “-” connections) were taken as an empty entry (i.e., absence of connection, $s = 0$) in the connectivity matrix following the procedures by Stephan et al. (Fig. 2) (for additional analyses excluding all connections of unknown strength, see Supporting Information, Table S1 and Fig. S1). In all, the examined connectivity matrix described 39 areas (nodes) of the WBB47 atlas, with 175 weak connections (edges), 20 medium strength connections, and 26 strong connections.

Regionwise Strychnine Functional Connectivity Strength

Basic graph analysis was used as a theoretical framework to explore topological structure of the strychnine-induced functional network (Fig. 2). For each cortical area, the regional out-strength defined as the sum across all outgoing projections of a region and in-strength defined as the sum across all ingoing connections of a region were computed.

Regional Neurotransmitter Receptor Levels

Information on the chemoarchitecture of macaque cortical regions was taken from the study of Kötter et al. (2001). Kötter’s study reports on densities of (in total) 9 excitatory and inhibitory neurotransmitter receptors (in fmol/mg protein) of 29 smaller subareas of the visual, motor, and somatosensory system of the macaque cortex, densities obtained by means of in vitro autoradiography using receptor-specific radiolabeled

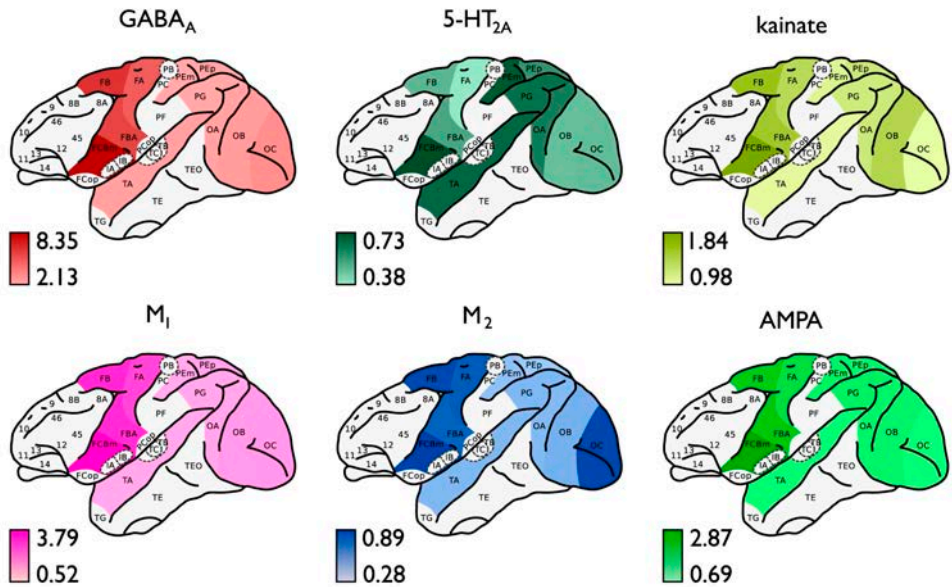


Figure 3. Cortical layout of mapped regional density levels. Figure shows the regional densities of the 6 examined receptors for the included macaque WBB47 cortical regions (Table II). Figure shows the density distributions of inhibitory receptors GABA_A (red) and M₂ (blue), and density distributions of excitatory receptors AMPA (light green), 5-HT_{2A} (dark green), M₁ (pink), and kainate (yellow). Binding density levels are depicted in fmol/mg · 10³ proteins ranging from minimum values (light colors) to maximum values (dark colors). Data as collated from the study of Kötter et al. (2001) (see main text).

To enable cross-modal analysis between the receptor data and macroscale strychnine functional connectivity data derived for the WBB47 cortical areas, the 29 smaller areas reported by Kötter et al. were manually mapped to the regions of the WBB47 parcellation atlas. The WBB47 atlas and mapping was used in previous studies of our group on macroscale anatomical connectivity of the macaque cortex, and provided a detailed description of the performed mapping (Table II) (Scholtens et al., 2014; van den Heuvel et al., 2015). Mapping of receptor density data to the WBB47 atlas resulted in receptor data for a total of 11 WBB47 cortical regions (FA, FB, FBA, FCBm, PEp, PEm, PG, TA, OA, OB, and OC) (Scholtens et al., 2014). The resulting receptor density levels for the 6 examined receptors of the 11 cortical regions are shown in Figure 3.

Excitatory–inhibitory ratio

For each region, a net excitatory character was examined by means of computation of the excitatory–inhibitory ExIn ratio, calculated as the mean excitatory receptor density (mean over AMPA, 5-HT_{2A}, kainate, and M₁) divided by the mean inhibitory receptor

density (mean over M_2 and $GABA_A$). As such, a larger ExIn ratio indicated less inhibitory neurotransmission as mediated by receptor densities (Kapogiannis et al., 2013). To eliminate potential influences of differences in absolute receptor densities, we calculated an alternative ExIn ratio using normalized receptor densities. Values for each receptor were rescaled by dividing each density by the largest value for that specific receptor, excluding any effect of differences in absolute receptor density.

Statistical Analysis

Pearson's correlation was used to test a potential interplay between regional receptor densities and functional connectivity, cross-correlating the 6 receptor density levels plus the ExIn ratio with nodal functional out- and in-strength. Area FBA lacked any recordings of efferent strychnine functional connectivity and with such (functional) disconnection believed to be related to a shortage of measurements rather than a true effect of regions being completely unconnected to the rest of the brain, FBA was excluded from further analysis. This resulted in a dataset on chemoarchitecture-connectomics comparison for 10 cortical regions. Across these 10 regions, a total of $7 \times 2 = 14$ statistical tests were performed (6 receptors plus ExIn ratio; in- and out-strength), yielding the need for correction for multiple testing. With a strongly dependent nature of the receptor density data (showing an average correlation of $r = .6296$ between the 6 receptor levels), a principal component analysis was performed to assess the true number of independent tests performed (Gao et al., 2008). PCA resulted in the identification of two components in the receptor data explaining $>99\%$ of the total variance, yielding a partial Bonferroni-corrected α of $.05 / (2 \times 2) = .0125$ correcting for the number of independent tests of 2 receptor components \times 2 functional connectivity metrics (i.e., out- and in-strength). Effects reaching this partial Bonferroni-corrected α of $.0125$ were taken as significant (Gao et al., 2008; Li and Ji, 2005; Scholtens et al., 2014). Further taking into account the notion of the data not being normally distributed, findings were verified with nonparametric Spearman's Rank correlations. Similar results were observed (Supporting Information), but we believe that due to the low power of the data ($n = 10$), Spearman's tests might have overestimated relationships (Supporting Information, Table S2), thus we favored Pearson's correlation analysis.

Results

Table I lists all correlations between receptor levels and regional functional out- and in-strength (see also Supporting Information, Figs. S2 and S3 for overview of all interactions). Correlating the 6 receptor densities with regional out-strength revealed a significant negative effect of inhibitory M_2 receptors and strychnine-induced functional

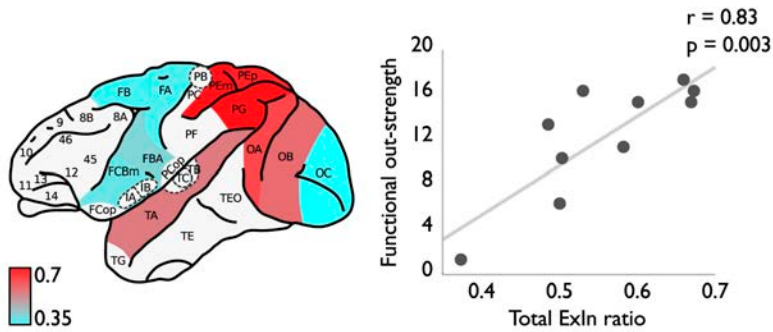


Figure 4. Interplay between receptor ExIn ratio and macroscale functional out-strength connectivity. Left panel shows the cortical ExIn ratios (high ratio values in red and low values in blue). Red regions depict cortical areas with an (relatively) excitatory chemoarchitecture, whereas blue regions depict regions with an (relatively) inhibitory character. Right panel depicts the observed positive association between local chemoarchitecture ExIn ratio (x -axis) and the level of macroscale strychnine functional out-strength of cortical areas (y -axis) ($r = .83$, $p = .0032$). Figure illustrates the main finding of our study of the local excitatory

Table 1. Pearson correlations (R) between neurotransmitter receptor level densities and total out-/in-strength of strychnine-induced functional connectivity of cortical areas.

	Out-strength		In-strength	
	R	p	R	p
AMPA	-0.1328	0.7146	-0.1741	0.6086
5-HT _{2A}	0.6194	0.0561	-0.0283	0.9342
Kainate	-0.0817	0.8224	-0.0873	0.7985
M ₁	-0.3278	0.3551	-0.2044	0.5466
M ₂	-0.7577	0.0111 ^a	-0.1292	0.7049
GABA _A	-0.3372	0.3408	-0.1861	0.5838
ExIn ratio	0.8259	0.0032 ^a	0.1256	0.7129

Receptor levels are based on autoradiography measurements reported by Kötter et al. (2001). Correlations were calculated between excitatory receptor levels (AMPA, 5-HT_{2A}, kainate, and M₁), inhibitory receptors (GABA_A and M₂), and the in- and out-strength of strychnine functional connectivity of cortical areas. ^a Effects reaching a partial Bonferroni corrected α of .0125.

out-strength ($r = -0.7577$, $p = .0111$, reaching partial Bonferroni correction) (Supporting Information, Fig. S4). No effects between regional variation of GABA_A, AMPA, kainate, 5-HT_{2A}, or M₁ neurotransmitter receptor densities and regional functional out-strength were observed (see Table I and Supporting Information, Fig. S2 for overview of all correlations). Moreover, in particular, receptor ExIn ratio and functional out-strength showed a strong positive correlation ($r = .8259$, $p = .0032$; Fig. 4), indicating an overall more excitatory and less inhibitory chemoarchitecture of cortical regions to be related to more and stronger outgoing macroscale effective functional projections. Using the normalized ExIn ratio yielded similar results ($r = .8439$, $p = .0021$). As hypothesized based on the workings of strychninization, no correlation was found between macroscale functional in-strength connectivity patterns and cortical variation in excitatory/inhibitory receptor level densities.

Table 2. Pearson correlations (R) between neurotransmitter receptor level densities and total out-/in-strength of strychnine-induced functional connectivity of cortical areas.

WBB47 region	Kötter et al. (2001) subregion								
FA	F1								
FB	F2v	F2d	F3	F6	F7				
FBA	F4v	F4d							
FCBm	F5								
PEm	VIP								
PEp	PO	MIP	PEP						
PG	LIP	PG	MST						
TA	FST								
OA	V3v	V3d	V3A	V4v	V4d	V6A	V4t	MT	MTp
OB	V2v	V2d							
OC	V1								

The first column lists all cortical regions of the WBB47 parcellation that were included in the analysis. Remaining columns show the included subregions from the Kötter et al. (2001) study (for which receptor density information was available) per WBB47 region.

Discussion

Our findings show evidence of a direct interplay between the excitatory chemoarchitecture of cortical areas and their effective functional connectivity pattern on the macroscale of brain organization. Supported by the receptor-driven neurobiological underpinnings of strychninization (Curtis et al., 1971), our study shows the out-strength of cortical connectivity of cortical areas to be related to the excitatory and inhibitory nature of cortical areas, and in particular, their balance herein. A micro–macro interplay between regional variation in receptor densities and macroscale functional cortical connectivity contributes to the hypothesis of the emergence of global brain patterns to be dependent on microscale neuronal properties (Scholtens et al., 2014; Zilles et al., 1995). Considering the original intentions of Dusser de Barenne to reveal the functional organization of regions of the visual, sensory, motor, and frontal cortex, it is not surprising that the strychnine functional modules as shown in the study of Stephan are in line with common functional (Stephan et al., 2000) and anatomical (Scholtens et al., 2014) subdivisions of the macaque cortex. Interestingly, multidimensional hierarchical clustering approaches in macaque did reveal first overlapping patterns of anatomical connectivity and receptor mappings, but did not observe direct relationships between receptor levels and total level of structural connectivity of cortical areas (Kötter et al., 2001; Scholtens et al., 2014). Pandya et al. showed in the macaque and human cortex that distinct cytoarchitectonic sub-regions have unique patterns of cortico-cortical connectivity (Pandya and Sanides, 1973; Petrides and Pandya, 1999, 2002). Furthermore, Beul et al. (2015) recently showed the relation between cytoarchitectonic type and structural connectivity, and we showed highly connected cortical areas to have higher neuronal complexity (Scholtens et al., 2014; van den Heuvel et al., 2016, 2015). Taken together, cytoarchitectonic

characteristics have been suggested to be potentially more directly related to anatomical projections and less to the smaller and more functionally operating scale of chemoarchitecture. In contrast, chemoarchitectural modulation – and in particular rich variation in cortical “receptor fingerprints” – has been hypothesized to rather relate to the functional organization of cortical regions (Zilles et al., 2002, 2004) with receptors and their corresponding neurotransmitters modulating neuronal signal transduction by means of integration and summation of excitatory and inhibitory input (Salling and Harrison, 2014). Our current observations are in favor of such an important role of the chemoarchitecture of cortical areas in the emergence of large-scale functional connectivity patterns across regions, showing evidence of the extent of effective functional connectivity of cortical regions to depend on their underlying chemical excitatory and inhibitory nature.

Whether the observed across-region relationship between microscale chemoarchitecture and macroscale functional connectivity also holds within an individual region across time (e.g., on the relatively short timescale of task performance or on the much longer timescale of brain development) would be an interesting topic for future research. Over time, neurotransmitter receptors traffic between intracellular compartments and the neuronal membrane, thereby changing the distribution of active excitatory and inhibitory receptors (Choquet and Triller, 2013; Kneussel et al., 2014). The receptor distributions included in this study are static snapshots of the macaque cortex at a certain time point and therefore do not enable examination of the influence of subtle changes in excitatory and inhibitory balance on the strength of functional connectivity within a region across time. Complementary research measuring changes in functional dynamics and receptor binding densities at different time points can contribute to a more complete understanding of the relationship between a region’s chemoarchitecture and functional connectivity.

Our findings of cortical chemoarchitecture to play a modulating role in large-scale functional processes are in line with earlier observations on positive interactions between functional connectivity as derived from resting-state fMRI recordings and magnetic resonance spectroscopy (MRS) estimations of the chemical balance of cortical regions. As recently reviewed by Duncan et al. (2014), human MRI studies have reported on inverse interactions between individual variation in functional MRI measured cortical activity and GABA levels (e.g., Donahue et al. (2010)), and positive relationships between functional connectivity and glutamate levels (e.g., Schmaal et al. (2012)). Furthermore, Kapogiannis et al. (2013) reported on higher levels of precuneus functional cortical activity and connectivity to be linked to local availability of glutamate and GABA transmitters, with in particular the ratio of excitatory glutamate and inhibitory GABA neurotransmission to show the strongest relationship with

resting-state fMRI functional connectivity patterns. This further underscores the importance of the excitatory/inhibitory chemical character of cortical regions in influencing global whole-brain functional connectivity patterns (Duncan et al., 2014).

Induced functional connectivity patterns by strychninization are a consequence of a net excitatory reaction to a cortical target area by suppressing the receptor function of inhibitory glycine receptors and (partially) GABA_A strychnine-sensitive receptors in the source regions (Dusser de Barenne and Mcculloch, 1938; Salling and Harrison, 2014). In this context, it is worth to note that as a result of the strychnine administration, the retained inhibitory role of M₂ receptors has been reported to become (relatively) more important in the local chemical balance of the source region, due to the temporary elimination of glycine and GABAergic receptor activity at the site of administration (Brown, 2010). This is consistent with our findings showing strychnine-induced functional connectivity out-strength to have an inverse relationship with regional M₂ receptor density (shown in Supporting Information, Fig. S4 and Table I). Moreover, while strychninization may modulate inhibitory receptor action in the source region, the inhibitory mechanisms of the target regions are thought to be left unaffected, with the overall incoming (i.e., afferent) level of influence of other regions on the target region believed to remain relatively unchanged (Stephan et al., 2000). Whether or not the target region will eventually become activated depends – among other things – on the neuron type, on which the majority of the efferents from the source region project, as well as on neuronal interactions within the target regions. As a result, strychninization is thought to have only a minimal influence on incoming signals of cortical areas, which is indeed consistent with our observations showing no strong relationships between receptor levels and cortical in-strength.

As noted by Stephan et al. (2000), functional connectivity patterns derived from strychninization are known to be highly stable within and between specimens, as well as to be highly comparable to electroencephalography patterns acquired from direct electrical stimulation (Dusser de Barenne and Mcculloch, 1938). Comparable modern-day examinations might include the study of effects of transcranial direct-current stimulation (tDCS) and transcranial magnetic stimulation (TMS) on functional brain connectivity, techniques that both modulate cortical activity and therewith connectivity, albeit – clearly – in a much less-invasive way than cortical strychninization (Pascual-Leone et al., 2000). TMS in the motor cortex has indeed been suggested to result in a temporary local decrease in GABAergic neurotransmission together with enhanced cortical excitability and to modulate global resting-state functional connectivity patterns of the motor system (Stagg et al., 2011, 2009).

Considerations about the receptor densities have to be kept in mind when interpreting

our presented findings on functional organization. First, it is important to note that neurotransmitter receptors are likely to act on multiple cellular mechanisms and may thus involve a long chain of both excitatory and inhibitory events, making the overall interpretation of their resulting modulatory effect on neuronal excitability considerably more complex. Ionotropic kainate receptors mediate postsynaptic glutamatergic neurotransmission having an overall excitatory effect on the postsynaptic neuron (Kandel et al., 2000). Kainate receptors have, however, also been reported to play an indirect modulating role in the release of presynaptic GABA (see (Contractor et al., 2011) for an overview on the workings of kainate receptors). Second, in addition to classifying receptors based on their inhibitory and excitatory role, receptors are also often categorized according to their ionotropic or metabotropic nature. Ionotropic receptors such as AMPA, GABA_A, and kainate (ion channels) are known for their fast and direct influence on the membrane potential, while slower acting metabotropic G-protein-coupled receptors such as M₁, M₂, and 5-HT_{2A} have been shown to have a more modulatory role on the membrane potential [see for an overview, Hammond (2008)]. We incorporated both types of receptors in our study, arguing that in the timespan of measured strychnine-induced cortical activity (ranging from 2 to 15 min, (Dusser de Barenne and McCulloch, 1938)), both types of receptors will have had an influence on neuronal activity. Third, autoradiography studies have noted the distribution of neurotransmitter receptors to vary widely across cortical layers (Geyer et al., 1998). Layer-specific information about connectivity modulation could thus have been lost when taking the average receptor density over cortical layers. High densities of kainate receptors have been reported in cortical layer 4 (described as an important layer for driving processes (Shipp, 2005) from subcortical and thalamic projections (Jones, 1998)), suggesting that kainate receptors may be particularly involved in reception of input from subcortical rather than cortico-cortical projections (Douglas and Martin, 2004). In contrast, the highest densities of AMPA receptors have been noted in layer 2/3 cortical motor areas (Geyer et al., 1998), described as important target and source layers for cortico-cortical projections (Douglas and Martin, 2004). Fourth, data on glutamatergic NMDA receptor levels was only available for a small number of WBB47 areas and we therefore excluded recordings of this type of receptor from our analysis. However, NMDA is one of the most prevalent excitatory receptors in the central nervous system, with receptor densities in the macaque visual, motor, and sensory cortex recorded to range from 19% to 46% of all excitatory synapses (Huntley et al., 1994). Examination of NMDA receptors in relation to macroscale functional connectivity patterns may thus include an interesting and important topic for future studies.

We report on a small but potentially important next step in understanding a

micro–macro interplay of mammalian brain organization. Our findings may be of interest to studies examining changes in functional connectivity in neurological and psychiatric disorders, as such conditions are often reported to involve alterations in both receptor and neurotransmitter levels (see, for example, a review about serotonin receptors (Naughton et al., 2000)) as well as large-scale changes in interareal functional connectivity (see for example (Greicius, 2008) for review). Considering the interplay between macroscale cortical patterns and (dys-)function of the chemoarchitecture of neural elements at the microscale may form a potential fruitful way to get insight into the biological underpinnings of large-scale disruptions of functional connectivity in brain disorders.

References

- Adachi Y, Osada T, Sporns O, Watanabe T, Matsui T, Miyamoto K, Miyashita Y (2011) Functional connectivity between anatomically unconnected areas is shaped by collective network-level effects in the macaque cortex. *Cerebral cortex* 22:1586–1592.
- Amunts K, von Cramon DY (2006) The anatomical segregation of the frontal cortex: what does it mean for function? *Cortex* 42:525–528.
- Beul SF, Grant S, Hilgetag CC (2015) A predictive model of the cat cortical connectome based on cytoarchitecture and distance. *Brain Structure and Function* 220:3167–3184.
- Brown DA (2010) Muscarinic acetylcholine receptors (machrs) in the nervous system: some functions and mechanisms. *Journal of molecular neuroscience* 41:340–346.
- Choquet D, Triller A (2013) The dynamic synapse. *Neuron* 80:691–703.
- Contractor A, Mulle C, Swanson GT (2011) Kainate receptors coming of age: milestones of two decades of research. *Trends in neurosciences* 34:154–163.
- Cossell L, Iacaruso MF, Muir DR, Houlton R, Sader EN, Ko H, Hofer SB, Mrsic-Flogel TD (2015) Functional organization of excitatory synaptic strength in primary visual cortex. *Nature* 518:399–403.
- Curtis D, Duggan A, Johnston G (1971) The specificity of strychnine as a glycine antagonist in the mammalian spinal cord. *Experimental brain research* 12:547–565.
- Davidoff R, Aprison M, Werman R (1969) The effects of strychnine on the inhibition of interneurons by glycine and γ -aminobutyric acid. *International journal of neuropharmacology* 8:191–194.
- Donahue MJ, Near J, Blicher JU, Jezzard P (2010) Baseline gaba concentration and fmri response. *Neuroimage* 53:392–398.
- Douglas RJ, Martin KA (2004) Neuronal circuits of the neocortex. *Annu. Rev. Neurosci.* 27:419–451.
- Duncan NW, Wiebking C, Northoff G (2014) Associations of regional gaba and glutamate with intrinsic and extrinsic neural activity in humans—a review of multimodal imaging studies. *Neuroscience & Biobehavioral Reviews* 47:36–52.
- Dusser de Barenne JG (1924) Experimental researches on sensory localization in the cerebral cortex of the monkey (macacus). *Proceedings of the Royal Society of London B: Biological Sciences* 96:272–291.
- Dusser de Barenne JG, Mcculloch WS (1938) Functional organization in the sensory cortex of the

- monkey (*macaca mulatta*). *Journal of Neurophysiology* pp. 69–85.
- Gao X, Starmer J, Martin ER (2008) A multiple testing correction method for genetic association studies using correlated single nucleotide polymorphisms. *Genetic epidemiology* 32:361–369.
- Geyer S, Matelli M, Luppino G, Schleicher A, Jansen Y, Palomero-Gallagher N, Zilles K (1998) Receptor autoradiographic mapping of the mesial motor and premotor cortex of the macaque monkey. *Journal of Comparative Neurology* 397:231–250.
- Greicius M (2008) Resting-state functional connectivity in neuropsychiatric disorders. *Current opinion in neurology* 21:424–430.
- Hammond C (2008) *Cellular and Molecular Neurophysiology* Academic Press.
- Honey CJ, Thivierge JP, Sporns O (2010) Can structure predict function in the human brain? *NeuroImage* 52:766–76.
- Huntley GW, Vickers JC, Morrison JH (1994) Cellular and synaptic localization of nmda and non-nmda receptor subunits in neocortex: organizational features related to cortical circuitry, function and disease. *Trends in neurosciences* 17:536–543.
- Jones E (1998) The core and matrix of thalamic organization. *Neuroscience* 85:331–345.
- Kandel ER, Schwartz JH, Jessell TM (2000) *Principles of neural science*, Vol. 4 McGraw-hill New York.
- Kapogiannis D, Reiter DA, Willette AA, Mattson MP (2013) Posteromedial cortex glutamate and gaba predict intrinsic functional connectivity of the default mode network. *Neuroimage* 64:112–119.
- Kneussel M, Triller A, Choquet D (2014) Snapshot: receptor dynamics at plastic synapses. *Cell* 157:1738–1738. e1.
- Kötter R, Stephan KE, Palomero-Gallagher N, Geyer S, Schleicher a, Zilles K (2001) Multimodal characterisation of cortical areas by multivariate analyses of receptor binding and connectivity data. *Anatomy and embryology* 204:333–50.
- Kötter R (2007) *Anatomical concepts of brain connectivity*, pp. 149–167 Springer.
- Li J, Ji L (2005) Adjusting multiple testing in multilocus analyses using the eigenvalues of a correlation matrix. *Heredity* 95:221–227.
- Naughton M, Mulrooney JB, Leonard BE (2000) A review of the role of serotonin receptors in psychiatric disorders. *Human Psychopharmacology: Clinical and Experimental* 15:397–415.
- Pandya DN, Sanides F (1973) Architectonic parcellation of the temporal operculum in rhesus

- monkey and its projection pattern. *Anatomy and Embryology* 139:127–161.
- Pascual-Leone A, Walsh V, Rothwell J (2000) Transcranial magnetic stimulation in cognitive neuroscience—virtual lesion, chronometry, and functional connectivity. *Current opinion in neurobiology* 10:232–237.
- Passingham RE, Stephan KE, Kötter R (2002) The anatomical basis of functional localization in the cortex. *Nature Reviews Neuroscience* 3:606–616.
- Petrides M, Pandya D (1999) Dorsolateral prefrontal cortex: comparative cytoarchitectonic analysis in the human and the macaque brain and corticocortical connection patterns. *European Journal of Neuroscience* 11:1011–1036.
- Petrides M, Pandya D (2002) Comparative cytoarchitectonic analysis of the human and the macaque ventrolateral prefrontal cortex and corticocortical connection patterns in the monkey. *European Journal of Neuroscience* 16:291–310.
- Rubinov M, Sporns O (2010) Complex network measures of brain connectivity: uses and interpretations. *NeuroImage* 52:1059–69.
- Salling MC, Harrison NL (2014) Strychnine-sensitive glycine receptors on pyramidal neurons in layers ii/iii of the mouse prefrontal cortex are tonically activated. *Journal of neurophysiology* 112:1169–1178.
- Schmaal L, Goudriaan AE, Meer J, Brink W, Veltman DJ (2012) The association between cingulate cortex glutamate concentration and delay discounting is mediated by resting state functional connectivity. *Brain and behavior* 2:553–562.
- Scholtens LH, Schmidt R, de Reus MA, van den Heuvel MP (2014) Linking macroscale graph analytical organization to microscale neuroarchitectonics in the macaque connectome. *The Journal of Neuroscience* 34:12192–12205.
- Shipp S (2005) The importance of being agranular: a comparative account of visual and motor cortex. *Philosophical Transactions of the Royal Society of London B: Biological Sciences* 360:797–814.
- Sporns O, Tononi G, Kötter R (2005) The human connectome: a structural description of the human brain. *PLoS computational biology* 1:e42.
- Stagg CJ, Bachtiar V, Johansen-Berg H (2011) The role of gaba in human motor learning. *Current Biology* 21:480–484.
- Stagg CJ, Best JG, Stephenson MC, O’Shea J, Wylezinska M, Kincses ZT, Morris PG, Matthews PM, Johansen-Berg H (2009) Polarity-sensitive modulation of cortical neurotransmitters by transcranial stimulation. *Journal of Neuroscience* 29:5202–5206.

- Stephan KE, Hilgetag CC, Burns GA, O'Neill MA, Young MP, Kötter R (2000) Computational analysis of functional connectivity between areas of primate cerebral cortex. *Philosophical transactions of the Royal Society of London. Series B, Biological sciences* 355:111–26.
- Ullo S, Nieuwenhuis TR, Sona D, Maccione A, Berdondini L, Murino V (2014) Functional connectivity estimation over large networks at cellular resolution based on electrophysiological recordings and structural prior. *Frontiers in neuroanatomy* 8.
- van den Heuvel MP, Scholtens LH, de Reus MA, Kahn RS (2016) Associated microscale spine density and macroscale connectivity disruptions in schizophrenia. *Biol Psychiatry* 80:293–301.
- van den Heuvel MP, de Reus MA, Feldman Barrett L, Scholtens LH, Coopmans FMT, Schmidt R, Preuss TM, Rilling JK, Li L (2015) Comparison of diffusion tractography and tract-tracing measures of connectivity strength in rhesus macaque connectome. *Human Brain Mapping* 36:3064–3075.
- van den Heuvel MP, Kahn RS, Goñi J, Sporns O (2012) High-cost, high-capacity backbone for global brain communication. *Proceedings of the National Academy of Sciences of the United States of America* 109:11372–11377.
- van den Heuvel MP, Scholtens LH, Feldman Barrett L, Hilgetag CC, de Reus MA (2015) Bridging cytoarchitectonics and connectomics in human cerebral cortex. *The Journal of Neuroscience* 35:13943–13948.
- van den Heuvel MP, Sporns O (2013) An anatomical substrate for integration among functional networks in human cortex. *The Journal of neuroscience : the official journal of the Society for Neuroscience* 33:14489–500.
- von Bonin G, Bailey P (1947) *The neocortex of Macaca mulatta* Univ. of Illinois Press, Urbana.
- Walker E (1940) A cytoarchitectural study of the prefrontal area of the macaque monkey. *The Journal of Comparative Neurology* 73:59–86.
- Yuste R (2011) Dendritic spines and distributed circuits. *Neuron* 71:772–781.
- Zilles K, Palomero-Gallagher N, Grefkes C, Scheperjans F, Boy C, Amunts K, Schleicher A (2002) Architectonics of the human cerebral cortex and transmitter receptor fingerprints: reconciling functional neuroanatomy and neurochemistry. *European neuropsychopharmacology : the journal of the European College of Neuropsychopharmacology* 12:587–99.
- Zilles K, Schlaug G, Matelli M, Luppino G, Schleicher A, Qü M, Dabringhaus A, Seitz R, Roland PE (1995) Mapping of human and macaque sensorimotor areas by integrating architectonic, transmitter receptor, MRI and PET data. *Journal of anatomy* 187:515–37.
- Zilles K, Palomero-Gallagher N, Schleicher A (2004) Transmitter receptors and functional anatomy

of the cerebral cortex. *Journal of anatomy* 205:417–32.

Supplemental Information

of

Cortical chemoarchitecture shapes macroscale effective functional connectivity patterns in macaque cerebral cortex

Supplemental Methods

Alternative Statistical analyses

For each cortical area the out- and in-strength of functional connectivity strength were re-examined, by excluding all connections of unknown strength from the matrix (i.e. all connections with X). Pearson's correlation was used to test the relation between regional receptor densities and functional connectivity (see Table S1 and Figure S1 for results), cross-correlating the 6 receptor density levels and the ExIn ratio with the nodal functional out- and in-strength values of the residual regions ($n = 6$).

Supplemental Results

Alternative Statistical results

	Out-strength		In-strength	
	R	p	R	p
AMPA	0.2073	0.6935	-0.1899	0.5760
5-HT _{2A}	0.8286	0.0416	-0.2038	0.5479
Kainate	-0.7710	0.0727	-0.1602	0.6381
M ₁	-0.8621	0.0272	-0.1557	0.6475
M ₂	-0.7554	0.0824	0.1171	0.7318
GABA _A	-0.9094	0.0119	-0.1292	0.7050
ExIn ratio	0.5254	0.2844	-0.2297	0.4969

Table S1. Correlations of regional receptor levels and functional outward connection strength. To validate our main findings we removed all (124) pathways with an unknown connection strength (i.e. depicted as an "X" in the connectivity matrix). Fourteen relations were represented between all excitatory receptor levels, inhibitory receptors, ExIn ratio and the (out or in-) strength of the functional connections. Similar correlation coefficients were found using the complete dataset (as reported in main text), although we believe that due to the low power of the data ($n = 6$) lower p -values are found when all unknown connection strengths are removed.

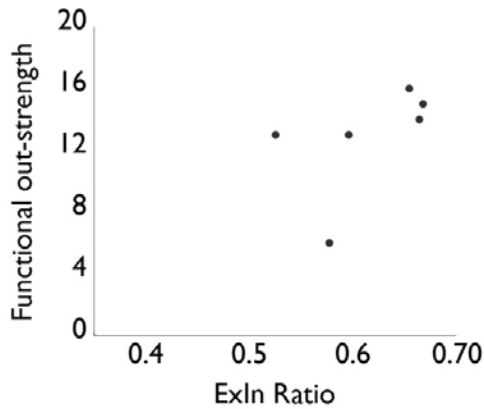


Figure S1. Interplay between receptor ExIn chemoarchitecture and macroscale functional out-strength connectivity. The graph shows a non-significant association between local chemoarchitecture ExIn ratio (x -axis) and the level of macroscale strychnine functional out-strength of cortical areas (y -axis, note that the out-strength is calculated without all unknown connections, $n = 6$). Figure illustrates the re-examined main finding of our study of the local excitatory chemoarchitecture of cortical areas to be of positive influence on outgoing global interregional functional influence of cortical areas when all unknown connections strength were removed (i.e. depicted as an “X” in the connectivity matrix).

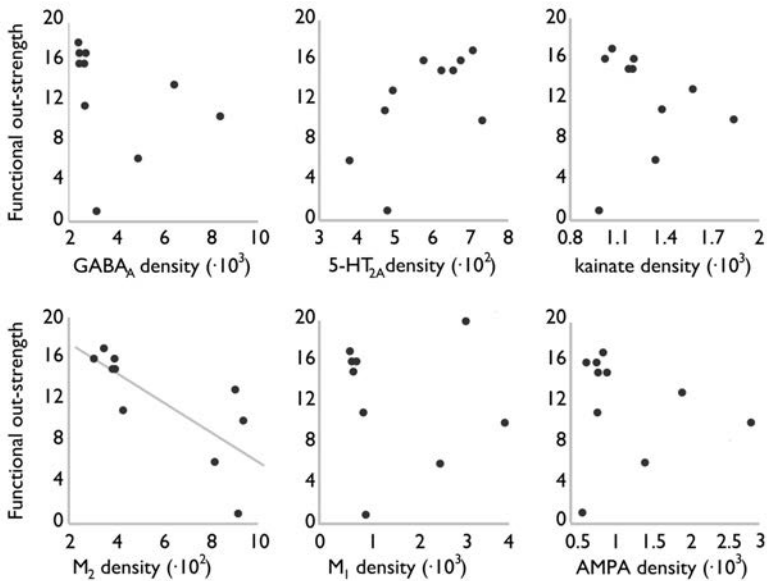


Figure S2. Overview of associations between receptor densities and out-strength. Figure shows the scatterplots of the 6 receptor densities (on x -axis, in $\text{fmol}/\text{mg} \cdot 10^3$ protein) and strychnine-induced functional out-strength (y -axis). Plots of inhibitory GABA_A and M₂ receptors are shown on the left, and plots of excitatory 5-HT_{2A}, M₁, kainate and AMPA receptors are presented in the middle and right. Figure illustrates an exclusive correlation between M₂ receptor densities and functional out-strength ($R = -.76$, $p = .0111$, see Figure S4).

	Out-strength		In-strength	
	<i>R</i>	<i>p</i>	<i>R</i>	<i>p</i>
AMPA	-0.1707	0.6372	0.0736	0.8298
5-HT _{2A}	0.5549	0.0959	-0.069	0.8403
Kainate	-0.2927	0.4118	-0.0782	0.8193
M ₁	-0.7988	0.0056*	-0.2253	0.5054
M ₂	-0.8659	0.0012*	-0.0598	0.8614
GABA _A	-0.7744	0.0085*	-0.2529	0.4531
ExIn ratio	0.7561	0.0114*	0.0966	0.7776

Table S2. Spearman Rank Correlations of regional receptor levels and functional connection strength. Spearman Rank correlation coefficients (*R*) between neurotransmitter receptor level densities and out-strength or in-strength of the strychnine-induced functional regions are represented. Receptor levels are collated from the study of Kötter and colleagues (Kötter et al., 2001). Relations were calculated between all excitatory receptor levels (AMPA, 5-HT_{2A}, kainate and M₁), inhibitory receptors (GABA_A and M₂), ExIn ratio and the (in or out) strength of the functional connections. Similar results were found using Pearson’s correlations (as reported in main text), although we believe that due to the low power of the data (*n* = 10) Spearman’s tests overestimates the relations. * Effects reaching a partial Bonferroni corrected α of .0125.

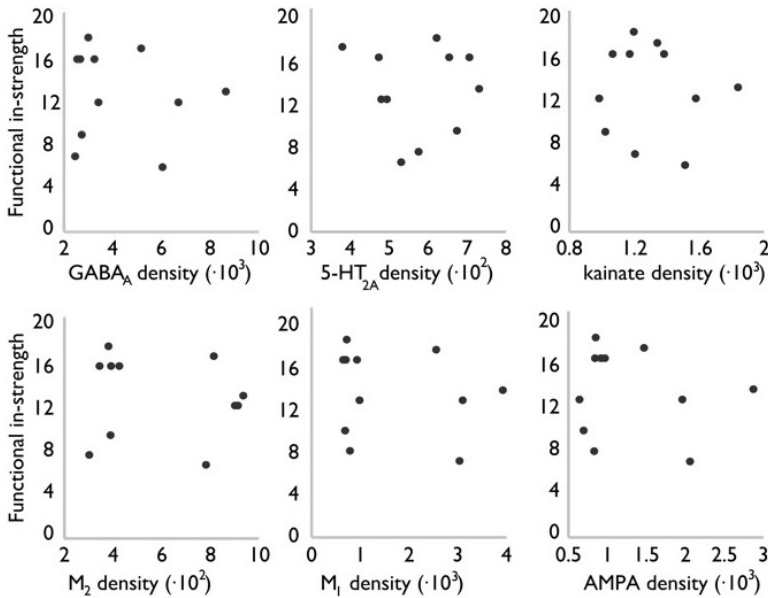


Figure S3. Overview of associations between receptor densities and in-strength. Figure shows the scatterplots of the 6 receptor densities (on *x*-axis, in fmol/mg·10³ protein) and strychnine-induced functional in-strength (*y*-axis). Plots of inhibitory GABA_A and M₂ receptors are shown on the left, and plots of excitatory 5-HT_{2A}, M₁, kainate and AMPA receptors are presented in the middle and on the right. As expected (see main text for description), correlations revealed no significant relationships.

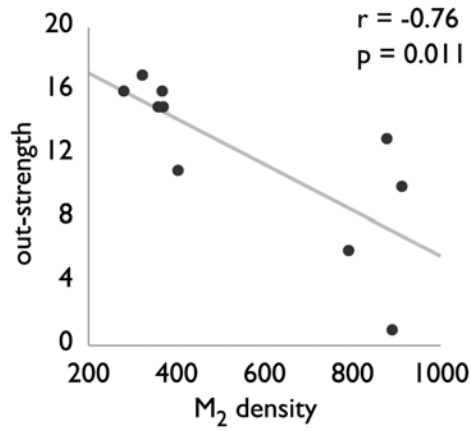
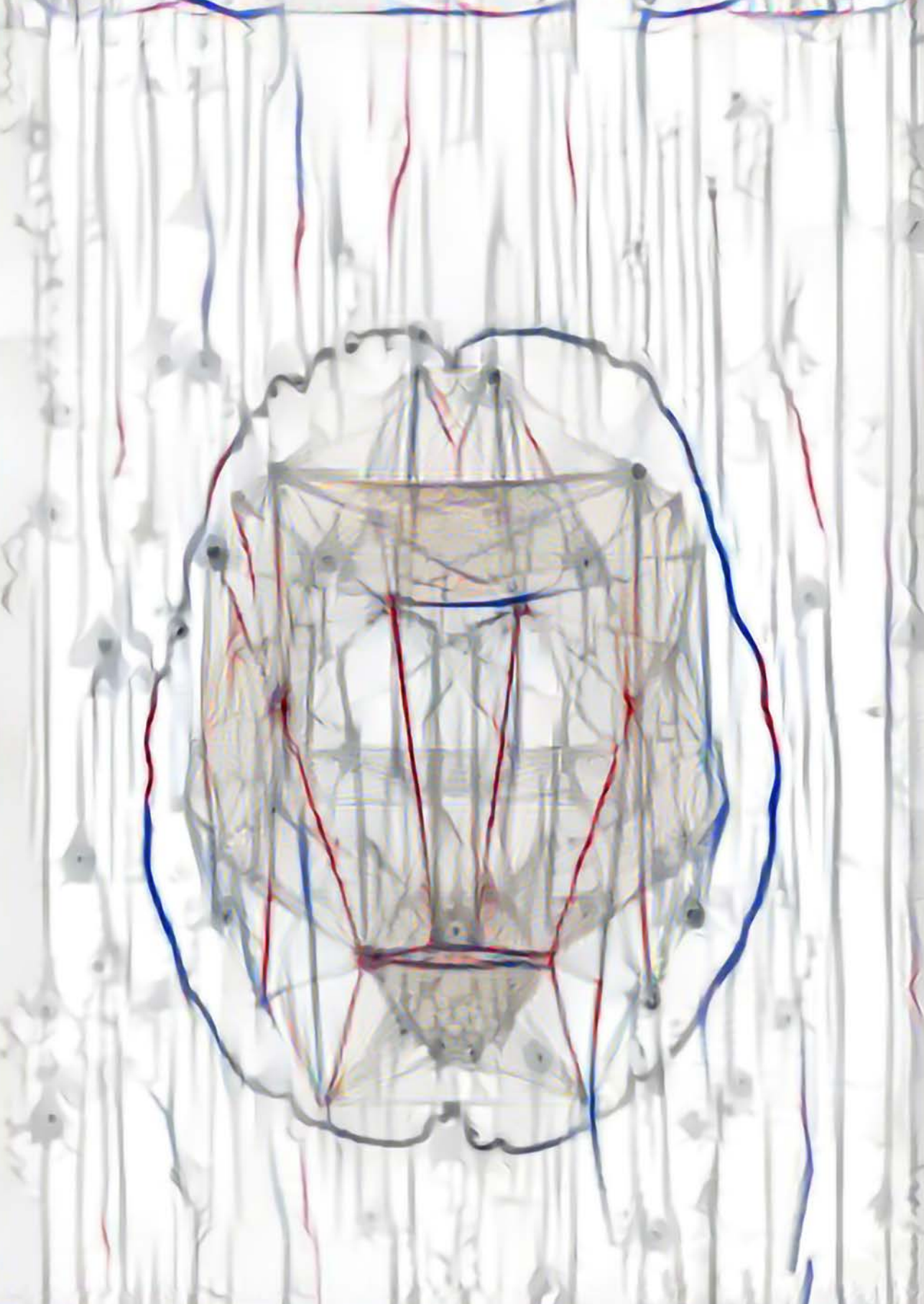


Figure S4. Association of M_2 receptor density and macroscale functional out-strength connectivity. Figure shows a negative correlation ($r = -0.76$, $p = .0111$), between regional M_2 density (on x -axis) and the level of strychnine-induced functional out strength (on y -axis), illustrating the influence of inhibitory M_2 receptors on the strength of cortico-cortical activity.

Supplemental References

Kötter R, Stephan KE, Palomero-Gallagher N, Geyer S, Schleicher a, Zilles K (2001) Multimodal characterisation of cortical areas by multivariate analyses of receptor binding and connectivity data. *Anatomy and embryology* 204:333–50.



Multimodal Analysis of Cortical Chemoarchitecture and Macroscale fMRI Resting-State Functional Connectivity

Martijn P. van den Heuvel, Lianne H. Scholtens, Elise Turk, Dante Martini, Wim VanDuffel, Lisa Feldman Barrett

Human Brain Mapping 2016; 37 (9): 3103–3113

The cerebral cortex is well known to display a large variation in excitatory and inhibitory chemoarchitecture, but the effect of this variation on global scale functional neural communication and synchronization patterns remains less well understood. Here, we provide evidence of the chemoarchitecture of cortical regions to be associated with large-scale region-to-region resting-state functional connectivity. We assessed the excitatory versus inhibitory chemoarchitecture of cortical areas as an Exc/In ratio between receptor density mappings of excitatory (AMPA, M_1) and inhibitory ($GABA_A$, M_2) receptors, computed on the basis of data collated from pioneering studies of autoradiography mappings as present in literature of the human (2 datasets) and macaque (1 dataset) cortex. Cortical variation in Exc/In ratio significantly correlated with total level of functional connectivity as derived from resting-state functional connectivity recordings of cortical areas across all three datasets (human I: $P = .0004$; human II: $P = .0008$; macaque: $P = .0007$), suggesting cortical areas with an overall more excitatory character to show higher levels of intrinsic functional connectivity during resting-state. Our findings are indicative of the microscale chemoarchitecture of cortical regions to be related to resting-state fMRI connectivity patterns at the global system's level of connectome organization.

Introduction

Brain function emerges from neural signaling and information transfer. At the cellular scale, a neuron's dendritic tree and axonal projections form the infrastructure for neuron-to-neuron signaling, with information transmitted from one neuron to another by means of chemical (or in some cases more direct electrical) transmission at a neuron's synapses (see for review Kandel et al. (2000)). Depending on type of neurotransmitter and receptor, the net effect of a neurotransmitter will be an excitatory (increasing the chance of a neuron to fire) or inhibitory (decreasing the chance of a neuron to fire) impulse to the postsynaptic neuron. Studies have shown a rich variety in the excitatory and inhibitory chemoarchitecture of cortical regions, with cortical areas showing varying densities of excitatory and inhibitory receptors. Some regions for example display relatively high levels of excitatory receptors such as glutamatergic NMDA, AMPA, and/or acetylcholine receptors M_1 and relatively low levels of inhibitory $GABA_A$ or M_2 receptors, while other regions show a much more overall inhibitory chemoarchitectural character (e.g., Caspers et al. (2015, 2012); Zilles et al. (2002); Zilles and Amunts (2009); Zilles et al. (2015)). However, while cellular neuroscience studies have delineated the effects of neurotransmitter type and accompanying receptors on the behavior of postsynaptic neurons, the effects of the chemoarchitecture of large-scale cortical areas on the emergence of global region-to-region activity patterns and interregional connectivity are less well understood (Kötter et al., 2007).

At this global scale of brain organization, neural communication and signaling is often inferred from synchronization patterns between cortical areas. In the last decade, the measurement of correlative patterns between intrinsic brain activity as derived from resting-state fMRI recordings has become a highly influential methodology for obtaining insight into the functional macroarchitecture of the human and animal brain (see for review Fox and Raichle (2007); Park and Friston (2013); van den Heuvel and Hulshoff Pol (2010); van den Heuvel et al. (2016)). Functional connectivity is defined as the synchronization pattern of activation time-series of large-scale cortical regions (Biswal et al., 1995; Friston et al., 1993), and in the human brain there is ample evidence of macroscale connectivity patterns to be linked to global brain function (Baggio et al., 2015; Bassett et al., 2009; Cole et al., 2012; Collin et al., 2016, 2013; Davis et al., 2012; Kong et al., 2015; Kunisato et al., 2011; van den Heuvel et al., 2010, 2009). As such, resting-state fMRI has become one of the workhorses of today's clinical, translational, and fundamental neuroscientist.

However, despite the clear impact of this type of measurement on contemporary neuroscience, the field does not yet have a fully clear picture of the biological underpinnings of resting-state fMRI functional connectivity patterns. Studies have

provided insight into the genetic underpinnings of resting-state correlations showing high heritability in twin studies (Bohlken et al., 2014; Fornito et al., 2011; Glahn et al., 2010; Jahanshad et al., 2013; van den Heuvel et al., 2013), SNPs to modulate brain connectivity (Esslinger et al., 2009) and gene expression patterns to be related to the fMRI signal (Cioli et al., 2014). Furthermore, studies combining anatomical information (such as tract-tracing in animals and/or in vivo DWI in humans) with resting-state fMRI have shown a clear link between the two modalities (Adachi et al., 2011; Cocchi et al., 2014; Hagmann et al., 2008; Honey and Sporns, 2009; van den Heuvel and Sporns, 2013a,b), suggesting that the brain's macroscale anatomical wiring forms the infrastructure for region-to-region functional interactions to emerge. Studies using advanced methods combining resting-state BOLD fMRI with more direct metrics of neural activity have further shown evidence of the resting-state signal to involve – or at least a significant part of the signal to include – a neural origin, hypothesizing that resting-state global patterns emerge from intrinsic firing patterns of neural populations (e.g., (Horwitz, 2004; Logothetis and Wandell, 2004; Niessing et al., 2005; Shmuel and Leopold, 2008)). However, still, there are several open questions about the origin of the observed intrinsic oscillating patterns and accompanying large-scale synchronization ordering of brain regions. In particular the question of why certain regions show more and stronger activity patterns during rest than others remains poorly understood. With our current study we aim to provide additional insight into this matter, suggesting that the chemoarchitecture of cortical areas may form a potential modulating factor of spontaneous large-scale region-to-region functional connectivity patterns.

Collating quantitative data on cortical receptor density levels of excitatory and inhibitory receptors of cortical regions in the macaque and human cortex from pioneering receptor mapping studies of Amunts and Zilles and coworkers (Amunts et al., 2010; Kötter et al., 2001; Zilles et al., 2015), and combining this data with whole brain fMRI functional connectivity measurements of the macaque and human cortex we show evidence of an association between the chemoarchitecture of cortical regions – and in particular a region's balance in excitatory and inhibitory receptors – and their level of resting-state fMRI global functional connectivity.

Materials and Methods

Human Dataset

Receptor density levels – human dataset I

Quantitative data on neurotransmitter receptor densities of eight cortical areas of human cortex, describing lateral frontal areas Brodmann Areas 4, 6, 6r1, 44, 45, 47, op8, and op9 (see Fig. 1, left panel and Supporting Information) were collated from the

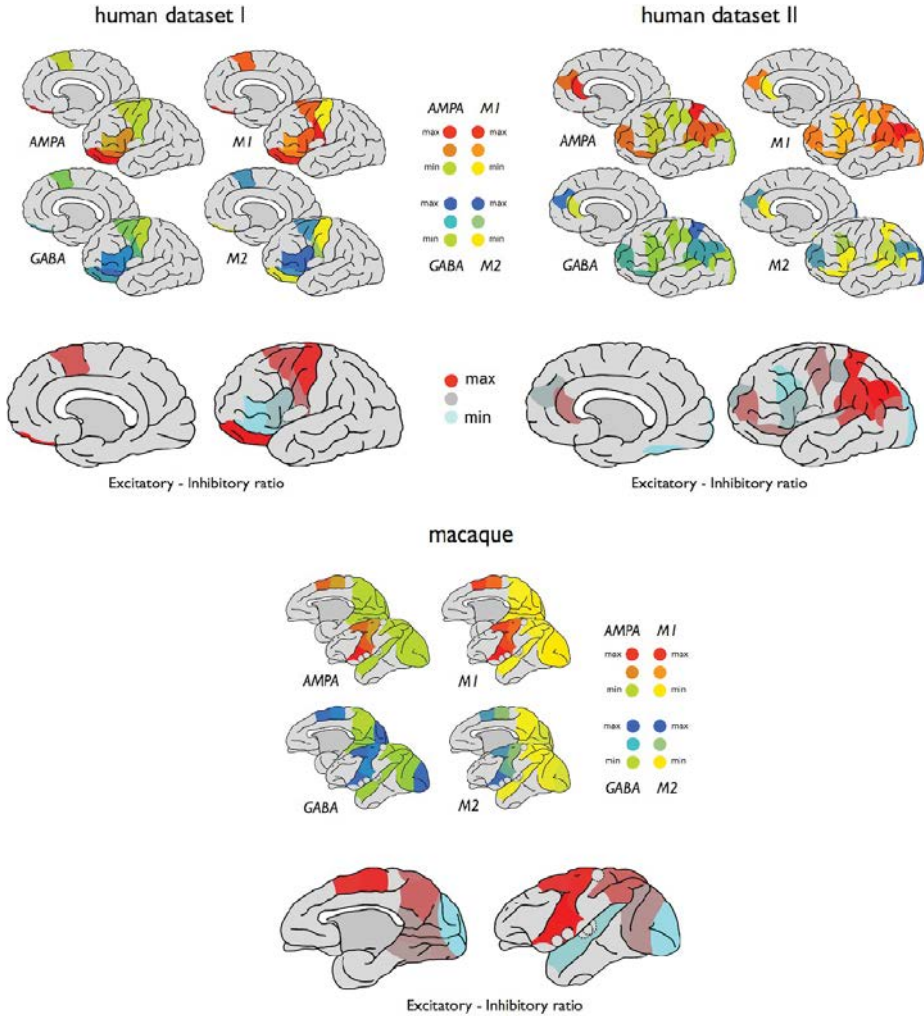


Figure 1. Regional mappings of receptor levels of regions of human cortex as derived from pioneering studies of Amunts et al. (Amunts et al., 2010) (human dataset I, 7 cortical areas, left panels) and Zilles et al. (Zilles et al., 2015) (human dataset II, 18 cortical areas, middle panels) on autoradiography recordings of postmortem cortical tissue. Figures depict measured receptor levels as mapped on the DK-57 cortical atlas (left hemisphere) depicting levels of excitatory working receptors AMPA and M₁ and inhibitory working receptors GABA_A and M₂. Right upper panel shows regional mappings of receptor levels of excitatory AMPA and M₁ and inhibitory GABA_A and M₂ of 11 regions of macaque cortex mapped to the WBB47 cortical atlas (see text and Supporting Information Fig. 1), as collated from the study of Kötter et al. (Kötter et al., 2001). Lower panels depict cortical variation in the *Ex/In* ratio between excitatory (AMPA + M₁) and inhibitory neurotransmitters (GABA_A and M₂) for human (left and middle) and macaque cortex (right).

study of Amunts and coworkers using in vitro autoradiography of binding ligands in six postmortem brains (averaging left and right hemispheres) (Amunts et al., 2010). Cortical receptor densities of four receptors were included, collected as maximum

intensity values for the radio labeled receptor-ligands in fmol/mg protein. Receptor levels of excitatory ionotropic glutamergic AMPA and metabotropic muscarinic acetylcholine type 1 (M_1) receptors and inhibitory ionotropic GABA_A and metabotropic muscarinic acetylcholine type 2 (M_2) receptors were collected. Examination was taken to include receptors that were consistently available across all 3 datasets (see below for human dataset II and the macaque dataset), with other receptor levels provided in the study of Amunts and colleagues (i.e., Kainate and serotonin 5-HT_{2A}) thus not taken into account in this study. In this context, we explicitly note that we excluded Kainate as it has been shown to have both an excitatory as well as (working through indirect pathways) an inhibitory effect on neuron activity (Contractor et al., 2011) and to be – as a notable difference to the other receptors – mostly present in infragranular layers (Zilles et al., 2015).

Using the detailed description of region location as provided in the paper of Amunts and coworkers, the eight reported areas were manually mapped (LHS, ET, MPvdH) to the 57 cortical region Desikan-Killiany (DK) atlas (114 regions across the two hemispheres) (Cammoun et al., 2012; Scholtens et al., 2015) to allow anatomical overlap with cortico-cortical resting-state functional connectivity data (see below; see Supporting Information Table 1 for the region-to-region mapping). The eight cortical areas mapped to seven cortical parcels of the DK-57 atlas (two regions reported by Amunts and coworkers overlapped with 1 region in the DK-57 atlas, and 1 region reported by Amunts and coworkers mapped to multiple subparcels of the DK atlas [see Supporting Information Table 1]). The DK-57 subdivision atlas was chosen as it includes a higher parcellation resolution than the 34 region cortical Desikan- Killiany atlas (Desikan et al., 2006) while still maintaining large enough regions to be able to have a robust region-wise measurement of the resting-state fMRI signal (see below). To express the overall excitatory versus inhibitory chemoarchitecture of a cortical region, for each region the regional excitatory-inhibitory receptor ratio $ExIn$ was determined computed as the ratio between the total sum of excitatory receptor levels (i.e., AMPA + M_1) and the total sum of inhibitory receptor levels (i.e., GABA_A + M_2) per region, as previously introduced by Kapogiannis and coworkers (Kapogiannis et al., 2013).

Receptor density levels – human dataset II

A second dataset on receptor density levels of cortical regions was collated from another seminal study of Zilles and coworkers (Zilles et al., 2015). This larger study described receptor mapping of 26 cortical regions using state-of-the-art high density autoradiography techniques, providing one of the most detailed and most complete receptor density mappings of human cortex present in literature. From the reported receptor fingerprint diagrams of 26 areas of cortex presented by Zilles and colleagues, levels of excitatory AMPA and M_1 and inhibitory receptor levels GABA_A, and M_2

(receptors overlapping with the other human and macaque dataset [see below]) were collected in levels of 50 units of absolute receptor densities (in fmol/mg protein), ranging from 100 to 2,500, with 50 being the finest level of scale that could be distinguished from the Zilles et al. study. (Besides the mentioned four receptors, the rich dataset of Zilles and colleagues also includes data on other receptor types [i.e., Kainate, NMDA, GABA_b, BZ, M₃, α_1 , α_2 , 5-HT_{1a}, 5-HT₂, D₁], but for consistency across the three datasets the set of four receptor types was taken to be overlapping with the human I and macaque dataset, see above). The 26 areas were mapped to regions of the DK-57 atlas (using the detailed descriptions and visualizations of the examined cortical regions as presented by Zilles and coworkers, with this mapping described in Supporting Information Table 2) obtaining receptor data of in total 18 of the 57 unihemisphere cortical regions of the DK-57 atlas. Similar as for the human dataset I, the *ExIn* ratio of a cortical region was computed as the ratio between excitatory receptor levels (i.e., AMPA + M₁) and inhibitory receptor levels (i.e., GABA_A + M₂). Figure 1 illustrates the receptor density levels as reported by the pioneering work of Zilles and coworkers mapped to the 18 areas of the DK-57 atlas (left hemisphere).

Resting-state fMRI functional connectivity

Resting-state functional connectivity between pairs of regions of the DK-57 cortical atlas was assessed by means of analysis of the high-quality resting-state fMRI data of the Human Connectome Project (Van Essen et al., 2013) (Q3 release, voxel-size 2mm isotropic, TR/TE 720/33.1 ms, 1,200 volumes, 14:33 min of data block 1, 215 subjects).

Data analysis included realignment of the fMRI time-series, coregistration of the fMRI time-series to the T1 image (using the mean fMRI over all 1,200 volumes), band-pass filtering of the time-series (.01 – .1 Hz), nuisance correction by regressing out the mean overall signal (mean over all cortical areas), correction for ventricle and white matter signals by means of linear regression, and motion-scrubbing for potential movement artifacts (Power et al., 2012) (performed as described in detail in van den Heuvel et al. (2013)). Next, using the individual T1 image (Q3, voxel size: .7 mm isotropic), tissue classification of cortical gray matter, white matter, and CSF was performed using FreeSurfer (Fischl and Dale, 2000) and the cortical mantle was parcellated in 114 cortical regions using the described DK-57 atlas. Next, for each of the individually segmented cortical regions an average time-series was computed by overlaying the DK-57 atlas with the fMRI time-series and by taking the average over the time-series of the selected voxels within a cortical region. For each individual dataset, a region-to-region functional connectivity matrix was computed by means of correlation analysis between the unique $114 \times (114-1)/2$ region pairs (Lynall et al., 2010; van den Heuvel et al., 2013). Next, a group-averaged weighted functional connectivity matrix (FC) was formed by averaging the individual matrices. The level of functional

connectivity of a region was computed as the total sum of all non-negative FC connections of a region ($FC > .1$, other thresholds revealed similar findings). Within graph theoretical examinations this metric is often referred to as “functional degree” (Lynall et al., 2010; Rubinov and Sporns, 2010; van den Heuvel and Hulshoff Pol, 2010; van den Heuvel et al., 2009). Focus was placed on positive connections, as our study was focused on the examination of excitatory long-range inter-areal connections (and thus expecting a positive correlation in time-series) and with the origin of negative correlations derived from functional resting-state fMRI recordings remaining a topic of investigation in the field. Overlapping the analysis of the macaque (see below), regional levels of functional connectivity were taken as the intra-hemispheric degree of each of the 57 regions (that is FC over all intrahemispheric connections of cortical areas). Including also interhemispheric connections (i.e., taking regional functional connectivity of a region as the sum of all 114-1 left and right hemispheric regions revealed similar findings (as additionally reported in the results section)).

Macaque Dataset

Receptor density levels

Data on neurotransmitter receptor density levels of cortical areas of the macaque cortex were collected from the study of Kötter and colleagues (Kötter et al., 2001), reporting on quantitative data of six receptors obtained by means of in vitro autoradiography in two macaque monkeys (*Macaca fascicularis* and *Macaca nemestrina* specimens), with receptor density levels provided as maximum intensity value for radio labeled receptor-ligands in fmol/mg protein. Regions described parts of the visual, motor, and somatosensory cortex. Data included – similar as in the human datasets – receptor density levels of excitatory AMPA and M_1 receptors and inhibitory $GABA_A$ and M_2 receptors. [The rich dataset of Kötter and colleagues also included information on Kainate, and serotonin 5-HT_{2A}, but our study was focused on the examination of AMPA, M_1 , M_2 , and $GABA_A$]. The examined cortical regions as reported by Kötter and colleagues (Kötter et al., 2001) were manually mapped to the Walker-vonBonin and Bailey WBB47 atlas of macaque cortex (Stephan et al., 2000; von Bonin and Bailey, 1947; Walker, 1940) (used for the functional connectivity mapping, see below and Supporting Information Fig. 1), resulting in a description of receptor density levels of in total 11 cortical regions of the 39 cortical areas of the WBB47 atlas of macaque cortex (Fig. 1, right panel). (This mapping was part of a recent study of our group on the link between anatomical macroscale connectome organization and microscale neuronal complexity (Scholtens et al., 2014) and is described in Supporting Information Table 3). Similar as in the human datasets, regional *ExIn* ratio of the 11 WBB47 cortical areas was computed as the ratio between excitatory receptor levels (i.e., AMPA + M_1) and

inhibitory receptor levels (i.e., GABA_A + M₂).

Resting-state fMRI functional connectivity

Overlapping the procedure as performed for the human dataset, functional connectivity between cortical areas of the macaque brain was derived from resting-state fMRI recordings. High-quality macaque resting-state fMRI data was acquired in four macaques with a 3T MR Siemens Trio scanner. The monkeys were trained in a mock scanner to continuously fixate on a red dot centered on a blank screen. When they reached 95% fixation performance, each monkey completed 10-min resting state scans on 5 or 6 different occasions over a period of 6 months, all unsedated (VanDuffel et al., 2001). The functional images were collected using a gradient-echo T2-weighted echo-planar sequence (40 slices, 84 × 84 in-plane matrix, repetition time (TR) = 2,000 ms, echo time (TE) = 19 ms, flip angle = 75°, voxel size = 1.25 mm × 1.25 mm × 1.25 mm, 300 volumes per run). Each of these four macaques were scanned during (on average) six sessions on different days (three macaques had six sessions, one macaque had five sessions), with each of the sessions containing (on average) 14 resting-state fMRI runs (minimum: 7, maximum: 24 sessions per run), bringing the total to 324 sessions of macaque imaging. In addition to the fMRI, T1-weighted anatomical scans (magnetization-prepared rapid gradient echo (MP-RAGE) sequence, TR = 2,200 ms, TE = 4.06 ms, voxel size = .5 mm × .5 mm × .5 mm) were collected during different scanning sessions in which the animals were sedated with ketamine/xylazine (ketamine 10mg/kg I.M. + Xylazine .5 mg/kg I.M., maintenance dose of .01 to .05 mg ketamine per minute I.V.). The macaque fMRI dataset and acquisition conditions are described in detail in (Mantini et al., 2013, 2011; VanDuffel et al., 2001). Analysis of each of the resting-state-fMRI time-series (i.e., each run separately) included a similar procedure as in the human dataset. Data processing included registration of the time-series for motion correction, co-registration of each of the runs with the anatomical T1 images, normalization of the time-series to a standard macaque average brain (using the transformation of the nonlinear normalization of the T1 to the standard macaque average brain). Data processing further included band-pass filtering of the time-series (.01 – .01 Hz), nuisance correction of the mean overall signal (mean over all cortical areas) and ventricle and white matter signal by means of regression analysis, and motion-scrubbing for potential movement artifacts (Power et al., 2012). The spatially normalized resting-state fMRI volumes were overlaid with the WBB47 parcellation atlas (van den Heuvel et al., 2015). For each of the 39 WBB47 cortical areas an average time-series was computed by taking the mean of the time-series of all voxels within each region, and the level of functional connectivity between all 39 × (39-1)/2 unique region pairs was computed as the Pearson correlation coefficient between these regional time-series, resulting in a 39 × 39 connectivity matrix for each macaque scan run. A

group-averaged weighted macaque functional connectivity matrix (macaque FC) was computed by averaging the connectivity matrices across runs per session, then across sessions, and finally across the four specimens, resulting in a group averaged macaque FC matrix. Next, similar as in the human dataset, level of functional connectivity of each of the 39 regions was computed as the sum of all non-negative FC connections of $FC > .1$ (other thresholds revealed similar findings) of a region. As the reported receptor density levels included values of one single hemisphere (with visual taken from the right, and motor regions taken from the left hemisphere) (Kötter et al., 2001) and with the WBB47 atlas not distinguishing between left and right hemisphere, regional levels of functional connectivity were taken from the left hemisphere.

Linking Receptor Density Levels to Macroscale resting-State Functional Connectivity

The focus of our study was the examination of the overall chemoarchitecture of cortical areas by means of the *ExIn* ratio in relationship to resting-state functional connectivity, as introduced by (Kapogiannis et al., 2013). For the human and macaque datasets, associations between a region's level of excitatory-inhibitory chemoarchitecture and total level of functional connectivity were examined by regression analysis (Pearson's correlation), cross-correlating regional *ExIn* ratios and resting-state fMRI derived functional connectivity levels. Effects reaching a *P*-value of an α of $.05/3 = .016$ (Bonferroni correction for the testing of three datasets) were taken as significant. Jarque-Bera test was performed to verify that *ExIn* values and functional connectivity values were normally distributed (which was the case for all *ExIn* and FC values, $P > .05$). Spearman's rho correlation was also performed for validation in post hoc analyses. In addition to the *ExIn* ratio, in post hoc analyses we also examined the relationship between individual receptor levels and regional FC.

Results

Human Dataset I

ExIn ratios of frontal areas of human cortex as measured across seven frontal regions significantly correlated to regional levels of functional connectivity ($r = .91$, $P = .0045$, Fig. 2), with cortical areas with a relatively higher excitatory and lower inhibitory character (i.e., a relatively high *ExIn* ratio) showing higher overall functional connectivity. Including interhemispheric connections in the computation of regional FC (see methods) revealed a similar positive correlation between cortical *ExIn* and regional functional connectivity ($r = .94$, $P = .0004$). Including region volume as a covariate in a post hoc regression analysis revealed the same association between *ExIn* ratio and regional FC ($P = .0165$). In addition, also the analyses of Spearman's rho correlation ($\rho = .95$, $P = .0112$) and a leave-one-out regression validation (in which each

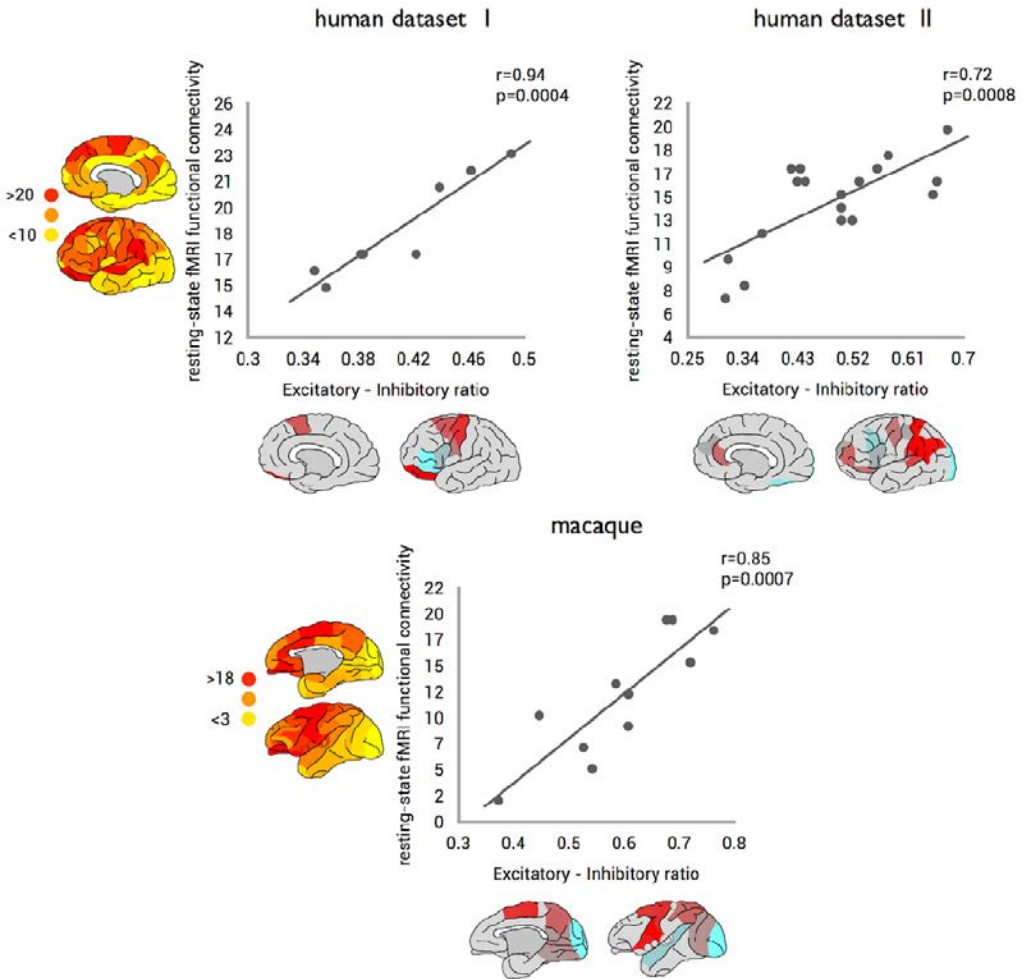


Figure 2. Interactions between the excitatory - inhibitory (*ExIn*) ratio of cortical regions and total strength of regional resting-state fMRI functional connectivity. Left and middle panels shows the correlations between *ExIn* ratio (*x*-axis) and regional functional connectivity (*y*-axis) for the human datasets (human dataset I and dataset II, respectively). Right panel shows the correlation between *ExIn* ratio (*x*-axis) and cortical resting-state functional connectivity (*y*-axis) for the macaque dataset (see Supporting Information Fig. 2 for region labels). All three datasets show a significant, positive association between the relative excitatory character of cortical areas and the level of cortico-cortical resting-state functional connectivity as derived from resting-state fMRI.

datapoint was left out one at the time and correlations were recomputed) revealed similar findings (min $r = .91$, $P = .0045$). A post hoc analysis in which individual receptor levels (i.e., AMPA, M_1 , M_2 , $GABA_A$) were correlated with FC revealed no significant relationships (Bonferroni corrected).

Human Dataset II

Receptor *ExIn* ratios of data of 18 regions of human cortex revealed a positive correlation with regional resting-state functional connectivity levels ($r = .72$, $P = .0008$, Fig. 2). Including interhemispheric FC connections revealed similar findings ($r = .57$, $P = .0134$). Post hoc testing of Spearman's rho correlation ($\rho = .50$, $P = .0348$), a leave-one-out regression validation (min $r = .55$, $P = .0224$) and a regression analysis with region volume as a covariate ($P = .0009$) all revealed similar findings. Post hoc analyses revealed no significant effects between individual receptor levels and FC (Bonferroni corrected).

Macaque Dataset

Consistent with the two human datasets, regional levels of resting-state functional connectivity of macaque cortical regions as measured across 11 cortical areas were found to be positively associated to regional variation in *ExIn* ratio ($r = .85$, $P = .00077$, Fig. 2). Including interhemispheric FC connections revealed similar findings ($r = .86$, $P = .00074$). Post hoc testing of Spearman's rho correlation ($\rho = .82$, $P = .0018$), a leave-one-out regression validation (min $r = .78$, $P = .0075$) and a regression analysis in which region volume was included as a covariate ($P = .0147$) all revealed consistent findings. Post hoc analysis revealed no significant effects between individual receptor levels and FC (Bonferroni corrected).

Discussion

This study suggests a potential interplay between chemoarchitectonic features of cortical areas and macroscale resting-state fMRI functional connectivity. Combining collated data on receptor density levels of excitatory and inhibitory neurotransmitters of areas of human and macaque cortex with resting-state functional MRI recordings, we show cortical areas with a relatively high excitatory and low inhibitory character to show a more elaborate resting-state functional connectivity profile to other areas of the cortex.

What might be a potential underlying mechanism of a higher excitatory chemoarchitecture to relate to a higher level of resting-state fMRI functional connectivity? A recent study of our group examined the cortical distribution of receptor levels in macaque cortex in context of strychnine effective connectivity, a unique type of functional connectivity resulting from a temporary excitatory reaction due to strychnine administration on the cortex (Turk et al., 2016). Strychnine works by blocking local GABA receptors, temporarily increasing the excitatory character of a cortical area. As a result of blocking GABA, the neural activity in the source region is increased, including the activity of the long-range projecting pyramidal neurons that connect the source

region to other sites of the cortex (Dusser de Barenne, 1924; Dusser de Barenne and McCulloch, 1938; Stephan et al., 2000). Consistent with the fMRI observations made here, we observed higher levels of effective strychnine connectivity to be related to the chemical balance of cortical areas, with overall more excitatory regions showing a stronger global strychnine connectivity profile. A possible mechanism behind the observed association between excitatory-inhibitory balance of cortical areas and their fMRI connectivity profile might thus include regions with a more overall excitatory character to be more prone to have a default level of excitatory effect on other areas of the cortex. These thoughts are in line with several studies reporting on inter-subject differences in neurotransmitter levels to impact functional connectivity and functional resting-state network formation. For example, combining resting-state fMRI recordings with magnetic resonance spectroscopy (MRS) measurements studies have reported higher Glx/Cr levels (an MRS metric of combined glutamate and glutamine concentrations normalized by individual differences in creatine) of anterior cingulate cortex to be related to higher levels of resting-state fMRI activity (Enzi et al., 2012) and modulation of regional functional connectivity (Duncan et al., 2011, 2013). MRS studies have further reported individual differences in higher concentrations of GABA to be inversely correlated to functional connectivity between the putamen and the default mode network during resting-state (Arrubla et al., 2014). This, as well as higher GABA levels within the primary motor cortex M_1 to be related to lower functional connectivity across the resting motor network (Stagg et al., 2014), an observation again in line with current resting-state fMRI findings. fMRI-MRS studies have shown findings of in particular the excitatory-inhibitory balance between glutamate and GABA levels – rather than one of the two separately – of precuneus cortex to be associated with individual variation in default mode network connectivity (Kapogiannis et al., 2013). In addition, studies reporting on a modulation of the glutamatergic system by means of pharmacotherapeutic intervention have reported effects on resting-state functional connectivity, with ketamine (an NMDA receptor antagonist blocking the function of excitatory receptors, having a net inhibitory effect on neural activity) administration resulting in decreased functional connectivity of the default mode network to regions of the dorsal medial prefrontal cortex and the pregenual anterior cingulate cortex (Scheidegger et al., 2012). Following up on their shown inverse relationship between individual differences in MRS estimates of GABA levels in M_1 and motor network functional connectivity, Stagg and colleagues reported on anodal transcranial direct current stimulation (tDCS, by the authors reported to reduce local GABA levels) of primary motor cortex M_1 to be related to increased resting-state functional connectivity within the motor system (Stagg et al., 2014). Extending these findings our findings now further suggest that cortical variation in excitatory-inhibitory character across areas may relate to region-to-region differences in global resting-state functional connectivity.

Taken together, these findings combined support the notion of the chemoarchitecture of the cerebral cortex to play a potential role in modulating intrinsic global functional connectivity patterns of mammalian cortex.

Neurophysiological investigations into the basis of the fMRI signal have noted hemodynamic signals to be coupled to synaptic processing and neural spiking patterns (Conner et al., 2011; Logothetis, 2002; Logothetis and Wandell, 2004; Niessing et al., 2005), and have in particular concluded the fMRI signal to be related to the input of cortical areas (Logothetis et al., 2001). While a correlation approach for the derivation of functional connectivity (as used in the current study) cannot make distinctions on the directionality of the functional interactions (i.e., whether region *A* is projecting to *B*, or *B* to *A*, or both), it is nevertheless interesting and encouraging to note that the receptor architecture of cortical areas – forming the modulation mechanisms of the input to neurons – are related to the resting-state fMRI signal. Future approaches using advanced techniques that go beyond simplistic correlation approaches and can provide information on the direction of functional interactions by employing techniques such as Granger Causality or Dynamic Causal Modeling (Miao et al., 2011; Stephan and Friston, 2010) might thus further delineate a possible link between cortical chemoarchitecture and the emergence of whole-brain spontaneous functional connectivity patterns.

Our findings are also interesting to interpret in context of recent studies suggesting an interplay between regional variation in microscale cytoarchitectural features of cortical areas and macroscale global anatomical connectivity. Beul and colleagues reported on the cortical type of cat cortex – classifying cortical areas into five classes based on supragranular laminar structure (Barbas and Rempel-Clower, 1997; Hilgetag and Grant, 2010) – to interact with macroscale anatomical connectivity (Beul et al., 2015). Furthermore, in a study on macaque (Scholtens et al., 2014) and human cortex (van den Heuvel et al., 2016, 2015) we revealed a positive association between regional variation in microscale cytoarchitectonic complexity of layer three pyramidal neurons and the number of efferent and afferent pathways of cortical areas. Interestingly, earlier multimodal studies reported on potential overlap in chemical and anatomical connectivity organization of motor and visual cortical areas, but did not report on direct associations between chemoarchitecture and the extent of anatomical connectivity of cortical regions across the global brain's network (Kötter et al., 2001). Combined with our current findings, this tends to speculatively suggest that perhaps not so much the anatomical connectivity of cortical areas, but more their functional connectivity is related to the intrinsic chemoarchitecture of cortical areas. Indeed, in a post hoc analysis we found no direct association between the number of anatomical connections of a cortical area and the *ExIn* ratio as measured in the macaque (in-degree: $P = .23$; out-degree: $P = .26$, connectivity data taken from the Bonin and Bailey anatomical

macaque connectome) (Scholtens et al., 2014). This is further strengthened by a post hoc partial correlation analysis in which *ExIn* ratio was included as the dependent variable and both functional degree (i.e., number of functional interactions) and structural degree (i.e., number of efferent and afferent structural pathways of a cortical area) were included as independent variables, which revealed a significant effect of functional degree on *ExIn* ($P = .0012$, partial correlation coefficient = .8924), but not of structural degree (in-degree: $P = .222$, out-degree: $P = .173$). Similar findings were observed for the two human datasets, with anatomical degree derived from analysis of diffusion weighted imaging data from the Human Connectome Project (Van Essen et al., 2013) [see de Reus and van den Heuvel (2014) and van den Heuvel et al. (2016)]. Here too, post hoc examinations using partial correlation revealed significant associations between the *ExIn* ratio and functional degree (human dataset I: $P = .005$, partial correlation coefficient = .9624; human dataset II: $P = .0163$, partial correlation coefficient = .5727), with no significant contribution from cortical structural degree (human dataset I: $P = .9037$; human dataset II: $P = .3393$).

Several remarks have to be made concerning the interpretation of the shown effects. We have to explicitly note that the spatial coverage of examined regions of human and macaque cortex is relatively limited. Data from autoradiography recordings included highly detailed mapping of receptor levels of cortical areas, including quantitative data on multiple receptors, but the number of cortical regions of which quantitative data could be extracted was still relatively low. Our study thus included “only” data of 7 and respectively 18 cortical areas of the human brain and of 11 regions of macaque cortex. Despite this coarse subsampling of the cortex, all three datasets revealed a positive correlation between the chemoarchitecture of cortical regions and resting-state BOLD fMRI derived functional connectivity, an association, as we argued above, consistent with earlier reports linking MRS findings to resting-state network formation. Nevertheless, future studies examining the relationship of resting-state fMRI connectivity using data of even more complete autoradiography mappings of human cortex are of high interest. In this context, it should also be noted that our study only included the examination of AMPA, M_1 , M_2 , and $GABA_A$, as these were consistently reported across humans and macaque, and we aimed for including similar receptors across the three 3 datasets. Future studies examining more and more detailed data including more types of receptor densities (e.g., $5HT_2$, Kainate, NMDA) and high-resolution layer-specific fMRI are of interest.

Our study puts forward a simple, but potentially important association between cortical chemoarchitecture and cortico-cortical resting-state functional connectivity. Providing insight into the biological underpinnings of the emergence of interareal functional connectivity, our cross-modal findings are suggestive of cortical areas with a relatively

high excitatory chemoarchitecture to show higher intrinsic resting-state functional connectivity. Understanding the chemical underpinnings of the resting-state fMRI signal may provide new leads to the examination of how drug intervention may effect functional (dys)connectivity patterns in the diseased brain.

Acknowledgments

We thank Marcel de Reus and Ruben Schmidt for help with the anatomical connectivity data and for interesting and inspiring discussions.

References

- Adachi Y, Osada T, Sporns O, Watanabe T, Matsui T, Miyamoto K, Miyashita Y (2011) Functional connectivity between anatomically unconnected areas is shaped by collective network-level effects in the macaque cortex. *Cerebral cortex* 22:1586–1592.
- Amunts K, Lenzen M, Friederici AD, Schleicher A, Morosan P, Palomero-Gallagher N, Zilles K (2010) Broca's region: novel organizational principles and multiple receptor mapping. *PLoS biology* 8:e1000489.
- Arrubla J, Desmond H, Amkreutz C, Neuner I, Shah NJ (2014) Gaba concentration in posterior cingulate cortex predicts putamen response during resting state fmri. *PLoS one* 9:e106609.
- Baggio HC, Segura B, Junque C, de Reus MA, Sala-Llonch R, Van den Heuvel MP (2015) Rich club organization and cognitive performance in healthy older participants. *Journal of Cognitive Neuroscience* 27:1801–1810.
- Barbas H, Rempel-Clower N (1997) Cortical structure predicts the pattern of corticocortical connections. *Cerebral cortex (New York, NY: 1991)* 7:635–646.
- Bassett DS, Bullmore ET, Meyer-Lindenberg A, Apud Ja, Weinberger DR, Coppola R (2009) Cognitive fitness of cost-efficient brain functional networks. *Proceedings of the National Academy of Sciences of the United States of America* 106:11747–52.
- Beul SF, Grant S, Hilgetag CC (2015) A predictive model of the cat cortical connectome based on cytoarchitecture and distance. *Brain Structure and Function* 220:3167–3184.
- Biswal B, Zerrin Yetkin F, Haughton VM, Hyde JS (1995) Functional connectivity in the motor cortex of resting human brain using echo-planar mri. *Magnetic resonance in medicine* 34:537–541.
- Bohlken MM, Mandl RC, Brouwer RM, van den Heuvel MP, Hedman AM, Kahn RS, Hulshoff Pol HE (2014) Heritability of structural brain network topology: A dti study of 156 twins. *Hum Brain Mapp* .
- Cammoun L, Gigandet X, Meskaldji D, Thiran JP, Sporns O, Do KQ, Maeder P, Meuli R, Hagmann P (2012) Mapping the human connectome at multiple scales with diffusion spectrum mri. *Journal of neuroscience methods* 203:386–97.
- Caspers J, Palomero-Gallagher N, Caspers S, Schleicher A, Amunts K, Zilles K (2015) Receptor architecture of visual areas in the face and word-form recognition region of the posterior fusiform gyrus. *Brain Structure and Function* 220:205–219.
- Caspers S, Schleicher A, Bacha-Trams M, Palomero-Gallagher N, Amunts K, Zilles K (2012) Organization of the human inferior parietal lobule based on receptor architectonics. *Cerebral*

- Cortex* 23:615–628.
- Cioli C, Abdi H, Beaton D, Burnod Y, Mesmoudi S (2014) Differences in human cortical gene expression match the temporal properties of large-scale functional networks. *PLoS One* 9:e115913.
- Cocchi L, Harding IH, Lord A, Pantelis C, Yucel M, Zalesky A (2014) Disruption of structure-function coupling in the schizophrenia connectome. *Neuroimage Clin* 4:779–87.
- Cole MW, Yarkoni T, Repovš G, Anticevic A, Braver TS (2012) Global connectivity of prefrontal cortex predicts cognitive control and intelligence. *Journal of Neuroscience* 32:8988–8999.
- Collin G, de Nijs J, Pol HH, Cahn W, van den Heuvel MP (2016) Connectome organization is related to longitudinal changes in general functioning, symptoms and iq in chronic schizophrenia. *Schizophrenia research* 173:166–173.
- Collin G, Kahn RS, de Reus Ma, Cahn W, van den Heuvel MP (2013) Impaired rich club connectivity in unaffected siblings of schizophrenia patients. *Schizophrenia bulletin* pp. 1–11.
- Conner CR, Ellmore TM, Pieters TA, DiSano MA, Tandon N (2011) Variability of the relationship between electrophysiology and bold-fmri across cortical regions in humans. *Journal of Neuroscience* 31:12855–12865.
- Contractor A, Mulle C, Swanson GT (2011) Kainate receptors coming of age: milestones of two decades of research. *Trends in neurosciences* 34:154–163.
- Davis FC, Knodt AR, Sporns O, Lahey BB, Zald DH, Brigidi BD, Hariri AR (2012) Impulsivity and the modular organization of resting-state neural networks. *Cerebral Cortex* 23:1444–1452.
- de Reus MA, van den Heuvel MP (2014) Simulated rich club lesioning in brain networks: a scaffold for communication and integration? *Frontiers in Human Neuroscience* 8.
- Desikan RS, Segonne F, Fischl B, Quinn BT, Dickerson BC, Blacker D, Buckner RL, Dale AM, Maguire RP, Hyman BT, Albert MS, Killiany RJ (2006) An automated labeling system for subdividing the human cerebral cortex on mri scans into gyral based regions of interest. *Neuroimage* 31:968–80.
- Duncan NW, Enzi B, Wiebking C, Northoff G (2011) Involvement of glutamate in rest-stimulus interaction between perigenual and supragenual anterior cingulate cortex: A combined fmri-mrs study. *Human brain mapping* 32:2172–2182.
- Duncan NW, Wiebking C, Tiret B, Marjańska M, Hayes DJ, Lyttleton O, Doyon J, Northoff G (2013) Glutamate concentration in the medial prefrontal cortex predicts resting-state cortical-subcortical functional connectivity in humans. *PLoS One* 8:e60312.
- Dusser de Barenne JG (1924) Experimental researches on sensory localization in the cerebral

- cortex of the monkey (macacus). *Proceedings of the Royal Society of London B: Biological Sciences* 96:272–291.
- Dusser de Barenne JG, McCulloch WS (1938) Functional organization in the sensory cortex of the monkey (macaca mulatta). *Journal of Neurophysiology* pp. 69–85.
- Enzi B, Duncan NW, Kaufmann J, Tempelmann C, Wiebking C, Northoff G (2012) Glutamate modulates resting state activity in the perigenual anterior cingulate cortex—a combined fmri-mrs study. *Neuroscience* 227:102–109.
- Esslinger C, Walter H, Kirsch P, Erk S, Schnell K, Arnold C, Haddad L, Mier D, Opitz von Boberfeld C, Raab K, Witt SH, Rietschel M, Cichon S, Meyer-Lindenberg A (2009) Neural mechanisms of a genome-wide supported psychosis variant. *Science* 324:605.
- Fischl B, Dale AM (2000) Measuring the thickness of the human cerebral cortex from magnetic resonance images. *Proceedings of the National Academy of Sciences* 97:11050–11055.
- Fornito A, Zalesky A, Bassett DS, Meunier D, Ellison-Wright I, Yücel M, Wood SJ, Shaw K, O'Connor J, Nertney D, Mowry BJ, Pantelis C, Bullmore ET (2011) Genetic influences on cost-efficient organization of human cortical functional networks. *The Journal of neuroscience : the official journal of the Society for Neuroscience* 31:3261–70.
- Fox MD, Raichle ME (2007) Spontaneous fluctuations in brain activity observed with functional magnetic resonance imaging. *Nature Reviews Neuroscience* 8:700–711.
- Friston K, Frith C, Liddle P, Frackowiak R (1993) Functional connectivity: the principal-component analysis of large (pet) data sets. *Journal of Cerebral Blood Flow & Metabolism* 13:5–14.
- Glahn DC, Winkler A, Kochunov P, Almasy L, Duggirala R, Carless M, Curran J, Olvera R, Laird A, Smith S (2010) Genetic control over the resting brain. *Proceedings of the National Academy of Sciences* 107:1223–1228.
- Hagmann P, Cammoun L, Gigandet X (2008) Mapping the structural core of human cerebral cortex. *PLoS biology* 6:e159.
- Hilgetag CC, Grant S (2010) Cytoarchitectural differences are a key determinant of laminar projection origins in the visual cortex. *Neuroimage* 51:1006–17.
- Honey C, Sporns O (2009) Predicting human resting-state functional connectivity from structural connectivity. *Proceedings of the National Academy of Sciences* 106:1–6.
- Horwitz B (2004) Relating fmri and pet signals to neural activity by means of large-scale neural models. *Neuroinformatics* 2:251–266.
- Jahanshad N, Rajagopalan P, Hua X, Hibar DP, Nir TM, Toga AW, Jack CR J, Saykin AJ, Green RC, Weiner MW, Medland SE, Montgomery GW, Hansell NK, McMahon KL, de Zubicaray

- GI, Martin NG, Wright MJ, Thompson PM (2013) Genome-wide scan of healthy human connectome discovers spon1 gene variant influencing dementia severity. *Proc Natl Acad Sci U S A* 110:4768–73.
- Kandel ER, Schwartz JH, Jessell TM (2000) *Principles of neural science*, Vol. 4 McGraw-hill New York.
- Kapogiannis D, Reiter DA, Willette AA, Mattson MP (2013) Posteromedial cortex glutamate and gaba predict intrinsic functional connectivity of the default mode network. *Neuroimage* 64:112–119.
- Kong F, Liu L, Wang X, Hu S, Song Y, Liu J (2015) Different neural pathways linking personality traits and eudaimonic well-being: a resting-state functional magnetic resonance imaging study. *Cognitive, Affective, & Behavioral Neuroscience* 15:299–309.
- Kötter R, Stephan KE, Palomero-Gallagher N, Geyer S, Schleicher a, Zilles K (2001) Multimodal characterisation of cortical areas by multivariate analyses of receptor binding and connectivity data. *Anatomy and embryology* 204:333–50.
- Kötter R, Maier J, Margas W, Zilles K, Schleicher A, Bozkurt A (2007) *Databasing Receptor Distributions in the Brain*, Vol. 401 of *Methods in Molecular Biology*, book section 15, pp. 267–284 Humana Press.
- Kunisato Y, Okamoto Y, Okada G, Aoyama S, Nishiyama Y, Onoda K, Yamawaki S (2011) Personality traits and the amplitude of spontaneous low-frequency oscillations during resting state. *Neuroscience letters* 492:109–113.
- Logothetis NK (2002) The neural basis of the blood–oxygen–level–dependent functional magnetic resonance imaging signal. *Philosophical Transactions of the Royal Society of London B: Biological Sciences* 357:1003–1037.
- Logothetis NK, Pauls J, Augath M, Trinath T, Oeltermann A (2001) Neurophysiological investigation of the basis of the fmri signal. *Nature* 412:150–157.
- Logothetis NK, Wandell BA (2004) Interpreting the bold signal. *Annu. Rev. Physiol.* 66:735–769.
- Lynall ME, Bassett DS, Kerwin R, McKenna PJ, Kitzbichler M, Muller U, Bullmore E (2010) Functional connectivity and brain networks in schizophrenia. *The Journal of Neuroscience* 30:9477–9487.
- Mantini D, Corbetta M, Romani GL, Orban GA, Vanduffel W (2013) Evolutionarily novel functional networks in the human brain? *Journal of Neuroscience* 33:3259–3275.
- Mantini D, Gerits A, Nelissen K, Durand JB, Joly O, Simone L, Sawamura H, Wardak C, Orban Ga, Buckner RL, Vanduffel W (2011) Default mode of brain function in monkeys. *The Journal of*

- neuroscience : the official journal of the Society for Neuroscience* 31:12954–62.
- Miao X, Wu X, Li R, Chen K, Yao L (2011) Altered connectivity pattern of hubs in default-mode network with alzheimer's disease: an granger causality modeling approach. *PloS one* 6:e25546.
- Niessing J, Ebisch B, Schmidt KE, Niessing M, Singer W, Galuske RA (2005) Hemodynamic signals correlate tightly with synchronized gamma oscillations. *science* 309:948–951.
- Park HJ, Friston K (2013) Structural and functional brain networks: from connections to cognition. *Science* 342:1238411.
- Power JD, Barnes KA, Snyder AZ, Schlaggar BL, Petersen SE (2012) Spurious but systematic correlations in functional connectivity mri networks arise from subject motion. *NeuroImage* 59:2142–2154.
- Rubinov M, Sporns O (2010) Complex network measures of brain connectivity: uses and interpretations. *NeuroImage* 52:1059–69.
- Scheidegger M, Walter M, Lehmann M, Metzger C, Grimm S, Boeker H, Boesiger P, Henning A, Seifritz E (2012) Ketamine decreases resting state functional network connectivity in healthy subjects: implications for antidepressant drug action. *PloS one* 7:e44799.
- Scholtens LH, de Reus MA, van den Heuvel MP (2015) Linking contemporary high resolution magnetic resonance imaging to the von economo legacy: A study on the comparison of mri cortical thickness and histological measurements of cortical structure. *Human Brain Mapping* 36:3038–3046.
- Scholtens LH, Schmidt R, de Reus MA, van den Heuvel MP (2014) Linking macroscale graph analytical organization to microscale neuroarchitectonics in the macaque connectome. *The Journal of Neuroscience* 34:12192–12205.
- Shmuel A, Leopold DA (2008) Neuronal correlates of spontaneous fluctuations in fmri signals in monkey visual cortex: implications for functional connectivity at rest. *Human brain mapping* 29:751–761.
- Stagg CJ, Bachtiar V, Amadi U, Gudberg CA, Ilie AS, Sampaio-Baptista C, O'Shea J, Woolrich M, Smith SM, Filippini N (2014) Local gaba concentration is related to network-level resting functional connectivity. *Elife* 3:e01465.
- Stephan KE, Hilgetag CC, Burns Ga, O'Neill Ma, Young MP, Kötter R (2000) Computational analysis of functional connectivity between areas of primate cerebral cortex. *Philosophical transactions of the Royal Society of London. Series B, Biological sciences* 355:111–26.
- Stephan KE, Friston KJ (2010) Analyzing effective connectivity with functional magnetic resonance imaging. *Wiley Interdisciplinary Reviews: Cognitive Science* 1:446–459.

- Turk E, Scholtens LH, van den Heuvel MP (2016) Cortical chemoarchitecture shapes macroscale effective functional connectivity patterns in macaque cerebral cortex. *Human Brain Mapping* 37:1856–1865.
- van den Heuvel MP, Scholtens LH, de Reus MA, Kahn RS (2016) Associated microscale spine density and macroscale connectivity disruptions in schizophrenia. *Biol Psychiatry* 80:293–301.
- van den Heuvel MP, van Soelen IL, Stam CJ, Kahn RS, Boomsma DI, Hulshoff Pol HE (2013) Genetic control of functional brain network efficiency in children. *Eur Neuropsychopharmacol* 23:19–23.
- van den Heuvel MP, de Reus MA, Feldman Barrett L, Scholtens LH, Coopmans FMT, Schmidt R, Preuss TM, Rilling JK, Li L (2015) Comparison of diffusion tractography and tract-tracing measures of connectivity strength in rhesus macaque connectome. *Human Brain Mapping* 36:3064–3075.
- van den Heuvel MP, Hulshoff Pol HE (2010) Exploring the brain network: a review on resting-state fmri functional connectivity. *European neuropsychopharmacology : the journal of the European College of Neuropsychopharmacology* 20:519–34.
- van den Heuvel MP, Mandl RCW, Stam CJ, Kahn RS, Hulshoff Pol HE (2010) Aberrant frontal and temporal complex network structure in schizophrenia: a graph theoretical analysis. *The Journal of neuroscience : the official journal of the Society for Neuroscience* 30:15915–26.
- van den Heuvel MP, Scholtens LH, Feldman Barrett L, Hilgetag CC, de Reus MA (2015) Bridging cytoarchitectonics and connectomics in human cerebral cortex. *The Journal of Neuroscience* 35:13943–13948.
- van den Heuvel MP, Scholtens LH, Turk E, Mantini D, Vanduffel W, Feldman Barrett L (2016) Multimodal analysis of cortical chemoarchitecture and macroscale fmri resting-state functional connectivity. *Human brain mapping* 37:3103–3113.
- van den Heuvel MP, Sporns O (2013a) An anatomical substrate for integration among functional networks in human cortex. *The Journal of neuroscience : the official journal of the Society for Neuroscience* 33:14489–500.
- van den Heuvel MP, Sporns O (2013b) Network hubs in the human brain. *Trends in cognitive sciences* 17:683–696.
- van den Heuvel MP, Sporns O, Collin G, Scheewe T, Mandl RCW, Cahn W, Goñi J, Hulshoff Pol HE, Kahn RS (2013) Abnormal rich club organization and functional brain dynamics in schizophrenia. *JAMA psychiatry (Chicago, Ill.)* 70:783–92.
- van den Heuvel MP, Stam CJ, Kahn RS, Hulshoff Pol HE (2009) Efficiency of functional brain networks and intellectual performance. *The Journal of neuroscience : the official journal of the*

Society for Neuroscience 29:7619–24.

Van Essen DC, Smith SM, Barch DM, Behrens TE, Yacoub E, Ugurbil K (2013) The wu-minn human connectome project: an overview. *Neuroimage* 80:62–79.

VanDuffel W, Fize D, Mandeville JB, Nelissen K, Van Hecke P, Rosen BR, Tootell RB, Orban GA (2001) Visual motion processing investigated using contrast agent-enhanced fmri in awake behaving monkeys. *Neuron* 32:565–577.

von Bonin G, Bailey P (1947) *The neocortex of Macaca mulatta* Univ. of Illinois Press, Urbana.

Walker E (1940) A cytoarchitectural study of the prefrontal area of the macaque monkey. *The Journal of Comparative Neurology* 73:59–86.

Zilles K, Palomero-Gallagher N, Grefkes C, Scheperjans F, Boy C, Amunts K, Schleicher a (2002) Architectonics of the human cerebral cortex and transmitter receptor fingerprints: reconciling functional neuroanatomy and neurochemistry. *European neuropsychopharmacology : the journal of the European College of Neuropsychopharmacology* 12:587–99.

Zilles K, Amunts K (2009) Receptor mapping: architecture of the human cerebral cortex. *Current opinion in neurology* 22:331–339.

Zilles K, Bacha-Trams M, Palomero-Gallagher N, Amunts K, Friederici AD (2015) Common molecular basis of the sentence comprehension network revealed by neurotransmitter receptor fingerprints. *Cortex* 63:79–89.

Supplemental Information

of

Multimodal analysis of cortical chemoarchitecture and macroscale fMRI resting-state functional connectivity

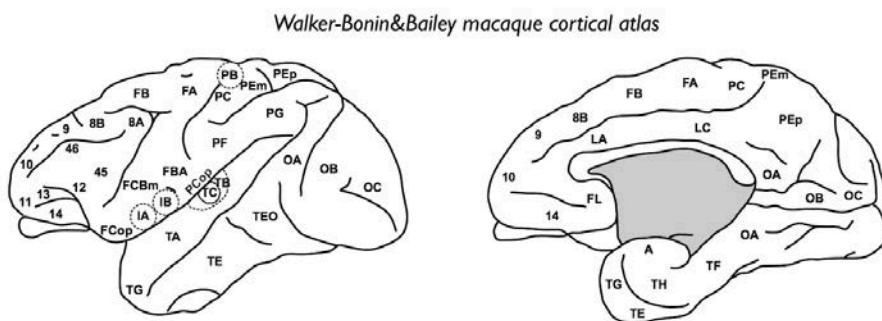


Figure S1. Combined Walker-Bonin&Bailey (WBB47) cortical atlas of the macaque.

Table S1.

Amunts regions	Regions in DK-57
4	precentral gyrus 1,2,3
6	superiorfrontal 3, caudalmiddlefrontal 1
6r1	precentral gyrus 4
44	parsopercularis 1
45	parstriangularis 1
47	lateralorbitofrontal 1
op8	parsopercularis 1
op9	parsorbitalis 1

Table describes the mapping of the original document regions to the regions of the Desikan-Kiliany atlas used for the functional connectivity.

Table S2.

Zilles regions	Regions in DK-57
IFS1/IFJ	rostralmiddlefrontal 1
pSTG/STS	superiortemporal 1
44v	parsopercularis 1
44d	rostralmiddlefrontal 1
45a	parsopercularis 1
45p	parsopercularis 1
47	parsorbitalis 1
Te2	transversetemporal 1
4v	precentral 3
4d	precentral 2
3b	postcentral 2
Te1	transversetemporal 1
V1	lateraloccipital 1
FG1	fusiform 1
FG2	fusiform 2
9	superiorfrontal 1
46	rostralmiddlefrontal 3
32	rostralanteriorcingulate 1
7	superiorparietal 1
PF	supramarginal 2
PFcm	supramarginal 2
PFm	supramarginal 2
Pfop	supramarginal 1
PFt	supramarginal 1
Pga	inferiorparietal 2
PGp	inferiorparietal 2

Table describes the mapping of the original document regions to the regions of the Desikan-Kiliany atlas used for the functional connectivity

Table S3.

Kötter regions	Regions in WBB47
F1	FA
F2v F2d	FB
F4v F4d	FBA
F5	FCBm
VIP	PEm
PO MIP	PEp
LIP PG	PG
FST	TA
V3v V3d	OA
V2v V2d	OB
V1	OC

Table describes the mapping of the original document regions to the regions of the Walker-Bonin&Bailey atlas used for the macaque functional connectivity

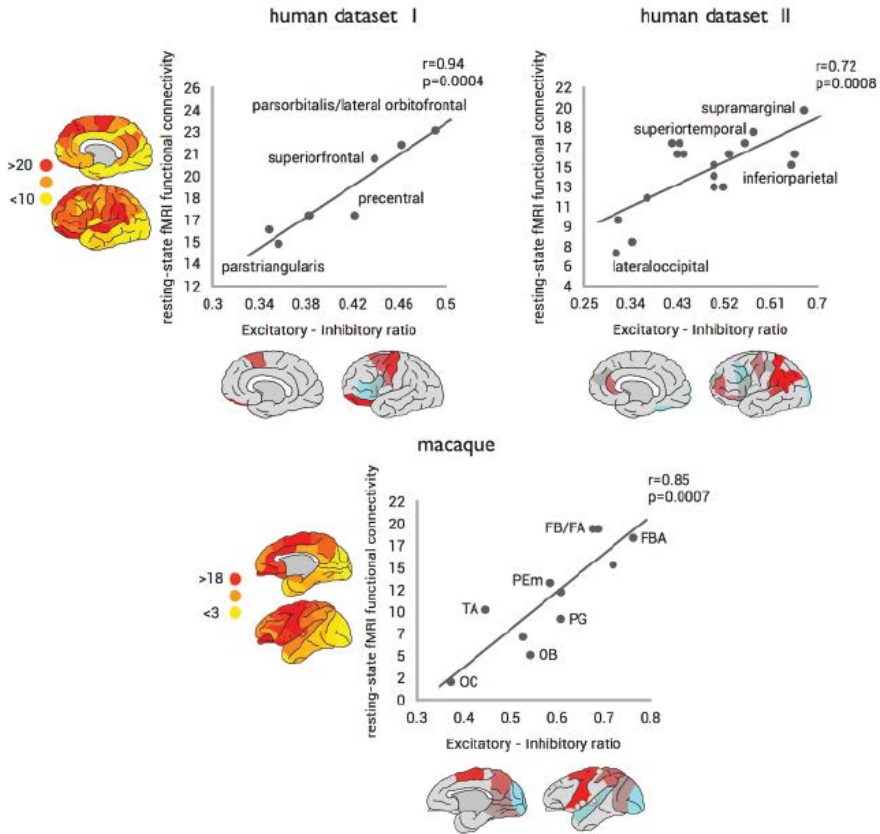
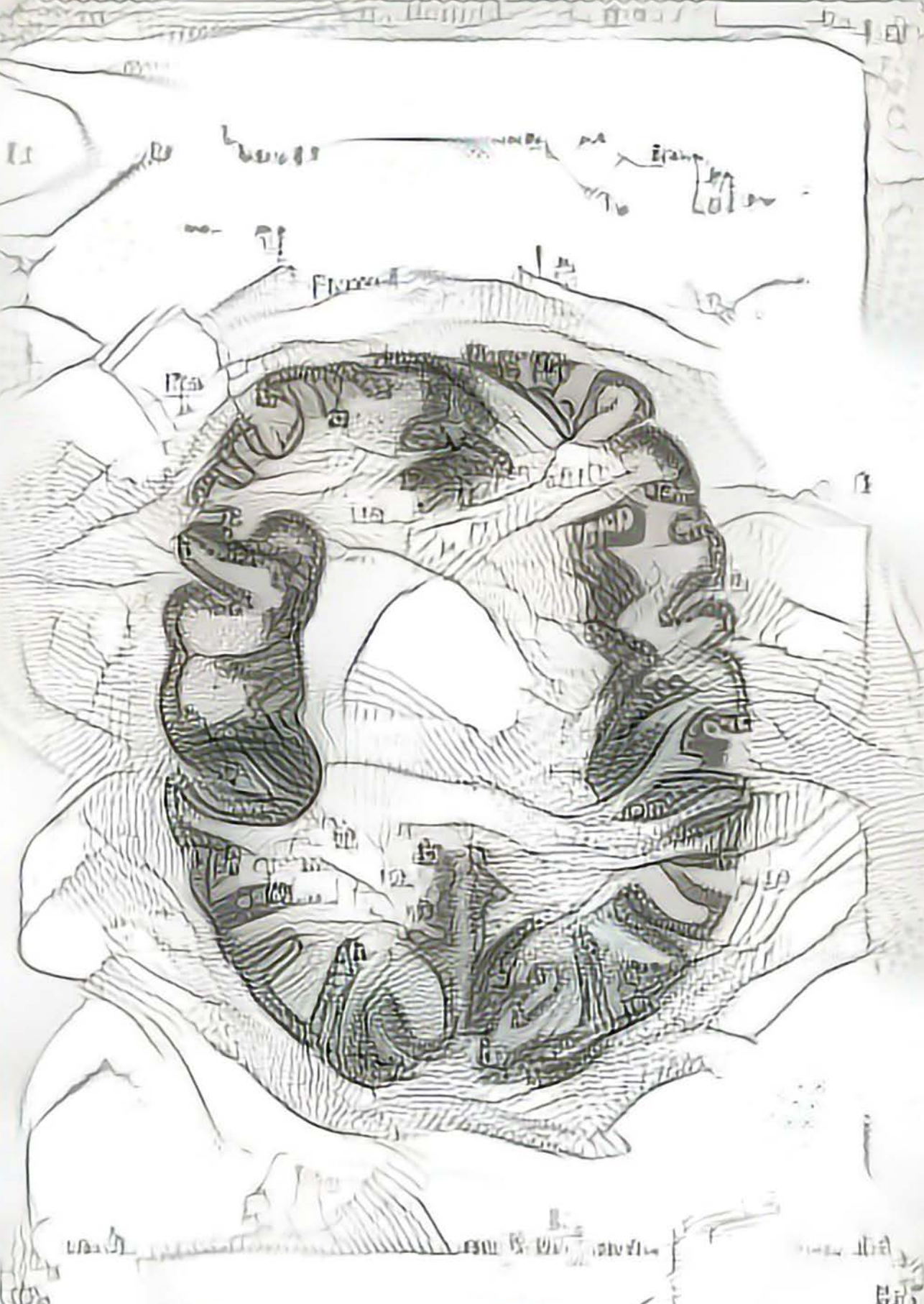


Figure S2. Same as Figure 2 in the main text, with region labels added. Interactions between the excitatory - inhibitory (ExIn) ratio of cortical regions and total strength of regional resting-state fMRI functional connectivity. Left and middle panels shows the correlations between ExIn ratio (x-axis) and regional functional connectivity (y-axis) for the human datasets (human dataset I and dataset II, respectively). Right panel shows the correlation between ExIn ratio (x-axis) and cortical resting-state functional connectivity (y-axis) for the macaque dataset. All three datasets show a significant, positive association between the relative excitatory character of cortical areas and the level of cortico-cortical resting-state functional connectivity as derived from resting-state fMRI.

Theme III – linking micro to macro scale across centuries



Linking Contemporary High Resolution Magnetic Resonance Imaging to the Von Economo Legacy: A Study on the Comparison of MRI Cortical Thickness and Histological Measurements of Cortical Structure

Lianne H. Scholtens, Marcel A. de Reus, and Martijn P. van den Heuvel

Human Brain Mapping 2015; 36 (8): 3038-3046

The cerebral cortex is a distinctive part of the mammalian nervous system, displaying a spatial variety in cyto-, chemico-, and myelinoarchitecture. As part of a rich history of histological findings, pioneering anatomists Von Economo and Koskinas provided detailed mappings on the cellular structure of the human cortex, reporting on quantitative aspects of cytoarchitecture of cortical areas. Current day investigations into the structure of human cortex have embraced technological advances in Magnetic Resonance Imaging (MRI) to assess macroscale thickness and organization of the cortical mantle in vivo. However, direct comparisons between current day MRI estimates and the quantitative measurements of early anatomists have been limited. Here, we report on a simple, but nevertheless important cross-analysis between the histological reports of Von Economo and Koskinas on variation in thickness of the cortical mantle and MRI derived measurements of cortical thickness. We translated the Von Economo cortical atlas to a subdivision of the commonly used Desikan–Killiany atlas (as part of the FreeSurfer Software package and a commonly used parcellation atlas in studies examining MRI cortical thickness). Next, values of “width of the cortical

mantle” as provided by the measurements of Von Economo and Koskinas were correlated to cortical thickness measurements derived from high-resolution anatomical MRI T1 data of 200+ subjects of the Human Connectome Project (HCP). Cross-correlation revealed a significant association between group-averaged MRI measurements of cortical thickness and histological recordings ($r = .54$, $P < .001$). Further validating such a correlation, we manually segmented the Von Economo parcellation atlas on the standardized Colin27 brain dataset and applied the obtained three-dimensional Von Economo segmentation atlas to the T1 data of each of the HCP subjects. Highly consistent with our findings for the mapping to the Desikan–Killiany regions, cross-correlation between in vivo MRI cortical thickness and Von Economo histology-derived values of cortical mantle width revealed a strong positive association ($r = .62$, $P < .001$). Linking today’s state-of-the-art T1-weighted imaging to early histological examinations our findings indicate that MRI technology is a valid method for in vivo assessment of thickness of human cortex.

Introduction

The human cerebral cortex occupies an average 550–600 ml of volume (Miller et al., 1980; Triarhou, 2007a), spans an impressive area of 2,000–2,500 cm² (Peters and Jones, 1984; Triarhou, 2007a) and includes an estimated, but widely varying, 25,000 neurons per mm³ (Alonso-Nanclares et al., 2008). A long history of histological examinations has identified a rich variation in cyto-, chemico-, and myeloarchitecture of the human cortex (Schüz and Miller, 2002; Zilles et al., 2002), identifying a large number of distinct cortical regions. Among pioneers of cortical mapping Korbinian Brodmann (1868–1918) (Brodmann, 1909) and Oskar (1870–1959) and Cecile Vogt (1875–1962) (see (Nieuwenhuys et al., 2014) for a recent meta-analysis), early anatomists Constantin Von Economo (1876–1931) and Georg Koskinas (1885–1975, see (Triarhou, 2006) for a biography of Von Economo’s life) provided detailed mappings of the complete human cortex by means of histological examination. In 1925 Von Economo and Koskinas presented the monumental work “Die Cytoarchitektonik der Hirnrinde des erwachsenen Menschen” (translated “Cytoarchitectonics of the Adult Human Cerebral Cortex”, from now on referred to as the Von Economo Atlas) (Von Economo and Koskinas, 1925) reporting on a complete parcellation of the human cortex in 54 distinct cortical areas (and 107 even more detailed smaller subregions) on the basis of quantified data on multiple aspects of cortical architecture, including neuronal count and width of the cortical mantle.

Following in the footsteps of these early pioneers in neuroanatomy, contemporary investigations into the human cortex have utilized technological advances in Magnetic

Resonance Imaging (MRI) to investigate the layout of the human cortex. Almost a hundred years after the pioneering work of Von Economo and Koskinas MR imaging is arguably one of the most popular techniques for studying the anatomy of the human cerebral cortex, with one of the advantages of this technique including the unique capability of examining cortical structure *in vivo*. This has led to a wide range of applications, including – among many others – investigations into delineation of distinct cortical regions, examinations of individual differences in cortical layout in relationship to cognitive functioning, mapping of changes in cortical structure in a wide range of psychiatric and neurological brain disorders, and so forth.

The number of studies directly comparing MRI derived estimates of cortical thickness with histological examinations is however surprisingly limited, but a few studies have made some important steps in bringing the two fields together. In their seminal work on the introduction of the FreeSurfer methodology to measure the thickness of the cortical mantle based on T1 MRI images, Fischl and Dale (2000) reported lobe averaged values of imaging derived cortical thickness levels to be within the range of values as reported by the histological measurements of Von Economo. Furthermore, comparing postmortem and MRI estimates they reported on a significant correlation between imaging derived estimates of cortical thickness of two postmortem brains and microscopy examinations in 7 brain regions (Rosas et al., 2002). In addition, a recent study reported overlapping levels of cortical thickness obtained by means of presurgery MRI and subsequent microscopy examination of a specific region removed from the temporal lobe during epilepsy surgery across a group of 26 patients (Cardinale et al., 2014). However, a systematic, region-wise whole-brain comparison between cytoarchitectural observations and MRI-based estimations of cortical structure remains missing. Connecting data from one of the most detailed – but perhaps by today's neuroscientist sometimes forgotten – cytoarchitectonic mappings of the human cortex with the best of what contemporary methods on anatomical MRI measurements have to offer (Van Essen et al., 2013) may provide a better understanding of the biological basis of the *in vivo* MRI cortical thickness measurements we do today. Here, we report on a cross-technique validation of cortical thickness estimations derived from MRI T1 imaging data of 215 subjects of the Human Connectome Project with the documented reports of pioneering anatomists Von Economo and Koskinas on the cellular structure of the human cerebral cortex.

Materials and Methods

Histological data

The detailed Von Economo atlas, originally published in 1925 by Von Economo and

Koskinas includes a parcellation of the total human cerebral cortex into 54 “Grundareae” (ground areas) based on a differentiating cytoarchitectonic layout of regions, with a more fine-grained division into 76 smaller “Varianten” (variants) and finally 107 even finer “Modifikationen” (modifications). As described in Von Economo’s 1927 writings that accompanied the atlas (titled “Zellaufbau der Grosshirnrinde des Menschen”, based on a series of teaching lectures by Von Economo (1927)), Von Economo stated that every region in the atlas was consistently observed in all investigated brain samples, with the atlas based on histological examination of the cortex of numerous brains (“zahlreichen Gehirnen”) of healthy (i.e., no reported history of neurological and/or psychiatric disorders) subjects in the age range of 30–40 years. Examples of cause of death as mentioned in the original text are hemoptysis in tuberculosis or a sudden death during surgery; the exact number of investigated samples was, however, not explicitly documented (Triarhou, 2007a; Von Economo, 2009). For the 51 most important regions described in the atlas (being 43 ground areas and 8 variants, of which 48 cortical and 3 hippocampal areas) Von Economo and Koskinas included overview tables with detailed quantified measures of cortical thickness and cytoarchitecture. Documentation of quantitative cytoarchitectonic values included reports of left and right hemispheric regions mixed together. A recent book translation by dr. L.C. Triarhou (Von Economo, 2009) of the 1927 accompanying textbook to English lists a detailed description of the cellular structure of the brain regions of the 1925 atlas, together with the information of Von Economo’s 1925 overview tables. In the study here, information on the width of the cortical mantle for the 48 cortical regions (40 ground regions and 8 variants) was included in our MRI versus Von Economo cortical thickness comparison, taken as the Von Economo and Koskinas reported overall width or the average of the cortical dome and cortical wall when separately provided (Von Economo, 2009).

MRI data

High-resolution T1-weighted imaging data of the Human Connectome Project was used for reconstruction of the human cerebral cortical mantle (Van Essen et al., 2013) (Q3 release, 215 subjects, voxel-size .7 mm isotropic, age-range 20–35 years). For each individual dataset, the FreeSurfer software package (Fischl et al., 2004) was used for automatic gray/white/cortical spinal fluid classification and subsequent reconstruction of the cortical mantle. A commonly used 114 region-subdivision of the Desikan–Killiany atlas (Desikan et al., 2006; Fischl et al., 2004) was used to parcellate the cortex into distinct brain regions, describing 57 unique cortical regions per hemisphere (a cortical parcellation as provided by (Cammoun et al., 2012; Hagmann et al., 2008)), being a subdivision based on the original Desikan–Killiany atlas describing 68 (34 single hemisphere) larger cortical regions (Desikan et al., 2006; Fischl et al., 2004). This

subdivision of 57 single hemisphere regions was used as it closely matched the number of cortical regions for which Von Economo–Koskinas cortical thickness was reported (48 regions). [Note that using other finer-grained subdivisions of the Desikan–Killiany atlas (dividing the original 34 cortical regions of the Desikan–Killiany atlas into respectively 111, 224, or 499 single hemisphere subregions (Hagmann et al., 2008)) revealed highly comparable results, as shown in Supporting Information Fig. S1]. Figure 1 illustrates the 57 single hemisphere subdivision of the Desikan–Killiany parcellation (Desikan et al., 2006).

Next, per individual dataset, FreeSurfer was used to compute the level of vertex-wise cortical thickness, and for each of the 114 cortical regions the average cortical thickness in that region was taken as the mean value over all cortical thickness measurements in that specific patch of the cortex. For the 114 regions group-averaged cortical thickness levels were computed as the average values over the total group of 215 subjects. To match the Von Economo atlas (which does not distinguish between left and right hemisphere, see description above), values of homologous regions of the left and right hemisphere were averaged to obtain MRI measurements of 57 single hemisphere cortical areas in total.

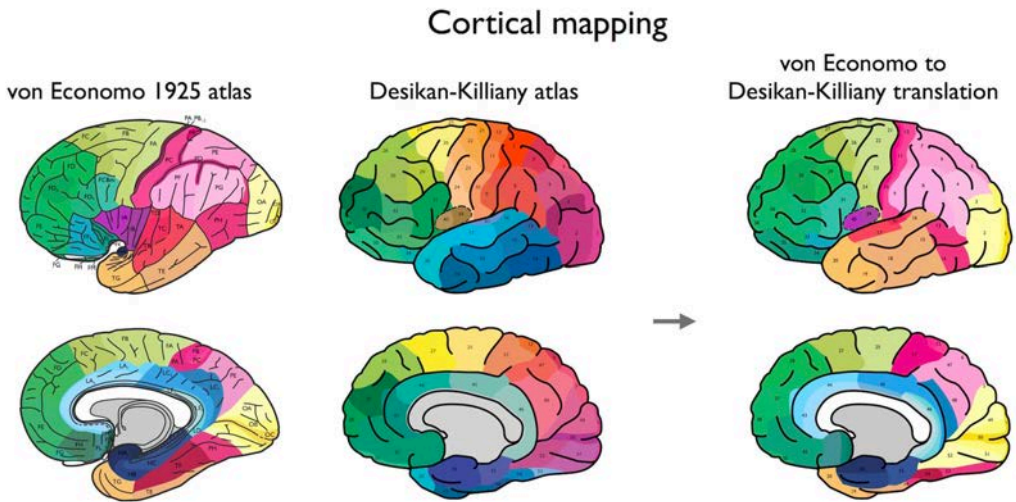


Figure 1. Cortical mapping. Left panel shows a remake of the original Von Economo atlas as published in (Triarhou, 2007b) (reprinted with permission), depicting the cortical areas as described and illustrated in (Von Economo, 1927, 2009). The middle panel shows the Desikan–Killiany atlas used for the computation of the MRI-based thickness of 114 cortical regions (57 per hemisphere, left hemisphere is shown). Right panel shows the regions of the Desikan–Killiany atlas (left hemisphere) as colored by the mapped Von Economo regions to our atlas. Supporting Information Table 1 gives a textual description of our mapping of the Von Economo regions to the Desikan–Killiany atlas.

Cortical mapping of atlases

The 48 cortical areas of Von Economo's atlas were manually mapped to the regions of the commonly used higher resolution 57 single hemisphere subdivision of the Desikan–Killiany atlas (Hagmann et al., 2008) (note that the three hippocampal regions as described by Von Economo and Koskinas were not included in our analysis as the hippocampus is not included as a cortical (but instead as a subcortical) structure in FreeSurfer). The Von Economo regions were manually mapped to the regions of the Desikan–Killiany atlas (LS, MvdH) using the information on the locations of the cortical regions as provided by visual illustrations of the 1925 atlas and the textual descriptions of the areas (Von Economo and Koskinas, 1925). For each region of the Desikan–Killiany atlas the best matching region(s) of the Von Economo atlas were selected, resulting in a mapping of the Von Economo regions to the 57 single-hemispheric regions of the subdivided Desikan–Killiany atlas. Figure 1 displays a one-to-one visual comparison between the digitized version of the Von Economo atlas and a schematic illustration of the Desikan–Killiany subdivided atlas (left hemisphere, 57 regions). Next, using the von Ecomomo to Desikan–Killiany atlas mapping, quantitative histological values were obtained for the 57 cortical regions: in case multiple Von Economo areas mapped to one single Desikan–Killiany region (e.g., regions FH, FL, FM, FN to medial orbitofrontal gyrus) the Von Economo and Koskinas reported levels were averaged; if one Von Economo area overlapped with two or more Desikan–Killiany regions (e.g., region FA to three Desikan–Killiany subareas of the precentral gyrus) each of the Desikan–Killiany regions obtained the histological levels as reported by Von Economo and Koskinas. Supporting Information Table 1 summarizes the Von Economo to Desikan–Killiany map-ping in text; Figure 1 illustrates the mapping visually. [A post hoc analysis of regions of which a 1-to-1 mapping between the Von Economo atlas and the Desikan–Killiany atlas (Supporting Information Table 1) was present (i.e., not involving averaging of cortical values) revealed highly consistent findings (see Supporting Information Results)].

Statistical analyses

Cross-technique examination was performed by means of correlation analysis between mapped histological values of the Von Economo atlas (i.e., reported width of the cortical mantle) and cortical thickness estimates as derived by MRI. Effects reaching a $P < .0045$ (reflecting a Bonferroni corrected alpha level of $< .05$, correcting for a total of 11 statistical tests performed in this study) were taken as significant.

Von Economo FreeSurfer atlas

In addition to a cross-technique analysis using MRI cortical thickness estimates based on the commonly used Desikan–Killiany atlas (see above), a second analysis was performed in which a direct mapping of 48 cortical Von Economo regions into

FreeSurfer was established. For this, first, we manually segmented the 48 cortical regions of the Von Economo atlas on the Colin27 brain (a standard reference brain in the field, consisting of an averaging of an individual brain that was scanned 27 times) (Holmes et al., 1998) using the label segmentation tools included in the FreeSurfer software suite. In this segmentation, region PB1 and PB2 were merged into one region PB (von Economo describes PB2 as being situated in an island-like fashion within area PB1 which we could not reliably draw onto the cortical surface) resulting in a total of 47 region labels. We note that during segmentation region FM and FN were found to be difficult to reliably draw onto the cortical surface due to their very small size and narrow shape (being the smallest segmented regions in the atlas, including only 2.6 and 3.1% of the average size of all Von Economo areas) (see also results). Second, the resulting manual segmentation was used to create a Von Economo FreeSurfer atlas using the atlas training tools as provided in FreeSurfer. Third, similar to our analysis for the Desikan–Killiany atlas, the Von Economo parcellation atlas was run on each of the individual HCP subjects (see Supporting Information Fig. S2 for five exemplary HCP subjects), individual MRI-based cortical thickness values for the Von Economo regions were extracted, and for each region a group average cortical thickness value was computed. Finally, region-wise group averaged cortical thickness estimates were cross-correlated with the Von Economo and Koskinas reported levels of width of the cortical mantle.

Results

Mapping of Von Economo–Koskinas to Desikan–Killiany

Region-wise MR T1-weighted imaging derived cortical thickness significantly correlated to Von Economo and Koskinas measurements of cortical width ($P = 2.00 \times 10^{-06}$, $r = .58$, surviving Bonferroni correction, Fig. 2A,B).

The Von Economo data does not distinguish between left and right hemisphere and in the mean analysis MRI data of the left and right hemisphere was thus averaged. Post hoc analysis, correlating Von Economo–Koskinas cortical width to MRI derived thickness of the left and right hemisphere separately, revealed similar strong correlations (right: $P = 2.69 \times 10^{-06}$, $r = .57$ | left: $P = 3.80 \times 10^{-06}$, $r = .57$).

Supplementary analyses describing (1) a subset of only the oldest HCP subjects (age range 31–35 years, 96 subjects) and (2) data of a set of $n = 40$ subjects drawn from a population of healthy participants of recent publications of our group (van den Heuvel et al., 2012; van den Heuvel and Sporns, 2011; van den Heuvel et al., 2013; Walhout et al., 2015) in the same age range as the Von Economo-Koskinas dataset (30–40 years)

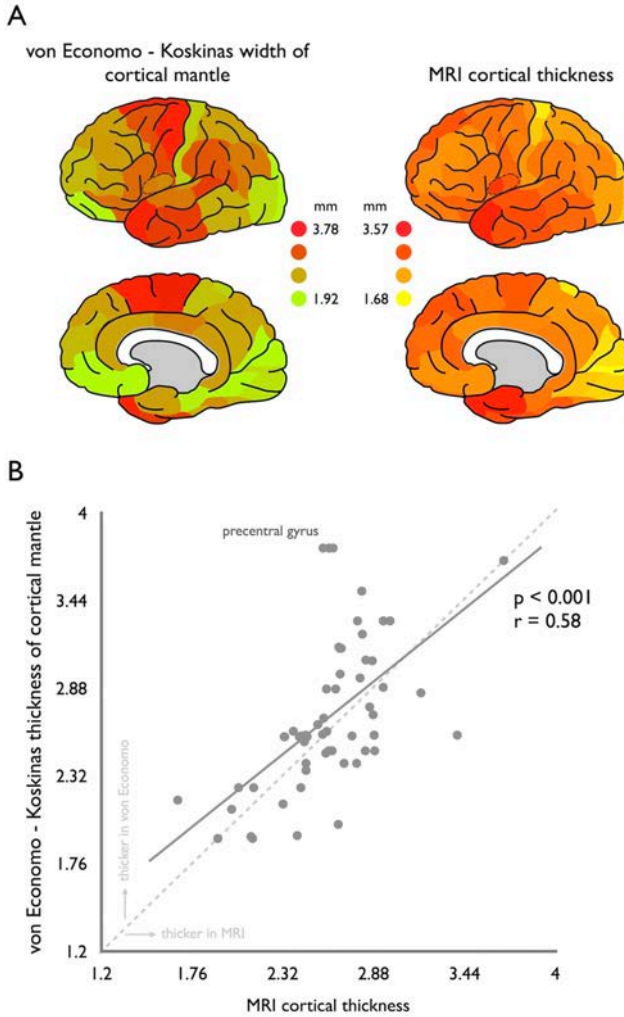


Figure 2. Association between Von Economo–Koskinas width of cortical mantle and MRI derived cortical thickness. Left panel of **A** shows the levels of total width of the cortical mantle as provided by Von Economo in millimeters (described as the average of the dome and wall width levels provided); right panel shows the cortical thickness as computed based on T1-weighted MRI data of 200+ subjects of the Human Connectome Project (see Methods) also in millimeters. **B** Correlation between region-wise Von Economo width of the cortical mantle (*y*-axis) and MRI derived cortical thickness (*x*-axis). Cross-technique comparison shows a strong relationship between Von Economo cortical width and MRI cortical thickness ($P < .001$, surviving Bonferroni correction for multiple testing). Points above the dashed middle line reflect regions of which the Von Economo histological measurements exceed the MRI derived estimates, points below this dashed line reflect regions of which MRI derived estimates of cortical thickness exceed those of the reports of Von Economo and Koskinas (see also Fig. 3). Regions of the precentral gyrus (marked) show a clear underestimation of cortical thickness as observed by means of MRI as compared to Von Economo reported cortical width (see results for a further investigation and possible explanation of this effect).

revealed highly consistent results to the main analysis (HCP 30–35 years: $r = .64$, $P = 1.15 \times 10^{-07}$; Utrecht set 30–40 years: $r = .56$, $P = 7.97 \times 10^{-06}$, data shown in Supporting Information Fig. S3).

Primary motor regions (region FA in the Von Economo 1925 atlas and subareas of the precentral gyrus in the Desikan–Killiany atlas, Supporting Information Table 1) showed deviating behavior from the general relationship, showing a clear underestimation of the thickness of the cortex as measured by MRI (over 31%, MRI: 2.60 mm, Von Economo total: 3.77 mm) as compared to the histological findings of Von Economo and Koskinas (points marked in Fig. 2B). Studies have noted a general difficulty of providing accurate MR measurements of cortical thickness of primary motor regions based on T1-weighted imaging (Han et al., 2006). This effect is possibly related to a suggested gradual transition of layer 6 to the white matter in the precentral gyrus (Brodmann, 1909) and thus relatively high T1 signal (Steen et al., 2000), making an accurate segmentation of the cortical and white matter boundary and subsequent estimates of the thickness of the cortical mantle particularly difficult in these regions (Han et al., 2006). Indeed, taking the Von Economo reports of the width of layer 1–layer 5 (i.e., excluding the heavily myelinated layer 6 of the precentral gyrus regions) revealed a much better overlap with the MR estimates of precentral gyrus thickness, reducing the effect to a small overestimation of 3.7% (MRI: 2.60 mm, von Economo layer 1–5: 2.46 mm).

Examining this effect across all regions, an underrepresentation of the thickness of the cortical mantle by MRI as compared to Von Economo–Koskinas reported values was mostly found in motor frontal, lateral parietal and primary visual cortical regions (e.g., pink to magenta regions, supramarginal cortex showing a Von Economo–MRI ratio: 1.17, pericalcarine gyrus: 1.30, Fig. 3), while an overestimation of MRI cortical thickness (i.e., Von Economo < MRI) was observed in lateral frontal and medial regions of the insular, frontal, and temporal cortex (yellow regions, ratio: .77, lateral orbitofrontal cortex, Fig. 3).

Von Economo FreeSurfer atlas

Consistent with the presented findings above, correlating MRI cortical thickness values extracted from the manually segmented VonEconomo FreeSurfer atlas with the Von Economo-Koskinas histological reports revealed a positive correlation ($P = .0016$, $r = .45$). Note that as illustrated in Figure 4, two points (indicated in pink in the figure) formed clear outliers to the overall correlation. Indeed, as noted, regions FM and FN were identified during manual segmentation process as difficult to segment subregions due to their very small size and narrow shape as compared to other cortical areas (see methods). Labeling FM and FN as outliers in the correlation analysis resulted in a

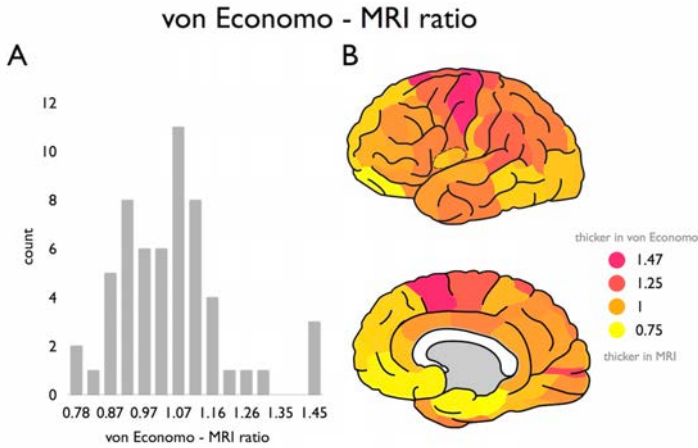


Figure 3. Von Economo–MRI ratio across regions. Panel A shows the distribution of the ratio between the Von Economo and Koskinas estimate of cortical width and MRI derived cortical thickness across all cortical regions of the 57 region Desikan–Killiany atlas; panel B shows the Von Economo–MRI ratio plotted on the cortical surface (left hemisphere). A ratio of > 1 reflects a level of cortical thickness higher in the Von Economo mapping as compared to the MRI derived estimate (pink to magenta regions). A ratio of < 1 reflects a level of cortical thickness higher as estimated by MRI as compared to the reports of Von Economo and Koskinas (yellow regions).

correlation of $r = .62$ ($P = 5.76 \times 10^{-06}$, Fig. 4). In addition, similar as for the mapping to the 57 single hemisphere Desikan–Killiany regions, the precentral gyrus (region FA in the Von Economo atlas) showed a clear underestimation by MRI (Von Economo/MRI ratio: 1.35). Further consistent with the results for the mapping of the Von Economo atlas to the Desikan–Killiany atlas (Fig. 3), MRI analysis resulted in an underestimation of the thick-ness of the cortical mantle for frontal motor, lateral parie-tal, and primary visual regions (e.g., frontal region FB showing a Von Economo–MRI ratio of 1.04, region PF 1.12, and region OC 1.09) and an overestimation of MRI derived thickness of medial temporal, frontal, and insular cortex (e.g., region FL showing a ratio of .75, region IB .90, region HC .76).

Discussion

The main finding of our study is a positive correlation between MRI derived measures of cortical thickness and width of the cortical mantle as reported in the histological work of pioneering neuroanatomists Von Economo and Koskinas (Von Economo, 1927; Von Economo and Koskinas, 1925). With MRI currently being one of today’s most used technologies to measure structure of the human cortex, linking and validating MRI derived metrics to histological reports is of importance to the use of such metrics in clinical, translational and cognitive neuroscience studies. Our technical report shows a

Linking MRI to Von Economo cortical thickness

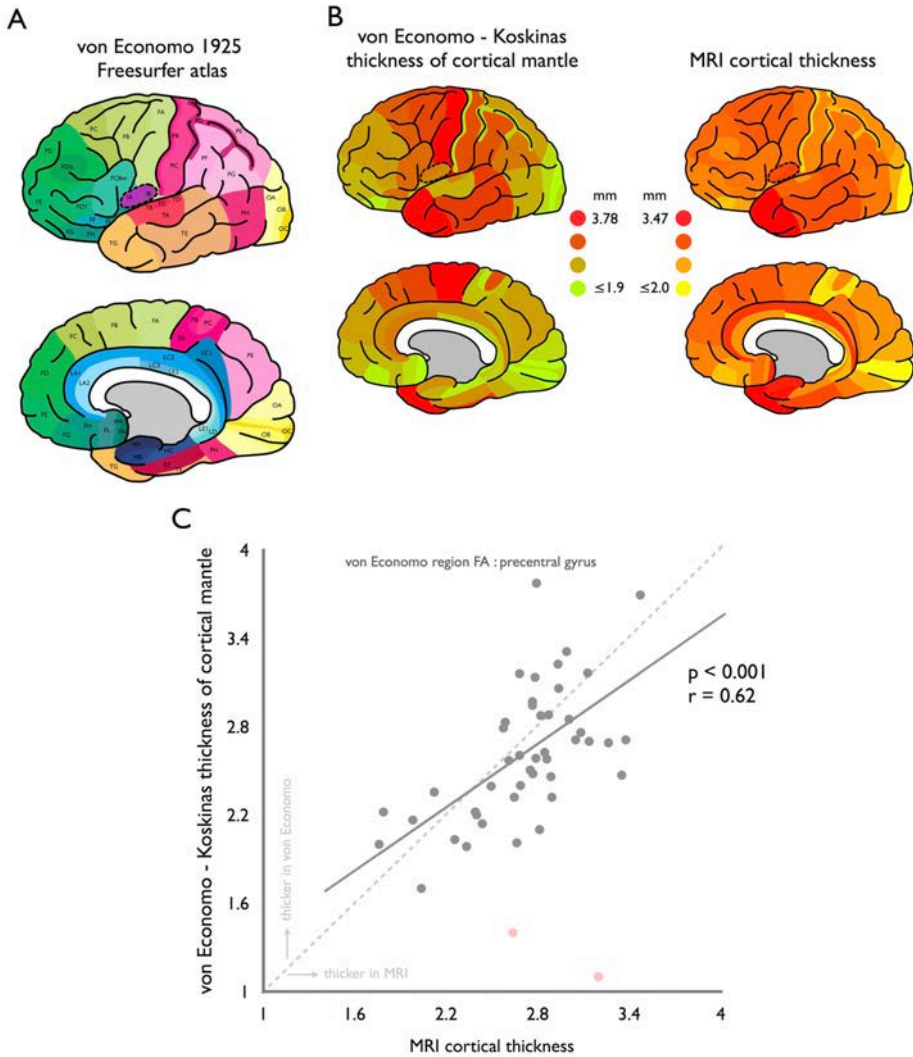


Figure 4. Von Economo–FreeSurfer atlas. Panel A illustrates the regions of the manually segmented Von Economo 1925 FreeSurfer atlas. Panel B shows for this atlas the Von Economo and Koskinas reported cortical width values (left panel) and MRI derived thickness estimates (right panel) of the cortical mantle. Panel C shows the significant region-wise correlation between Von Economo–Koskinas measurements of width of the cortical mantle (*y*-axis) and MRI derived measurements of cortical thickness (*x*-axis). Panel D shows the ratio between the Von Economo and Koskinas reported cortical width values and MRI derived estimates of cortical thickness (with a ratio > 1 (pink-magenta) indicating Von Economo > MRI, and a ratio of < 1 (yellow) indicating Von Economo < MRI). [Note the high overlap with the results shown for the manual mapping to the Desikan–Killiany atlas as presented in Fig. 3B].

simple, but potentially important correlation between MRI derived metrics of cortical thickness and cortical width as measured by histological techniques.

At least three technical remarks have to be kept in mind when interpreting the findings of this study. First, post-mortem examinations are known to suffer from volume shrinkage after death related to dehydration of the tissue, thus leading to a general underestimation of measurements of size of postmortem tissue. The data of von Economo and Koskinas have not been corrected for shrinkage effects, which could be argued as having led to a possible global underestimation of measurements of volume and thickness (Amunts et al., 2007). However, the section procedure as used by Von Economo and Koskinas has been noted to lead to an overestimation of tissue volume, factors argued to counter balance shrinkage effects (Amunts et al., 2007). Amunts et al. (2007), documenting and analyzing the used procedures in detail, thus concluded the Von Economo and Koskinas estimates to be accurate and comparable to other techniques. Second, how the brain samples included in the Von Economo 1925 atlas exactly correspond to HCP MRI data can unfortunately not be quantified (as trivially no MRI data of the samples as examined by Von Economo and Koskinas exists), but it is clear from their detailed writings on differences between individual samples that they investigated a number of brains, presumably of both men and women combined in an age range of 30–40 years. Concerning the latter, supplementary analysis of examining HCP and Utrecht MRI samples in the age range of 30–40 years revealed consistent findings (See Supporting Information Materials and Supporting Information Fig. 3). Third, MRI estimations of the cortical thickness of regions were taken as an average over a large group of subjects thus ignoring individual differences in thickness of the cortical mantle related to for example gender (e.g., (Amunts et al., 2007; Sowell et al., 2006)) and/or variation in cognitive abilities (Karama et al., 2011; Schnack et al., 2014).

Our conclusion is threefold. First, today's MRI technology is a good method for a quick, automated estimation of thickness of the cortical mantle *in vivo*. Second, translating detailed histology data to an MRI framework provides new opportunities to test algorithms for automated gray/white matter segmentations. And third, findings show that MRI-based observations can be examined and interpreted in light of cytoarchitectonic observations, suggesting that the “gap” between MRI derived and histology derived measurements of human cortical structure may not be as big as sometimes thought.

Acknowledgments

The authors would like to thank Leonard van den Berg, and Ruben Schmidt for kindly sharing T1 MRI data (as part of the analyzed supplementary Utrecht dataset). We thank Claus Hilgetag for fruitful and enjoyable discussions on this topic.

References

- Alonso-Nanclares L, Gonzalez-Soriano J, Rodriguez JR, DeFelipe J (2008) Gender differences in human cortical synaptic density. *Proceedings of the National Academy of Sciences of the United States of America* 105:14615–14619.
- Amunts K, Armstrong E, Malikovic A, Hömke L, Mohlberg H, Schleicher A, Zilles K (2007) Gender-specific left-right asymmetries in human visual cortex. *Journal of Neuroscience* 27:1356–1364.
- Brodmann K (1909) *Vergleichende Lokalisationslehre der Grosshirnrinde in ihren Prinzipien dargestellt auf Grund des Zellenbaues* Barth.
- Cammoun L, Gigandet X, Meskaldji D, Thiran JP, Sporns O, Do KQ, Maeder P, Meuli R, Hagmann P (2012) Mapping the human connectome at multiple scales with diffusion spectrum mri. *Journal of neuroscience methods* 203:386–97.
- Cardinale F, Chinnici G, Bramerio M, Mai R, Sartori I, Cossu M, Lo Russo G, Castana L, Colombo N, Caborni C, De Momi E, Ferrigno G (2014) Validation of freesurfer-estimated brain cortical thickness: comparison with histologic measurements. *Neuroinformatics* 12:535–42.
- Desikan RS, Segonne F, Fischl B, Quinn BT, Dickerson BC, Blacker D, Buckner RL, Dale AM, Maguire RP, Hyman BT, Albert MS, Killiany RJ (2006) An automated labeling system for subdividing the human cerebral cortex on mri scans into gyral based regions of interest. *Neuroimage* 31:968–80.
- Fischl B, van der Kouwe A, Destrieux C, Halgren E, Segonne F, Salat DH, Busa E, Seidman LJ, Goldstein J, Kennedy D, Caviness V, Makris N, Rosen B, Dale AM (2004) Automatically parcellating the human cerebral cortex. *Cereb Cortex* 14:11–22.
- Fischl B, Dale AM (2000) Measuring the thickness of the human cerebral cortex from magnetic resonance images. *Proceedings of the National Academy of Sciences* 97:11050–11055.
- Hagmann P, Cammoun L, Gigandet X (2008) Mapping the structural core of human cerebral cortex. *PLoS biology* 6:e159.
- Han X, Jovicich J, Salat D, van der Kouwe A, Quinn B, Czanner S, Busa E, Pacheco J, Albert M, Killiany R, Maguire P, Rosas D, Makris N, Dale A, Dickerson B, Fischl B (2006) Reliability of mri-derived measurements of human cerebral cortical thickness: the effects of field strength, scanner upgrade and manufacturer. *Neuroimage* 32:180–94.
- Holmes CJ, Hoge R, Collins L, Woods R, Toga AW, Evans AC (1998) Enhancement of mr images using registration for signal averaging. *Journal of computer assisted tomography* 22:324–333.
- Karama S, Colom R, Johnson W, Deary IJ, Haier R, Waber DP, Lepage C, Ganjavi H, Jung R, Evans AC (2011) Cortical thickness correlates of specific cognitive performance accounted for by the

- general factor of intelligence in healthy children aged 6 to 18. *Neuroimage* 55:1443–1453.
- Miller A, Alston R, Corsellis J (1980) Variation with age in the volumes of grey and white matter in the cerebral hemispheres of man: measurements with an image analyser. *Neuropathology and applied neurobiology* 6:119–132.
- Nieuwenhuys R, Broere CA, Cerliani L (2014) A new myeloarchitectonic map of the human neocortex based on data from the vogt-vogt school. *Brain Struct Funct* .
- Peters A, Jones EG (1984) *Comparative Structure and Evolution of Cerebral Cortex, Part I*, Vol. 8A of *Cerebral Cortex* Springer US.
- Rosas H, Liu A, Hersch S, Glessner M, Ferrante R, Salat D, van Der Kouwe A, Jenkins B, Dale A, Fischl B (2002) Regional and progressive thinning of the cortical ribbon in huntington's disease. *Neurology* 58:695–701.
- Schnack HG, van Haren NE, Brouwer RM, Evans A, Durston S, Boomsma DI, Kahn RS, Hulshoff Pol HE (2014) Changes in thickness and surface area of the human cortex and their relationship with intelligence. *Cerebral Cortex* 25:1608–1617.
- Schüz A, Miller R (2002) *Cortical areas: unity and diversity* Conceptual advances in brain research. Taylor & Francis, London; New York.
- Sowell ER, Peterson BS, Kan E, Woods RP, Yoshii J, Bansal R, Xu D, Zhu H, Thompson PM, Toga AW (2006) Sex differences in cortical thickness mapped in 176 healthy individuals between 7 and 87 years of age. *Cerebral cortex* 17:1550–1560.
- Steen RG, Reddick WE, Ogg RJ (2000) More than meets the eye: significant regional heterogeneity in human cortical t 1*. *Magnetic resonance imaging* 18:361–368.
- Triarhou LC (2007a) The economo-koskinas atlas revisited: Cytoarchitectonics and functional context. *Stereotactic and Functional Neurosurgery* 85:195–203.
- Triarhou LC (2007b) A proposed number system for the 107 cortical areas of economo and koskinas, and brodmann area correlations. *Stereotactic and Functional Neurosurgery* 85:204–215.
- Triarhou LC (2006) The signalling contributions of constantin von economo to basic, clinical and evolutionary neuroscience. *Brain Research Bulletin* 69:223–243.
- van den Heuvel MP, Kahn RS, Goñi J, Sporns O (2012) High-cost, high-capacity backbone for global brain communication. *Proceedings of the National Academy of Sciences of the United States of America* 109:11372–11377.
- van den Heuvel MP, Sporns O (2011) Rich-club organization of the human connectome. *The Journal of neuroscience : the official journal of the Society for Neuroscience* 31:15775–86.

- van den Heuvel MP, Sporns O, Collin G, Scheewe T, Mandl RCW, Cahn W, Goñi J, Hulshoff Pol HE, Kahn RS (2013) Abnormal rich club organization and functional brain dynamics in schizophrenia. *JAMA psychiatry (Chicago, Ill.)* 70:783–92.
- Van Essen DC, Smith SM, Barch DM, Behrens TE, Yacoub E, Ugurbil K (2013) The wu-minn human connectome project: an overview. *Neuroimage* 80:62–79.
- Von Economo C (1927) *Zellaufbau der Grosshirnrinde des Menschen* Springer, Berlin.
- Von Economo C (2009) *Cellular structure of the human cerebral cortex* Karger Medical and Scientific Publishers, Basel.
- Von Economo CF, Koskinas GN (1925) *Die Cytoarchitektonik der Hirnrinde des erwachsenen Menschen* J. Springer.
- Walhout R, Westeneng HJ, Verstraete E, Hendrikse J, Veldink JH, Van Den Heuvel MP, Van Den Berg LH (2015) Cortical thickness in als: towards a marker for upper motor neuron involvement. *J Neurol Neurosurg Psychiatry* 86:288–294.
- Zilles K, Palomero-Gallagher N, Grefkes C, Scheperjans F, Boy C, Amunts K, Schleicher a (2002) Architectonics of the human cerebral cortex and transmitter receptor fingerprints: reconciling functional neuroanatomy and neurochemistry. *European neuropsychopharmacology : the journal of the European College of Neuropsychopharmacology* 12:587–99.

Supplemental Information

of

Linking Contemporary High Resolution Magnetic Resonance Imaging to the Von Economo Legacy: A Study on the Comparison of MRI Cortical Thickness and Histological Measurements of Cortical Structure

Supplemental methods

Von Economo – MRI analysis for non-overlapping regions

To match regions of the Von Economo and Desikan–Killiany atlas, cortical values were averaged in the case of multiple smaller Von Economo areas linked to one single Desikan–Killiany region (see methods). To rule out any potential effect of this averaging, a second post-hoc analysis was performed in which only regions were included that involved a 1 to 1 mapping between the two atlases (23 regions, Supplemental Table 1, see also methods), revealing highly consistent findings with the main analysis ($p = 7.65 \times 10^{-04}$, $r = .65$).

Consistency of Von Economo – MRI cortical thickness measurements in a 30-40 year subset.

Several studies have reported a modest, but relevant association between age and reduction in cortical thickness in the age range between 20 and 40 years (for example (Lemaitre et al., 2012; Schnack et al., 2014)). To verify whether our results are influenced by the difference in age range between our 215 included Human Connectome Project (HCP) subjects (aged 20-35 years, in age classes of 5 years) and the Von Economo-Koskinas dataset (30-40 years) we performed two additional analyses. First, we compared the Von Economo-Koskinas cortical width measurements to only the subset of MRI thickness values derived from the oldest included HCP subjects (in age class 31-35). Similar to our main findings (see main text), this resulted in a strong positive correlation between MRI cortical thickness and Von Economo-Koskinas thickness of the cortical mantle (HCP 30-35 years, $n = 96$: $r = .64$, $p = 1.15 \times 10^{-07}$, data shown in Supplemental Figure S3-A). Second, we examined the cross-technique correlation for a dataset of $n = 40$ healthy participants within the exact age range as examined by Von Economo and Koskinas (all subjects ranging between 30-40 years, mean/std: 34.1/3.4 years) taken from recent studies of our group (all datasets acquired on the same 3 Tesla Philips Achieva scanner, all with the same T1-weighted imaging protocol, 3D FFE using parallel imaging, TR/TE 10ms/4.6ms, 200 slices, 0.75 mm voxel size). Analyzing this new dataset in the same way as the HCP data, again revealed a significant, positive correlation between MRI estimates of cortical thickness and cortical width values of the Von Economo atlas (Utrecht set 30-40 years: $r = .56$, $p = 7.97 \times 10^{-06}$, data shown in Supplemental Figure S3-B).

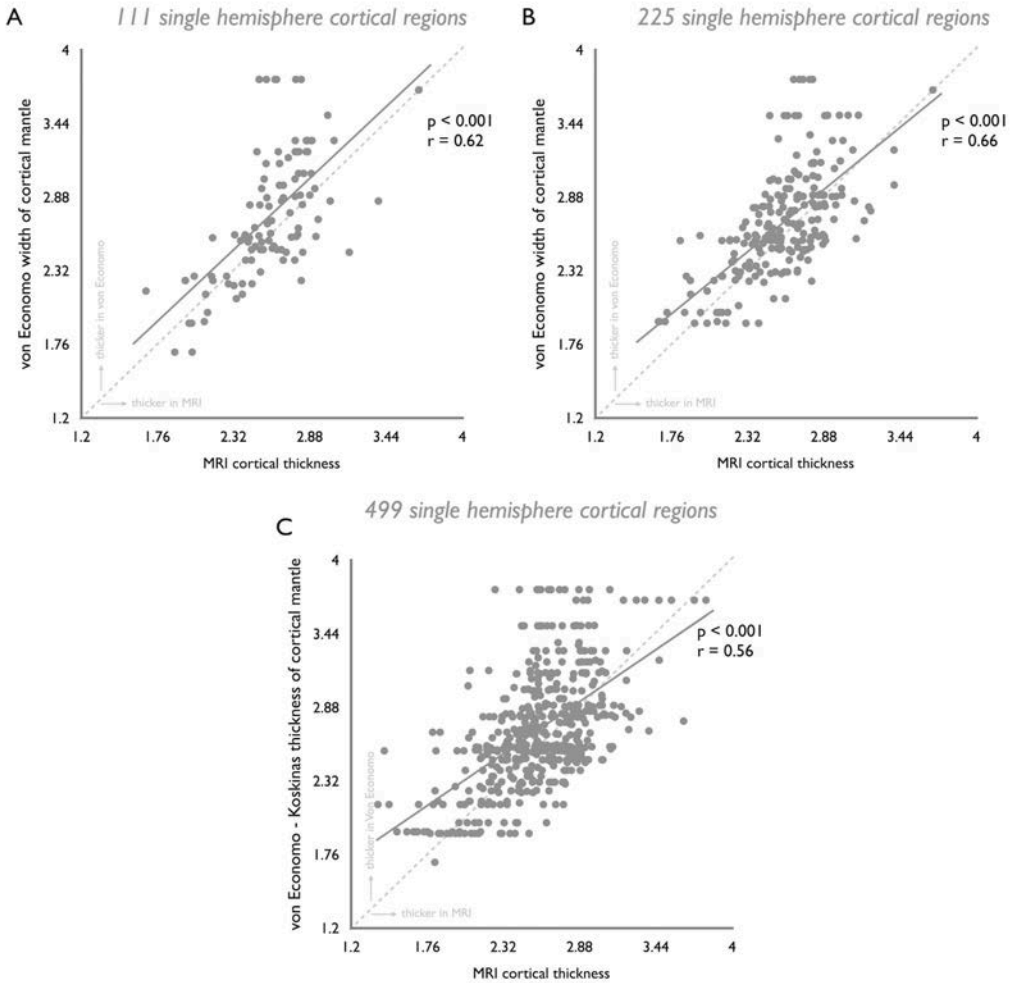


Figure S1. In the main part of our study, a mapping of the Von Economo data to the Desikan–Killiany subdivided atlas of 114 (57 single hemisphere) regions was used. Using other (also commonly used) more fine-grained subdivisions of the Desikan–Killiany atlas (as made by Hagmann and colleagues (Cammoun et al., 2012; Hagmann et al., 2008)) revealed highly consistent results. Panel A, B and C show correlations between the Von Economo and Koskinas estimates of width of the cortical mantle and MRI derived cortical thickness when the 219 (111 single left hemisphere regions), 448 (225 single left hemisphere regions) and 998 (499 single left hemisphere regions) subdivisions of the Desikan–Killiany atlas are used. All three additional subdivisions revealed high correlations (and highly significant effects), being DK-228 ($r = .62$, $p = 8.04 \times 10^{-13}$), DK-500 ($r = .66$, $p = 3.844 \times 10^{-29}$) and DK-1000 ($r = .56$, $p = 1.95 \times 10^{-42}$).

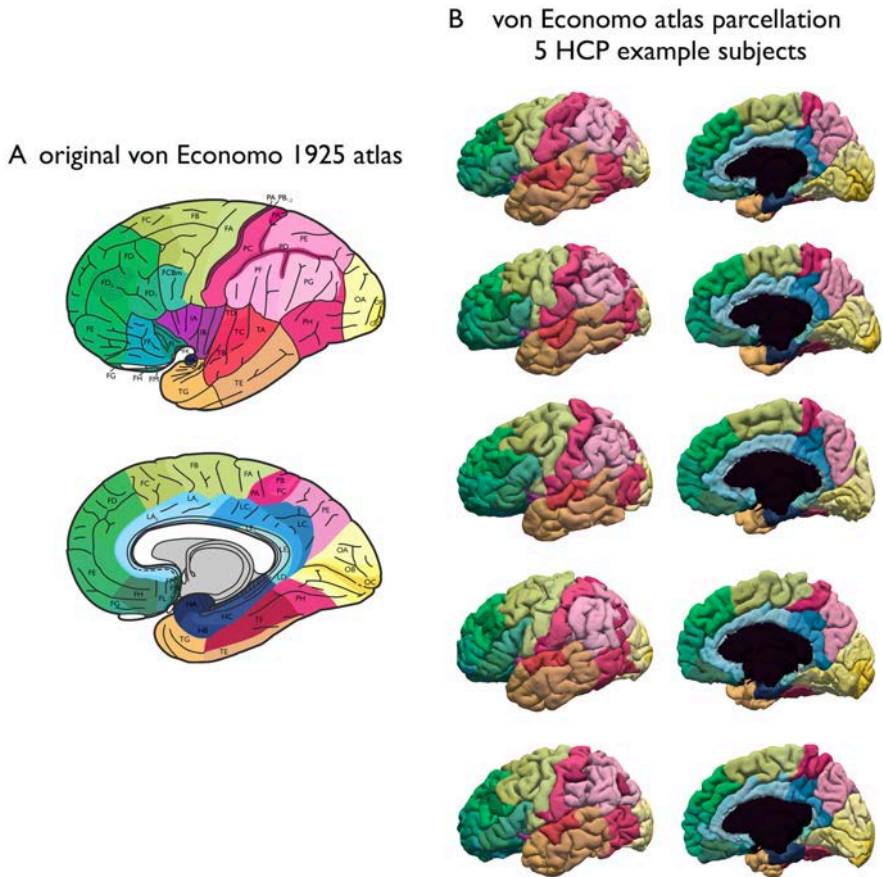


Figure S2. In addition to a cross-technique analysis using MRI cortical thickness values based on a common subdivision of the Desikan–Killiany atlas (see main text), a second analysis was performed using a direct mapping of the cortical Von Economo regions to a newly segmented atlas in FreeSurfer (see main text, and Supplemental Figure S1 for this mapping). Panel A shows the original Von Economo – Koskinas atlas. Panel B shows a lateral (left panel) and medial (right panel) view of the new FreeSurfer–VonEconomo atlas on the 3D cortical surface rendering of five random exemplary subjects of the Human Connectome Project.

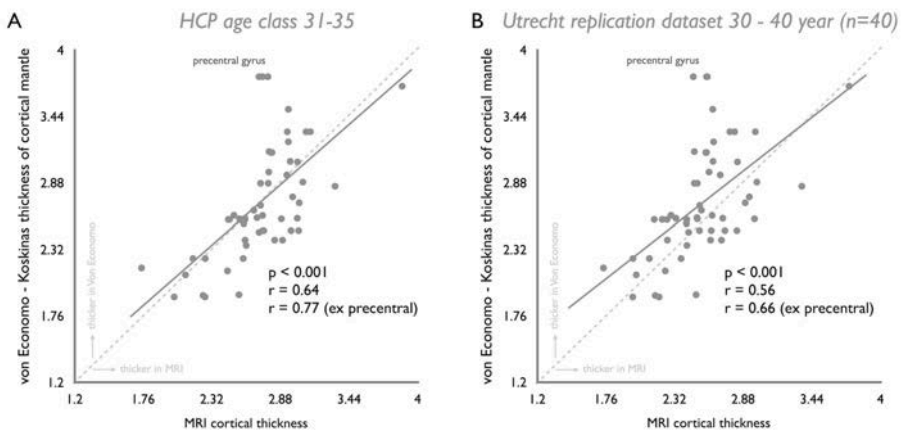


Figure S3. Panel A shows the correlation between Von Economo and Koskinas measurements of cortical width and MRI derived cortical thickness values for the subset of HCP subjects in the age class of 31-35 (96 subjects, Desikan–Killiany atlas 57 single hemisphere subregions). Panel B shows the Von Economo – MRI correlation for the $n = 40$ Utrecht subset (age 30-40 years, Desikan–Killiany atlas 57 single hemisphere subregions).

Table S1. Mapping Von Economo atlas to Desikan-Killiany atlas.

region code	Von Economo - Koskinas atlas region name	Desikan - Killiany atlas region number(s) & region name(s)*
Frontal pole		
FA	precentral gyrus	precentral_1, precentral_2, precentral_3, superiorfrontal_4
FB	granular frontal area	precentral_4, superiorfrontal_4, caudalmiddlefrontal_1
FC	intermediate frontal area	superiorfrontal_3, caudalmiddlefrontal_1
FCBm	magnocellular agranular intermediated frontal	parsopercularis_1
FD	granular frontal area	superiorfrontal_2, rostralmiddlefrontal_1
FDdelta	middle granular frontal area	rostralmiddlefrontal_2
FDT	triangular granular frontal area	parstriangularis_1
FE	frontalpolar area	parsorbitalis_1, rostralmiddlefrontal_3, superiorfrontal_1, frontalpole_1
FF	orbital area (agranular orbital area FFalpha)	parsorbitalis_1, lateralorbitofrontal_1, lateralorbitofrontal_2
FG	straight area	lateralorbitofrontal_2
FH	prefrontal area	medialorbitofrontal_1
FI	frontoinsular area	lateralorbitofrontal_1
FK	frontal piriform area	lateralorbitofrontal_1
FL	parolfactory area	medialorbitofrontal_1
FM	geniculate area	medialorbitofrontal_1
FN	precommissural	medialorbitofrontal_1
Parietal lobe		
PA	postcentral giant pyramidal area PA1 and postparacentral giant pyramidal area PA2	postcentral_1, postcentral_2, postcentral_3, paracentral_1
PB1	oral postcentral area granulosa	postcentral_1, postcentral_2, postcentral_3
PB2	oral postcentral area simplex	postcentral_1, postcentral_2, postcentral_3
PC	intermediate postcentral area	postcentral_1, postcentral_2, postcentral_3
PD	caudal postcentral area	postcentral_1, postcentral_2, postcentral_3
PE	superior parietal area	superiorparietal_1, superiorparietal_2, superiorparietal_3, precuneus_2, precuneus_1
PF	supramarginal area	supramarginal_2, supramarginal_1
PG	angular area	inferiorparietal_1, inferiorparietal_2
PH	basal temporo-occipital parietal area	inferiortemporal_2, middletemporal_1, bankssts_1, fusiform_1, lingual_1
Insular cortex		
IA	precentral insular area	insula_2
IB	postcentral insular area	insula_1
Occipital lobe		
OA	peristriate area	lateraloccipital_2, inferiorparietal_1, superiorparietal_3, cuneus_1, lingual_1, lingual_2
OB	parastriate area	cuneus_1, lingual_1, lingual_2, lateraloccipital_1
OC	striate area	lateraloccipital_1, pericalcarine_1

* region subnumbers are study specific.

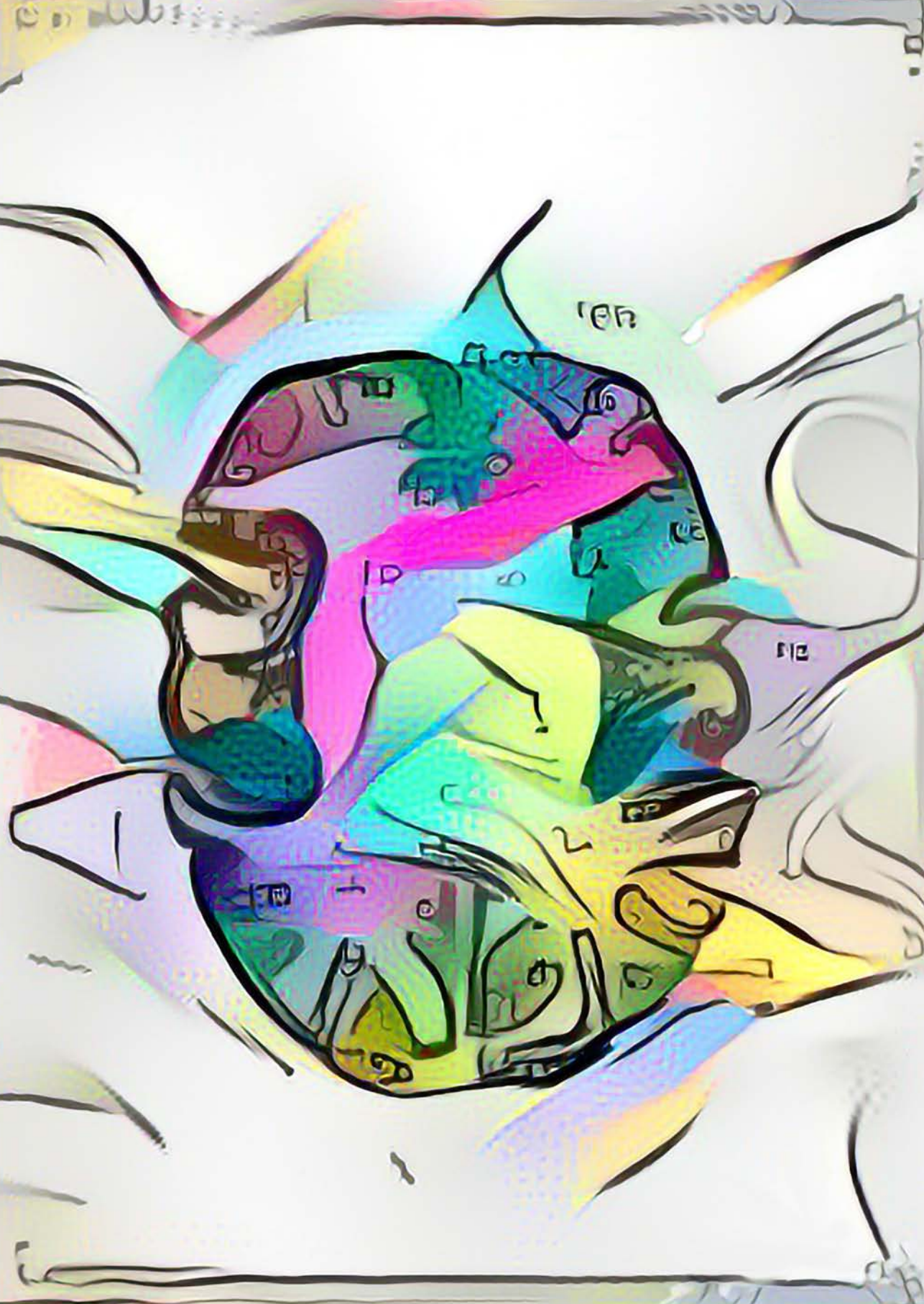
Table S1 – continued.

region code	Von Economo - Koskinas atlas region name	Desikan - Killiany atlas region number(s) & region name(s)*
Temporal lobe		
TA	superior temporal area	transversetemporal_1, superiortemporal_2
TB	supratemporal area simplex	transversetemporal_1
TC	supratemporal area granulosa	transversetemporal_1
TD	intercalated supratemporal area	transversetemporal_1
TE	temporal area proper	inferiortemporal_2, middletemporal_1, superiortemporal_2, middletemporal_2, inferiortemporal_1, superiortemporal_1
TF	fusiform area	fusiform_2
TG	temporopolar area	temporalpole_1, inferiortemporal_1
Cingulate cortex		
LA1	precingulate agranular anterior limbic area	rostralanteriorcingulate_1, caudalanteriorcingulate_1
LA2	precingulate agranular anterior limbic area	rostralanteriorcingulate_1, caudalanteriorcingulate_1
LC1	dorsal posterior cingulate area	precuneus_2
LC2	ventral posterior cingulate area	posteriorcingulate_1, isthmuscingulate_1
LC3	precingulate agranular anterior limbic area	posteriorcingulate_1
LD	angranular retrosplenial area	isthmuscingulate_1
LE1	superior retrosplenial area granulosa	isthmuscingulate_1
LE2	inferior retrosplenial area granulosa	isthmuscingulate_1
Hippocampal lobe		
HA	uncinate area	entorhinal_1
HB	parauncinate area	entorhinal_1
HC	rhinal area limitans	parahippocampal_1

* region subnumbers are study specific.

Supplemental References

- Cammoun L, Gigandet X, Meskaldji D, Thiran JP, Sporns O, Do KQ, Maeder P, Meuli R, Hagmann P (2012) Mapping the human connectome at multiple scales with diffusion spectrum mri. *Journal of neuroscience methods* 203:386–97.
- Hagmann P, Cammoun L, Gigandet X (2008) Mapping the structural core of human cerebral cortex. *PLoS biology* 6:e159.
- Lemaitre H, Goldman AL, Sambataro F, Verchinski BA, Meyer-Lindenberg A, Weinberger DR, Mattay VS (2012) Normal age-related brain morphometric changes: nonuniformity across cortical thickness, surface area and gray matter volume? *Neurobiology of Aging* 33:617.e1–617.e9.
- Schnack HG, van Haren NE, Brouwer RM, Evans A, Durston S, Boomsma DI, Kahn RS, Hulshoff Pol HE (2014) Changes in thickness and surface area of the human cortex and their relationship with intelligence. *Cerebral Cortex* 25:1608–1617.



Chapter 10

An MRI Von Economo Koskinas atlas

Lianne H. Scholtens, Marcel A. de Reus, Siemon C. de Lange, Ruben Schmidt, Martijn P. van den Heuvel

NeuroImage in press

The cerebral cortex displays substantial variation in cellular architecture, a regional patterning that has been of great interest to anatomists for centuries. In 1925, Constantin von Economo and George Koskinas published a detailed atlas of the human cerebral cortex, describing a cytoarchitectonic division of the cortical mantle into over 40 distinct areas. Von Economo and Koskinas accompanied their seminal work with large photomicrographic plates of their histological slides, together with tables containing for each described region detailed morphological layer-specific information on neuronal count, neuron size and thickness of the cortical mantle. Here, we aimed to make this legacy data accessible and relatable to *in vivo* neuroimaging data by constructing a digital Von Economo – Koskinas atlas compatible with the widely used FreeSurfer software suite. In this technical note we describe the procedures used for manual segmentation of the Von Economo – Koskinas atlas onto individual T1 scans and the subsequent construction of the digital atlas. We provide the files needed to run the atlas on new FreeSurfer data, together with some simple code of how to apply the atlas to T1 scans within the FreeSurfer software suite. The digital Von Economo – Koskinas atlas is easily applicable to modern day anatomical MRI data and is made publicly available online.

Introduction

The cerebral cortex shows large variation in cytoarchitectonic organization. In the early twentieth century, building on the scientific foundation provided by preceding neuroanatomist pioneers such as Carl Hammarberg (Hammarberg, 1895), Alfred Walter Campbell (Campbell, 1905) and Korbinian Brodmann (Brodmann, 1909), Constantin von Economo and George Koskinas (Fig. 1A) worked on a detailed mapping of the cytoarchitectural anatomy of the human cerebral cortex (Von Economo and Koskinas, 1925). Their joint efforts resulted in a detailed atlas of the human cerebral cortex including, as they describe, 54 large main cortical areas (which they called “Grund Areae”), 76 smaller variants (“Varianten”) and 107 finer modification areas (“Modifikationen”) (von Economo and Koskinas, 1925). In total, Von Economo and Koskinas marked 48 cortical and 3 hippocampal regions (composed of 43 main regions and 8 variants) to be the most consistent and distinct regions of the cortex and included detailed tables in their 1925 textbook describing the cytoarchitectural characteristics of these regions; including layer-specific neuronal cell size, cell count and width of the cortical mantle.

Today, imaging techniques such as Magnetic Resonance Imaging (MRI) allow for assessment of structural brain measures in large groups of healthy subjects and patient populations *in vivo*. A wide range of different brain atlases in MRI space have been constructed, using a variety of different techniques. Well-known examples of these include the gyral based Desikan-Killiany (Desikan et al., 2006) and Automated Anatomical Labeling (AAL) (Tzourio-Mazoyer et al., 2002) atlases, the probabilistic International Consortium for Brain Mapping atlas (ICBM, (Mazziotta et al., 2001)), and the postmortem histology based JuBrain Cytoarchitectonic Atlas (Zilles and Amunts, 2010). More recently, atlases have strived to combine multiple modalities in parcellating the human cerebral cortex (Toga et al., 2006), cumulating in a multimodal brain map based on combined borders in microscale cortical architecture together with task fMRI-based feature maps, resting state connectivity, and folding patterns (Glasser et al., 2016). In spirit of these endeavors, we here make the legacy of histological morphological data (Fig. 1B) of Von Economo and Koskinas accessible – and of use – to today’s MRI scientists. The goal of this technical note is to report and make freely available a digital atlas of the Von Economo and Koskinas data in MRI space, one that is easy to use in the well-known FreeSurfer imaging processing pipeline (Fischl, 2012). Using the original atlas and the original descriptions in the accompanying 1925 textbook of Von Economo and Koskinas (Von Economo and Koskinas, 1925) we segmented the by Von Economo and Koskinas identified 48 cortical regions onto the cortical surface reconstruction of 20 T1 datasets and subsequently constructed a group-averaged digital Von Economo – Koskinas atlas suited for the FreeSurfer software

suite.

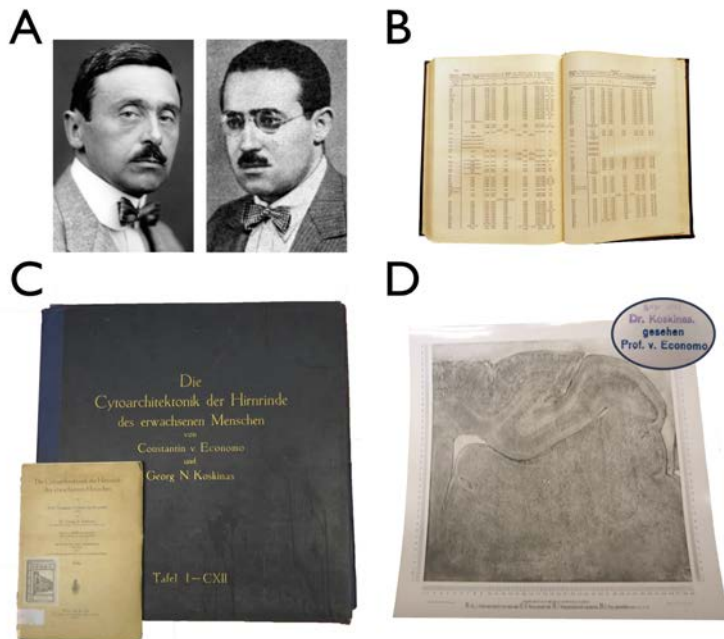


Figure 1. The 1925 Von Economo – Koskinas atlas. **(A)** Figure shows portraits of Constantin von Economo (left) and George Koskinas (right). **(B)** An example table from the 1925 accompanying textbook containing cytoarchitectonic data **(C)** The 1925 Von Economo – Koskinas atlas (von Economo and Koskinas, 1925): the folder containing 112 photomicrographs (right) and the manual to the folder (left). **(D)** A photograph of one of the original photomicrographs included in the atlas (showing a cross section of the hippocampus), with stamps of approval of Von Economo and Koskinas (inset).

In what follows we first describe the original 1925 work of Von Economo and Koskinas, followed by a description of our procedures to create a digital Von Economo – Koskinas atlas. We document our manual segmentations of the 48 cortical regions on high-resolution T1 scans, followed by the procedures we used to construct a group-averaged atlas usable in FreeSurfer. We describe easy to use exemplary code to run the atlas on FreeSurfer segmented T1 scans and conclude with a validation of the atlas usability by comparing the cortical width of areas of the cortical mantle as provided by Von Economo and Koskinas with corresponding MRI-based estimates on 400+ *in vivo* T1 scans from the Human Connectome Project. The resulting FreeSurfer Von Economo – Koskinas atlas and accompanying exemplary code are provided as Supplementary Material to this paper and are made publicly available for download online at www.dutchconnectomelab.nl/economo.

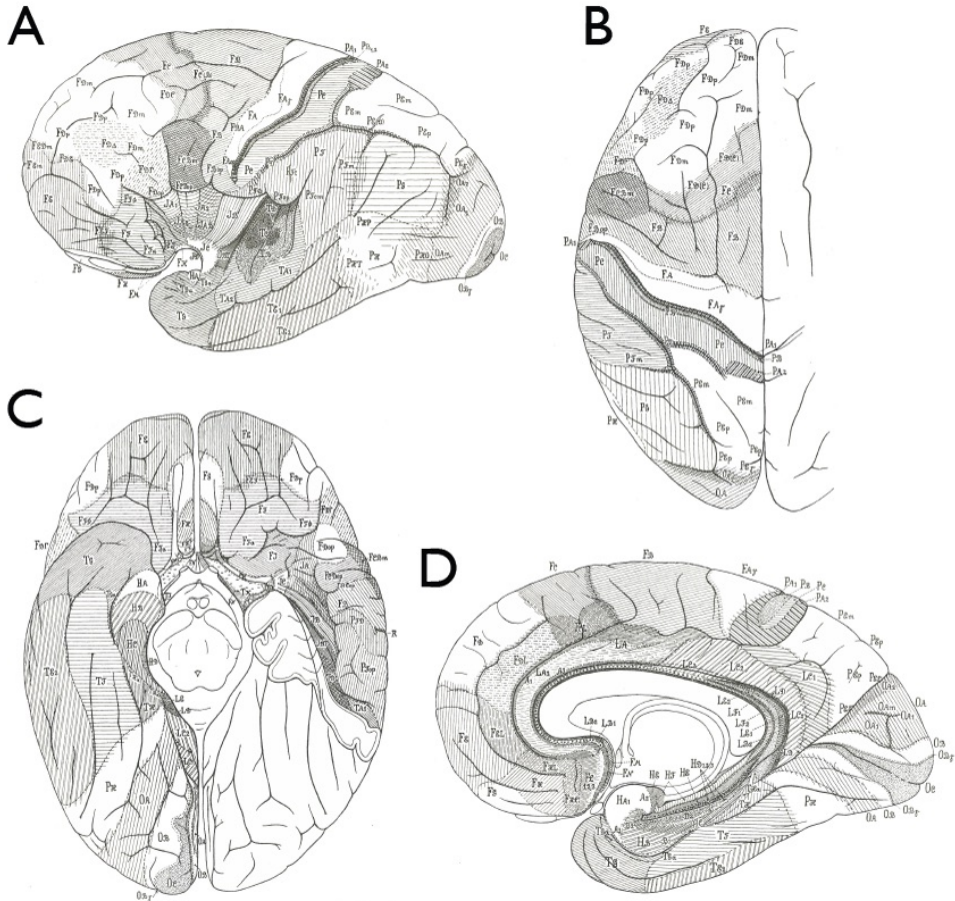


Figure 2. 1925 Von Economo – Koskinas atlas illustrations. Figure shows illustrations as included in the original 1925 Von Economo – Koskinas atlas: (A) lateral view of the cortical mapping, (B) dorsal view, (C) ventral view, (D) medial view.

Atlas segmentation procedures and validation

The 1925 Von Economo – Koskinas atlas

Constantin von Economo started his work on mapping the cytoarchitecture of the brain in 1912 and was joined in his labors in 1919 by neuroanatomist George Koskinas (Triarhou, 2005; Von Economo and Koskinas, 1925) (Fig. 1A). Their combined 1925 neuroanatomical work consisted of three volumes: 1) a textbook providing the literature background, methods and a full description of each distinct cortical area, together with tables containing detailed quantitative information of regional cytoarchitecture and layer-specific cortical thickness for the (as labeled by Von Economo

and Koskinas) 48 most important cortical regions (Fig. 1B) (the tables were recently reproduced by Karger AG in (Von Economo, 2009)) 2) a folder containing 112 panels with photomicrographic plates of size 40×40 cm of representative histological examples of each described brain area and its variants (von Economo and Koskinas, 1925) (folder with photographic plates reproduced by Karger AG, Basel (Von Economo et al., 2008)) (Fig. 1D), and 3) a manual for the folder, with a brief description of the brain mapping as well as details on the exact cortical location of each histological slice included in the folder (Fig. 1C). In their textbook, Von Economo and Koskinas provided a comprehensive description of their defined cortical areas, together with detailed illustrations showing lateral, medial, ventral and dorsal views of their constructed 1925 cortical atlas (Von Economo and Koskinas, 1925) (Fig. 2, Supplemental Fig. S1). A historical overview of the lives and work of Von Economo and Koskinas is outlined by Lazaros C. Triarhou (Triarhou, 2005, 2006).

Von Economo and Koskinas were pioneers in many aspects, setting new standards to the field. They devised a structured histological processing pipeline to precisely and with consistent quality document the cytoarchitecture of the human cerebral cortex. As they documented in their 1925 writings on their work (Fig. 1C) (Von Economo and Koskinas, 1925), they were keen on carefully standardizing and documenting each step in their multi-day process. They used photography to record all donor samples on which the locations of the later studied brain slices were noted (Von Economo and Koskinas, 1925). Furthermore, instead of making coronal or horizontal sections through the entire brain, Von Economo and Koskinas devised a new, custom method of slicing brain material, cutting blocks perpendicular to the cortical surface and gyral axis of each winding of the brain to allow the cortical thickness to be measured accurately (straight) at each location in the cortex (Von Economo and Koskinas, 1925). Each tissue block was labeled and its location marked onto the whole brain photographs. After all blocks were cut, they were all processed together in an identical fashion, resulting in identical Nissl (toluidine blue) staining quality and intensity. Next, again unique for their time and introducing a new way of documenting anatomical work, high-resolution photographs (Zeiss planar 1:4.5 F=2 cm, final magnification 100x) were taken of each of the stained sections. These plates formed the basis of their presented atlas in 1925 (Fig. 1D) (Von Economo and Koskinas, 1925).

Data demographics

Von Economo and Koskinas based their mappings on detailed analysis and observations of several healthy brain samples. As described in their 1925 writings (see Supplemental Materials for quotes of their textual description) (Von Economo and Koskinas, 1925) they only included brains of people without psychiatric abnormalities or neurological symptoms within the age range of 30 to 40 years (textbook, page 8). Furthermore, most

likely they included information on left and right hemispheres of male as well as female donors together, as they explicitly mentioned in their 1925 writings that they did not have sufficient information to draw conclusions on gender or hemispheric differences (see e.g. page 284, 309, 320 of (Von Economo and Koskinas, 1925)).

Cortical areas

Von Economo and Koskinas started out by first dividing the cortical mantle into 7 lobes (occipital, parietal, temporal, frontal, cingulate, hippocampal and insular) and then subdivided these lobes into 54 basic regions, followed by the smaller 76 variants and 107 modification areas. The basic 54 regions were grouped per lobe and for each region they provided a description in 7 subsections, including 1) Macroscopic appearance; 2) Microscopic appearance; 3) Ratios of the layers to each other; 4) Description of individual layers; 5) General overview: extent, borders and variants; 6) Historic contemplations and myelination; 7) Physiological considerations. It is on these 7 categories that they based their original mapping of the cortex into cortical regions. Region names are constructed as follows: the first letter indicates the lobe the region can be found on (for instance occipital lobe – O), followed by the second letter indicating the region number (for instance A – the first region labeled on the lobe), an optional lower caps Greek symbol indicates a smaller subregion. From these regions Von Economo and Koskinas identified 48 as the most important distinct regions of the human cortex (see for the full name and description of each region Supplemental Table S1). It was of this cortical subdivision that we set out to make a digital version usable in modern-day MRI analysis software suites.

MRI dataset

We now describe the procedures used to make a digital version of the 1925 Von Economo – Koskinas atlas usable in FreeSurfer. We started out by selecting T1 scans (3 T Philips Achieva scanner, 3D FFE using parallel imaging, TR/TE 10ms/4.6ms, 200 slices, acquisition: 0.75 mm isotropic voxel size, resliced: $1 \times 1 \times 1$ mm voxels) of $n = 20$ individuals, randomly drawn from a large group of healthy controls of previous studies of our group (van den Heuvel et al., 2012; van den Heuvel and Sporns, 2011, 2013; van den Heuvel et al., 2013). Similar to the reported set of Von Economo and Koskinas (Von Economo and Koskinas, 1925) subjects were selected to be in the age range of 30 – 40 years (mean age 33.3 years (std:3.7)) and included data from both males ($n = 11$) and females ($n = 9$). Each of the individual T1 scans was processed using the FreeSurfer software package (Fischl, 2012) (<http://freesurfer.net/>; RRID:SCR_001847, version 5.3.0), resulting in individual tissue segmentation and cortical surface reconstruction. Tissue classifications and surface reconstructions were manually checked for proper segmentation.

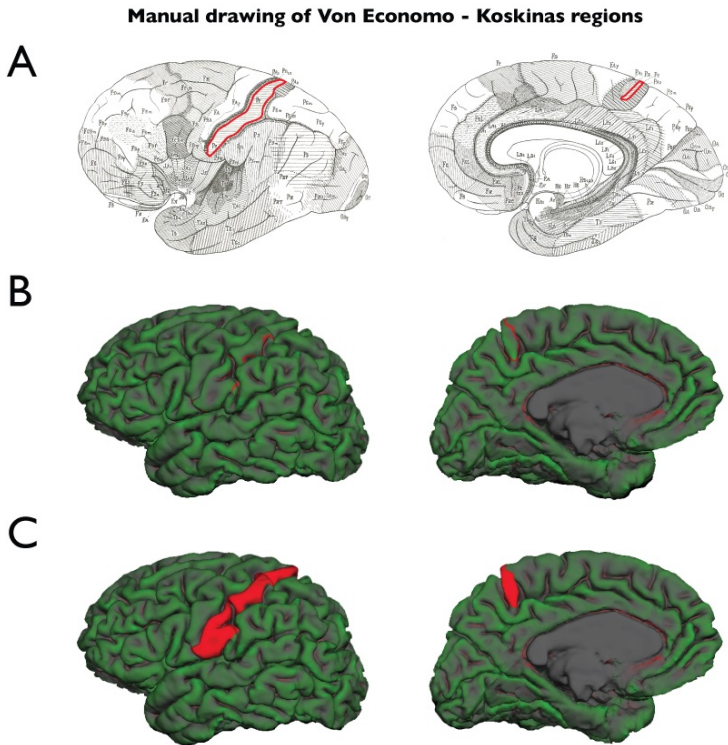


Figure 3. Drawing cortical labels. Figure illustrates the process of how we segmented a Von Economo – Koskinas region (here shown region FA) onto an exemplary cortical surface reconstruction. **(A)** Figures shows the region outlined in red on the 1925 Von Economo – Koskinas lateral and medial illustration, **(B)** the plotted outline of the region on the cortical surface reconstruction, **(C)** completed and filled-in region label. Shades of green indicate the curvature of the cortex. (For interpretation of the references to color in this figure legend, the reader is referred to the web version of this article.).

Manual segmentation of Von Economo – Koskinas areas

Next, using the tksurfer label segmentation and editing tools included in the FreeSurfer toolset (version 5.3.0), the 48 cortical regions of the 1925 Von Economo and Koskinas atlas were manually segmented onto both hemispheres of the FreeSurfer cortical surface reconstruction. The region boundaries as illustrated and described in detail in the textbook of the 1925 Von Economo – Koskinas atlas (Figs. 1, 2) were used to segment each region on the cortical rendering (Von Economo and Koskinas, 1925). First, for each region separately, we carefully plotted individual landmark points onto the surface using the saydrawing tool of tksurfer. This was followed by connecting the dots and filling the label with the “paint label tool”. The result was saved as a.label file (Fig. 3). This procedure was repeated for all regions separately. Next, after drawing all individual regions, a visual crosscheck was performed of all labels together to correct

any gaps and/or overlap between labels and to compare their position with the descriptions in the 1925 Von Economo – Koskinas atlas. Label segmentation was performed by primary researcher LHS to ensure constant segmentation quality, in close conjunction with the other authors.

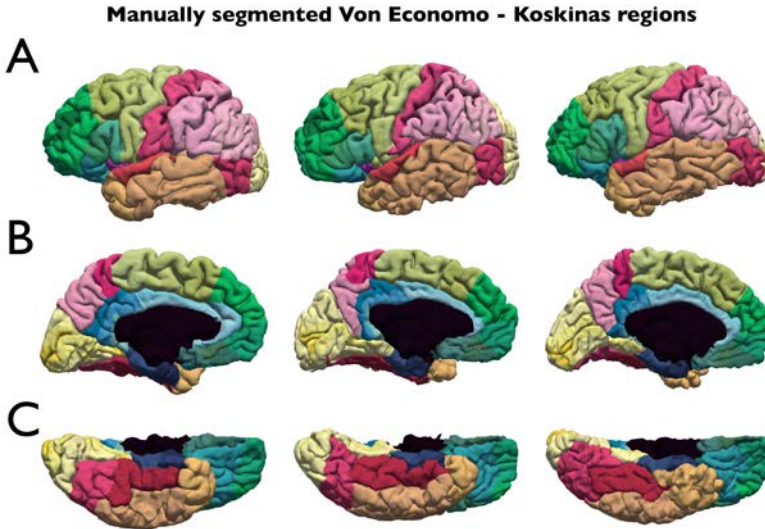


Figure 4. Manually drawn individual FreeSurfer Von Economo – Koskinas regions. Figure shows screenshots of lateral (A), medial (B) and ventral (C) aspects of the Von Economo – Koskinas regions as manually plotted onto individual FreeSurfer cortical surface reconstructions. Figure shows final segmentations of three exemplary subjects.

Three specific comments on the manual segmentations are noted. Of the 48 regions, region PB2 was described by Von Economo and Koskinas as being situated in an island-like fashion within PB1, and we therefore merged PB1 and PB2 into one region for cortical segmentation. Second, 6 small and narrow ribbon-like regions (LE1, LE2, FJ, FK, FM, FN) were hard to reliably segment onto cortical surface reconstructions (Fig. 2). These regions are predominantly situated on the outer boundary of the cortical gray matter and are generally only a few millimeters in width. We therefore merged the thin regions LE1 and LE2 into one region LE, FJ and FK into region FJK and FM and FN together with FL into region FLMN (see Supplemental Fig. S1) to ensure consistent cross-subject segmentation of all regions included in the FreeSurfer Von Economo – Koskinas atlas. In summary, this resulted in manual segmentations of in total 43 regions per hemisphere, for $n = 20$ individual datasets. Fig. 4 shows three exemplary individual segmentations. Third, the majority of the Von Economo – Koskinas regions do not occupy the entire extent of a gyrus or sulcus (with the exception of region PC, OC, TF and sulcal wall regions PA, PB and PD) and thus had at least one edge which was not delimited

by macroscale landmarks (sulci). To segment these regions, we determined the size and location of the Von Economo – Koskinas region on the FreeSurfer cortical surface reconstructions based on the relative size of that region in relation to the total size of the gyrus it occupied as presented in the visual representations of the cortical atlas provided by Von Economo and Koskinas (Von Economo and Koskinas, 1925). As such, in case a region occupied e.g. X cm on the total Y cm length of the gyrus in the 1925 atlas descriptions, the boundary was segmented on the X/Y part of the gyrus in the MRI cortical surface reconstructions. An example of this is region TE, located on the lateral and ventral surface of the temporal lobe (see atlas Fig. 2). The border of area TE with temporal pole area TG cannot be determined based on a clear macroscale landmark and was therefore drawn based on its location relative to the total (caudal to frontal) length of the temporal lobe as illustrated and described in the 1925 atlas (Fig. 3). Another example includes frontal areas FH and FG, which on the medial surface are partially separated by the sulcus rostralis superior, but more caudally have a border that diverges away from this sulcus and does not overlap with clear landmarks. After consideration of the original 1925 atlas descriptions by Von Economo and Koskinas, the location of this diversion was segmented proportionally to the full length (anterior – rostral) of the medial orbitofrontal lobe (Supplemental Fig. S2). An overview of all label borders is given in Supplemental Table S2.

Individual variation

In their 1925 textbook accompanying the photomicrographic plates, Von Economo and Koskinas reported variation in total brain volume and gyrification patterns between their studied individuals. As a result, defined cortical areas and boundaries varied from one subject to another. Meticulous as Von Economo and Koskinas were, they closely examined multiple subjects, of which they observed and described individual variation in region boundaries. To capture (to the extent possible) macroscale individual variation in gyrification patterns and accompanying architectural boundaries, the cortical atlas was manually segmented on $n = 20$ individuals (rather than a single average standardized T1 scan, as for example the Colin27 average brain (Holmes et al., 1998) in (Scholtens et al., 2015)), and the original documentation and schematic illustrations of Von Economo and Koskinas was used to map boundaries in the individual subjects (Von Economo and Koskinas, 1925). For this we used the region-specific descriptions in which Von Economo and Koskinas provided insight into the between-subject variation in gross cortical architecture they encountered in their postmortem examinations. For those regions of which they encountered large individual variation (such as the occipital pole region OC), Von Economo and Koskinas included exemplary illustrations, showing alternative folding patterns (See for examples Supplementary Fig. S3). For each individual T1 scan, LHS studied and used the original

German text to get the best matching location for each cortical region was selected in the textbook to segment the matching regions on the cortical surface reconstructions (Fig. 5).

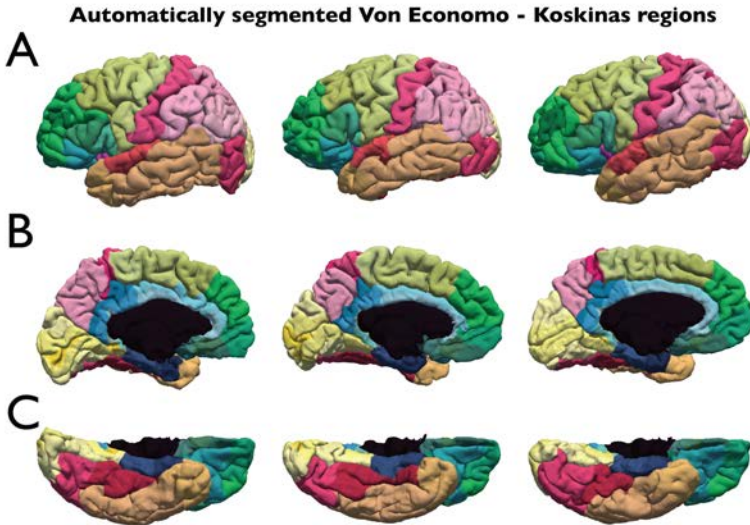


Figure 5. Automated FreeSurfer parcellation of Von Economo – Koskinas regions onto individual scans. Figure shows screenshots of lateral (A), medial (B) and ventral (C) aspects of the automatically parcellated FreeSurfer Von Economo – Koskinas atlas on cortical surface reconstructions of the HCP dataset. Figure shows 3 exemplary subjects of the 438 sets examined.

FreeSurfer Von Economo – Koskinas atlas training

After manual segmentation on each of the individual datasets, the FreeSurfer `mris_label2annot` function was used to merge each of the manually created `.label` files with a `.ctab` color table (containing a RGB color label for each of the regions) obtaining individual annotation files (`.annot` files). Next, across the group of subjects, individual `.annot` files were taken as input for the `mris_ca_train` function, training a cortical parcellation atlas file by combining geometric (curvature) information from the cortical model with the manually assigned labels from the individual `.annot` files. This resulted in a group atlas `.gcs` file.

Running the atlas on individual T1 scans

The resulting parcellation atlas is suitable for implementation in future FreeSurfer analyses to automatically assign the Von Economo – Koskinas neuroanatomical labels to cortical surface reconstructions. Running this digital atlas on a FreeSurfer dataset produces two parcellation annotation files, `lh.economo.annot` describing the atlas parcellation for the left and `rh.economo.annot` describing the atlas parcellation for the

right hemisphere. Individual.annot files can then be used in the `mris_anatomical_stats` function to extract MRI-based anatomical properties for each Von Economo – Koskinas region for both hemispheres, resulting in an output statistics data file added to the FreeSurfer stats directory describing morphological metrics of each of the automatically labeled regions. Example code to run the atlas on a FreeSurfer dataset includes:

```
DATA_DIR= # describing the directory that includes the
lh.colortable.txt, rh.colortable.txt, lh.economo.gcs,
rh.economo.gcs datafiles
SUBJECTS_DIR= # the FreeSurfer subject directory containing
FreeSurfer output
SUBJECTNAME= # FreeSurfer Subjectname

# Formation of Von Economo - Koskinas annotation files
mris_ca_label -t ${DATA_DIR}/lh.colortable.txt ${SUBJECTNAME} lh
${SUBJECTS_DIR}/ ${SUBJECTNAME}/surf/lh.sphere.reg
${DATA_DIR}/lh.economo.gcs
${SUBJECTS_DIR}/${SUBJECTNAME}/label/lh.economo.annot

mris_ca_label -t ${DATA_DIR}/rh.colortable.txt ${SUBJECTNAME} rh
${SUBJECTS_DIR}/ ${SUBJECTNAME}/surf/rh.sphere.reg
${DATA_DIR}/rh.economo.gcs
${SUBJECTS_DIR}/${SUBJECTNAME}/label/rh.economo.annot

# Create anatomical stat files
mris_anatomical_stats -a ${SUBJECTNAME}/label/lh.economo.annot -f
${SUBJECTNAME}/stats/lh.economo.stats ${SUBJECTNAME} lh
mris_anatomical_stats -a ${SUBJECTNAME}/label/rh.economo.annot -f
${SUBJECTNAME}/stats/rh.economo.stats ${SUBJECTNAME} rh
```

Segmentation consistency

We examined the consistency of the digitally segmented Von Economo – Koskinas atlas from three different perspectives: 1) manual label consistency; 2) comparison of the automated and manual segmentations; 3) between-subject atlas consistency. Furthermore, 4) we validated the digital atlas by comparing cortical thickness measurements as obtained from MRI with the histological width of the cortical mantle data as reported by Von Economo and Koskinas.

Manual label consistency

Consistency in manual label drawing was assessed by resampling each manually labeled FreeSurfer surface to the fsaverage FreeSurfer average brain (yielding a resampled to fsaverage `economo.annot` file for each individual hemisphere) and calculating the overlap in vertex label assignment between the $n = 20$ resampled individual annotation files. Across all manually labeled FreeSurfer reconstructions, the vertex-wise label consistency was 74.6% (std 2.9%).

Comparison of automated and manual segmentations

To quantify the consistency of the automated Von Economo – Koskinas parcellation with the ground truth of the manually segmented atlas files, we implemented a sliding window approach, building the atlas on 19 of the 20 T1 scans included in the manually drawn training set and applying it to the remaining scan. Then, for every individual scan in the training set, we calculated the overlap between the label assignment of all vertices in the surface reconstruction of the automatic parcellation and the manual segmentation. Comparing the automatic and manual segmentations yielded an atlas-wide average vertex label consistency of 78.7% (std 2.5%), with average consistency varying between labels from 50.4 to 93.7%. With substantial variation in both label size (ranging from on average 65 to 12063 vertices) and shape (from large and almost square to a narrow ribbon shape), we further investigated the influence of both factors on the observed label consistency. We hypothesized that an individual label's consistency score is affected by both its size (a large label will have a larger portion of its vertices in its center, with a very low chance of switching label affiliation), as well as its shape (an oblong label has more border vertices and thus more opportunity to switch labels). Implementing a generalized linear model with each label's fraction of edge vertices (number of edge vertices/total vertex count) as a predictor and the manual-automatic segmentation consistency as an outcome variable shows this edge vertex fraction to explain 56% of the variance in the segmentation consistency outcome variable. Leaving out the top 10% most elongated regions resulted in an automated – manual vertex label consistency of 82.3%.

Across-subject atlas consistency

Consistency of the automatic parcellation atlas across subjects was computed by resampling the datasets in the HCP validation dataset ($N = 511$) to the fsaverage FreeSurfer average brain, mapping each vertex and its label to its corresponding fsaverage vertex (yielding a resampled to fsaverage `economo.annot` file for each hemisphere), which enabled vertex-wise comparison between the automated atlas parcellation of the individual HCP validation scans. The average overlap between vertex labels across all subjects was computed, resulting in an across subject consistency of 92.9% (std 1.14%). Similar to the comparison with the manual ground truth, label consistency varied from 56.1 to 98.0% (std 9.1%), with those labels with the largest

proportion of edge vertices (the smallest and thinnest regions) showing the largest variability.

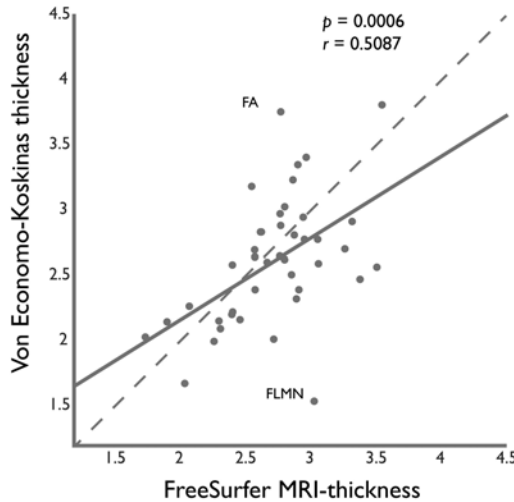


Figure 6. MRI – Histology cortical thickness comparison. Region-wise correlation between Von Economo – Koskinas histological measurements of width of the cortical mantle (*y*-axis) and MRI based cortical thickness (*x*-axis) derived using the FreeSurfer Von Economo – Koskinas atlas.

Atlas verification using histological data

We validated the new MRI atlas by comparing MRI based estimates of cortical thickness with the original reports of width of the cortical mantle as reported by Von Economo and Koskinas (von Economo and Koskinas, 1925). For this, we analyzed 438 high-resolution T1- weighted datasets of the Human Connectome Project (S500 release, voxel-size 0.7 mm isotropic, age-range 22–35 years) using the FreeSurfer package (Fischl, 2012) for automatic tissue classification and subsequent 3D cortical surface reconstruction. The FreeSurfer Von Economo – Koskinas atlas was applied to these datasets, subdividing both hemispheres into 43 unique cortical regions using the lines of code described above. T1-based cortical thickness estimates of the 43 cortical areas were obtained from the FreeSurfer stats files. The resulting individual regional MRI cortical thickness estimates were then averaged across both hemispheres as the investigations of Von Economo and Koskinas most likely contained data encompassing both hemispheres (at least no clear description is made of which hemisphere was examined in which donor brain (Von Economo and Koskinas, 1925)). Values were averaged across all subjects, which yielded 43 group-averaged regional cortical thickness values. Region HA was excluded from this comparison. Although HA is described as being partially of cortical composition (containing the most upper part of the parahippocampal gyrus) and was thus included in the FreeSurfer Von Economo –

Koskinas atlas, the largest portion of this region is hippocampal (uncus and Ammon's horn), which is labeled as subcortical in the FreeSurfer suite and therefore cannot be used for cortical thickness measurements. Pearson correlation analysis between MRI and histology derived metrics of cortical thickness revealed a high correlation (Fig. 6; $p = .0006$, $r = .5087$). In line with our earlier observations (Scholtens et al., 2015) MRI-based measurements of cortical thickness of primary motor cortex (region FA) showed a clear underestimation compared to the histological data (2.7 vs 3.7 mm thickness), likely related to the described strong myelination of infragranular layers of FA (Von Economo and Koskinas, 1925) and a related undifferentiated border with the underlying white matter (Han et al., 2006). In addition, the narrow and difficult to segment Von Economo – Koskinas regions FM and FN showed a clear overestimation of their MRI thickness compared to histological width of the cortical mantle. Excluding these outliers from our comparison resulted in a stronger correlation between the two modalities in measurements of cortical thickness ($p < .0001$, $r = .6282$).

Conclusion

We present a digital Von Economo – Koskinas atlas usable in the popular FreeSurfer suite. The atlas is accompanied by exemplary code and acquired FreeSurfer data files to be easily applied on new individual T1 scans, allowing for a subdivision of the cortical mantle according to the cytoarchitectonic regions defined by Von Economo and Koskinas. When using the atlas the following points should be considered.

First, the cortical mapping presented in the original 1925 Von Economo – Koskinas atlas is based on differences in cytoarchitectonic organization between cortical regions, with individual cytoarchitectonic information combined into a more general cortical mapping based on combined region localization (Von Economo and Koskinas, 1925). The final 1925 Economo – Koskinas atlas does therefore not reflect any inter-individual variability, and since it is represented on a single hemisphere does not convey any information on interhemispheric variation. It is this averaged atlas that we aimed to project to MRI-space. Second, the implementation of our FreeSurfer Von Economo – Koskinas atlas is based on a manual drawing onto cortical surface reconstructions of in vivo measured T1 scans, and thus does not – similar to other MRI atlases – incorporate any information on the cytoarchitecture of the individual in vivo scanned brains on which it is applied.

Adding to previous publications that brought cytoarchitectonic atlases into stereotaxic space (such as the atlas describing the Von Economo – Koskinas parietal lobe (Caspers et al., 2008, 2006)), the here presented MRI Von Economo – Koskinas atlas does not only cover the entire cortical surface, like the well-known mapping of the Brodmann

atlas (Brodmann, 1909) by (Talairach and Tournoux, 1988), but also provides an opportunity to directly relate the mapped regions back to the morphological data on which the mapping was based (information which is not accessible for the Brodmann atlas). Most importantly, different from for example the atlas of Brodmann (Brodmann, 1909), Von Economo and Koskinas meticulously reported rich details on the cytoarchitecture of all regions on which they based their atlas, reporting on layer specific information on cell density, cell size and layer width. This data as recently reproduced and documented by LC Triarhou in (Von Economo, 2009) can be applied to modern-day neuroimaging studies in a variety of ways. Implementations include comparisons of MRI-based and histological cortical thickness (as in (Scholtens et al., 2015) and briefly shown here), or relating (functional) connectivity profiles to cytoarchitectonic features such as layer-wise neuron size (van den Heuvel et al., 2015) or cortical type (Wylie et al., 2015). Our hope is that implementation of the FreeSurfer Von Economo – Koskinas atlas into existing MR processing pipelines will facilitate further incorporation of healthy cytoarchitectonic data into imaging studies.

The atlas is presented as Supplemental material, will be made publicly available online at www.dutchconnectomelab.nl/economo and is free to use under a Creative Commons Attribution-NonCommercial-ShareAlike 4.0 International License.

Acknowledgments

This work was supported by the Netherlands Organization for Scientific Research VIDI grant (MPvdH, VIDI-452-16-015).

References

- Brodmann K (1909) *Vergleichende Lokalisationslehre der Grosshirnrinde in ihren Prinzipien dargestellt auf Grund des Zellenbaues* Barth.
- Campbell AW (1905) *Histological studies on the localisation of cerebral function* University Press.
- Caspers S, Eickhoff SB, Geyer S, Scheperjans F, Mohlberg H, Zilles K, Amunts K (2008) The human inferior parietal lobule in stereotaxic space. *Brain Struct Funct* 212:481–95.
- Caspers S, Geyer S, Schleicher A, Mohlberg H, Amunts K, Zilles K (2006) The human inferior parietal cortex: cytoarchitectonic parcellation and interindividual variability. *Neuroimage* 33:430–48.
- Desikan RS, Segonne F, Fischl B, Quinn BT, Dickerson BC, Blacker D, Buckner RL, Dale AM, Maguire RP, Hyman BT, Albert MS, Killiany RJ (2006) An automated labeling system for subdividing the human cerebral cortex on mri scans into gyral based regions of interest. *Neuroimage* 31:968–80.
- Fischl B (2012) Freesurfer. *NeuroImage* 62:774–781.
- Glasser MF, Coalson TS, Robinson EC, Hacker CD, Harwell J, Yacoub E, Ugurbil K, Andersson J, Beckmann CF, Jenkinson M, Smith SM, Van Essen DC (2016) A multi-modal parcellation of human cerebral cortex. *Nature* .
- Hammarberg C (1895) *Studien über Klinik und Pathologie der Idiotie, nebst untersuchungen über die normale Anatomie der Hirnrinde* Druck der Edv. Berling.
- Han X, Jovicich J, Salat D, van der Kouwe A, Quinn B, Czanner S, Busa E, Pacheco J, Albert M, Killiany R, Maguire P, Rosas D, Makris N, Dale A, Dickerson B, Fischl B (2006) Reliability of mri-derived measurements of human cerebral cortical thickness: the effects of field strength, scanner upgrade and manufacturer. *Neuroimage* 32:180–94.
- Holmes CJ, Hoge R, Collins L, Woods R, Toga AW, Evans AC (1998) Enhancement of mr images using registration for signal averaging. *Journal of computer assisted tomography* 22:324–333.
- Mazziotta J, Toga A, Evans A, Fox P, Lancaster J, Zilles K, Woods R, Paus T, Simpson G, Pike B, Holmes C, Collins L, Thompson P, MacDonald D, Iacoboni M, Schormann T, Amunts K, Palomero-Gallagher N, Geyer S, Parsons L, Narr K, Kabani N, Le Goualher G, Feidler J, Smith K, Boomsma D, Pol HH, Cannon T, Kawashima R, Mazoyer B (2001) A four-dimensional probabilistic atlas of the human brain. *Journal of the American Medical Informatics Association : JAMIA* 8:401–430.
- Scholtens LH, de Reus MA, van den Heuvel MP (2015) Linking contemporary high resolution magnetic resonance imaging to the von economo legacy: A study on the comparison of mri cortical thickness and histological measurements of cortical structure. *Human Brain*

- Mapping* 36:3038–3046.
- Talairach J, Tournoux P (1988) *Co-planar stereotaxic atlas of the human brain. 3-Dimensional proportional system: an approach to cerebral imaging* Thieme, New York.
- Toga AW, Thompson PM, Mori S, Amunts K, Zilles K (2006) Towards multimodal atlases of the human brain. *Nature Reviews Neuroscience* 7:952–966.
- Triarhou LC (2005) Georg n. koskinas (1885-1975) and his scientific contributions to the normal and pathological anatomy of the human brain. *Brain Res Bull* 68:121–39.
- Triarhou LC (2006) The signalling contributions of constantin von economo to basic, clinical and evolutionary neuroscience. *Brain Research Bulletin* 69:223–243.
- Tzourio-Mazoyer N, Landeau B, Papathanassiou D, Crivello F, Etard O, Delcroix N, Mazoyer B, Joliot M (2002) Automated anatomical labeling of activations in spm using a macroscopic anatomical parcellation of the mni mri single-subject brain. *Neuroimage* 15:273–89.
- van den Heuvel MP, Kahn RS, Goñi J, Sporns O (2012) High-cost, high-capacity backbone for global brain communication. *Proceedings of the National Academy of Sciences of the United States of America* 109:11372–11377.
- van den Heuvel MP, Scholtens LH, Feldman Barrett L, Hilgetag CC, de Reus MA (2015) Bridging cytoarchitectonics and connectomics in human cerebral cortex. *The Journal of Neuroscience* 35:13943–13948.
- van den Heuvel MP, Sporns O (2011) Rich-club organization of the human connectome. *The Journal of neuroscience : the official journal of the Society for Neuroscience* 31:15775–86.
- van den Heuvel MP, Sporns O (2013) An anatomical substrate for integration among functional networks in human cortex. *The Journal of neuroscience : the official journal of the Society for Neuroscience* 33:14489–500.
- van den Heuvel MP, Sporns O, Collin G, Scheewe T, Mandl RCW, Cahn W, Goñi J, Hulshoff Pol HE, Kahn RS (2013) Abnormal rich club organization and functional brain dynamics in schizophrenia. *JAMA psychiatry (Chicago, Ill.)* 70:783–92.
- Von Economo C (2009) *Cellular structure of the human cerebral cortex* Karger Medical and Scientific Publishers, Basel.
- Von Economo CF, Koskinas GN (1925) *Die Cytoarchitektonik der Hirnrinde des erwachsenen Menschen* J. Springer.
- Von Economo CF, Koskinas GN, Triarhou LC (2008) *Atlas of cytoarchitectonics of the adult human cerebral cortex* Karger Basel.

Wylie KP, Kronberg E, Maharajh K, Smucny J, Cornier MA, Tregellas JR (2015) Between-network connectivity occurs in brain regions lacking layer iv input. *NeuroImage* 116:50–58.

Zilles K, Amunts K (2010) Centenary of brodmann’s map—conception and fate. *Nature reviews. Neuroscience* 11:139–45.

Supplemental Information

of

A FreeSurfer MRI Von Economo – Koskinas Atlas

Supplemental Methods

Data demographics

Von Economo and Koskinas based their mappings on detailed analysis and observations of several healthy brain samples. In their 1925 writings, they state (page 8 (Von Economo and Koskinas, 1925)):

“Wir haben natürlich von vornherein immer bloß Gehirne von Personen in den Kreis unserer Untersuchungen gezogen, welche von jeder geistigen Abnormität frei waren und überhaupt keine Symptome von selten des Nervensystems geboten hatten”,

which in English translates to: “We have of course from the beginning only included brains in our research of people who were without psychiatric abnormalities and displayed no neurological symptoms”.

They do not explicitly mention the number of specimens included in their research, but about the quantitative regional morphological data presented they state (page 34): “Das Bild stellt ein Durchschnittsresultats vieler Rindenmessungen an zahlreichen Gehirnen schematisch dar, welche wir immer an homologen Stellen der Hemisphären vorgenommen haben.” [“The illustration shows the average result of many cortical measurements done at homologous locations in hemispheres of numerous brains.”]

Although Von Economo and Koskinas further do not specifically mention the exact age of the subjects included in their study, they selected their subjects within the age range of 30–40 years, writing (page 41): “Nochmals möchten wir hier erwähnen, daß sich alle unsere Befunde auf Gehirne Erwachsener, im 4. Lebensdezennium stehender Personen beziehen.” [“We would like to again mention that all our results are from adult brains of individuals in their 4th decade of life.”]

Furthermore, as they mention that they did not have sufficient information to draw conclusions on gender or hemispheric differences, it is highly likely that they included information on left and right hemispheres of male as well as female donors (page 284):

“nur eines möchten wir hier speziell erwähnen, daß wir betreffs der Unterschiede, die BETZ zwischen rechts und links an den Hemisphären gemacht hat, sowie zwischen männlichen und

weiblichen Gehirnen, keine die betreffenden Aussprüche dieses Autors bestätigenden Resultate erhalten haben; vielleicht war es ein Zufall, daß gerade die weiblichen Gehirne, die ich untersucht habe, vielfach eine schönere Ausbildung betreffs Größe sowohl als Form der Pyramidenzellen aufgewiesen haben als die männlichen.”

[“We would like to specially mention that regarding the differences BETZ [Vladimir Betz (1834-1894), pioneering neuroanatomist after whom the giant pyramidal cells in the primary motor cortex were named (Betz, 1874)] found between the right and left hemisphere, as well as between male and female brains, we have not been able to confirm any of his statements; maybe was it a coincidence that precisely those female brains that I examined frequently had a more beautiful formation regarding size and shape of the pyramidal cells than the male brains.”]

Supplemental Tables

Von Economo – Koskinas abbreviation	Full region name
FA	Area praecentralis
FB	Area frontalis agranularis
FC	Area frontalis intermedia
FCBm	Area (frontalis intermedio agranularis magnocellularis in) Broca
FD	Area frontalis granularis
FDdelta	Area frontalis granularis media
FDT	Area frontalis granularis triangularis
FE	Area frontopolaris
FF	Area orbitalis (granularis)
FG	Area gyri recti (Ar. recta)
FH	Area praefrontalis
FJK	Area frontoinsularis + Area piriformis frontalis
FLMN	Area parolfactoria + Area geniculata + Area praecommissuralis
HA	Area uncinata
HB	Area parauncinata
HC	Area rhinalis limitans
IA	Area insulae praecentralis
IB	Area insulae postcentralis
LA1	Area limbicus anterior agranularis - praecingularis
LA2	Area limbicus anterior agranularis - cingularis anterior
LC1	Area cingularis posterior dorsalis
LC2	Area cingularis posterior ventralis
LC3	Area cingularis limitans posterior
LD	Area retrosplenialis agranularis
LE	Area retrosplenialis granulosa
OA	Area peristriata
OB	Area parastriata
OC	Area striata (granulosa)
PA	Area postcentralis gigantopyrimidalis + Area postparacentralis gigantopyrimidalis
PB	Area postcentralis oralis simplex + Area postcentralis oralis granulosa
PC	Area postcentralis intermedia
PD	Area postcentralis caudalis
PE	Area parietalis superior
PF	Area supramarginalis
PG	Area angularis
PH	Area parietalis (temporo-occipital) basalis
TA	Area temporalis superior
TB	Area supratemporalis magnocellularis simplex
TC	Area supratemporalis granulosa
TD	Area supratemporalis intercalata
TE	Area temporalis propria
TF	Area fusiformis
TG	Area temporoporalis

Table S1. List of abbreviations and region names. The table details the region names included in the FreeSurfer Von Economo – Koskinas atlas in the left column, and their precise region description in the right column. For each short region name, the first letter indicates the cerebral lobe the region belongs to (F-frontal, H-hippocampal, I-insular, L-limbic, O-occipital, P-parietal, T-temporal).

Von Economo – Koskinas abbreviation	Region border description
FA	<p>Laterally this region covers most of the precentral gyrus, its anterior border overlaps with the precentral sulcus and its the inferior end continues further down to the Sylvian fissure. The posterior region border is formed by the central sulcus, the inferior border by the sulcus subcentralis. On the medial aspect of the hemisphere the anterior region border is formed by the paracentral sulcus, with the inferior border at the sulcus callosomarginalis. The posterior border on the medial side runs through the fossa paracentralis.</p>
FB	<p>On the lateral aspect of the brain, the anterior border of this region has been drawn in a straight line up from the sulcus frontalis inferior (starting at the level of the sulcus diagonalis operculi) to the dorsal aspect of the hemisphere and from there down on the medial side to the first branching of the sulcus callosomarginalis. The inferior border is defined by the Sylvian fissure. Posteriorly (on the lateral aspect of the hemisphere), the region is bordered by the precentral sulcus, medially the border runs along the paracentral sulcus until it reaches the sulcus callosomarginalis.</p>
FC	<p>The anterior border of this region is drawn as a line going up from the sulcus frontalis inferior along the anterior end of the sulcus frontalis medius to the dorsal aspect of the hemisphere. From there the same line continues down to the sulcus intralimbicus, passing the posterior branches of the sulcus callosomarginalis on its way. The posterior border of this region has been drawn as a line starting at the sulcus frontalis inferior just above the sulcus diagonalis operculi going up to the dorsal aspect of the hemisphere and from there down on the medial side to the first branching of the sulcus callosomarginalis.</p>
FCBm	<p>This region covers the pars opercularis, bordered on two sides by the Sylvian fissure and its vertical ramus. The other two borders are formed by the inferior branch of the precentral sulcus and the sulcus frontalis inferior.</p>
FD	<p>This region spans a large portion of the frontal lobe. Laterally, its posterior border is formed by a line drawn up from the sulcus frontalis inferior along the anterior end of the sulcus frontalis medius to the dorsal aspect of the hemisphere. From there the same line continues down to the sulcus intralimbicus, passing the posterior branches of the sulcus callosomarginalis on its way. Starting on the medial surface of the hemisphere, its inferior border is drawn as a straight line spanning medially from the most anterior point of the cingulate gyrus to the end of the sulcus orbitalis lateralis on the lateral surface. The posterior border on the lateral surface is formed by the sulcus frontalis inferior and by a line connecting the two ends of the ramus verticalis and horizontalis Sylvii. The final border on the medial aspect is defined as the sulcus intralimbicus.</p>
FDdelta	<p>The borders of this region are ambiguous. The region has been taken to be on the center of the medial frontal sulcus.</p>
FDT	<p>This region covers the gyrus triangularis. It is delineated on three sides by the Sylvian fissure and its ramus verticalis and horizontalis. The fourth border is formed by a line drawn between the ends of both rami.</p>
FE	<p>This region covers the pole of the frontal lobe, on the lateral as well as the ventral and medial sides of the hemisphere. On the ventral surface the posterior border of this region runs from the junction of the sulcus orbitalis lateralis and transversalis to the anterior tip of the gyrus rectus. Medially, the inferior border is drawn from the anterior tip of the gyrus rectus to the most inferior point of the cingulate cortex and the superior border is drawn as a straight line spanning medially from the most anterior point of the cingulate gyrus to the end of the sulcus orbitalis lateralis on the lateral surface. Laterally, the inferior border of the region runs from the anterior tip of the gyrus rectus to the end of the ramus horizontalis fissurae Sylvii.</p>

Table S2. Border definitions of the Von Economo – Koskinas regions included in the digitized atlas. The definitions used to describe the gyri and sulci have been derived from the nomenclature as used by Von Economo and Koskinas in their atlas description (von Economo and Koskinas, 1925).

Von Economo – Koskinas abbreviation	Region border description
FF	<p>This region occupies a large part of the ventral surface of the frontal lobe and extends from the sulcus olfactorius on the ventral aspect up to the lateral aspect until it reaches the ramus horizontalis fissurae Sylvii. On the ventral aspect its anterior border is drawn as a line spanning from the junction of the sulcus orbitalis lateralis and transversalis to the anterior tip of the gyrus rectus, its posterior border is formed by the margo anterior. On the lateral surface of the hemisphere its anterior border is drawn up from the anterior tip of the gyrus rectus to the end of the ramus horizontalis fissurae Sylvii.</p>
FG	<p>Situated on the anterior ? of the gyrus rectus, the posterior border of this region is drawn as a line perpendicular to the axis of the gyrus rectus. Medially the region extends from the gyrus rectus onto the orbitofrontal cortex, up to the sulcus rostralis superior.</p>
FH	<p>Located on the medial and ventral aspect of the frontal lobe, the anterior border of this region is drawn as a straight line from the cingulate sulcus to the most anterosuperior point of region FG and from there follows the sulcus rostralis superior; at 1/3 of the distance to the edge of the cortical mantle the line diverges diagonally to the ventral aspect of the gyrus rectus, where it continues in a straight line across the gyrus rectus (at 1/2 of the length of the gyrus) to the sulcus olfactorius. Its posterior border is drawn as a line perpendicular to the axis of the gyrus rectus at 5/6 of the rostro-caudal length of the gyrus. Superiorly the region is bordered by the cingulate sulcus, inferiorly by the sulcus olfactorius.</p>
FJK	<p>This region is situated in the fold between the insular cortex and the edge of the frontal cortex.</p>
FLMN	<p>This region is located on the most caudoinferior edge of the frontal cortex. The extend of this region runs from the cingulate culcus to by the edge of the gyrus rectus and the edge of the orbitofrontal gyrus. The region occupies the most caudal 5/6th of the gyrus rectus and its border on the medial aspect of the hemisphere is formed by the sulcus olfactorius.</p>
HA	<p>This region occupies the uncus of the hippocampal gyrus and has been segmented to occupy the thickest portion of the anterior part of the hippocampal gyrus. Superiorly this region is delineated by the sulcus hippocampi. The inferior border is drawn from the most posterior edge of the uncus in a diagonal line (in anterior direction) to the fissura rhinalis.</p>
HB	<p>Located on the hippocampal gyrus, the anterior border of this region is drawn from the most posterior edge of the uncus in a diagonal line anteriorly to the fissura rhinalis. Posteriorly, the border is drawn from the most posterior edge of the uncus in a straight line down to the fissura rhinalis. Superiorly, the border is defined as the sulcus hippocampi, inferiorly as the fissura rhinalis.</p>
HC	<p>Situated on the hippocampal gyrus, the anterior border of this region was drawn from the most posterior edge of the uncus in a straight line down to the fissura rhinalis. Posteriorly, the region is delimited by the edge of the hippocampal gyrus, taken as the point where the "truncus fissurae parietooccipitalis et calcarinae" ends. Superiorly, the border is defined as the sulcus hippocampi, inferiorly as the fissura rhinalis.</p>
IA	<p>Located on the anterior part of the insular gyrus, the anterior border of this region is formed by the sulcus brevis primus insulae, while the posterior border is formed by the sulcus centralis insulae. All other borders are defined as the edge of the insular gyrus.</p>
IB	<p>Located on the posterior part of the insular gyrus, the anterior border of this region is formed by the sulcus centralis insulae. All other borders are defined as the edge of the insular gyrus.</p>

Table S2 – continued.

Von Economo – Koskinas abbreviation	Region border description
LA1	<p>Situated on the upper anterior portion of the cingulate cortex, the posterior border of this region is formed by a line drawn just anterior of the paracentral sulcus, diagonally (in anterior direction) to the sulcus corporis callosi. The superior border is most anteriorly (up to the gyrus frontolimbicus anterior) defined as the sulcus intralimbicus, from there the border coincides with the sulcus callosomarginalis. The inferior border of this region is formed by a line drawn at 1/5 of the width of the cingulate gyrus removed from the superior border; dividing the anterior cingulate cortex into two elongated ribbons.</p>
LA2	<p>Situated on the lower half of the anterior portion of the cingulate cortex. Its posterior border is formed by the a line drawn just anterior of the paracentral sulcus, diagonally (in anterior direction) to the sulcus corporis callosi. Its superior border is a line drawn a distance of 1/5 of the width of the anterior cingulate gyrus away from the sulcus intralimbicus and de sulcus callosomarginalis; dividing the anterior cingulate cortex into two elongated ribbons. The inferior border is the sulcus corporis callosi.</p>
LC1	<p>Situated on the caudal portion of the cingulate cortex and part of the medial superior parietal cortex. The anterior border of this region is formed by the ramus verticalis sulci callosomarginalis. Posteriorly, the region is bordered by the fissura parietooccipitalis. The superior border of this region is drawn as a curved line drawn in anterior direction from the most superior point of the sulcus subparietalis to the start of the ramus verticalis sulci callosomarginalis and in posterior direction to the fissura parietooccipitalis at the level of the anterior end of the sulcus sagittalis cunei inferior. The region's superior border was traced from the sulcus callosomarginalis at the level of the Fossa paracentralis in a curved line to the anterior tip of the sulcus subparietalis and from there to a point just below the posterior tip of the sulcus subparietalis, after which it continues to the "truncus fissurae parietooccipitalis et calcarinae".</p>
LC2	<p>This region is situated on the caudal portion of the limbic lobe. Its anterior border divides the cingulate cortex just anterior of the paracentral sulcus, diagonally (in anterior direction) to the sulcus corporis callosi. Its posterior border is formed by the truncus fissurae parietooccipitalis et calcarinae. The region's superior border is less obvious, it was traced from the sulcus callosomarginalis at the height of the Fossa paracentralis in a curved line to the anterior tip of the sulcus subparietalis and from there to a point just below the posterior tip of the sulcus subparietalis, after which it continues to the "truncus fissurae parietooccipitalis et calcarinae". The inferior border is for the most anterior portion of the region formed by the sulcus corporis callosi. More posteriorly the border diverges away from the sulcus corporis callosi towards the truncus fissurae parietooccipitalis et calcarinae.</p>
LC3	<p>This small region occupies a portion of the gyrus intralimbicus and a small edge of the limbic gyrus, bordered anteriorly at the same height as region LC2 and posteriorly at the height of the fossa paracentralis.</p>
LD	<p>Occupies the edge between the limbic gyrus and the intralimbic gyrus, starting at the height of the fossa paracentralis and ending at the truncus fissurae parietooccipitalis et calcarinae.</p>
LE	<p>Occupies the intralimbic gyrus starting at the height of the fossa paracentralis up to the posterior edge of the hippocampal gyrus.</p>
OA	<p>Anteriorly on the lateral surface this region is bordered by a line starting at the intersection between the sulcus occipitalis primus and the sulcus parietalis transversus. From this intersection the line goes down towards the ventral surface just posterior of the Incisura praeoccipitalis and continues on the medial side parallel to the calcarine sulcus to the truncus fissurae parietooccipitalis et calcarinae. Laterally, up from the aforementioned intersection, the line goes to the fissura parietooccipitalis on the superior aspect of the hemisphere and follows this fissure to the medial side. The posterior border on the lateral surface is placed parallel and just anterior of the sulcus lunatus. On the medial aspect, one line descends from the superior surface and follows the sulcus sagittalis cunei inferior until it reaches the fissura parietooccipitalis. The second border line ascends from the ventral surface and runs parallel to the calcarine sulcus, intersecting with the anterior branch point of the sulcus lingualis.</p>

Table S2 – continued.

Von Economo – Koskinas abbreviation	Region border description
OB	Laterally occupies the zone from the edge of the occipital pole up to just anterior of the sulcus lunatus. Medially lies between the lip of the calcarine sulcus and region OA.
OC	This region occupies the walls and lip of the calcarine sulcus, as well as the occipital pole.
PA	Laterally occupies the anterior wall of the central sulcus, medially extends out from the central sulcus onto the paracentral lobule with its anterior boundary running through the fossa paracentralis. Its inferior border is defined by the sulcus callosomarginalis, ventrally it follows the ramus verticalis of the sulcus callosomarginalis back up to the dorsal aspect, where it covers a small portion of the postcentral gyrus up to the end of the sulcus postcentralis superior.
PB	This region lies on the posterior wall of the central sulcus and extends out halfway onto the paracentral lobule.
PC	Laterally this region covers the postcentral gyrus, except for the parietal operculum, medially it extends onto the paracentral lobule, where it covers a narrow strip 1/4th of the width of the lobule and 2/3 of the height.
PD	Is situated in the sulcus postcentralis and its branches.
PE	Laterally this region spans from a line connecting the sulcus postcentralis superior and the ramus verticalis of the sulcus callosomarginalis to a line between the sulcus parietalis transversus and the fissura parietooccipitalis. Its ventral border is formed by the edge of the sulcus interparietalis. Medially, it is located between the ramus verticalis of the sulcus callosomarginalis and the fissura parietooccipitalis, with its ventral border drawn as a curved line starting at the beginning of the ramus verticalis sulci callosomarginalis running posteriorly along the most superior point of the sulcus subparietalis down to the fissura parietooccipitalis at the height of the anterior end of the sulcus sagittalis cunei inferior.
PF	Covers the gyrus supramarginalis, including the parietal operculum and the operculum Rolando. Its superior border is formed by the sulcus postcentralis inferior and the interparietal sulcus. The posterior border extends from the sulcus intermedius down to the inferior end of the caudal branch of the sulcus temporalis superior, from where the inferior border of the region runs to the ramus posterior fissurae Sylvii.
PG	Lies on the angular gyrus, with its anterior border formed by a line extending from the sulcus intermedius down to the end of the caudal branch of the sulcus temporalis, from where its inferior border extends to the sulcus occipitalis secundus lateralis at the height of the inferior end of the sulcus occipitalis lateralis primus. Its posterior border is formed by the sulcus occipitalis lateralis primus and the interparietal sulcus.
PH	Described as the basal portion of the parietal lobe, laterally the anterior border of this region is formed by a line stretching from the caudal branch of the superior temporal sulcus to the beginning of the main superior temporal sulcus, connecting down along the posterior end of the inferior temporal sulcus where it continues onto the ventral portion of the temporal lobe. There region PH runs all the way to the truncus fissurae parietooccipitalis et calcarinae on the medial side parallel to region OA, covering a strip of the most posterior section (1/5) of the fusiform gyrus and gyrus retrolimbicus (1/4).
TA	Covers part of the dorsal and lateral aspect of the superior temporal lobe, with its border starting at the ramus posterior fissurae Sylvii, running to the superior temporal sulcus which it follows for 1/3 of the length of the temporal lobe. There the border extends upwards to the Margo posterior sulci circularis insulae. The center of this region is occupied by smaller regions TB, TC and TD.
TB	Lies within region TA, only on the dorsal aspect of the superior temporal lobe. Its outer border is drawn such that region TB is not visible on the lateral view of the hemisphere. This region covers 2/3 of the dorsal superior temporal gyrus delineated by region TA. Region TC and TD are situated within TB.

Table S2 – continued.

Von Economo – Koskinas abbreviation	Region border description
TC	Is drawn to cover the middle 1/3 of region TB, it lies flush with the margo posterior sulci circularis insulae and leaves 1/5 of the most posterior surface of TB open for region TD.
TD	Is situated on the most posterior part of the dorsal surface of the superior temporal gyrus, just below the parietal operculum. Posterior-anterior it extends about 1/5 of the length of TB from the parietal operculum.
TE	The largest temporal region. Laterally this region covers the posterior part (1/3) of the superior temporal gyrus and the posterior 2/3rd of the middle and inferior temporal gyrus.
TF	Covers the anterior 4/5th of the fusiform gyrus.
TG	This region covers the anterior tip of the temporal lobe, as well as the most anterior 1/3rd of the superior, middle and inferior temporal gyrus.

Table S2 – continued.

Supplemental Figures

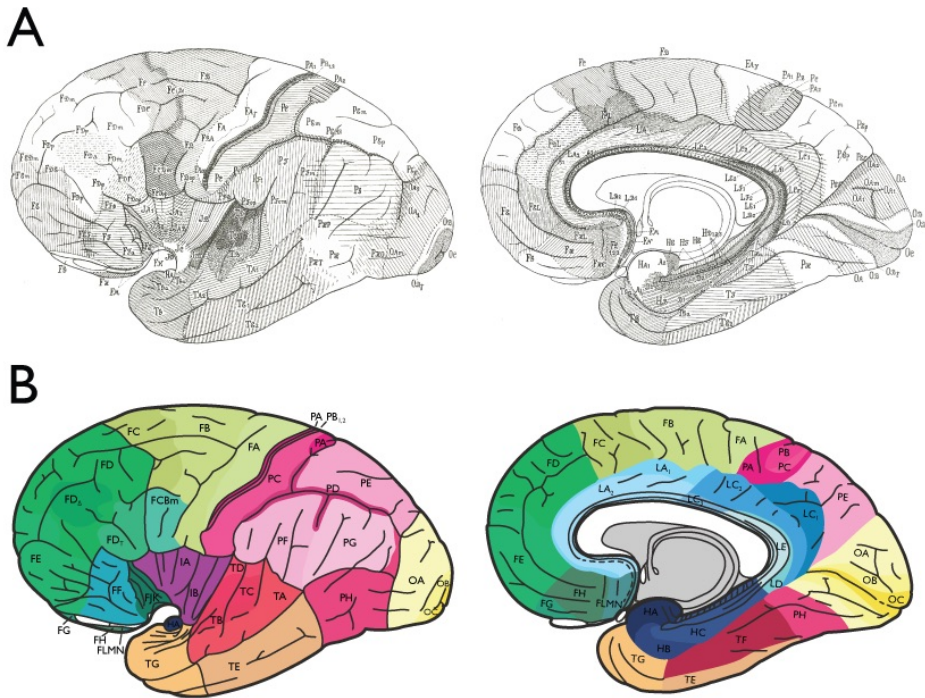


Figure S1. Colored version of the 1925 Von Economo – Koskinas atlas illustrations. (A) Figure shows the lateral and medial view of the original illustration described in the Von Economo – Koskinas atlas as included in their 1925 textbook (von Economo and Koskinas, 1925). **(B)** Figure shows a digitized and colored version of the illustrations showing the 43 merged regions as included in the FreeSurfer Von Economo – Koskinas atlas, which were described as the most important cortical regions and were included in the tables with histological data provided by Von Economo and Koskinas (von Economo and Koskinas, 1925).

Manual drawing of Von Economo - Koskinas region

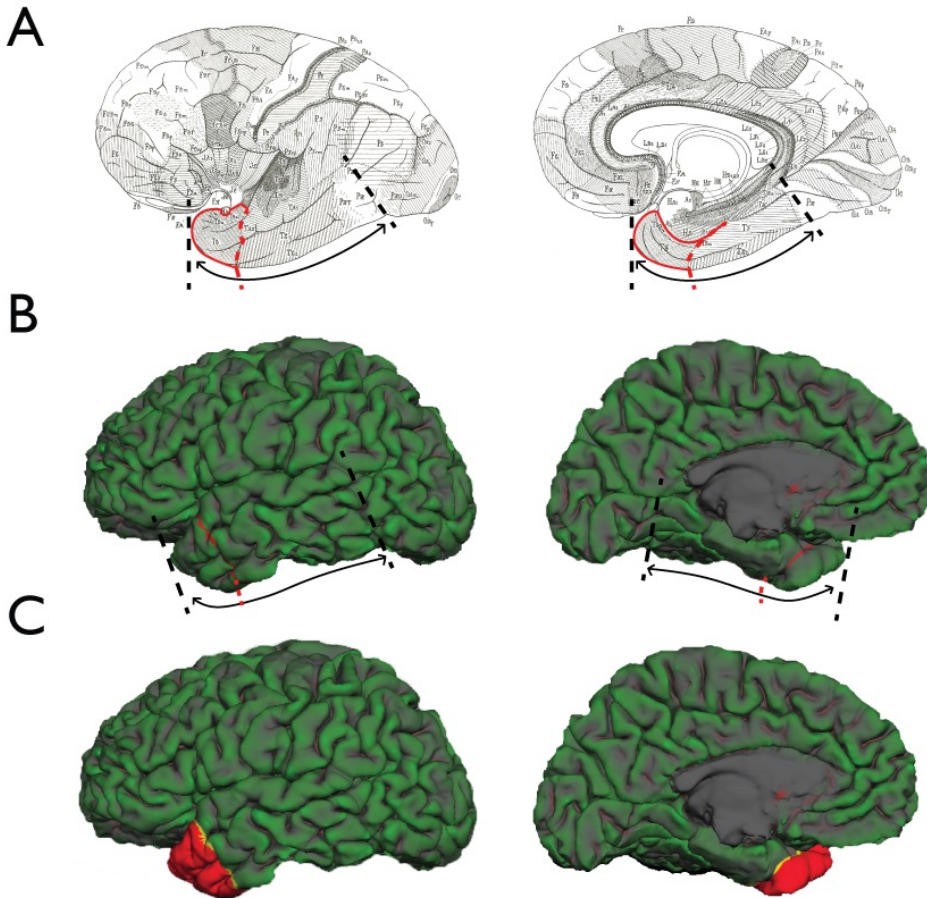


Figure S2. Drawing cortical labels. Figure illustrates the process of drawing Von Economo - Koskinas region TG onto an exemplary cortical surface reconstruction. **(A)** Figures shows the region outlined in red on the 1925 Von Economo - Koskinas lateral and medial illustration, **(B)** the plotted outline of the region on the cortical surface reconstruction, **(C)** completed and filled-in region label.

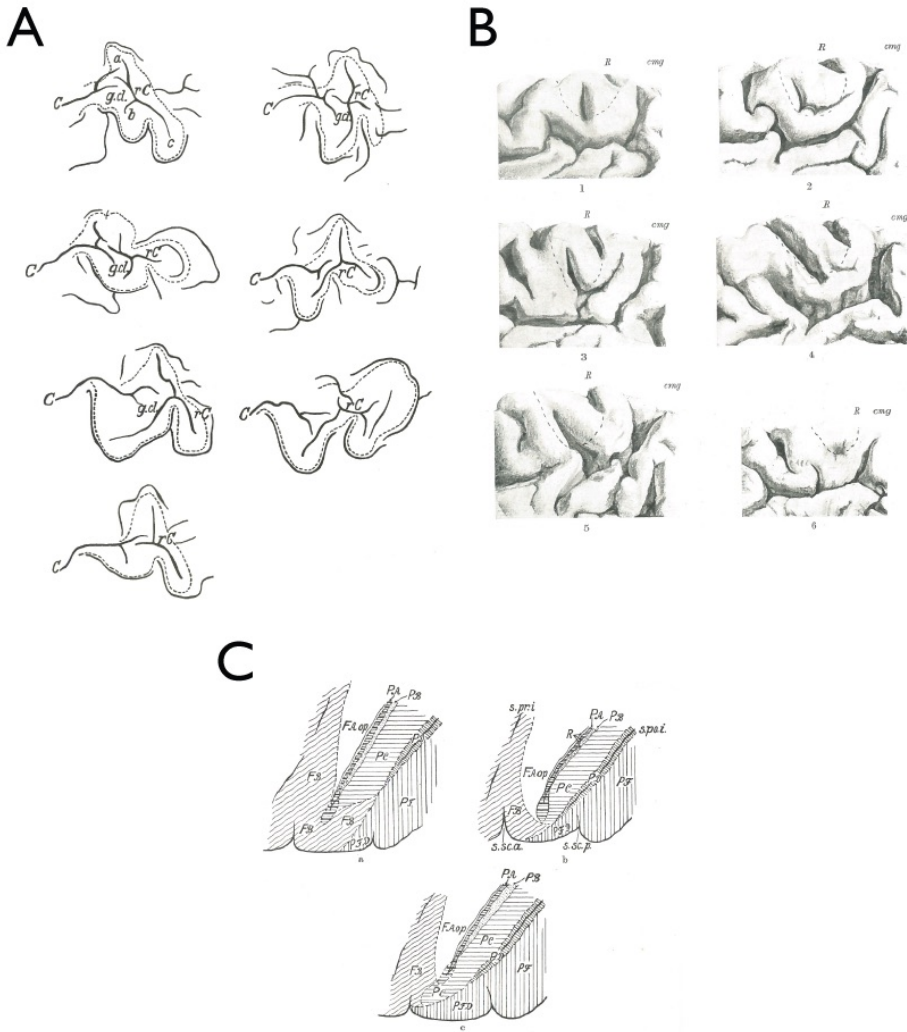


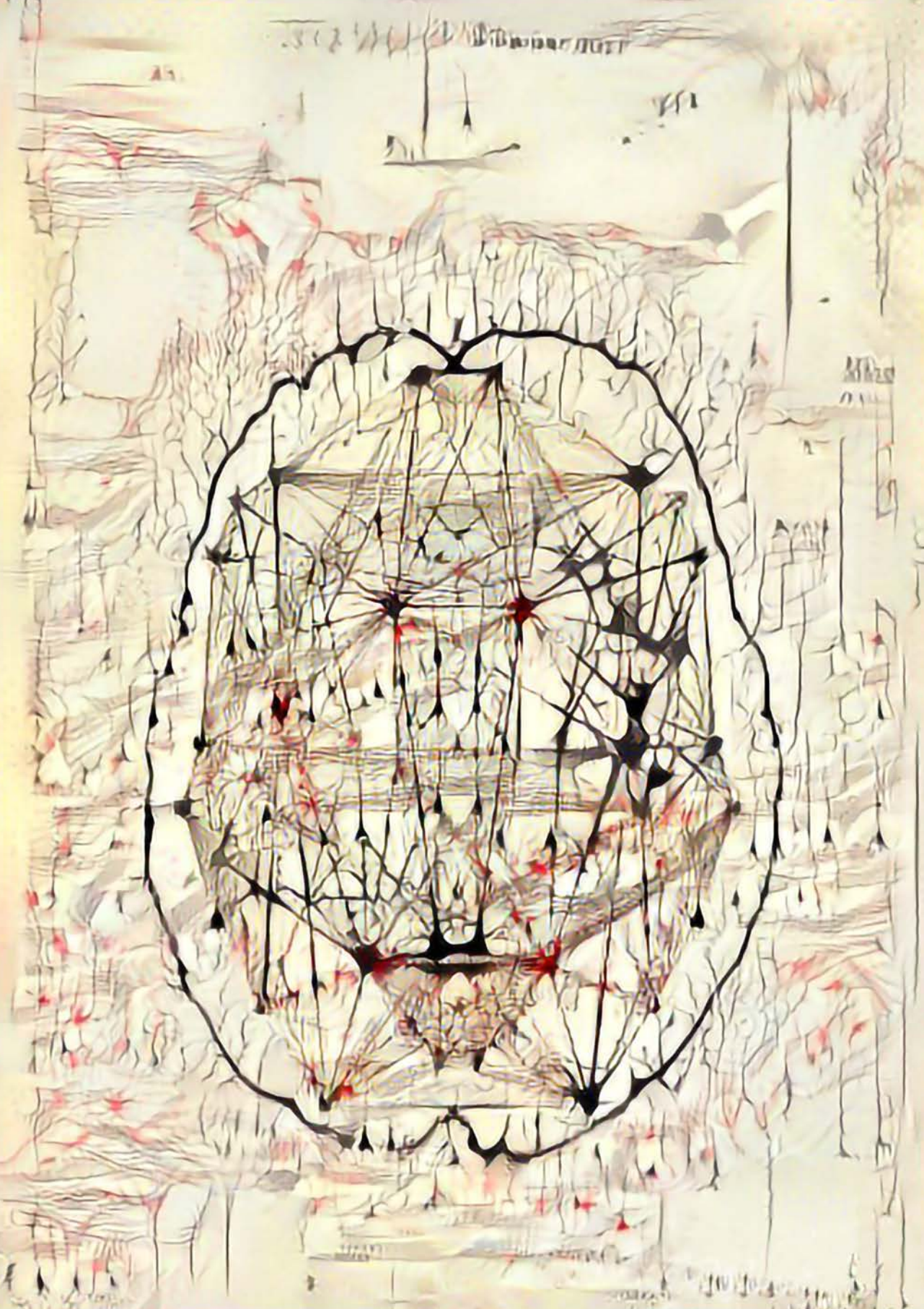
Figure S3. Examples of variation in cortical folding. Figure shows examples of between-subject variation in cortical folding patterns, as included in the 1925 Von Economo – Koskinas textbook for (A) calcarine sulcus, (B) paracentral lobule, (C) central sulcus.

Supplemental References

Betz W (1874) Anatomischer nachweis zweier gehirncentra. *Zentralbl Med Wiss* 12.

Von Economo CF, Koskinas GN (1925) *Die Cytoarchitektur der Hirnrinde des erwachsenen Menschen* J. Springer.

Theme IV – macroscale connectomics in young offspring of schizophrenia and bipolar disorder patients



Affected anatomical rich club and structural-functional coupling in young offspring of schizophrenia and bipolar disorder patients

Guusje Collin, Lianne H. Scholtens, René S. Kahn, Manon H.J. Hillegers and Martijn P. van den Heuvel

Biological Psychiatry 2017; 82 (10): 746-755

BACKGROUND: Emerging evidence suggests disruptions in the wiring organization of the brain's network in schizophrenia (SZ) and bipolar disorder (BD). As the importance of genetic predisposition has been firmly established in these illnesses, children (offspring) of patients constitute an at-risk population. This study examines connectome organization in children at familial high risk for psychosis.

METHODS: Diffusion-weighted magnetic resonance imaging scans were collected from 127 nonpsychotic offspring 8 to 18 years of age (average age = 13.5 years) of a parent diagnosed with SZ (SZ offspring; $n = 28$) or BD (BD offspring; $n = 60$) and community control subjects ($n = 39$). Resting-state functional magnetic resonance imaging scans were available for 82 subjects. Anatomical and functional brain networks were reconstructed and examined using graph theoretical analysis.

RESULTS: SZ offspring were found to show connectivity deficits of the brain's central rich club (RC) system relative to both control subjects and BD offspring. The disruption in anatomical RC connectivity in SZ offspring was associated with increased modularity of the functional connectome. In addition, increased coupling between structural and

functional connectivity of long-distance connections was observed in both SZ offspring and BD offspring.

CONCLUSIONS: This study shows lower levels of anatomical RC connectivity in nonpsychotic young offspring of SZ patients. This finding suggests that the brain's anatomical RC system is affected in at-risk youths, reflecting a connectome signature of familial risk for psychotic illness. Moreover, finding no RC deficits in offspring of BD patients suggest a differential effect of genetic predisposition for SZ versus BD on the developmental formation of the connectome.

Introduction

Elucidating the patterns of brain development that lead up to the manifestation of major psychiatric disorders is a pressing issue in current biological psychiatry. A valuable paradigm to explore brain development in relation to psychiatric vulnerability is the study of young individuals at increased risk for schizophrenia (SZ) and bipolar disorder (BD) (Hameed and Lewis, 2016; Mesman et al., 2013; Rasic et al., 2013). Given that these illnesses are genetically mediated (Consortium, 2014; Mühleisen et al., 2014), offspring of SZ and BD patients constitute an at-risk population. In addition to genetic predisposition, having a parent with mental illness has been associated with an increased burden of environmental stressors in childhood (Schreuder et al., 2016; Yehuda et al., 2001) that further increase the risk of developing a psychiatric disorder. Identifying neurobiological disturbances in these at-risk offspring may help clarify the developmental origins of brain abnormalities observed in established illness and contribute to the development of early detection and intervention strategies aimed to ameliorate or prevent psychotic illness (Yung and Nelson, 2011).

SZ and BD are characterized by symptoms in a range of behavioral, cognitive, and affective domains. These higher-order brain functions depend on flexible interactions among functionally specialized neural circuits, shaped by the brain's network of anatomical connections, the connectome (Sporns et al., 2005). Graph theoretical studies suggest that the connectome is organized according to a cost-efficient wiring pattern (Bullmore and Sporns, 2012), with a modular community structure (Meunier et al., 2010), short communication relays (Collin et al., 2013; Hagmann et al., 2008) and a central "rich club" (RC) core of highly connected hubs (van den Heuvel and Sporns, 2011) that is thought to have a crucial role in whole-brain integration (van den Heuvel et al., 2012, 2016). Emerging evidence suggests that the brain's wiring organization is disrupted in SZ [for review see (Fornito et al., 2012; van den Heuvel and Fornito, 2014)] and BD (Collin et al., 2016; Forde et al., 2015; Roberts et al., 2016), but

whether connectome abnormalities are present in unaffected young offspring of SZ and BD patients remains to be determined.

In this study, we examine connectome organization in young offspring of SZ and BD patients. These high-risk offspring between 8 and 18 years of age are younger than the typical age at onset of SZ and BD, which peaks in late teens to early twenties (Häfner et al., 1994; Sham et al., 1994). Studying this at-risk population thus provides an opportunity to assess the impact of genetic vulnerability for psychotic illness on brain development well before the age at which psychosis typically manifests. Investigating anatomical and functional brain network topology, we aim to determine whether disruptions in connectome organization are present in nonpsychotic young at-risk offspring and how putative deficits in connectome topology relate to early psychopathology.

Materials and methods

Participants

This study includes 127 participants between 8 and 18 years of age from a total of 93 families, including 28 offspring of a SZ patient (SZ offspring), 60 offspring of a BD patient (BD offspring), and 39 community control subjects (Table 1). The offspring are referred to as nonpsychotic because none met DSM-IV criteria for SZ or a related psychotic disorder at the time of baseline assessment (present and lifetime). For each family, all offspring in the appropriate age range entered our study to prevent a biased selection of participants within the family, as offspring with (subthreshold) symptoms may otherwise be more likely to be signed up for study participation than offspring with no (subthreshold) symptoms. Clinical diagnoses of parents were confirmed using the Structured Clinical Interview for DSM-IV Axis I Disorders (First et al., 2002). Control parents were screened for psychopathology using the mini-Schedules for Clinical Assessment in Neuropsychiatry (Nienhuis et al., 2010). The medical ethics committee of the University Medical Center Utrecht approved the study, and all participating children and their parents provided written informed consent.

The Schedule for Affective Disorders and Schizophrenia for School-Age Children – Present and Lifetime Version (Kaufman et al., 1997) was used to evaluate symptoms and DSM-IV diagnoses of all participants (Supplement). As evidence suggests that intelligence relates to brain changes during development (Pol et al., 2006; Ramsden et al., 2011; Shaw et al., 2006) and intellectual underperformance is a risk factor for SZ (Kahn and Keefe, 2013), IQ was also assessed. Overall IQ was estimated using four subtests (block design, picture completion, information, and vocabulary) of the

	Schizophrenia Offspring, <i>n</i> = 28	Bipolar Disorder Offspring, <i>n</i> = 60	Community Controls, <i>n</i> = 39	Statistics
Age, Mean (SD)	13.1 (3.1)	14.2 (2.5) ^a	12.7 (2.2) ^a	$F = 3.92, p = .022$
Gender, Male/Female, <i>n</i>	9/19	33/27	19/20	$\chi^2 = 4.13, p = .127$
Estimated IQ, ^b Mean (SD)	10.4 (2.5) ^c	104.0 (19.1) ^a	116.9 (12.7) ^{a,c}	$F = 8.69, p < .001$
Clinical Diagnosis, ^d <i>n</i> (%)				
No diagnosis	11 (39.3) ^c	28 (46.7) ^a	32 (82.1) ^{a,c}	$\chi^2 = 15.03, p = .001$
Mood disorder ^e	6 (21.4)	18 (3.0) ^a	4 (1.3) ^a	$\chi^2 = 6.05, p = .049$
Anxiety disorder ^f	3 (1.7)	4 (6.7)	1 (2.6)	$\chi^2 = 1.85, p = .397$
ADHD	1 (3.6)	1 (1.7)	0 (.0)	$\chi^2 = 1.32, p = .516$
ASD	4 (14.3) ^c	2 (3.3)	0 (.0) ^c	$\chi^2 = 7.63, p = .022$
Other ^g	3 (1.7)	4 (6.7)	2 (5.1)	$\chi^2 = .77, p = .682$
K-SADS Sum Scores, ^h Mean (SD)				
Total	138.6 (14.0) ^c	136.8 (19.2) ^a	122.7 (7.2) ^{a,c}	$\chi^2 = 12.06, p < .001$
Psychosis	34.6 (3.8) ^c	33.5 (3.4)	32.3 (.6) ^c	$\chi^2 = 4.82, p = .010$
Depression	1.6 (2.8) ^c	1.5 (2.8) ^a	8.9 (1.3) ^{a,c}	$\chi^2 = 5.95, p = .003$
Mania	4.6 (1.1)	4.7 (1.7) ^a	4.0 (.0) ^a	$\chi^2 = 3.65, p = .029$
Anxiety	17.0 (3.2)	17.0 (3.5)	15.5 (2.2)	$\chi^2 = 2.83, p = .063$
Behavior	2.4 (4.6) ^c	2.3 (4.2) ^a	17.5 (2.0) ^{a,c}	$\chi^2 = 7.50, p = .001$
Psychotropics Medication, ⁱ <i>n</i> (%)	3 (1.7)	3 (5.0)	0 (0)	$\chi^2 = 3.95, p = .139$

Table 11.1: Statistical comparison was performed using analysis of variance for continuous and chi-squared tests for categorical variables.

ADHD, attention-deficit/hyperactivity disorder; ASD, autism spectrum disorder (including Asperger syndrome and childhood disintegrative disorder); K-SADS, Schedule for Affective Disorders and Schizophrenia for School-Age Children.

^a Significant bivariate difference (post hoc test): bipolar disorder offspring vs. controls.

^b Data missing for 4 subjects.

^c Significant bivariate difference (post hoc test): schizophrenia offspring vs. controls.

^d Data missing for 3 subjects.

^e Mood disorders include major depressive disorder, bipolar disorder, dysthymic disorder, cyclothymic disorder, mood disorder not otherwise specified, and adjustment disorder with depressed mood.

^f Anxiety disorders include panic disorder, specific phobia, generalized anxiety disorder, obsessive-compulsive disorder, and anxiety disorder not otherwise specified.

^g Other includes tic disorder not otherwise specified, eating disorder not otherwise specified, enuresis, adjustment disorder with mixed disturbances of emotions and conduct, oppositional defiant disorder, and cannabis use disorder.

^h Data missing for 9 subjects.

ⁱ Psychotropic medications include methylphenidate, dexamphetamine, fluoxetine, citalopram, haloperidol, and melatonin. Data missing for 10 subjects.

Wechsler Intelligence Scale for Children–Third Edition Revised (for participants <16 years of age) (Wechsler, 1991) or the Wechsler Adult Intelligence Scale–Third Edition (for participants >16 years of age) (Wechsler, 1997). The majority of the offspring (>85%) were naïve to psychotropic medication.

Image Acquisition and Preprocessing

Magnetic resonance imaging (MRI) was performed on a 3T clinical MRI scanner at the University Medical Center Utrecht (Philips Achieva, the Netherlands), including anatomical T1-weighted scans for tissue classification and cortical parcellation, diffusion-weighted imaging scans for reconstruction of white matter pathways, and resting-state functional MRI scans to compute interregional functional connectivity (Supplement).

Anatomical Connectome Reconstruction

One anatomical brain network was reconstructed for each individual subject, consisting of 114 cortical areas, reflecting a subdivision of the Desikan–Killiany atlas (Cammoun et al., 2012; Hagmann et al., 2008), and reconstructed streamlines between these areas. Network connections were included when two nodes (i.e., brain regions) were connected by at least five tractography streamlines (de Reus and van den Heuvel, 2013). For each participant, the network information was stored in a structural connectivity (SC) matrix, with rows and columns reflecting cortical brain regions, and matrix entries representing the weights of the graph edges taken as the number of tractography streamlines. The main results were confirmed using streamline density (number of streamlines corrected for the average volume of the connecting brain regions) as connection weights (Supplement). In addition, effects were confirmed using a higher resolution parcellation of the cortex into 448 approximately equally sized parcels (Cammoun et al., 2012) (Supplement).

Functional Connectome Reconstruction

Resting-state functional MRI data were available for 82 of the 127 subjects (Supplement). These subjects originated from a total of 69 families and included 29 controls, 38 BD offspring, and 15 SZ offspring. For each subject, the level of functional connectivity between the nodes of the network ($N = 114$) was computed as the Pearson correlation between the regions' time series and was stored in the individual functional connectivity (FC) matrix.

Anatomical Connectome Topology

The topological organization of the anatomical brain networks was assessed using a selection of graph measures (Rubinov and Sporns, 2010). Overall connectivity strength (S) was computed as the total sum of the weights of all connections in the network.

Global efficiency (GE) was computed as the average inverse shortest path length between all node pairs, commonly interpreted as a metric of overall communication capacity. Clustering (C) was computed as the average likelihood that the neighbors of a node are also mutually connected, as a measure of operational segregation. The modularity index (Q_{sc}) was computed to assess the extent to which the networks could be decomposed into coherent communities promoting specialized processing (Newman, 2006).

Rich Club Organization

RC organization of complex networks expresses the tendency of high-degree hubs to be more strongly interconnected than is to be expected based on their high degree alone (Colizza et al., 2006; van den Heuvel and Sporns, 2011). The presence of RC organization was verified in the current sample (Supplemental Figure S1). RC regions – i.e., brain hubs – were defined for each subject individually as the top 20 high-degree nodes, corresponding to the top 18% highest-ranking nodes in terms of degree. RC effects as reported in this study were found over a range of hub definitions (Supplement). Based on the categorization of network nodes into RC (i.e., hub) and non-RC nodes, network edges were classified into three categories, with RC edges connecting hub nodes, feeder edges connecting hub to peripheral nodes, and local edges connecting peripheral nodes (van den Heuvel et al., 2012). For each individual dataset, RC, feeder, and local connectivity was computed as the sum of the weights of each edge class.

Functional Communities

Using the constructed functional connectomes, functional communities were determined using the Louvain community detection algorithm (100 runs per subject, selecting the highest functional modularity [Q_{fc}] index) (Blondel et al., 2008). The Louvain algorithm was used because it is suitable for networks with both positively and negatively weighted connections, as is the case in resting-state functional MRI functional networks (Rubinov and Sporns, 2011). In addition, the sum of FC between functional modules was calculated as a measure of intermodular functional integration.

Structural–Functional Coupling

The coupling between structural and functional connectivity (SC–FC coupling) was assessed. To this end, all nonzero entries of the structural connectome were selected and rescaled to a Gaussian distribution, and a correlation analysis was performed between the strength of the structural connections and the associated level of FC (Hagmann et al., 2008; Honey and Sporns, 2009; van den Heuvel et al., 2013). Using a log transformation to obtain a normal distribution of SC or applying Spearman rank correlations to the empirical SC data resulted in the same overall findings.

Intrahemispheric Versus Interhemispheric Connections. To explore possible group differences in SC–FC coupling for connections within versus those between the hemispheres, intra- and interhemispheric connections were examined separately.

Fiber Length. To assess the potential impact of fiber length on SC–FC coupling, short (<50 mm), intermediate (50–100 mm), and long-distance (>100 mm) structural connections (i.e., corresponding to the bottom 55%, middle 25%, and top 20% of connections, respectively) were examined.

Statistical Analysis

A linear mixed model procedure was used to examine group differences in metrics of brain network topology, accounting for effects of age and gender, and within-family dependence (i.e., ≥ 2 siblings participating in the study). Group status, age, and gender entered into the model as fixed effects terms, and within-family dependencies between individual subjects as random effects terms (Supplement). Visual inspection of residual plots did not reveal evidence for any obvious deviations from normality.

The examined network metrics showed a substantial level of correlation (mean [SD] = .42 [.32]), as commonly reported in brain network studies (Lynall et al., 2010; Scholtens et al., 2014; van den Heuvel and Sporns, 2011). To control for type I error while taking the correlation between network metrics into account, a method designed to estimate the effective number of performed tests was used to compute a “partial Bonferroni” corrected α (Gao et al., 2008; Li and Ji, 2005; Shriner et al., 2008). Methods that provide more stringent control for familywise error rate reduce the probability of even one false positive discovery (type I error) but may inflate type II error. A principal component analysis (PCA) was performed to transform the data matrix of connectome metrics into a set of linearly uncorrelated variables (i.e., principal components). The first two components were found to explain .95% of the variance. Based on this result, results with an $\alpha < .05 / 2 = .025$ (Scholtens et al., 2014) were submitted to post hoc bivariate comparison using the linear mixed model, with the contrast differentiating each pair of subject groups separately. Partial Bonferroni-adjusted p values ($p_{adj} = p \times c$, with $c =$ the number of PCA components) are reported throughout. For adjusted p values exceeding 1, $p_{adj} = 1.0$ is reported. To verify that the informative signal is in the first two principal components, rather than the remaining variance not accounted for by partial Bonferroni, the components were also tested directly (Supplement). For metrics with significant group effects, the mean adjusted difference (M_{diff}), quantified as the percentage difference in a graph metric between a pair of subject groups, and standard error (SE) are reported.

Influence of Age and Relatedness on Main Findings

Age and relatedness were included as predictors in the main analysis. To verify that age and relatedness were not driving group effects, main effects were reassessed using an age-matched subgroup of BD offspring and in a subset of unrelated individuals ($n = 93$), which confirmed our findings (Supplement).

Linking Functional Modularity to Structural Rich Club Connectivity

It has been suggested that the RC system serves as an anatomical infrastructure for the integration of information among functional modules. To test how RC connectivity impacts the level of functional integration, the association between structural RC connectivity and Q_{fc} , as well as the level of intermodular functional integration, was assessed in each subject group using linear regression analysis, correcting for the effects of age and gender.

Clinical Correlates

Connectome metrics showing significant group effects were examined for an association with total symptoms, sum scores on five symptom domains (i.e., psychosis, depression, mania, anxiety, and behavior), and overall IQ. Partial correlations between clinical and connectome metrics were computed in the total sample and separate subject groups, controlling for the effects of age and gender. Performing a PCA on the data matrix of clinical measures yielded three principal components explaining .95% of the variance. Based on this result, partial Bonferroni-adjusted p values were computed to correct for the product of the number of the clinical and connectome PCA components (i.e., $3 \times 2 = 6$).

Results

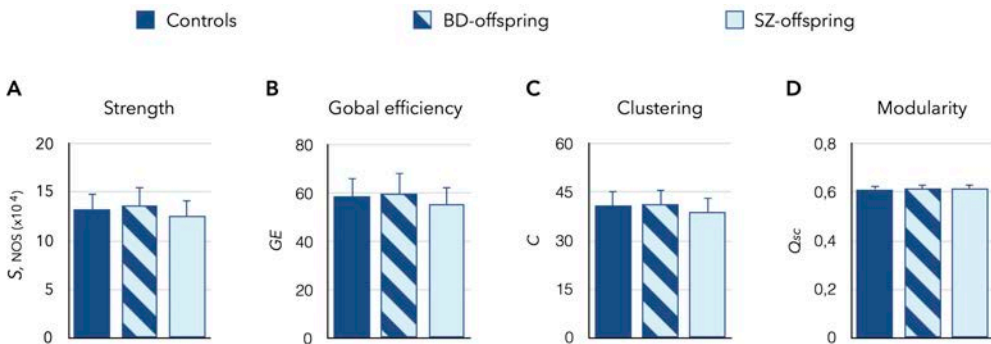


Figure 1. Anatomical connectome topology. Bar charts showing mean values of overall (A) strength (S), (B) global efficiency (GE), (C) clustering (C), and (D) modularity index (Q_{sc}) for each of the three subject groups (i.e., schizophrenia [SZ] offspring, bipolar disorder [BD] offspring, and control subjects), with whiskers indicating standard deviations. $*p < .05$, uncorrected. NOS, number of streamlines.

Global Connectome Topology

Group analysis revealed a marginal effect of overall S ($F_{2,122} = 3.40, p_{adj} = .070$) and GE ($F_{2,122} = 3.13, p_{adj} = .094$) (Figure 1A, B). These effects were mild and did not survive multiple comparison correction, suggesting that the global organization of the connectome is relatively intact in young offspring of SZ and BD patients. No significant group effects of overall C ($F_{2,122} = 2.47, p_{adj} = .178$) or Q_{sc} ($F_{2,122} = .74, p_{adj} = .962$) were found (Figure 1C, D). Reassessing global network topology in high-resolution connectome maps yielded similar results (S : $F_{2,122} = 2.97, p_{adj} = .108$; GE : $F_{2,122} = 3.98, p_{adj} = .041$; C : $F_{2,122} = 1.19, p_{adj} = .302$; and Q_{sc} : $F_{2,122} = .79, p_{adj} = .908$).

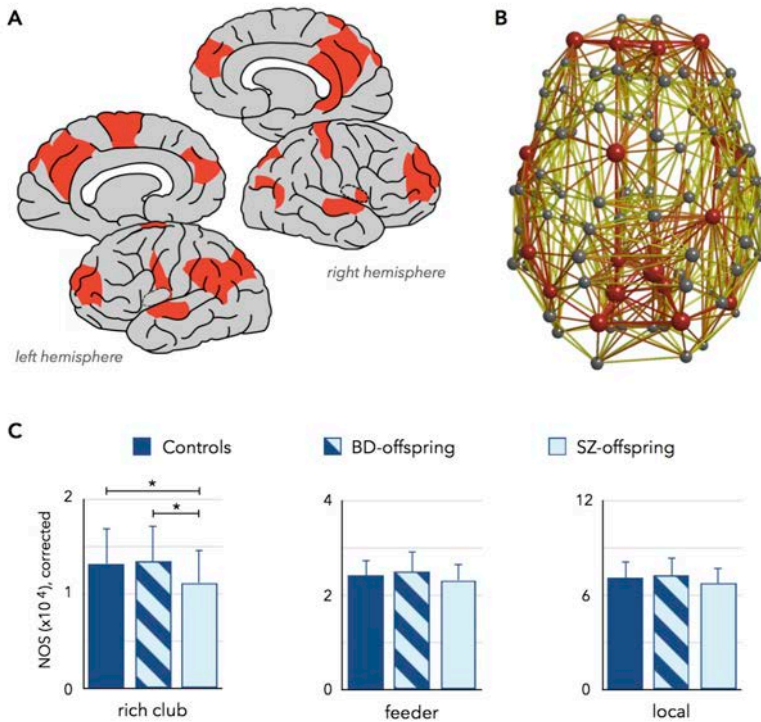


Figure 2. Rich club organization. Rich club regions defined as the top 20 high-degree brain regions (averaged over subjects) depicted on a cortical surface (A). (B) Connectome reconstruction, with nodes (i.e., brain regions) scaled to indicate how many nodes they connect to and colored to indicate hub (red) or nonhub (gray) brain regions. Edges are colored to indicate rich club (red), feeder (orange), and local (yellow) connections. (C) Bar charts show mean (SD) values of rich club, feeder, and local connectivity per subject group. *Indicates a significant reduction in rich club connectivity in the schizophrenia (SZ) offspring relative to both controls and bipolar disorder (BD) offspring. NOS, number of streamlines.

Rich Club Organization

Across subjects, RC regions included portions of the bilateral precuneus; superior frontal, superior parietal, and superior temporal gyri; rostral middle frontal gyrus and inferior

parietal gyrus; as well as the left supramarginal gyrus and precentral gyrus and right postcentral gyrus; isthmus cingulate gyrus; and insula (Figure 2A, B). Group analysis indicated a significant group effect of RC connectivity ($F_{2,122} = 3.90$, $p_{adj} = .046$) but not feeder ($F_{2,122} = 1.91$, $p_{adj} = .306$) or local ($F_{2,122} = 2.57$, $p_{adj} = .162$) connections (Figure 2C). Post hoc bivariate comparison indicated a reduction in RC connectivity in the SZ offspring group compared with control subjects ($M_{diff} = -16.8\%$, $SE = 7.0\%$, $p = .018$) and BD offspring ($M_{diff} = 16.8\%$, $SE = 6.4\%$, $p = .010$). These results were confirmed over a range of hub thresholds (i.e., top 16–29% of brain regions, with a maximal group effect at the top 25% [$F_{2,122} = 5.93$, $p_{adj} = .006$]) (Supplemental Figure S2). The group effect of RC connectivity was replicated using a high-resolution cortical parcellation scheme ($F_{2,122} = 4.30$, $p_{adj} = .032$). In addition, using strength rather than degree to define hubs also confirmed the effect ($F_{2,122} = 4.92$, $p_{adj} = .018$).

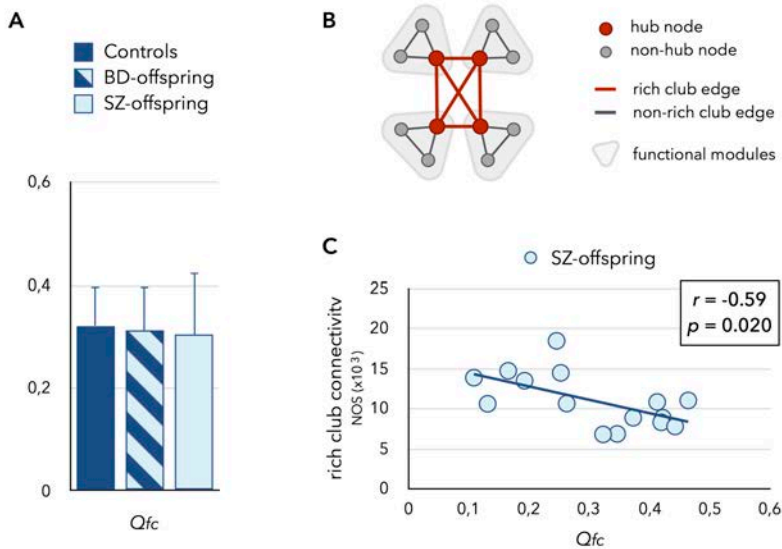


Figure 3. Functional modularity (Q_{fc}). (A) Bar chart showing mean (SD) level of Q_{fc} per subject group. (B) Toy network illustrating how the rich club collective may serve as an anatomical infrastructure linking functional modules. (C) Scatter plot showing the association between anatomical rich club connectivity and the level of Q_{fc} in the schizophrenia (SZ) offspring. NOS, number of streamlines.

Functional Communities

The level of Q_{fc} of brain networks was similar between subject groups ($F_{2,77} = .56$, $p_{adj} = 1.0$) (Figure 3A), and there were no significant group differences in consensus modular topology (Supplement and Supplemental Figure S3). Assessing the relationship between functional modularity and anatomical RC connectivity (Figure 3B), there was a negative correlation between Q_{fc} and RC connectivity in the SZ offspring ($r = -.59$, $p = .020$) (Figure 3C), but not controls or BP offspring. In line with this finding, RC

connectivity showed a positive association with intermodular functional integration in SZ offspring ($r = .56, p = .029$). These findings suggest that affected RC connectivity in SZ offspring is associated with decreased intermodular functional integration.

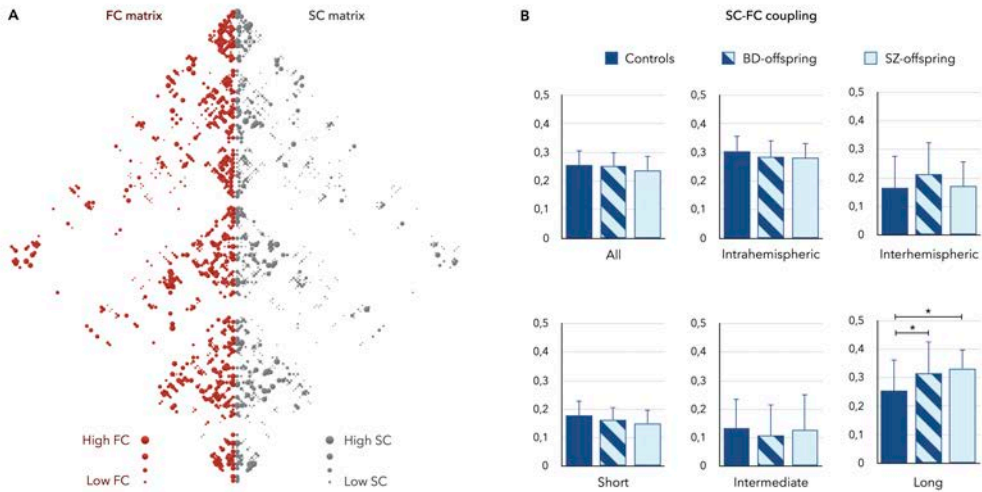


Figure 4. Structural connectivity (SC) – functional connectivity (FC) coupling. (A) Matrix representation of group-averaged SC and FC matrices masked to include functional connections for which a structural connection was present, suggesting a high degree of overlap between levels of SC and FC. (B) Bar charts showing mean (SD) values of SC–FC coupling per subject group for all structural connections, for intra- and interhemispheric connections, and for short, intermediate, and long connections. *Indicates significant group effects in SC–FC coupling of long-distance connections. BD, bipolar disorder; SZ, schizophrenia.

Structural–Functional Coupling

Whole-brain SC–FC coupling was not significantly different across subject groups ($F_{2,77} = .16, p_{adj} = 1.0$) (Figure 4A, B). Analyzing connection classes separately, there was a trend-level effect of interhemispheric SC–FC coupling ($F_{2,77} = 3.17, p_{adj} = .096$) (Figure 4B), and a significant effect of long-distance SC–FC coupling ($F_{2,77} = 7.23, p_{adj} = .002$), with post hoc bivariate tests indicating increased SC–FC coupling in both SZ offspring ($M_{diff} = 34.3\%$, $SE = 12.1\%$, $p = .002$) and BD offspring ($M_{diff} = 29.9\%$, $SE = 9.6\%$, $p = .002$) relative to controls (Figure 4B). This was not observed for intermediate and short-range [often intramodular (Hagmann et al., 2010)] connections (intermediate: $F_{2,77} = .12, p_{adj} = 1.0$; short: $F_{2,77} = 1.55, p_{adj} = .438$).

Clinical Correlates

There were no clear associations between connectome metrics showing significant group effects and clinical variables in the total offspring sample. Adding diagnoses as a categorical variable (i.e., mood disorders, anxiety disorders, attention-deficit/hyperactivity disorder, autism spectrum disorders, and “other”) to the

linear mixed model did not reveal a significant effect of diagnosis. Correcting for psychotropic medication use (yes/no) in the model confirmed the main results (RC connectivity: $F_{2,122} = 4.45$, $p_{adj} = .028$; long-distance SC–FC coupling: $F_{2,77} = 6.01$, $p_{adj} = .008$). Repeating the analyses after excluding all participants with any current or previous antipsychotic or antidepressant medication attenuated the main effect of RC connectivity (RC connectivity: $F_{2,122} = 3.37$, $p_{adj} = .075$; long-distance SC–FC coupling: $F_{2,77} = 5.93$, $p_{adj} = .008$), which may relate to reduced sample size or because excluding medicated subjects leads to an overly healthy subgroup of offspring that is not representative of the overall familial high-risk population.

Discussion

The main finding of this study is that the anatomical RC system connecting brain hubs is affected in nonpsychotic young offspring of SZ patients. This finding suggests that deficits in RC connectivity are present in children and adolescents with a genetic predisposition for SZ well before the age at which psychosis typically manifests.

SZ offspring were found to show lower levels of anatomical RC connectivity compared to both healthy controls and offspring of BD patients. This finding is consistent with studies in patients with established illness, showing RC disruptions in SZ (Griffa et al., 2015; van den Heuvel et al., 2013; Wang et al., 2015; Yeo et al., 2016; Yu et al., 2013) but not BD (Collin et al., 2016) patients. Moreover, unaffected siblings of SZ patients (Collin et al., 2013) and subjects with prodromal symptoms suggestive of impending psychosis (Schmidt et al., 2016) have been noted to exhibit RC deficits, while emerging evidence suggests a possible opposite effect in first-degree relatives of BD patients (Lord et al.), lending further support to our findings. In all, previous studies and our current findings suggest that genetic predisposition for SZ versus BD may have a differential effect on the developmental formation of the connectome's central RC system. Specifically, RC deficits appear to be a unique connectome disturbance in those affected by, or at elevated risk for, SZ.

An open question is at which time – in the course of neurodevelopment – brain network deficits evolve in children with a genetic predisposition for SZ. Studies of normative brain development indicate that hallmark organizational features of the connectome, including RC organization, are already present at 30 weeks' gestation (Ball et al., 2014; van den Heuvel et al., 2014). Nonetheless, hub-to-hub RC connections and SC–FC coupling have been found to strengthen with age in childhood and adolescence (Baker et al., 2015; Collin et al., 2013; Hagmann et al., 2010). Meta-analytical evidence indicates that children who later develop SZ show cognitive impairments by early

adolescence at the latest (Dickson et al., 2012; Kahn and Keefe, 2013), suggesting that the neurobiological process underlying SZ predates first psychosis by many years. Our finding that young SZ offspring show anatomical connectome deficits is consistent with this hypothesis. Indeed, a post hoc analysis including only subjects under 12 years of age (Supplement) demonstrated a significant group effect of RC connectivity, indicating that deficits in the anatomical RC system in SZ offspring are already present by late childhood.

RC connectivity was found to show a negative correlation with functional connectome modularity in SZ offspring, suggesting that deficits in anatomical connectivity among central brain hubs may reduce the brain's capacity for intermodular functional integration. This finding supports the notion that the RC system forms an anatomical infrastructure for the integration of neural information between segregated functional communities in the brain (van den Heuvel and Sporns, 2013). Healthy brain function is thought to depend on flexible interactions among specialized neural circuits to support a diverse repertoire of cognitive and behavioral functions (Fair et al., 2009). A longstanding hypothesis on SZ is that a disruption in the integration of neural information among functional brain circuits may underlie psychotic symptoms and cognitive deficits (Collin et al., 2016; Friston and Frith, 1995; Stephan et al., 2009). Our current study suggests that abnormal developmental formation of the central RC system in youths at risk for SZ may form the anatomical substrate for disturbed functional integration, which may in turn predispose to cognitive maldevelopment and vulnerability to psychosis.

There were no clear associations between RC connectivity and early psychopathology or IQ. The lack of association with (subclinical) symptoms may be due to insufficient power. It may also relate to the young age of our sample (i.e., 13.5 years of age on average), as the emergence of subthreshold (psychotic) symptoms is a relatively late occurring phenomenon in the trajectory from elevated risk to psychosis onset (Keshavan et al., 2011).

Another finding of our study is that both SZ offspring and BD offspring exhibit an increased level of SC-FC coupling of long-distance connectome edges, suggesting that this may be a shared disturbance in youth at risk for both affective and nonaffective psychotic illnesses. The underlying biology or functional consequences of abnormal SC-FC coupling remain to be determined, but elevated SC-FC coupling has been suggested to reflect higher anatomical constraint over functional brain dynamics (Griffa et al., 2015; van den Heuvel et al., 2013; Yu et al., 2013), invoking a reduced capacity for dynamic reconfigurations of functional connectivity patterns. Whether, and if so how, this might impact cognitive behavioral functioning remains to be elucidated.

Intriguing recent findings suggest that the brain's capacity for dynamic reconfigurations in functional connectivity among neural circuits relates to aspects of executive cognition, such as cognitive flexibility (Braun et al., 2015). This capacity has been noted to increase from childhood to adulthood (Hutchison and Morton, 2015). Increased structural constraint over functional connectivity may thus reflect a reduced capacity for flexible brain dynamics due to a deviant pattern of brain development in at-risk offspring.

Some issues should be considered when interpreting the findings of our study. First, diffusion imaging relies on water diffusion as an indirect probe of axon geometry and, as a result, suffers from a number of inherent limitations (Jbabdi and Johansen-Berg, 2011). Many factors influence streamline count, and it is not straightforward to interpret changes in streamline count in terms of underlying biology (Jones, 2008). Nonetheless, studies linking diffusion MRI to tract-tracing measures of anatomical connectivity indicate that diffusion tractography-derived streamline count provides a fairly realistic estimate of projection strength (Donahue et al., 2016; van den Heuvel et al., 2014). Second, the sample size of the SZ offspring group is relatively modest; these subjects are difficult to recruit because of issues such as reduced fecundity in patients with mental illness in general (Power et al., 2013) and SZ in particular (Laursen and Munk-Olsen, 2010; Power et al., 2013; Semple et al., 1997), and the disorganization of families as a result of the illness. Moreover, various tests were performed to capture different aspects of the same brain network data. In all, six metrics of global network topology (i.e., strength, efficiency, clustering, structural and functional modularity, and RC organization) and six measures of structural–functional coupling (i.e., whole-brain and for five connection classes) were examined. As metrics of network topology exhibit nontrivial correlations (Lynall et al., 2010; Scholtens et al., 2014) related to the way they are mathematically defined (De Vico Fallani et al., 2014), a partial Bonferroni method was used to account for the dependence between network metrics. While this approach is thought to balance type I and type II error (Scholtens et al., 2014), it should be noted that it does not hold the statistical rigor of standard Bonferroni correction. Considering the number of performed tests and the modest size of our SZ offspring sample, external replication of our findings is warranted. A third limitation to our study is that we did not assess environmental risk factors for psychotic illness, while these may impact the risk for developing a psychotic disorder directly or in association with genetic factors. Fourth, detailed neuropsychological data were not available, limiting the possibility of assessing the potential impact of brain network alterations on cognitive functioning. Fifth, the offspring groups are necessarily heterogeneous, including both individuals that will remain psychiatrically healthy as well as those that will go on to develop a minor or major psychiatric disorder. Longitudinal follow-up of

our offspring cohort may offer new insights into how connectome organization relates to later development of psychotic illness and, conversely, resilience.

Our study shows that young offspring of SZ patients exhibit deficits in anatomical connectivity of the brain's central RC system, which may represent a connectome signature of genetic risk for SZ. We did not find evidence for RC deficits in offspring of BD patients, in line with previous findings in adult patients, suggesting a differential influence of genetic predisposition for SZ versus BD on connectome development. Elucidating how early genetic and environmental risk factors impact RC formation may help unravel the neurobiological mechanisms underlying emerging SZ and offer directions for early detection and treatment.

Acknowledgments

This work was supported by Vidi Grant No. 452-16-015 from the Netherlands Organization for Scientific Research (to MPvdH), an MQ Fellowship (to MPvdH), a NARSAD Independent Investigator Grant No. 20244 from the Brain and Behavior Research Foundation (to MHJH), and the Consortium on Individual Development, Grant No. 024-001-003, funded by the Netherlands Organization for Scientific Research (to RSK, as co-primary investigator). There was no involvement by the funding bodies at any stage of the study. The authors report no biomedical financial interests or potential conflicts of interest.

References

- Baker ST, Lubman DI, Yücel M, Allen NB, Whittle S, Fulcher BD, Zalesky A, Fornito A (2015) Developmental changes in brain network hub connectivity in late adolescence. *Journal of Neuroscience* 35:9078–9087.
- Ball G, Aljabar P, Zebari S, Tumor N, Arichi T, Merchant N, Robinson EC, Ogunjide E, Rueckert D, Edwards AD (2014) Rich-club organization of the newborn human brain. *Proceedings of the National Academy of Sciences* 111:7456–7461.
- Blondel VD, Guillaume JL, Lambiotte R, Lefebvre E (2008) Fast unfolding of communities in large networks. *Journal of statistical mechanics: theory and experiment* 2008:P10008.
- Braun U, Schäfer A, Walter H, Erk S, Romanczuk-Seiferth N, Haddad L, Schweiger JJ, Grimm O, Heinz A, Tost H (2015) Dynamic reconfiguration of frontal brain networks during executive cognition in humans. *Proceedings of the National Academy of Sciences* 112:11678–11683.
- Bullmore E, Sporns O (2012) The economy of brain network organization. *Nature reviews. Neuroscience* 13:336–49.
- Cammoun L, Gigandet X, Meskaldji D, Thiran JP, Sporns O, Maeder P, Meuli R, Hagmann P (2012) Mapping the human connectome at multiple scales with diffusion spectrum mri. *Journal of neuroscience methods* 203:386–97.
- Colizza V, Flammini A, Serrano M, Vespignani A (2006) Detecting rich-club ordering in complex networks. *Nat Phys* 2:110–115.
- Collin G, de Nijs J, Pol HH, Cahn W, van den Heuvel MP (2016) Connectome organization is related to longitudinal changes in general functioning, symptoms and iq in chronic schizophrenia. *Schizophrenia research* 173:166–173.
- Collin G, Sporns O, Mandl RCW, van den Heuvel MP (2013) Structural and functional aspects relating to cost and benefit of rich club organization in the human cerebral cortex. *Cerebral cortex (New York, N.Y. : 1991)* .
- Consortium SWGotPG (2014) Biological insights from 108 schizophrenia-associated genetic loci. *Nature* 511:421–427.
- de Reus M, van den Heuvel M (2013) Estimating false positives and negatives in brain networks. *Neuroimage* 70:402–9.
- De Vico Fallani F, Richiardi J, Chavez M, Achard S (2014) Graph analysis of functional brain networks: practical issues in translational neuroscience. *Phil. Trans. R. Soc. B* 369:20130521.
- Dickson H, Laurens K, Cullen AE, Hodgins S (2012) Meta-analyses of cognitive and motor function

- in youth aged 16 years and younger who subsequently develop schizophrenia. *Psychological medicine* 42:743–755.
- Donahue CJ, Sotiropoulos SN, Jbabdi S, Hernandez-Fernandez M, Behrens TE, Dyrby TB, Coalson T, Kennedy H, Knoblauch K, Van Essen DC (2016) Using diffusion tractography to predict cortical connection strength and distance: a quantitative comparison with tracers in the monkey. *Journal of Neuroscience* 36:6758–6770.
- Fair DA, Cohen AL, Power JD, Dosenbach NU, Church JA, Miezin FM, Schlaggar BL, Petersen SE (2009) Functional brain networks develop from a "local to distributed" organization. *PLoS Comput Biol* 5:e1000381.
- First M, Spitzer R, Gibbon M, William J (2002) Structured clinical interview for DSM-IV-TR axis I disorders, research version, patient edition (SCID-I/P) New York, NY: New York State Psychiatric Institute. *Biometric research* 73.
- Forde NJ, O'Donoghue S, Scanlon C, Emsell L, Chaddock C, Leemans A, Jeurissen B, Barker GJ, Cannon DM, Murray RM (2015) Structural brain network analysis in families multiply affected with bipolar I disorder. *Psychiatry Research: Neuroimaging* 234:44–51.
- Fornito A, Zalesky A, Pantelis C, Bullmore ET (2012) Schizophrenia, neuroimaging and connectomics. *NeuroImage* 62:2296–2314.
- Friston KJ, Frith CD (1995) Schizophrenia: a disconnection syndrome? *Clin Neurosci* 3:89–97.
- Gao X, Starmer J, Martin ER (2008) A multiple testing correction method for genetic association studies using correlated single nucleotide polymorphisms. *Genetic epidemiology* 32:361–369.
- Griffa A, Baumann PS, Ferrari C, Do KQ, Conus P, Thiran J, Hagmann P (2015) Characterizing the connectome in schizophrenia with diffusion spectrum imaging. *Human brain mapping* 36:354–366.
- Häfner H, Maurer K, Löffler W, Fätkenheuer B (1994) The epidemiology of early schizophrenia influence of age and gender on onset and early course. *The British journal of psychiatry* .
- Hagmann P, Sporns O, Madan N, Cammoun L, Pienaar R, Wedeen VJ, Meuli R, Thiran JP, Grant PE (2010) White matter maturation reshapes structural connectivity in the late developing human brain. *Proc Natl Acad Sci U S A* 107:19067–72.
- Hagmann P, Cammoun L, Gigandet X (2008) Mapping the structural core of human cerebral cortex. *PLoS biology* 6:e159.
- Hameed MA, Lewis AJ (2016) Offspring of parents with schizophrenia: A systematic review of developmental features across childhood. *Harvard review of psychiatry* 24:104–117.
- Honey C, Sporns O (2009) Predicting human resting-state functional connectivity from structural

- connectivity. *Proceedings of the National Academy of Sciences* 106:1–6.
- Hutchison RM, Morton JB (2015) Tracking the brain's functional coupling dynamics over development. *Journal of Neuroscience* 35:6849–6859.
- Jbabdi S, Johansen-Berg H (2011) Tractography: where do we go from here? *Brain Connect* 1:169–83.
- Jones DK (2008) Studying connections in the living human brain with diffusion mri. *Cortex* 44:936–52.
- Kahn RS, Keefe RS (2013) Schizophrenia is a cognitive illness: time for a change in focus. *JAMA psychiatry* 70:1107–1112.
- Kaufman J, Birmaher B, Brent D, Rao UMA, Flynn C, Moreci P, Williamson D, Ryan N (1997) Schedule for affective disorders and schizophrenia for school-age children-present and lifetime version (k-sads-pl): Initial reliability and validity data. *Journal of the American Academy of Child & Adolescent Psychiatry* 36:980–988.
- Keshavan MS, DeLisi LE, Seidman LJ (2011) Early and broadly defined psychosis risk mental states. *Schizophrenia research* 126:1–10.
- Laursen TM, Munk-Olsen T (2010) Reproductive patterns in psychotic patients. *Schizophrenia research* 121:234–240.
- Li J, Ji L (2005) Adjusting multiple testing in multilocus analyses using the eigenvalues of a correlation matrix. *Heredity* 95:221–227.
- Lord A, Roberts G, Breakspear M, Mitchell P The rich club of the brain in bipolar disorder In *Front Hum Neurosci Conference Abstract: XII International Conference on Cognitive Neuroscience (ICON-XII)*, Lord2015. Available at: doi:10.3389/conf.fnhum.2015.217.00272. Accessed June 12, 2017.
- Lynall ME, Bassett DS, Kerwin R, McKenna PJ, Kitzbichler M, Muller U, Bullmore E (2010) Functional connectivity and brain networks in schizophrenia. *The Journal of Neuroscience* 30:9477–9487.
- Mesman E, Nolen WA, Reichart CG, Wals M, Hillegers MH (2013) The dutch bipolar offspring study: 12-year follow-up. *American Journal of Psychiatry* 170:542–549.
- Meunier D, Lambiotte R, Bullmore E (2010) Modular and hierarchically modular organization of brain networks. *Frontiers in neuroscience* 4:200.
- Mühleisen TW, Leber M, Schulze TG, Strohmaier J, Degenhardt F, Treutlein J, Mattheisen M, Forstner AJ, Schumacher J, Breuer R (2014) Genome-wide association study reveals two new risk loci for bipolar disorder. *Nature communications* 5:3339.

- Newman ME (2006) Modularity and community structure in networks. *Proceedings of the national academy of sciences* 103:8577–8582.
- Nienhuis FJ, van de Willige G, Rijnders CAT, de Jonge P, Wiersma D (2010) Validity of a short clinical interview for psychiatric diagnosis: the mini-scan. *The British Journal of Psychiatry* 196:64–68.
- Pol HEH, Schnack HG, Posthuma D, Mandl RC, BaarÃƒ WF, van Oel C, van Haren NE, Collins DL, Evans AC, Amunts K (2006) Genetic contributions to human brain morphology and intelligence. *Journal of Neuroscience* 26:10235–10242.
- Power JD, Schlaggar BL, Lessov-Schlaggar CN, Petersen SE (2013) Evidence for hubs in human functional brain networks. *Neuron* 79:798–813.
- Ramsden S, Richardson FM, Josse G, Thomas MS, Ellis C, Shakeshaft C, Seghier ML, Price CJ (2011) Verbal and non-verbal intelligence changes in the teenage brain. *Nature* 479:113–116.
- Rasic D, Hajek T, Alda M, Uher R (2013) Risk of mental illness in offspring of parents with schizophrenia, bipolar disorder, and major depressive disorder: a meta-analysis of family high-risk studies. *Schizophrenia bulletin* 40:28–38.
- Roberts G, Perry A, Lord A, Frankland A, Leung V, Holmes-Preston E, Levy F, Lenroot R, Mitchell P, Breakspear M (2016) Structural dysconnectivity of key cognitive and emotional hubs in young people at high genetic risk for bipolar disorder. *Molecular psychiatry* .
- Rubinov M, Sporns O (2010) Complex network measures of brain connectivity: uses and interpretations. *NeuroImage* 52:1059–69.
- Rubinov M, Sporns O (2011) Weight-conserving characterization of complex functional brain networks. *NeuroImage* 56:2068–79.
- Schmidt A, Crossley NA, Harrisberger F, Smieskova R, Lenz C, Riecher-RÃƒussler A, Lang UE, McGuire P, Fusar-Poli P, Borgwardt S (2016) Structural network disorganization in subjects at clinical high risk for psychosis. *Schizophrenia bulletin* 43:583–591.
- Scholtens LH, Schmidt R, de Reus MA, van den Heuvel MP (2014) Linking macroscale graph analytical organization to microscale neuroarchitectonics in the macaque connectome. *The Journal of Neuroscience* 34:12192–12205.
- Schreuder MM, Vinkers CH, Mesman E, Claes S, Nolen WA, Hillegers MH (2016) Childhood trauma and hpa axis functionality in offspring of bipolar parents. *Psychoneuroendocrinology* 74:316–323.
- Semple SJ, Patterson TL, Shaw WS, Grant I, Moscona S, Koch W, Jeste D (1997) The social networks of older schizophrenia patients. *International Psychogeriatrics* 9:81–94.
- Sham P, MacLean C, Kendler K (1994) A typological model of schizophrenia based on age at onset,

- sex and familial morbidity. *Acta Psychiatrica Scandinavica* 89:135–141.
- Shaw P, Greenstein D, Lerch J, Clasen L, Lenroot R, Gogtay N, Evans A, Rapoport J, Giedd J (2006) Intellectual ability and cortical development in children and adolescents. *Nature* 440:676–679.
- Shriner D, Baye TM, Padilla MA, Zhang S, Vaughan LK, Loraine AE (2008) Commonality of functional annotation: a method for prioritization of candidate genes from genome-wide linkage studies. *Nucleic acids research* 36:e26–e26.
- Sporns O, Tononi G, Kötter R (2005) The human connectome: a structural description of the human brain. *PLoS computational biology* 1:e42.
- Stephan KE, Friston KJ, Frith CD (2009) Dysconnection in schizophrenia: from abnormal synaptic plasticity to failures of self-monitoring. *Schizophr Bull* 35:509–27.
- van den Heuvel MP, Kersbergen KJ, de Reus MA, Keunen K, Kahn RS, Groenendaal F, de Vries LS, Benders MJ (2014) The neonatal connectome during preterm brain development. *Cereb Cortex* 25:3000–3013.
- van den Heuvel MP, Kahn RS, Goñi J, Sporns O (2012) High-cost, high-capacity backbone for global brain communication. *Proceedings of the National Academy of Sciences of the United States of America* 109:11372–11377.
- van den Heuvel MP, Scholtens LH, Turk E, Mantini D, Vanduffel W, Feldman Barrett L (2016) Multimodal analysis of cortical chemoarchitecture and macroscale fmri resting-state functional connectivity. *Human brain mapping* 37:3103–3113.
- van den Heuvel MP, Sporns O (2011) Rich-club organization of the human connectome. *The Journal of neuroscience : the official journal of the Society for Neuroscience* 31:15775–86.
- van den Heuvel MP, Sporns O (2013) An anatomical substrate for integration among functional networks in human cortex. *The Journal of neuroscience : the official journal of the Society for Neuroscience* 33:14489–500.
- van den Heuvel MP, Sporns O, Collin G, Scheewe T, Mandl RCW, Cahn W, Goñi J, Hulshoff Pol HE, Kahn RS (2013) Abnormal rich club organization and functional brain dynamics in schizophrenia. *JAMA psychiatry (Chicago, Ill.)* 70:783–92.
- van den Heuvel M, Fornito A (2014) Brain networks in schizophrenia. *Neuropsychology Review* pp. 1–17.
- Wang Z, Dai Z, Gong G, Zhou C, He Y (2015) Understanding structural-functional relationships in the human brain: a large-scale network perspective. *The Neuroscientist* 21:290–305.
- Wechsler D (1991) *WISC-III: Wechsler intelligence scale for children* Psychological Corporation.

- Wechsler D (1997) *WAIS-III, Wechsler adult intelligence scale: Administration and scoring manual* Psychological Corporation.
- Yehuda R, Halligan SL, Grossman R (2001) Childhood trauma and risk for ptsd: relationship to intergenerational effects of trauma, parental ptsd, and cortisol excretion. *Development and psychopathology* 13:733–753.
- Yeo RA, Ryman SG, Van Den Heuvel MP, De Reus MA, Jung RE, Pommy J, Mayer AR, Ehrlich S, Schulz SC, Morrow EM (2016) Graph metrics of structural brain networks in individuals with schizophrenia and healthy controls: group differences, relationships with intelligence, and genetics. *Journal of the International Neuropsychological Society* 22:240–249.
- Yu Q, Sui J, Liu J, Plis SM, Kiehl KA, Pearlson G, Calhoun VD (2013) Disrupted correlation between low frequency power and connectivity strength of resting state brain networks in schizophrenia. *Schizophr Res* 143:165–71.
- Yung AR, Nelson B (2011) Young people at ultra high risk for psychosis: a research update. *Early intervention in psychiatry* 5:52–57.

Supplemental Information

of

Affected anatomical rich club and structural-functional coupling in young offspring of schizophrenia and bipolar disorder patients

Supplementary methods

K-SADS-PL

The Schedule for Affective Disorders and Schizophrenia Present and Lifetime Version for Children (K-SADS-PL) is a semi-structured diagnostic interview designed to assess current (past 2 months) and past symptoms resulting in DSM-Axis I diagnoses in children and adolescents by interviewing the child and parent(s) separately. Symptoms were rated using a 1 to 3-point scale: 1) symptom not present; 2) symptom at sub-threshold level; 3) symptom at threshold level. Sum scores reflecting symptom severity [i.e., current or past symptoms, selecting highest symptom scores] were derived for the following domains: psychosis, depression, mania, anxiety and behavior.

Neuroimaging

Anatomical T1-weighted imaging. For each participant, a T1-weighted image was acquired using a 3D Fast Field Echo using parallel imaging sequence (TR/TE 10 ms/4.6 ms; FOV 240×240×160 mm, 200 slices, .75 mm isotropic voxel size). Anatomical T1-scans were preprocessed using FreeSurfer software (Fischl, 2012), including tissue classification and parcellation of the cortex into 114 regions reflecting a subdivision of the Desikan-Killiany atlas (Cammoun et al., 2012; Hagmann et al., 2008).

Diffusion weighted imaging. Two sets of DWI-scans were acquired for each participant; each consisting of 5 unweighted B₀-scans ($b = 1000 \text{ s/mm}^2$) and 30 diffusion-weighted scans (SENSE, p-reduction 3; gradient set of 30 weighting directions; TR/TE = 7035/68 ms, EPI factor 35; FOV 240×240 mm, 2 mm isotropic voxels, non-angulated 75 slices). The second diffusion set was acquired with a reversed k-space readout (van den Heuvel and Sporns, 2011). DWI images were realigned and corrected for eddy currents and susceptibility distortions (Andersson and Skare, 2002). Diffusion directions were determined in each voxel using the compressed sensing based CFARI algorithm (Landman et al., 2012), capable of resolving complex fiber orientations such as crossing fibers. Based on the diffusion profiles, white matter pathways were reconstructed using deterministic tractography. To this end, eight seeds were started per voxel, and for each seed, a tractography streamline was constructed by following the main diffusion direction from voxel to

voxel. Stop criteria included reaching a voxel with a fractional anisotropy $< .1$, making a sharp turn of $> 45^\circ$, reaching a gray matter voxel or exiting the brain mask (van den Heuvel et al., 2013).

Resting-state functional MRI. Resting-state BOLD signals were recorded during 8 minutes (3D PRESTOSENSE, effective TR/TE 22/32 ms with shifted echo, flip-angle 9 degrees, p/s reduction 2/2; dynamic scan time 1.6s, 4mm isotropic voxels, 32 slices covering whole-head). The PRESTOSENSE sequence uses echo shifting, which allows echo times longer than the sequence repetition time and is thus fast enough for fMRI, while maintaining a sufficiently long TE for optimal contrast (van den Heuvel et al., 2008; van Gelderen et al., 2012). Resting-state time series were realigned and co-registered to the T1 image to ensure overlap with the cortical parcellation maps. Time-series were corrected for global effects – including white matter, ventricle and global mean signals and 6 motion parameters – using linear regression, and band-pass filtered (.01 – .1 Hz). To minimize the influence of head-motion on the rs-fMRI data, each slice with frame-wise displacement exceeding .5 (defined as the sum of the absolute derivatives of the six realignment parameters) was scrubbed following the procedure of (Power et al., 2012). There was no significant difference in the number of scrubbed scans between the subject groups (ANOVA, $F = 1.95$, $p = .15$).

Functional connectome reconstruction

Resting-state fMRI data was acquired in a total of 102 out of 127 participants. The rs-fMRI data were examined for outliers in the total number of scrubbed volumes, excluding scans with more than 50% scrubbed volumes, or with major image distortions on visual inspection. This resulted in a total of 25 fMRI scans being discarded, leaving 82 functional connectivity matrices for further analysis. Repeating functional connectome analyses in subjects with a minimum of 5 min fMRI data (Birn et al., 2013) ($N = 74$) did not change the nature of our results.

Rich club organization

A weighted group-averaged network was reconstructed by creating a binary network representation from all connections identified in at least 50% of subjects and, for each connection, averaging connection weights across subjects. A weighted rich club curve was computed for the empirical group-network and examined relative to the average rich club curve of a set of 1000 comparable random networks to determine the extent to which the empirical curve exceeds the random model (van den Heuvel and Sporns, 2011). A normalized rich club curve, computed as the ratio between the empirical and random rich club curve, significantly exceeding 1 over a range of degree k suggests the existence of rich club organization.

Rich club effects at other hub thresholds

In the main analysis, rich club regions were selected for each subject individually as the top 20 ranked highest degree brain regions (reflecting the top 18% highest ranking nodes in terms of degree). To ensure that reported effects were not limited to one particular threshold, rich club connectivity was recomputed for each individual subject over a range of hub thresholds. For each threshold, group-differences in rich club connectivity were examined using the linear mixed model

described in the main text (see “Statistical analysis”).

Linear mixed model

Group-differences in brain network metrics were assessed using a linear mixed model procedure, allowing us to correct for age and gender, as well as family relatedness within the subject groups. Formally:

$$Y = \text{intercept} + \beta_1(\text{group}) + \beta_2(\text{age}) + \beta_3(\text{gender}) + \alpha_1(\text{family}) + \epsilon$$

with β_1 , β_2 , and β_3 representing fixed-effects parameters of the effects of group, age and gender respectively, α representing the random effect of family dependence, and ϵ representing the normally distributed residual error.

Streamline density weighting

Main effects were replicated using streamline density (SD) edge-weights, computed as the number streamlines (NOS) corrected for the average volume of the connecting brain regions.

Effect of age on main findings

The mean age of the BD-offspring was significantly higher than the average age of the SZ-offspring and controls. To assess the influence of age differences on the main findings, an age-matched subgroup of BD-offspring ($N = 39$), with mean (std) age of 12.9 (2.0) years, was identified. This subgroup did not significantly differ in age from either SZ-offspring or controls (both $p > .7$). Main effects were reanalyzed using this BD-offspring subgroup.

Influence of relatedness on main findings

The participants ($N = 127$) originated from a total of 93 families. In the main analyses, within-family dependency entered into the linear mixed model procedure as a random effect term to account for the effect of relatedness. To further assess the influence of within-family dependence, the main findings were reanalyzed in a subset of unrelated individuals ($N = 93$), consisting of all subjects without a participating sibling were included, as well as one randomly selected individual from each set of siblings.

Effect of streamline threshold

A streamline count threshold was used to limit the inclusion of false-positive edges (de Reus and van den Heuvel, 2013) and reduce variance. To examine the influence of this threshold on our findings, the analyses were repeated without applying a streamline threshold.

Supplementary results

Rich club organization

Rich club organization was verified in the current sample, as indicated by an increasing normalized rich club coefficient, significantly exceeding 1 over a range of k (Figure S1).

Rich club effects at other hub thresholds

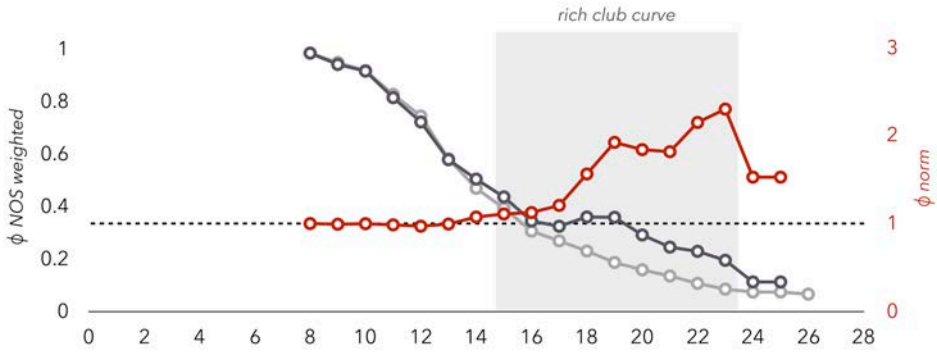


Figure S1. Rich club curve for weighted group-averaged network, with empirical and random curves in dark and light grey respectively, and normalized rich club curve in red, showing an increasing normalized rich club coefficient over a range of $k = 15 - 23$.

Significant group-differences in rich club connectivity were found across a range of rich club thresholds. Specifically, a significant group difference (all $F > 3.25$, $p < .05$) in rich club connectivity was present for each rich club definition between the top 16% – 29% highest-ranking brain regions in terms of degree (see Figure S2).

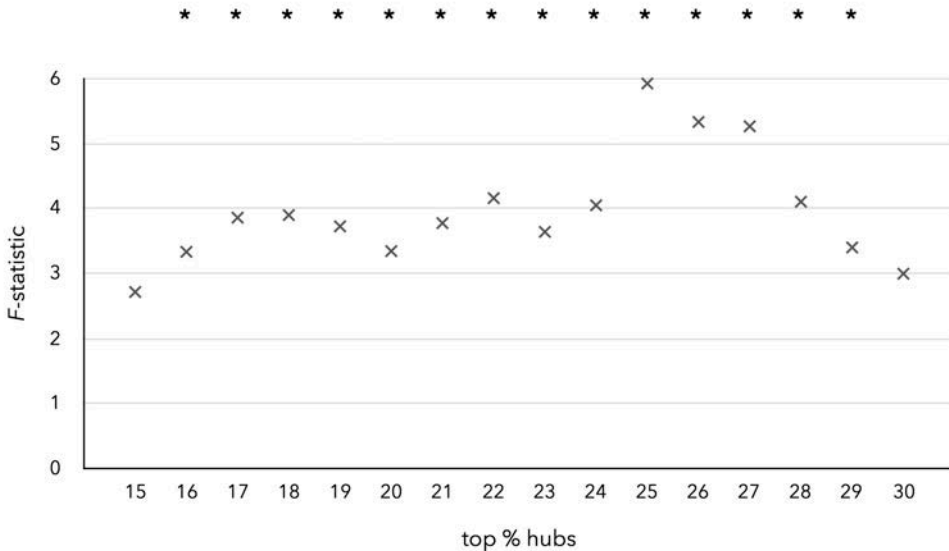


Figure S2. Chart showing F-statistics of group-differences in rich club connectivity for hub thresholds ranging from the top 15% and top 30% highest-degree brain regions. * indicates $p < .05$.

Modular decomposition of functional connectomes

Figure S3 summarizes consensus modular decomposition of functional connectomes for each subject group. Using default resolution parameter $\gamma = 1$, the community detection algorithm (Blondel et al., 2008) resulted in 3 functional modules for each group (Figure S3A), with no significant differences in consensus modular topology between subject groups (controls vs. BD-offspring and SZ-offspring: $p = .39$ and $p = .41$ respectively; BD-offspring vs. SZ-offspring: $p = .58$). Resolution parameter of $\gamma = 1.5$ yielded a total of 8, 9, and 10 modules for controls, BD-offspring, and SZ-offspring respectively (Figure S3B). However, differences between groups in modular decomposition at this resolution were not significant (controls vs. BD-offspring and SZ-offspring: $p = .19$ and $p = .20$ respectively, and BD-offspring vs. SZ-offspring: $p = .94$), indicating that similar group-differences were also common in the random condition.

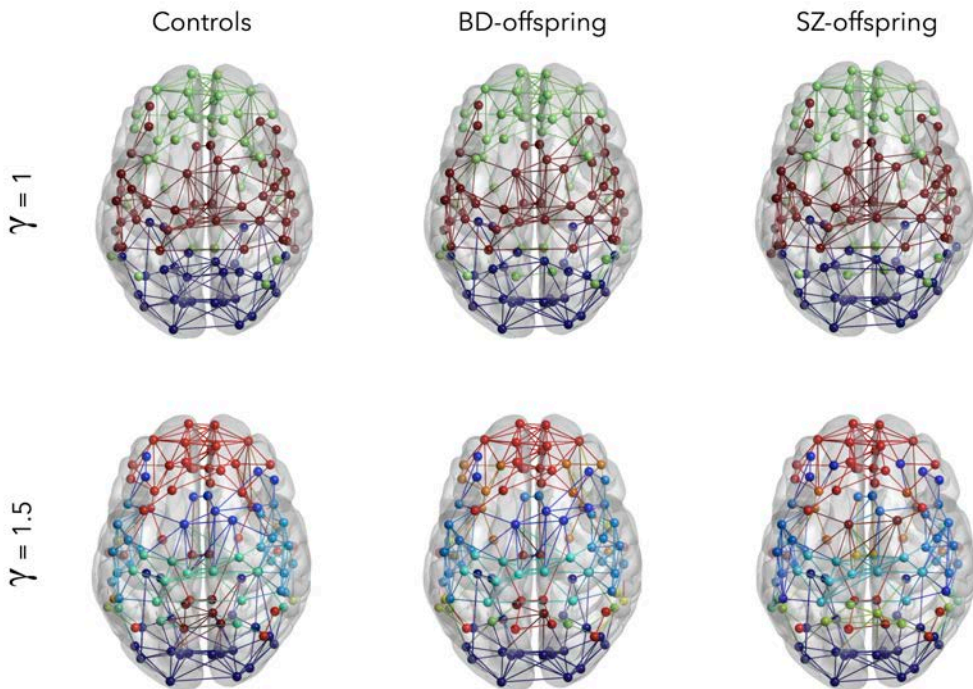


Figure S3. A. Consensus modular decomposition of functional brain networks per subject group with “default” resolution parameter $\gamma = 1$. B. Modular decomposition per subject group using resolution parameter of $\gamma = 1.5$ to detect smaller modules. No significant group-differences in modular decomposition were found at either resolution (both $p > .1$).

Streamline density weighting

Streamline density (SD) weighting (rather than NOS-weighting) of connectome edges did not change the nature of our findings.

Rich club connectivity. Using SD-weighting, there was a marginal effect of rich club connectivity ($F_{(2,122)} = 3.27$, $p_{adj} = .080$). Examining rich club connectivity across a range of hub thresholds revealed (marginally) significant group effects between the top 18% – 32% highest-ranking brain regions in terms of degree, with top 25% yielding maximal group-effects. At this hub threshold, there was a significant group-effect of rich club connectivity ($F_{(2,122)} = 4.82$, $p_{adj} = .019$), with post-hoc tests revealing a significant reduction in SD connectivity in SZ-offspring as compared to both controls ($M_{diff} = -11.4\%$, $SE = 5.0\%$, $p = .023$) and BD-offspring ($M_{diff} = -14.0\%$, $SE = 4.6\%$, $p = .003$).

Functional modularity. Assessing the association between functional modularity and structural rich club SD connectivity revealed a significant negative correlation between Q_{fc} and rich club connectivity in the SZ-offspring ($r = -.69$, $p = .004$), confirming our main results with NOS weighting.

Structural-functional coupling. SD weighting confirmed the main effect of SC-FC coupling of long-distance connections ($F_{(2,77)} = 6.99$, $p_{adj} = .004$), with post-hoc tests indicating a significant increase in SC-FC coupling in both offspring groups relative to controls (SZ-offspring; $M_{diff} = 38.8\%$, $SE = 12.2\%$, $p = .002$ | BD-offspring: $M_{diff} = 3.3\%$ $SE = 9.7\%$, $p = .002$).

Effect of age on main findings

Replicating the analyses using a subgroup of BD-offspring matched on age to the controls ($N = 39$) confirmed our main findings, again showing significant group-effects of rich club connectivity ($F_{(2,122)} = 4.36$, $p_{adj} = .029$) and long-distance SC-FC coupling ($F_{(2,77)} = 7.50$, $p_{adj} = .002$).

Influence of relatedness on main findings

The main results were also replicated in a subset of unrelated individuals ($N = 93$), which confirmed our findings, with significant group-effects of rich club connectivity ($F_{(2,122)} = 3.80$, $p_{adj} = .052$), and long-distance SC-FC coupling ($F_{(2,77)} = 6.88$, $p_{adj} = .004$).

Effect of streamline threshold on main findings

The group-effect of long-distance SC-FC coupling remained intact in the absence of a streamline threshold ($F_{(2,77)} = 6.15$, $p_{adj} = .006$). In the absence of a streamline threshold, the group-effect of rich club connectivity was no longer significant ($F_{(2,122)} = 2.85$, $p_{adj} = .124$). This likely relates to less robust hub definitions when low-streamline connections are included in binary network reconstructions. Indeed, using strength rather than degree as a more sensitive method to define hubs and then reassessing hub-to-hub connectivity in the absence of a streamline threshold did confirm the group-effect of rich club connectivity ($F_{(2,122)} = 4.75$, $p_{adj} = .020$).

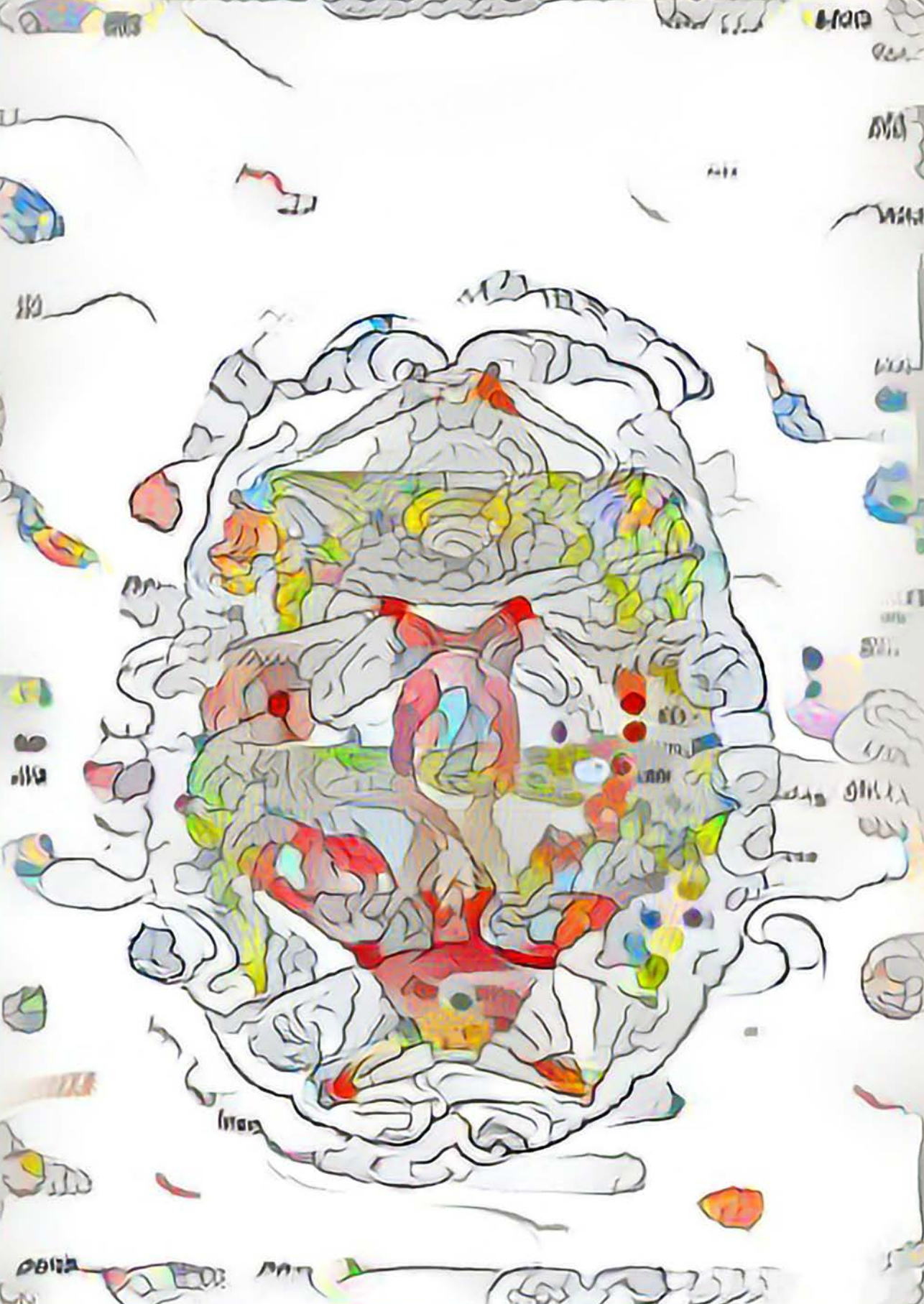
Rich club connectivity in subjects below age 12

To further assess the timing of connectome disruptions in children with genetic predisposition for psychotic illness, a post-hoc analysis was performed subjects below 12 years of age, including 13 SZ-offspring, 14 BP-offspring, and 16 controls with mean (std) ages of 1.3 (.9), 1.7 (.8) and 1.6 (1.0) respectively. Repeating the group-analysis of rich club connectivity in these subjects confirmed the group-effect ($F_{(2,38)} = 6.71$, $p_{adj} = .006$), with significantly lower rich club

connectivity in SZ-offspring relative to controls ($M_{diff} = -31.8\%$, $SE = 8.7\%$, $p_{adj} = .002$).

Supplemental References

- Andersson JL, Skare S (2002) A model-based method for retrospective correction of geometric distortions in diffusion-weighted epi. *Neuroimage* 16:177–99.
- Birn RM, Molloy EK, Patriat R, Parker T, Meier TB, Kirk GR, Nair VA, Meyerand ME, Prabhakaran V (2013) The effect of scan length on the reliability of resting-state fmri connectivity estimates. *Neuroimage* 83:550–558.
- Blondel VD, Guillaume JL, Lambiotte R, Lefebvre E (2008) Fast unfolding of communities in large networks. *Journal of statistical mechanics: theory and experiment* 2008:P10008.
- Cammoun L, Gigandet X, Meskaldji D, Thiran JP, Sporns O, Do KQ, Maeder P, Meuli R, Hagmann P (2012) Mapping the human connectome at multiple scales with diffusion spectrum mri. *Journal of neuroscience methods* 203:386–97.
- de Reus M, van den Heuvel M (2013) Estimating false positives and negatives in brain networks. *Neuroimage* 70:402–9.
- Fischl B (2012) Freesurfer. *NeuroImage* 62:774–781.
- Hagmann P, Cammoun L, Gigandet X (2008) Mapping the structural core of human cerebral cortex. *PLoS biology* 6:e159.
- Landman BA, Bogovic JA, Wan H, ElShahaby FEZ, Bazin PL, Prince JL (2012) Resolution of crossing fibers with constrained compressed sensing using diffusion tensor mri. *NeuroImage* 59:2175–2186.
- Power JD, Barnes KA, Snyder AZ, Schlaggar BL, Petersen SE (2012) Spurious but systematic correlations in functional connectivity mri networks arise from subject motion. *NeuroImage* 59:2142–2154.
- van den Heuvel M, Mandl R, Pol HH (2008) Normalized cut group clustering of resting-state fmri data. *PLoS one* 3:e2001.
- van den Heuvel MP, Sporns O (2011) Rich-club organization of the human connectome. *The Journal of neuroscience : the official journal of the Society for Neuroscience* 31:15775–86.
- van den Heuvel MP, Sporns O, Collin G, Scheewe T, Mandl RCW, Cahn W, Goñáls J, Hulshoff Pol HE, Kahn RS (2013) Abnormal rich club organization and functional brain dynamics in schizophrenia. *JAMA psychiatry (Chicago, Ill.)* 70:783–92.
- van Gelderen P, Duyn JH, Ramsey NF, Liu G, Moonen CT (2012) The presto technique for fmri. *Neuroimage* 62:676–681.



Chapter 12

Summary and Discussion

[Parts of this summary and discussion have been submitted as a review paper to Biological Psychiatry: Cognitive Neuroscience and Neuroimaging]

Studies in the healthy brain have repeatedly demonstrated strong associations between modalities of both micro and macro scales of brain organization in multiple mammalian species. These consistent observations point towards potential common organizational principles where regions with a microscale architecture supportive of a larger computational load have more and stronger connections in the brain network on the macroscale, and where disruptions observed on one organizational scale could modulate the other. In this chapter, we first provide an overview of recent findings on associations between micro and macroscale organization observed in the healthy brain, including both general brain-wide relations and features specific to the topology of highly connected hub regions. Next, we continue with a summary of micro-macro findings reported in the context of brain disorders. We conclude with suggestions for future multiscale connectome comparisons linking multiple scales and modalities, and suggest how such comparisons could contribute to a more complete fundamental understanding of brain organization and associated disease related alterations.

Integrating micro and macro scale information in health

Recent studies combining information on microscale cortical characteristics with macroscale connectivity data have shown micro-macro associations to be present across a wide range of micro and macroscale modalities. These observations have been made in the brains of multiple different mammalian species, including the rodent, cat, macaque and human brain (see for review (van den Heuvel et al., 2016)). Here, we first describe general cortex-wide micro – macro associations in the structural and functional connectome, followed by an overview of characteristics specific to highly connected hub regions.

Structural connectome

Extending the observations of cortical microscale heterogeneity made on the microscale, studies employing tract tracing to study connections of specific regions in the macaque monkey (e.g. (Rockland and Pandya, 1979; Seltzer and Pandya, 1978)) and cat brain (as collated and analyzed by (Scannell et al., 1995)) have shown that the majority of cortical regions are predominantly connected to regions with a similar cytoarchitectural layout, hypothesizing that a large portion of cortical connections occur between regions with similar functional profiles (Barbas, 2015). Most notably layer III pyramidal cell complexity, neuron density, cortical type and gene expression have been shown to be associated with regional macroscale connectivity patterns (e.g. (Beul et al., 2015; Beul and Hilgetag, 2017; Goulas et al., 2016; Krienen et al., 2016; Scholtens et al., 2014)).

Furthermore, neuronal complexity of cortical layer III pyramidal cells – the neuron type and layer hypothesized to constitute the majority of corticocortical connectivity – was associated with the extent of regional corticocortical connectivity. Correlating the degree of corticocortical connectivity of macroscale regions to layer III pyramidal cell complexity in the tract-tracing based macaque connectome (CoCoMac database (Stephan et al., 2001)) showed that those regions with more corticocortical connections also tend to have larger, more branched and more spinous layer III pyramidal cells (Scholtens et al., 2014) [**chapter 2**], indicative of a larger computational capacity in these regions on both the micro and the macro scale. Investigating the relation between microscale characteristics and macroscale connectivity in a different dataset of macaque macroscale tract tracing based connectivity (Markov et al., 2012) showed cortical neuron density to have the strongest association with regional macroscale connectivity (Beul and Hilgetag, 2017), with regions with a lower neuron density having more macroscale connectivity.

In the human brain, cortical regions characterized by larger layer III neuron size tend to have a larger macroscale connectivity strength compared to regions with small neurons in

cortical layer III (van den Heuvel et al., 2015) [**chapter 4**]. A comparison using collated information on morphometry of Golgi-stained layer III pyramidal cells has further shown regions in which layer III pyramidal cells have longer basal dendrites, more spines and higher spine density to have a larger number of corticocortical connections than regions with smaller, less complex layer III pyramidal cells (van den Heuvel et al., 2016) (Figure 1b) [**chapter 3**].

The cytoarchitectonic structural type of cortical regions may also play an important role in the formation of long-range connectivity. Combining regional cytoarchitectural cortical type and tract-tracing based corticocortical connectivity in the cat connectome showed that the majority of regions generally connect with other regions of the same cortical type (Beul et al., 2015), and that more agranular multimodal association regions tend to have a larger number of macroscale corticocortical connections than regions of other cortical types (Beul et al., 2015). Furthermore, architectonic similarity has been shown to be strongly related to a region's laminar projection pattern as well as its number of corticocortical connections. This suggests microscale cortical architecture to be a strong predictor for macroscale connectivity patterns (Beul et al., 2017). These findings were supported by observations in rodents, reporting on a similar association between cytoarchitectural similarity and corticocortical connectivity (Goulas et al., 2017). Extending these observations, studies in the human brain have shown similar findings with cytoarchitecturally similar regions, showing strong correspondence specifically in supragranular neuron density to be preferentially connected to each other (Goulas et al., 2016) (Figure 1a).

Further evidence of a potential relationship between cytoarchitectonic organization of cortical areas and their connectivity may come from studies combining information from genetics and imaging. A first study combining information on cortical gene expression with the macroscale structural connectome in the rodent brain showed that regions with similar gene expression profiles tend to have similar projection patterns and that connected regions have more similar gene expression (French and Pavlidis, 2011).

Taken together, observations are indicative of a cortical organization in which the majority of connections in the network occur locally between regions of similar macroscale makeup. Furthermore, regions with microscale morphology supportive of larger computational capacity tend to have more macroscale corticocortical connections, facilitating high integration of information across modalities.

Functional connectome

Multimodal studies investigating the putative relation between microscale

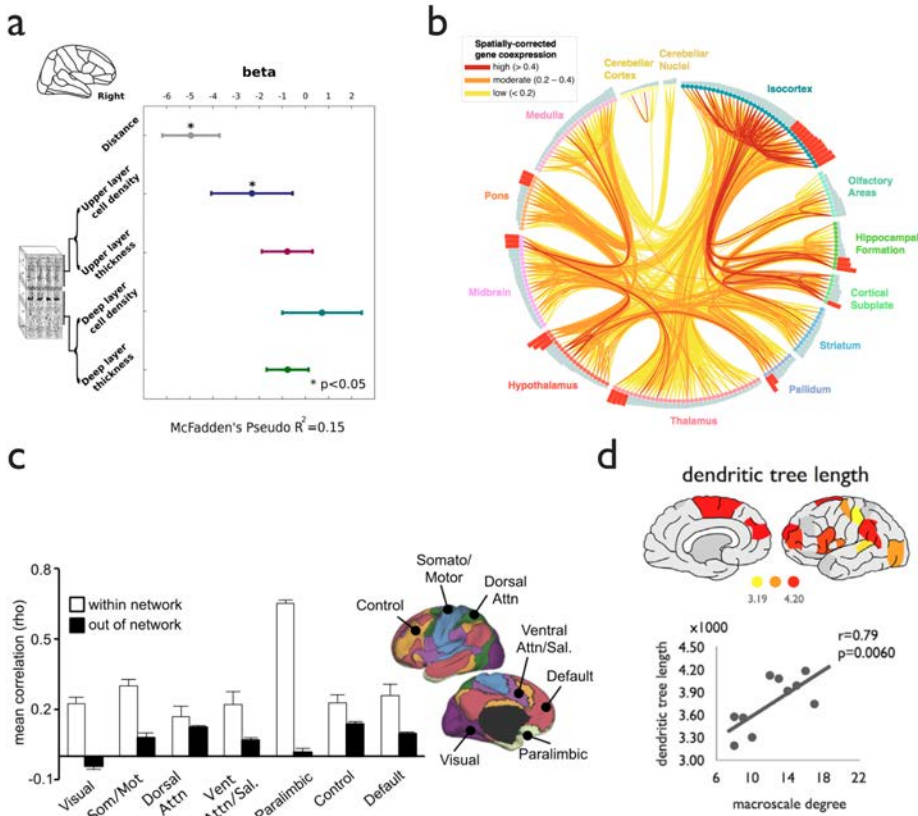


Figure 1. Examples of associations between micro and macroscale organization in the healthy brain. A) Investigating the relation between the presence and absence of macroscale connections and microscale structural traits resulted in a good fit for physical distance between regions and similarity in supragranular neuron density (figure shows results for the right hemisphere)(Goulas et al., 2016); B) Combining regional gene expression data with connectivity in the mouse brain revealed a link between molecular function and neuronal connectivity, showing highly correlated gene expression of hub regions specifically in genes involved in synthesis and metabolism of ATP (the primary energetic currency of neuronal communication) (Fulcher and Fornito, 2016); C) Linking regional gene expression profiles with information on resting state functional network membership showed regions that are part of the same functional network to have highly correlated gene expression patterns (Krienen et al., 2016); D) Combining microscale data on Golgi-based layer III pyramidal cell morphology with macroscale data on diffusion-weighted MRI-based corticocortical connectivity showed larger microscale pyramidal cell complexity to be associated with more macroscale structural connections (van den Heuvel et al., 2016).

chemoarchitecture and functional connectivity measures have shown regions with a larger proportion of excitatory vs inhibitory neurotransmitter receptor levels to have stronger functional connections (Turk et al., 2016; van den Heuvel et al., 2016), [chapter 7 & 8]. Linking a region's microscale cytoarchitectural profile with its

macroscale connectivity to different resting state functional networks (such as described in e.g. (Yeo et al., 2011)) showed cortical regions with high between-network connectivity to have a cytoarchitectural makeup characterized by an absent or disrupted layer IV (Wylie et al., 2015). This is suggestive of an absence of layer IV to be a potential organizational characteristic for inter-network communication hubs (Wylie et al., 2015), in line with observations in micro-macro associations in the structural connectome of the cat (Beul et al., 2015). Likewise, similarity in cortical microstructural myeloarchitecture has been related to shared membership of functional connectivity networks (modules) in MEG (Hunt et al., 2016) as well as in resting state fMRI (Huntenburg et al., 2017). Additionally, analysis of the postsynaptic proteome in 12 Brodmann Areas of the human cortex revealed each region to have a distinct proteomic signature reflecting regional functional differences, when linked to fMRI and positron emission tomography (PET), as well as genetic and behavioral data (Roy et al., 2018).

Furthermore, studies combining functional connectomics with information on gene expression showed cortical gene expression of genes enriched in human supragranular cortical layers to be more similar within than between functional networks (Krienen et al., 2016) (Figure 1c), and correlated gene expression of genes enriched for ion channels to be associated with membership of resting state functional networks (Richiardi et al., 2015). These findings are again indicative of regions with similar microscale organization to have an increased likelihood of being interconnected.

Micro-macro in highly connected hub regions

Adding to these general cortex-wide trends, comparisons between highly connected hub regions and less well connected peripheral regions have shown hub regions to be associated with differential microscale regional profiles. Combining tract tracing connectivity and regional gene expression profiles in the rat brain showed hub regions to have increased expression of genes involved in cellular energy metabolism (Fulcher and Fornito, 2016) (Figure 1b). Additionally, hub regions in the macaque as well as in the human connectome have larger layer III pyramidal cells, with a higher spine density than peripheral regions (Scholtens et al., 2014; van den Heuvel et al., 2016) [**chapter 2 & 3**], characteristics hypothesized to be related to a neuron's larger integrative and computational capacity (Koch, 1997; McCulloch and Pitts, 1943). Hub regions in the cat brain have been demonstrated to on average be of a more agranular structural type than non-hubs (Beul et al., 2015).

Interestingly, these findings are supported by computer simulations. In line with the findings based on histological microscale measures in the mammalian cortex, a recent *in silico* study implementing graph theoretical analyses within a set of simulated rat somatosensory cortical columns showed those neurons with the largest dendritic trees to

be highly connected hubs within the microscale cortical column (Gal et al., 2017).

Taken together, combining micro and macroscale information on brain organization provides a promising novel avenue in gaining better understanding of the function of the brain as a whole.

Micro and macroscale integration in brain disorders

Alterations in relation to neuropsychiatric disorders have been reported by studies on both the micro and macroscale of cortex organization. In recent years, some first studies have been presented that combine both scales of observation in brain disorders. Such across-scale approaches to understanding brain function in disease could provide promising new mechanistic insights. In the following paragraphs, we overview and discuss recent micro-macro findings reported in Alzheimer's disease and schizophrenia.

Alzheimer's disease is neuroanatomically characterized by amyloid-beta plaque depositions and tau-tangles, as well as regional loss of dendritic spines, together with progressive loss of cortical gray and white matter (Tackenberg et al., 2009). On the macroscale, neuroimaging studies investigating brain structure have consistently reported on loss cortical volume in line with observations on the microscale (McDonald et al., 2009; Thompson et al., 2003). Connectome studies in Alzheimer's have reported highly connected hub regions to consistently be affected, both in resting-state functional connectivity (Buckner et al., 2009) as well as in the DWI derived structural connectome (Lo et al., 2010). These observations suggest hub regions to somehow be more vulnerable or to at least play a contributing role in the disease processes of the disorder. Indeed, Buckner and colleagues showed a clear voxel-to-voxel association between PET amyloid-beta deposition estimates and degree of resting-state functional connectivity in Alzheimer's disease (Buckner et al., 2009) (Figure 2a), demonstrating that – also on the microscale – more highly connected regions tend to be preferentially affected in Alzheimer's disorder. These findings have since been replicated in the structural connectome of Alzheimer's patients (Prescott et al., 2014).

There are multiple hypotheses as to why highly connected hub regions tend to be most affected in Alzheimer's disease. Their central position in the brain network could mean that any disease-related alterations starting in the periphery could accumulate in the hubs (Crossley et al., 2014). In addition to the contribution of topology, hub connections have been suggested to be biologically expensive. Hub connections span longer distances (van den Heuvel et al., 2012), and the higher blood flow and metabolic rate observed in hub regions (Bullmore and Sporns, 2012; Vaishnavi et al., 2010) has been hypothesized to reflect an increased demand posed on the cellular infrastructure

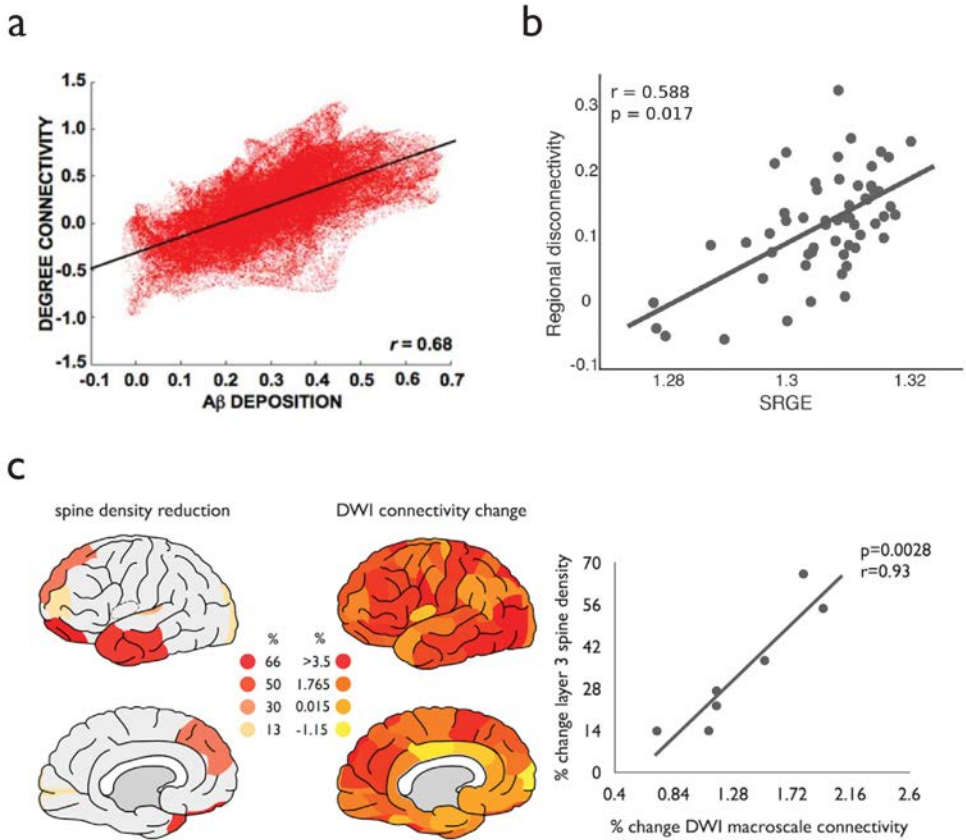


Figure 2. Examples of associations between micro and macroscale organization in brain disorders. **A)** Buckner and colleagues combined PET-based data on β -amyloid deposition with resting state functional connectivity in Alzheimer's disease, showing a larger voxel-wise β -amyloid deposition (x -axis) to be associated with larger functional connectivity (y -axis) (Buckner et al., 2009); **B)** Combining Allan Human Brain Atlas data on gene expression in the healthy human brain with data on region-wise corticocortical disconnectivity in schizophrenia patients showed those regions with higher schizophrenia risk gene expression (SRGE, x -axis) to have larger regional disconnectivity (y -axis) in schizophrenia patients (Romme et al., 2017); **C)** Linking collated literature data on regional changes in microscale layer III pyramidal cell spine density in schizophrenia patients to information on macroscale disconnectivity in schizophrenia showed a positive association between % change in macroscale connectivity (x -axis) and % change in layer III spine density (y -axis) (van den Heuvel et al., 2016).

within hub regions. This increased demand on hub regions and their connections has been hypothesized to lead to increased wear and tear and ultimately to an increased accumulation of amyloid beta depositions in hub regions in Alzheimer's disease (Buckner et al., 2009). Indeed, micro scale *in vivo* regional synaptic activity has been associated with increased vulnerability to amyloid beta deposition (Bero et al., 2011;

Cirrito et al., 2005; Walker and Jucker, 2011). In a simulation study combining both scales of information, degradation of highly connected hub regions in Alzheimer's disease was reported to be dependent on the spike density within a region (de Haan et al., 2012). Together, these findings provide an illustration of how functional characteristics at the micro and macro scale of a brain disorder interact, and how alterations on one scale can modulate the other.

Multiple observations of a potential interaction between disease effects on the microscale and macroscale of brain organization have been reported in schizophrenia. Schizophrenia is a heterogeneous disorder characterized by hallucinations, delusions, loss of initiative and cognitive dysfunction, and has since long been hypothesized to be a disorder of brain dysconnectivity (e.g. (Friston, 1998; Stephan et al., 2009)). Magnetic resonance imaging studies have revealed consistent wide-spread disconnectivity patterns in schizophrenia patients (e.g. (Ellison-Wright et al., 2008; Kanaan et al., 2005; Kubicki et al., 2005; Stephan et al., 2009)). Additionally, connectomics studies in both resting-state functional connectivity and diffusion-weighted connectomes have reported abnormalities in network organization (Bassett et al., 2008; Fornito et al., 2012; He et al., 2008; Lynall et al., 2010), and specifically in connection strength (Griffa et al., 2015; Skudlarski et al., 2010; van den Heuvel et al., 2013) between hubs in the connectome.

On the microscale, studies have reported on reductions in spine density in cortical association areas (e.g. (Garey et al., 1998; Glantz and Lewis, 2000)), and Lewis and colleagues have suggested a specific role of layer III pyramidal cells in schizophrenia (Kolluri et al., 2005; Pierrri et al., 2001). Furthermore, observations have been made of abnormal cell migration (more neurons found remaining in subcortical white matter, indicating potential problems in neuronal migration (Connor et al., 2011)), altered distribution and density of cortical interneurons (e.g. (Akbarian et al., 1993; Ikeda et al., 2004)) and a potential increased neuroinflammatory response in schizophrenia (Trépanier et al., 2016). While mostly examined separately, these reported effects on the macro- and microscale are potentially related to each other.

Linking both scales of information in schizophrenia, a potential association between microscale spine density reductions on layer III pyramidal cells and macroscale disruptions of rich club connectivity has been observed (van den Heuvel et al., 2016) (Figure 2c) [**chapter 3**]. Furthermore, combining regional gene expression profiles of the healthy brain has shown those regions with higher schizophrenia risk gene expression to display more severely affected macroscale connectivity (Romme et al., 2017) (Figure 2b).

Summary and future perspectives

Strong micro-macro associations have been observed in connectomes of many species and across a wide range of modalities. Microscale regional characteristics are consistently associated to, or even predictive of macroscale connectivity patterns. Similar multiscale connectomics patterns have been reported in both the structural and in the functional connectome, with most brain regions primarily connecting to other regions with similar microscale characteristics. Conversely, a relatively small subset of highly connected multimodal hub regions is characterized on the microscale by an agranular cortical type, larger neuron complexity and gene expression profiles supportive of increased cellular signaling and metabolism.

Considering the wide variety of measures reported to be associated with macroscale connectivity, some notable overlap between characteristics can be observed. Broadly, two types of micro-macro associations can be observed. The first concerns a general observation that regions that share a connection (be it structural or functional) tend to have larger microscale architectural similarity than unconnected regions (see for instance (Beul et al., 2017; Goulas et al., 2016; Huntenburg et al., 2017; Krienen et al., 2016)). The second observation is that cortical regions that have a larger number of connections to the rest of the brain tend to have a different microscale architecture than regions with fewer connections. More highly connected (hub) regions tend to be of a more agranular structural type (Beul et al., 2015; Wylie et al., 2015) and to have a more complex neuronal morphology (Scholtens et al., 2014; van den Heuvel et al., 2016) [chapter 2 & 3] supportive of increased integrative and computational capacities.

Multiscale connectomics studies into (early) brain development could provide novel insights as to *when* and *how* the micro – macro associations observed in the adult brain arise. Exploring potential temporal dynamics of plasticity and aging in the interplay between micro and macroscale brain organization would be of great interest. In parallel, studies into mechanisms of brain disorders employing multiscale connectomics could extend micro-macro comparisons to other brain disorders, such as for example autism spectrum disorder, attention deficit hyperactivity disorder, amyotrophic lateral sclerosis or Huntington’s disease.

Advancing from comparisons employing information collated across different sources and individuals for multiscale connectomics studies, ideally future endeavors would aim to directly compare high resolution brain-wide multiscale data within individual subjects. A non-exhaustive list of measures of interest could include “classical” measures such as neuron density, neuron morphometry, myelination, and synapse

density such as collated previously across literature. These could be complimented by quantification of other microscale measures such as glial and specific interneuron density, inflammatory markers, or brain-wide layer specific gene expression profiles together with high-resolution neuroimaging protocols. Such a broad large-scale data acquisition is a monumental task, and the feasibility of such an endeavor would arguably be for a large part dependent on innovations in automated tissue processing and quantification, as well as big data type analyses. Nevertheless, direct multiscale observations in multiple subjects, or even across control and patient groups could provide a great leap in our understanding of the interplay of multiple scales of brain organization in health, as well as in brain disease.

Final words

This thesis examined the interplay of microscale cortical architecture and macroscale connectomics. Specifically, we aimed to assess how regional variability observed on the microscale of cortex organization is associated to a region's macroscale connectivity pattern. We indeed observed a clear association between microscale architecture and macro scale connectivity. Based on our findings, regions with a microscale cortical architecture supportive of more complex integrative and computational processing tend to have more macroscale connectivity. We observed a similar relation in schizophrenia – described as a disorder of disconnectivity – where alterations in microscale spine density are associated with disconnectivity on the macroscale. Taken together, we propose that multiscale, multimodal connectomics such as applied in this thesis is a promising new avenue of neuroscience research that could contribute to a more complete fundamental understanding of brain organization and associated disease related alterations.

References

- Akbarian S, Bunney WE, Potkin SG, Wigal SB, Hagman JO, Sandman CA, Jones EG (1993) Altered distribution of nicotinamide-adenine dinucleotide phosphate diaphorase cells in frontal lobe of schizophrenics implies disturbances of cortical development. *Archives of general psychiatry* 50:169–177.
- Barbas H (2015) General cortical and special prefrontal connections: Principles from structure to function. *Annual Review of Neuroscience* 38:269–289.
- Bassett DS, Bullmore E, Verchinski BA, Mattay VS, Weinberger DR, Meyer-Lindenberg A (2008) Hierarchical organization of human cortical networks in health and schizophrenia. *J Neurosci* 28:9239–48.
- Bero AW, Yan P, Roh JH, Cirrito JR, Stewart FR, Raichle ME, Lee JM, Holtzman DM (2011) Neuronal activity regulates the regional vulnerability to amyloid- β deposition. *Nature neuroscience* 14:750–756.
- Beul SF, Barbas H, Hilgetag CC (2017) A predictive structural model of the primate connectome. *Scientific Reports* 7:43176.
- Beul SF, Grant S, Hilgetag CC (2015) A predictive model of the cat cortical connectome based on cytoarchitecture and distance. *Brain Structure and Function* 220:3167–3184.
- Beul SF, Hilgetag CC (2017) Neuron density is a fundamental determinant of structural connectivity in the primate cerebral cortex. *bioRxiv* p. 117051.
- Buckner RL, Sepulcre J, Talukdar T, Krienen FM, Liu H, Hedden T, Andrews-Hanna JR, Sperling RA, Johnson KA (2009) Cortical hubs revealed by intrinsic functional connectivity: mapping, assessment of stability, and relation to alzheimer’s disease. *J Neurosci* 29:1860–73.
- Bullmore E, Sporns O (2012) The economy of brain network organization. *Nature reviews. Neuroscience* 13:336–49.
- Cirrito JR, Yamada KA, Finn MB, Sloviter RS, Bales KR, May PC, Schoepp DD, Paul SM, Mennerick S, Holtzman DM (2005) Synaptic activity regulates interstitial fluid amyloid- β levels in vivo. *Neuron* 48:913–922.
- Connor CM, Crawford BC, Akbarian S (2011) White matter neuron alterations in schizophrenia and related disorders. *International Journal of Developmental Neuroscience* 29:325–334.
- Crossley NA, Mechelli A, Scott J, Carletti F, Fox PT, McGuire P, Bullmore ET (2014) The hubs of the human connectome are generally implicated in the anatomy of brain disorders. *Brain* 137:2382–95.

- de Haan W, Mott K, van Straaten ECW, Scheltens P, Stam CJ (2012) Activity dependent degeneration explains hub vulnerability in alzheimer's disease. *PLOS Computational Biology* 8:e1002582.
- Ellison-Wright I, Glahn DC, Laird AR, Thelen SM, Bullmore E (2008) The anatomy of first-episode and chronic schizophrenia: an anatomical likelihood estimation meta-analysis. *American Journal of Psychiatry* 165:1015–1023.
- Fornito A, Zalesky A, Pantelis C, Bullmore ET (2012) Schizophrenia, neuroimaging and connectomics. *NeuroImage* 62:2296–2314.
- French L, Pavlidis P (2011) Relationships between gene expression and brain wiring in the adult rodent brain. *PLoS computational biology* 7:e1001049.
- Friston KJ (1998) The disconnection hypothesis. *Schizophr Res* 30:115–25.
- Fulcher BD, Fornito A (2016) A transcriptional signature of hub connectivity in the mouse connectome. *Proceedings of the National Academy of Sciences of the United States of America* 113:1435–1440.
- Gal E, London M, Globerson A, Ramaswamy S, Reimann MW, Muller E, Markram H, Segev I (2017) Rich cell-type-specific network topology in neocortical microcircuitry. *Nat Neurosci* 20:1004–1013.
- Garey LJ, Ong WY, Patel TS, Kanani M, Davis A, Mortimer AM, Barnes TRE, Hirsch SR (1998) Reduced dendritic spine density on cerebral cortical pyramidal neurons in schizophrenia. *Journal of Neurology, Neurosurgery & Psychiatry* 65:446–453.
- Glantz LA, Lewis DA (2000) Decreased dendritic spine density on prefrontal cortical pyramidal neurons in schizophrenia. *Arch Gen Psychiatry* 57:65–73.
- Goulas A, Uylings HB, Hilgetag CC (2017) Principles of ipsilateral and contralateral cortico-cortical connectivity in the mouse. *Brain Structure and Function* 222:1281–1295.
- Goulas A, Werner R, Beul SF, Saering D, van den Heuvel M, Triarhou LC, Hilgetag CC (2016) Cytoarchitectonic similarity is a wiring principle of the human connectome. *bioRxiv* p. 068254.
- Griffa A, Baumann PS, Ferrari C, Do KQ, Conus P, Thiran J, Hagmann P (2015) Characterizing the connectome in schizophrenia with diffusion spectrum imaging. *Human brain mapping* 36:354–366.
- He Y, Chen Z, Evans A (2008) Structural insights into aberrant topological patterns of large-scale cortical networks in alzheimer's disease. *The Journal of Neuroscience* 28:4756–4766.
- Hunt BAE, Tewarie PK, Mouglin OE, Geades N, Jones DK, Singh KD, Morris PG, Gowland PA, Brookes MJ (2016) Relationships between cortical myeloarchitecture and electrophysiological

- networks. *Proceedings of the National Academy of Sciences of the United States of America* 113:13510–13515.
- Huntenburg JM, Bazin PL, Goulas A, Tardif CL, Villringer A, Margulies DS (2017) A systematic relationship between functional connectivity and intracortical myelin in the human cerebral cortex. *Cereb Cortex* 27:981–997.
- Ikeda K, Ikeda K, Iritani S, Ueno H, Niizato K (2004) Distribution of neuropeptide y interneurons in the dorsal prefrontal cortex of schizophrenia. *Progress in Neuro-Psychopharmacology and Biological Psychiatry* 28:379–383.
- Kanaan RA, Kim JS, Kaufmann WE, Pearlson GD, Barker GJ, McGuire PK (2005) Diffusion tensor imaging in schizophrenia. *Biol Psychiatry* 58:921–9.
- Koch C (1997) Computation and the single neuron. *Nature* 385:207–210.
- Kolluri N, Sun Z, Sampson AR, Lewis DA (2005) Lamina-specific reductions in dendritic spine density in the prefrontal cortex of subjects with schizophrenia. *Am J Psychiatry* 162:1200–2.
- Krienen FM, Yeo BTT, Ge T, Buckner RL, Sherwood CC (2016) Transcriptional profiles of supragranular-enriched genes associate with corticocortical network architecture in the human brain. *Proceedings of the National Academy of Sciences* 113:E469–E478.
- Kubicki M, Park H, Westin CF, Nestor PG, Mulkern RV, Maier SE, Niznikiewicz M, Connor E, Levitt JJ, Frumin M (2005) Dti and mtr abnormalities in schizophrenia: analysis of white matter integrity. *Neuroimage* 26:1109–1118.
- Lo CY, Wang PN, Chou KH, Wang J, He Y, Lin CP (2010) Diffusion tensor tractography reveals abnormal topological organization in structural cortical networks in alzheimer's disease. *The Journal of Neuroscience* 30:16876–16885.
- Lynall ME, Bassett DS, Kerwin R, McKenna PJ, Kitzbichler M, Muller U, Bullmore E (2010) Functional connectivity and brain networks in schizophrenia. *The Journal of Neuroscience* 30:9477–9487.
- Markov NT, Ercsey-Ravasz MM, Ribeiro Gomes aR, Lamy C, Magrou L, Vezoli J, Misery P, Falchier a, Quilodran R, Gariel Ma, Sallet J, Gamanut R, Huissoud C, Clavagnier S, Giroud P, Sappey-Marinié D, Barone P, Dehay C, Toroczkai Z, Knoblauch K, Van Essen DC, Kennedy H (2012) A weighted and directed interareal connectivity matrix for macaque cerebral cortex. *Cerebral cortex (New York, N.Y. : 1991)* pp. 1–20.
- McCulloch WS, Pitts W (1943) A logical calculus of the ideas immanent in nervous activity. *The bulletin of mathematical biophysics* 5:115–133.
- McDonald CR, McEvoy LK, Gharapetian L, Fennema-Notestine C, Hagler DJ, Holland D, Koyama

- A, Brewer JB, Dale AM, For the Alzheimer's Disease Neuroimaging I (2009) Regional rates of neocortical atrophy from normal aging to early alzheimer disease. *Neurology* 73:457–465.
- Pierri JN, Volk CL, Auh S, Sampson A, Lewis DA (2001) Decreased somal size of deep layer 3 pyramidal neurons in the prefrontal cortex of subjects with schizophrenia. *Archives of general psychiatry* 58:466–473.
- Prescott JW, Guidon A, Doraiswamy PM, Choudhury KR, Liu C, Petrella JR, Initiative FtADN (2014) The alzheimer structural connectome: Changes in cortical network topology with increased amyloid plaque burden. *Radiology* 273:175–184.
- Richiardi J, Altmann A, Milazzo AC, Chang C, Chakravarty MM, Banaschewski T, Barker GJ, Bokde AL, Bromberg U, Buchel C, Conrod P, Fauth-Buhler M, Flor H, Frouin V, Gallinat J, Garavan H, Gowland P, Heinz A, Lemaitre H, Mann KF, Martinot JL, Nees F, Paus T, Pausova Z, Rietschel M, Robbins TW, Smolka MN, Spanagel R, Strohle A, Schumann G, Hawrylycz M, Poline JB, Greicius MD (2015) Brain networks. correlated gene expression supports synchronous activity in brain networks. *Science* 348:1241–4.
- Rockland K, Pandya D (1979) Laminar origins and terminations of cortical connections of the occipital lobe in the rhesus monkey. *Brain research* 179:3–20.
- Romme IAC, de Reus MA, Ophoff RA, Kahn RS, van den Heuvel MP (2017) Connectome disconnectivity and cortical gene expression in patients with schizophrenia. *Biological Psychiatry* 81:495–502.
- Roy M, Sorokina O, Skene N, Simonnet C, Mazzo F, Zwart R, Sher E, Smith C, Armstrong JD, Grant SG (2018) Proteomic analysis of postsynaptic proteins in regions of the human neocortex. *Nature neuroscience* 21:130.
- Scannell JW, Blakemore C, Young MP (1995) Analysis of connectivity in the cat cerebral cortex. *The Journal of neuroscience : the official journal of the Society for Neuroscience* 15:1463–83.
- Scholtens LH, Schmidt R, de Reus MA, van den Heuvel MP (2014) Linking macroscale graph analytical organization to microscale neuroarchitectonics in the macaque connectome. *The Journal of Neuroscience* 34:12192–12205.
- Seltzer B, Pandya DN (1978) Afferent cortical connections and architectonics of the superior temporal sulcus and surrounding cortex in the rhesus monkey. *Brain Research* 149:1–24.
- Skudlarski P, Jagannathan K, Anderson K, Stevens MC, Calhoun VD, Skudlarska BA, Pearlson G (2010) Brain connectivity is not only lower but different in schizophrenia: a combined anatomical and functional approach. *Biol Psychiatry* 68:61–9.
- Stephan KE, Friston KJ, Frith CD (2009) Dysconnection in schizophrenia: from abnormal synaptic plasticity to failures of self-monitoring. *Schizophr Bull* 35:509–27.

- Stephan KE, Kamper L, Bozkurt a, Burns Ga, Young MP, Kötter R (2001) Advanced database methodology for the collation of connectivity data on the macaque brain (cocomac). *Philosophical transactions of the Royal Society of London. Series B, Biological sciences* 356:1159–86.
- Tackenberg C, Ghori A, Brandt R (2009) Thin, stubby or mushroom: spine pathology in alzheimer's disease. *Current Alzheimer research* 6:261–268.
- Thompson PM, Hayashi KM, de Zubicaray G, Janke AL, Rose SE, Semple J, Herman D, Hong MS, Dittmer SS, Doddrell DM, Toga AW (2003) Dynamics of gray matter loss in alzheimer's disease. *J Neurosci* 23:994–1005.
- Trépanier M, Hopperton K, Mizrahi R, Mechawar N, Bazinet R (2016) Postmortem evidence of cerebral inflammation in schizophrenia: a systematic review. *Molecular psychiatry* .
- Turk E, Scholtens LH, van den Heuvel MP (2016) Cortical chemoarchitecture shapes macroscale effective functional connectivity patterns in macaque cerebral cortex. *Human Brain Mapping* 37:1856–1865.
- Vaishnavi SN, Vlassenko AG, Rundle MM, Snyder AZ, Mintun MA, Raichle ME (2010) Regional aerobic glycolysis in the human brain. *Proceedings of the National Academy of Sciences* 107:17757–17762.
- van den Heuvel MP, Bullmore ET, Sporns O (2016) Comparative connectomics. *Trends Cogn Sci* 20:345–61.
- van den Heuvel MP, Scholtens LH, de Reus MA, Kahn RS (2016) Associated microscale spine density and macroscale connectivity disruptions in schizophrenia. *Biol Psychiatry* 80:293–301.
- van den Heuvel MP, Kahn RS, Goñi J, Sporns O (2012) High-cost, high-capacity backbone for global brain communication. *Proceedings of the National Academy of Sciences of the United States of America* 109:11372–11377.
- van den Heuvel MP, Scholtens LH, Feldman Barrett L, Hilgetag CC, de Reus MA (2015) Bridging cytoarchitectonics and connectomics in human cerebral cortex. *The Journal of Neuroscience* 35:13943–13948.
- van den Heuvel MP, Scholtens LH, Turk E, Mantini D, Vanduffel W, Feldman Barrett L (2016) Multimodal analysis of cortical chemoarchitecture and macroscale fmri resting-state functional connectivity. *Human brain mapping* 37:3103–3113.
- van den Heuvel MP, Sporns O, Collin G, Scheewe T, Mandl RCW, Cahn W, Goñi J, Hulshoff Pol HE, Kahn RS (2013) Abnormal rich club organization and functional brain dynamics in schizophrenia. *JAMA psychiatry (Chicago, Ill.)* 70:783–92.

- Walker LC, Jucker M (2011) Amyloid by default. *Nature neuroscience* 14:669–670.
- Wylie KP, Kronberg E, Maharajh K, Smucny J, Cornier MA, Tregellas JR (2015) Between-network connectivity occurs in brain regions lacking layer iv input. *NeuroImage* 116:50–58.
- Yeo BT, Krienen FM, Sepulcre J, Sabuncu MR, Lashkari D, Hollinshead M, Roffman JL, Smoller JW, Zöllei L, Polimeni JR (2011) The organization of the human cerebral cortex estimated by intrinsic functional connectivity. *Journal of neurophysiology* 106:1125–1165.

List of publications

First and second author

- Scholtens LH**, van den Heuvel MP (submitted) Multimodal connectomics in psychiatry: bridging scales from micro to macro. *Biological Psychiatry: Cognitive Neuroscience & Neuroimaging*.
- Collin G, **Scholtens LH**, Kahn RS, Hillegers MH, van den Heuvel MP, (2017) Affected anatomical rich club and structural-functional coupling in young offspring of schizophrenia and bipolar disorder patients. *Biological Psychiatry* 82: 746–755.
- Scholtens LH**, de Reus MA, de Lange SC, Schmidt R, van den Heuvel MP (2016) An MRI Von Economo – Koskinas atlas. *NeuroImage* epub Dec 28.
- Turk* E, **Scholtens LH***, van den Heuvel MP (2016) Cortical chemoarchitecture shapes macroscale effective functional connectivity patterns in macaque cerebral cortex. *Human Brain Mapping* 37:1856–1865.
- van den Heuvel MP, **Scholtens LH**, Turk E, Mantini D, Vanduffel W, Feldman Barrett L (2016) Multimodal analysis of cortical chemoarchitecture and macroscale fmri resting-state functional connectivity. *Human Brain Mapping* 37:3103–3113.
- Scholtens LH**, de Reus MA, van den Heuvel MP (2015) Linking contemporary high resolution magnetic resonance imaging to the von economo legacy: A study on the comparison of MRI cortical thickness and histological measurements of cortical structure. *Human Brain Mapping* 36:3038–3046.
- Marqués-Iturria I, **Scholtens LH**, Garolera M, Pueyo R, García-García I, González-Tartiere P, Segura B, Junqué C, Sender-Palacios M, Vernet-Vernet M et al. (2015) Affected connectivity organization of the reward system structure in obesity. *NeuroImage* 111:100–106.
- van den Heuvel MP, **Scholtens LH**, de Reus MA, Kahn RS (2015) Associated microscale spine density and macroscale connectivity disruptions in schizophrenia. *Biological Psychiatry* 80:293–301.
- van den Heuvel MP, **Scholtens LH**, Barrett LF, Hilgetag CC, de Reus MA (2015) Bridging cytoarchitectonics and connectomics in human cerebral cortex. *The Journal of Neuroscience* 35:13943–13948.
- van den Heuvel MP, **Scholtens LH**, de Reus MA (2015) Topological organization of connectivity strength in the rat connectome. *Brain Structure and Function* pp. 1–18.
- Scholtens LH**, Schmidt R, de Reus MA, van den Heuvel MP (2014) Linking macroscale graph analytical organization to microscale neuroarchitectonics in the macaque connectome. *The*

List of publications

Journal of Neuroscience 34:12192–12205.

Other publications

Keunen K, Benders MJ, Leemans A, van Haastert IC, Fieret-Stam PC, **Scholtens LH**, Viergever MA, Kahn RS, Groenendaal F, de Vries LS, van den Heuvel MP (2017) White matter maturation in the neonatal brain is predictive of school age cognitive capacities in children born very preterm. *Dev Med Child Neurol* 59: 939–946.

Chang X, Collin G, Xi Y, Cui L, **Scholtens LH**, Sommer IE, Wang H, Yin H, Kahn RS, van den Heuvel MP (2017) Resting-state functional connectivity in medication-naive schizophrenia patients with and without auditory verbal hallucinations: A preliminary report. *Schizophrenia Research* 188: 75–81.

Schmidt R, de Reus MA, **Scholtens LH**, van den Berg LH, van den Heuvel MP (2015) Simulating disease propagation across white matter connectome reveals anatomical substrate for neuropathology staging in amyotrophic lateral sclerosis. *Neuroimage* 124: 762–769.

van den Heuvel MP, de Reus MA, Feldman Barrett L, **Scholtens LH**, Coopmans FM, Schmidt R, Preuss TM, Rilling JK, Li L (2015) Comparison of diffusion tractography and tract- tracing measures of connectivity strength in rhesus macaque connectome. *Human brain mapping* 36: 3064-3075.

Conference abstracts

Scholtens LH, van den Heuvel MP (2017) Highly connected regions in macaque cortex show increased cortical expansion towards human. *Society for Neuroscience*.

Scholtens LH, de Reus MA, van den Heuvel MP (2015) Layer-specific comparison of high resolution MRI cortical thickness with the von Economo legacy. *Society for Neuroscience*.

Scholtens LH, de Reus MA, van den Heuvel MP (2015) Comparing high resolution MRI cortical thickness measurements with the von Economo atlas. *Human Brain Mapping*.

Nederlandse samenvatting

Hersenconnectiviteit van micro- tot macroschaal

Het brein is een bijzonder complex orgaan, bestaande uit een groot aantal hersengebieden met verschillende functies die door een netwerk van verbindingen onderling zijn verbonden. Het complete netwerk van verbindingen tussen deze gebieden wordt ook wel het connectoom genoemd, en verbindt de gebieden in het brein op zo'n manier dat informatie op een efficiënte manier wordt samengebracht en verwerkt. De verbindingen in het brein zijn niet gelijkmatig verdeeld. Sommige gebieden hebben veel lange connecties die wijd verspreid zijn over het brein en kunnen daardoor informatie uit een groot aantal gebieden (modaliteiten) combineren en verwerken. Dit soort bovengemiddeld verbonden gebieden worden ook wel "hubs" genoemd, en bevinden zich verspreid door het brein in gebieden betrokken bij het verwerken van complexe informatie. Andere gebieden in het brein hebben minder verbindingen en wisselen informatie uit op een meer lokaal niveau, zoals bijvoorbeeld de gebieden betrokken bij de verwerking van primaire visuele informatie.

Hoewel de verbindingen tussen verschillende delen van het brein voortkomen uit neuronen (op de cellulaire *microschaal*), worden deze in het humane hersenonderzoek vaak met behulp van MRI (magnetic resonance imaging) scans gereconstrueerd. Deze techniek heeft een relatief lage resolutie – in een MRI voxel (3D pixel) kunnen zich wel 10^4 neuronen bevinden – en het resulterende connectoom beschouwen wij in de context van dit proefschrift daarom als *macroschaal* informatie. Naast de regionale variatie in macroschaal verbindingen zoals gevonden wordt in het connectoom, is er ook op de microschaal van corticale neuronale architectuur grote variatie tussen gebieden van het brein. Het grootste deel van de cortex (ofwel, hersenschors – de buitenste laag van de grote hersenen) is opgebouwd uit 6 lagen. Deze lagen worden gedefinieerd op basis van het type, de grootte en de dichtheid van neuronen in de cortex, waarbij elke laag een net andere samenstelling heeft. De populaties van neuronen in zo'n laag hebben vrij specifieke verbindingspatronen. Zo zijn neuronen in laag III van de cortex met name verbonden met andere gebieden in de cortex (corticocorticale verbindingen), terwijl neuronen in laag V en VI vaker naar andere dieper gelegen delen van het brein en het ruggenmerg verbinden. Naast deze differentiatie in functie en verbinding tussen corticale lagen is er ook tussen gebieden in de cortex grote variatie in architectuur. Deze laatstgenoemde variatie wordt op basis van apenonderzoek genoemd als een van de belangrijkste voorspellende factoren voor het patroon van macroschaal corticocorticale verbindingen in het brein (zie ook **hoofdstuk 1** – Introduction).

In dit proefschrift combineren we informatie uit verschillende bronnen op zowel de micro- als de macroschaal, om zo meer te weten te komen over de interactie tussen de hersenorganisatie op beide schalen. Daarvoor maken we gebruik van drie soorten macroschaal informatie: 1) structurele connectiviteit, een reconstructie van de anatomische verbindingen (vezelbanen) tussen hersengebieden; 2) functionele connectiviteit, gebaseerd op de mate van samenhang in de regionale activatiepatronen van het brein in rust; 3) hersenstructuur, zoals de vouwingen en dikte van de cortex.

Micro–macro in het structureel connectoom

Hoofdstuk 2 beschrijft een brede vergelijking van micro en macroschaal eigenschappen in het connectoom van de muis. Hieruit komt naar voren dat gebieden met veel corticocorticale verbindingen en een centrale rol in het connectoom grotere pyramidecellen hebben in corticale laag III, met grotere dendrietbomen en een hogere synapsdichtheid. Ook hubgebieden hebben neuronen met grote wijdvertakte dendrieten, passend bij hun rol in de integratie van complexe informatie in het macroschaal connectoom. **Hoofdstuk 3** borduurt voort op de bevindingen in de muis, en laat in **deel I** zien dat ook in het structureel connectoom van het menselijk brein grotere pyramidecellen in laag III met een hogere synapsdichtheid op de microschaal samengaan met een grotere corticale verbondenheid op de macroschaal. Ook in de mens gaat de centrale rol en het grote aantal macroschaal verbindingen van hubgebieden samen met een microschaal architectuur met grote, complexe neuronen in laag III. **Deel II** van hoofdstuk 3 beschrijft de samenhang tussen de verminderde macroschaal connectiviteit in schizofreniepatiënten en afname in de synapsdichtheid van pyramidecellen in laag III, waarbij een sterke relatie bestaat tussen afname in connectiviteit en afname in synapsdichtheid. **Hoofdstuk 4** verdiept de micro–macro relatie beschreven in hoofdstuk 2 en 3 verder, door te kijken naar de laag-specifieke relatie tussen de grootte van neuronale cellichamen en macroschaal connectiviteit. Hieruit blijkt dat alleen de grootte van cellichamen in laag III – de belangrijkste laag voor corticocorticale verbindingen – geassocieerd is met de mate van macroschaal verbondenheid. In **hoofdstuk 5** wordt de micro – macro associatie tussen de grootte van neuronale cellichamen en connectiviteit verbreed door eenzelfde analyse te doen in het connectoom van de rat en de muis, en deze nogmaals te verifiëren in de mens. Alle voorgaande vergelijkingen zijn gedaan met microschaal informatie uit literatuur of online beschikbare databases. **Hoofdstuk 6** beschrijft een pilotstudie waarin nieuw verkregen data over de microschaal grootte van dendrietbomen van laag III pyramidecellen (op basis van de Golgi-Cox kleuring) wordt gerelateerd aan macroschaal connectiviteit en aan vergelijkbare data uit de literatuur (zoals gebruikt in hoofdstuk 3). Samengevat laten deze hoofdstukken zien dat de regionale corticale

microstructuur – en dan specifiek de grootte en complexiteit van laag III pyramidecellen – een passende microschaal infrastructuur biedt voor de op de macroschaal geobserveerde rol van een hersengebied in het connectoom.

Micro-macro in het functioneel connectoom

Het tweede deel van dit proefschrift beschrijft twee vergelijkingen tussen de regionale variatie in de ratio tussen inhibitoire (remmende) en excitatoire (stimulerende) neurotransmitters op de microschaal en functionele connectiviteit op de macroschaal. **Hoofdstuk 7** laat zien dat in het effectieve (strychnine-geïnduceerde activatie) functionele connectoom van de makaak een meer excitatoir neurotransmitterprofiel samengaat met een groter aantal uitgaande verbindingen naar de rest van de cortex. **Hoofdstuk 8** verbreedt deze vergelijking naar het resting-state fMRI gebaseerd functioneel connectoom van zowel de makaak als de mens, en laat zien dat ook hier gebieden met een meer excitatoir neurotransmitterprofiel een groter aantal functionele verbindingen hebben.

Micro-macro met historische data

Eén van de meest volledige bronnen van informatie over de microschaal corticale architectuur van het menselijk brein is de historische Von Economo – Koskinas atlas uit 1925. Deze beschrijft voor een groot aantal gebieden van de corticale mantel per laag het aantal neuronen, de grootte van neuronale cellichamen (gebruikt in hoofdstuk 4) en de dikte van de corticale laag, gemeten in histologische *post mortem* preparaten van meerdere humane breinen. Tegenwoordig meten veel neurowetenschappers corticale dikte met behulp van MRI-scans in levende proefpersonen. **Hoofdstuk 9** beschrijft een vergelijking tussen de regionale corticale dikte van het menselijke brein zoals beschreven door Von Economo en Koskinas en MRI-afgeleide corticale dikte, en laat een duidelijke associatie tussen de twee meetmethoden zien. Om de historische Von Economo – Koskinas atlas bereikbaar te maken voor een breder neurowetenschappelijk publiek, wordt in **hoofdstuk 10** een gedigitaliseerde versie van de atlas beschreven, die een directere vergelijking tussen de historische histologische data en moderne neuroimaging moet faciliteren.

Macroschaal connectoom verschillen in kinderen van patiënten met schizofrenie en bipolaire stoornis

Uit connectoomonderzoek in patiënten met schizofrenie is gebleken dat de hubs van het brein – betrokken bij de integratie van informatie uit verschillende bronnen – minder

goed verbonden zijn dan in gezonde controles. Dit verschil werd in mindere mate geobserveerd in broers en zussen zonder schizofrenie. In patiënten met bipolaire stoornis – een psychiatrische ziekte met een deels met schizofrenie overlappend ziektebeeld – is juist een ander patroon van verbidingsverschillen gevonden.

Hoofdstuk 11 beschrijft een studie in kinderen van mensen met schizofrenie of bipolaire stoornis, waarin opnieuw een verminderde hub connectiviteit wordt geobserveerd in kinderen van mensen met schizofrenie, maar niet in kinderen van mensen met bipolaire stoornis. Dit wijst erop dat er een mogelijk erfelijk verschil is in de ontwikkeling van het macroschaal connectoom in (familieleden van) schizofreniepatiënten, iets wat zeker een interessant startpunt is voor verder onderzoek in de context van de micro–macro associaties in het gezonde brein en in schizofrenie beschreven in dit proefschrift.

Tot slot bespreekt **hoofdstuk 12** hoe de observaties uit dit proefschrift aansluiten bij de literatuur, en verschillende mogelijkheden voor vervolgstudies. Een van de meest veelbelovende mogelijkheden hierin is het combineren van metingen op de micro- en macroschaal binnen hetzelfde individu, zodat de associaties die nu van metingen op groepsniveau tussen verschillende studiepopulaties zijn afgeleid direct meetbaar worden. Multimodaal connectoom onderzoek kan een verbindende factor vormen tussen niveaus van observatie in de neurowetenschappen, en zodoende bijdragen aan een meer compleet fundamenteel begrip van hersenorganisatie en ziektegerelateerde veranderingen in het brein.

Acknowledgments – Dankwoord

Dit dankwoord – het meest gelezen deel van ieder proefschrift – vormt de afsluiting van mijn boekje en van $4\frac{1}{2}$ mooie jaren als promovendus in het Dutch Connectome Lab. Ik wil graag heel veel mensen bedanken: collega's, vrienden en familie.

Als eerste wil ik graag mijn promotor professor Kahn bedanken. U stond altijd klaar met een aandachtig luisterend oor en scherpe suggesties. Uw geheugen en oog voor detail zijn uitzonderlijk, zodat u zelfs tijdens onze korte ontmoetingen nog uitstekend de vinger aan de pols van mijn project hield. Bedankt voor de kans om bij u op de afdeling mijn promotieonderzoek te doen.

Beste copromotor, dr. van den Heuvel, Martijn, het was een plezier om met je samen te werken. Dankzij jouw scherpe brein zat ik geen moment zonder ideeën, iets wat denk ik mede af te zien is aan het aantal hoofdstukken dat dit boekje rijk is. Omgekeerd stond jouw deur ook altijd open voor mijn vragen, opmerkingen en hersenspinsels, iets wat voor mij heel prettig was en mooi de flow in het onderzoek hield. Ik ben heel blij dat we de komende tijd onze samenwerking nog voort kunnen zetten. Aan goede ideeën geen gebrek!

Members of the Dutch Connectome Lab (both current and former), it's been a pleasure to work with you all. It's a true privilege to work in a team that is at the same time so diverse and so integrated. Marcel, Guusje, Ruben, Fraukje, Kristin, Maurits, Suus, Koen, Lizzy, Kirsten, Femke, Jet, Hannelore, Xiao, Idoia, Bauke, Siemon, Elise, Yongbin, Rory, Alessandra, Jil and Dirk Jan, without you guys I would not have enjoyed my research journey nearly as much as I did. Thanks for your friendship and for sharing your knowledge on programming, statistics, neuroanatomy, Chinese food, baking, terrible tv shows, fashion and the art of tafelvoetbal with this bookish neurobiologist. Let's meet up and go get some ice cream to remember the good old days. Visitors from across the globe – Karl, Carlo, Zach, Hugo, Tim, Julia, Longbiao, Jiahe and others – thanks for stopping by our lab, it was a pleasure meeting you.

Ook de collega's van de rivaliserende Kantoortuin 1 wil ik graag bedanken, voor de gezellige sinterklaasavonden, voor de koekjes die altijd klaarlagen, voor de goede gesprekken over huizen, koffie, bier en vakantiebestemmingen. Jessica – oud-kamergenootje, het was fijn kletsen.

Lieve collega's op het NIN. Inge – bedankt voor de kans om deel uit te maken van je groep. Mark, Nina, Marlijn en Adelia, bedankt voor jullie gastvrijheid. Het is een groot plezier om deel uit te mogen maken van jullie groep, bij jullie voelde ik me vanaf dag één

Dankwoord

welkom. Ik hoop dat we onze samenwerking nog lang voort mogen zetten! Beste Corbert – ook jou kan ik in dit dankwoord niet vergeten, zeer veel dank voor je ondersteuning in het opzetten van het Golgi project. Zonder jou was dat alles me nooit gelukt.

To my gracious hosts during my visits abroad – Lisa Feldman Barrett at Northeastern University and John Allman at Caltech Pasadena, many thanks for giving me the opportunity to be part of your labs.

Jelmer – Het was inderdaad prima forenzen.

Annemoon – Bedankt voor alle fijne lunchdates, en bedankt voor het aanhoren van mijn eindeloze vertellingen over papers, deadlines en andere wetenschapsongein.

Dear Doug & Azu, thanks for your incredible openness, hospitality and friendship. It's a rare thing to connect so easily, and to so seamlessly live together after knowing each other for such a short time. You made our time in Cambridge unforgettable.

Lieve vrienden en vriendinnen – bedankt voor alle gezelligheid tussen de bedrijven door. Jullie helpen me eraan denken dat ik ook de leuke dingen buiten de wetenschap niet moet vergeten. Waggachickies – super leuk dat we na al die jaren nog altijd zoveel contact hebben, tot gauw weer! Beste vrienden in Nijmegen – na al die jaren trouw ga ik nu toch echt het Nijmeegse land verruilen voor een meer centraal gelegen plekje. Wees niet bang, ik verlaat jullie niet echt. Andrei – oudste huisgenoot, dankzij jou en Ruud voelde Nijmegen direct als thuis. Ook nu is jouw plekkie in Maastricht mijn favoriete ontsnappingsoord als ik even geen wetenschap meer wil verdragen. Sjors – ik hoop je gauw weer spontaan bij ons aan de eettafel te zien, prachtige afleiding na een dag hard werken. Sem & Inge – dank voor de gezelligheid en fijne discussie met goed eten. Door jullie ogen zie ik een wereld vol mogelijkheden.

Lieve familie – lieve pap & mam, bedankt voor jullie steun en vertrouwen in mijn kunnen. Dankzij jullie voorbeeld en geduldige antwoorden op mijn eindeloos nieuwsgierige vragen beleeft dit nieuwsgierig Aagje nog altijd veel plezier in het uitvogelen van nieuwe dingen. Jullie groene Wageningse paradijsje is een oase van rust geweest in mijn soms hectische leven, zeker in deze laatste promotiejaren. Karlijn – lieve zus, ik ben ontzettend trots op je. Je bent een ontzettende doorzetter, die laatste stappen tot het architect-zijn gaan met jouw inzet helemaal goedkomen. Toin & Jackie bedankt voor de gezellige weekenden in het Brabantse land, ook jullie huis is een rustpunt te midden van de drukte waar Ruud en ik ons in stortten. Lieve, ik vind het hartstikke mooi om te zien hoe je bent opgebloeid tot een lekker eigenwijs individu. Je bent net zo'n doorzetter als je grote broer.

Maar nog het meest van allemaal gaat mijn dank uit naar **Ruud**. Zonder jou was dit alles me nooit gelukt. Jij helpt me met beide benen op de grond te staan. Als ik mezelf tijdens mijn promotietraject weer eens uit puur enthousiasme voorbij dreigde te lopen. Als ik me druk maakte over zaken die anderen zeker weten al lang waren vergeten. Als ik vergat dat anderen heus niet zo streng zijn als ik voor mezelf vaak ben. Als ik door de bomen het bos niet meer zag. Dankzij jou heb ik enigszins geleerd *schijt* te hebben aan dingen en mijn eigen pad te volgen. Nogmaals, zonder jouw steun had ik nooit zo veel kunnen bereiken en was dit boekje zeker weten een minder dik boekwerk geweest. Ik ben ontzettend trots en een ook een beetje jaloers dat je me nog bijna hebt weten in te halen in je vliegensvlugge superefficiënte, vernieuwende en diepgaande PhD-project. Ik heb groot respect voor hoe scherp jij je doelen voor ogen weet te houden. Ik ben blij dat we het wetenschappelijke promotiepad zij aan zij hebben weten te doorlopen, op naar het volgende avontuur?

Curriculum Vitae

Lianne Scholtens was born on May 11th, 1989 in Wageningen, the Netherlands. After graduating high school in 2007 (Gymnasium, Regionale Scholengemeenschap Pantarijn in Wageningen) she started her bachelor's degree in *Biology* at the Radboud University in Nijmegen. During her studies in Biology, she participated in all available courses on neuroscience and psychology, and obtained a minor in medial biology.

After completing her Bachelor's in 2010 with an internship investigating the effect of diet on amyloid plaque formation in a mouse model for Alzheimer's disease, Lianne started the *Cognitive Neuroscience* research masters program (also at Radboud University Nijmegen). Here, Lianne further developed her interest in multidisciplinary neuroscience, as evidenced by the topic of her masters internship and thesis, in which she sought to link neuroimaging and genetics in the study of pain sensitivity.

In 2013, Lianne joined the *Dutch Connectome Lab* to start her PhD at the Psychiatry department of University Medical Center Utrecht under supervision of professor dr. René Kahn and dr. Martijn van den Heuvel. Here, she applied her multidisciplinary knowledge to link multimodal and multiscale data on cortical structure and corticocortical connectivity to learn more about the biology behind the structure and function of the brain network. Lianne will continue her work at the Dutch Connectome Lab as a postdoctoral researcher, aiming to expand her multiscale connectome research across species to examine the brain network from an evolutionary perspective.



